

# **Thermosensitive hydrogels for 3D bioprinting of cartilage constructs**

**Anna Abbadessa**

The printing of this thesis was financially supported by:

Utrecht Institute for Pharmaceutical Sciences (UIPS), Utrecht, The Netherlands

Netherlands society for Biomaterials and Tissue Engineering (NBTE)

PolyVation BV, Groningen, The Netherlands

© Anna Abbadessa, 2017

Printed by Proefschriftmaken

ISBN: 978-90-393-6714-8

Cover design: angular view of a 3D printed hydrogel, Abbadessa *et al.*,  
*Carbohydrate Polymers*, 2016, 149, pp 163-174.

# **Thermosensitive hydrogels for 3D bioprinting of cartilage constructs**

Temperatuurgevoelige hydrogelen  
voor het 3D bioprinten van kraakbeenconstructen  
(met een samenvatting in het Nederlands)

## **Proefschrift**

ter verkrijging van de graad van doctor aan de Universiteit Utrecht  
op gezag van de rector magnificus, prof.dr. G.J. van der Zwaan,  
ingevolge het besluit van het college voor promoties in het openbaar  
te verdedigen op maandag 6 maart 2017 des middags te 2.30 uur

door

***Anna Abbadessa***

geboren op 26 februari 1986, te San Severo, Italië

**Promotor:** Prof. dr. ir. W.E. Hennink

**Copromotoren:** Dr. ir. T. Vermonden  
Dr. ir. J. Malda

This thesis was (partly) accomplished with financial support from the European Community's Seventh Framework Programme (FP7/2007-2013) under grant agreement n° 309962 (HydroZONES).



“Of course, one never knows what’s going to come out,  
but as soon as the drawing gets underway, a story or an idea is born.  
And that’s it. Then the story grows, like theater or life and the drawing is  
turned into other drawings, a real novel.”

From “Forever Picasso: an intimate look at his last years”  
by Roberto Otero



## **Table of contents**

<b>Chapter 1</b> General introduction	9
<b>Chapter 2</b> A thermo-responsive and photo-polymerizable chondroitin sulfate-based hydrogel for 3D printing applications	31
<b>Chapter 3</b> A synthetic thermo-sensitive hydrogel for cartilage bioprinting and its biofunctionalization with polysaccharides	59
<b>Chapter 4</b> Two-component thermosensitive hydrogels: phase separation affecting rheological behavior	91
<b>Chapter 5</b> Monodisperse hyaluronic acid-based microgels loaded in thermosensitive hydrogels for a sustained release of proteins: an introductory study	123
<b>Chapter 6</b> Bio-ink development for the fabrication of composite cartilage repair constructs	147
<b>Chapter 7</b> PolyHPMA-lac-PEG triblock copolymer/HAMA hydrogels for cartilage regeneration: <i>in vivo</i> studies in mice, mini-pigs and horses	173
<b>Chapter 8</b> Summary and Perspectives	197
<b>Appendix A</b> Nederlandse Samenvatting	207
<b>Appendix B</b> Curriculum Vitae and List of Publications	211
<b>Appendix C</b> Acknowledgements	215





# **Chapter 1**

## **General Introduction**

The field of Regenerative Medicine (RM) and Tissue Engineering (TE) aims to develop treatments for tissue damage by using biomaterials and/or cells, often in the presence of bioactive molecules, such as growth factors. Especially for poorly self-healing tissues, such as for the articular cartilages, TE strategies can represent promising alternatives to the non-ideal clinical procedures currently used. To develop an effective regenerative approach for the treatment of a certain tissue defect, a deep understanding of the anatomy, physiology and pathology of that tissue is required. Moreover, current treatments with their advantages and limitations must be examined, since they can serve as guidance for the development of rationally designed and superior novel treatments. Current progress in polymer chemistry, cell biology, biomaterial science and biomedical engineering offers a vast range of possible materials, cell types and culture procedures, as well as manufacturing technologies. In this context, rational and bio-inspired choices can be made to select the most appropriate material, cell type and processing technology. In the first chapter of this thesis, structure and function of articular cartilage, current treatments for cartilage damage and more advanced TE-based strategies are discussed.

## 1.1 Cartilage

### 1.1.1 General introduction to cartilage

Cartilage is a connective tissue containing specific cells, *i.e.* the chondrocytes, embedded in an extracellular matrix consisting of predominantly collagen and proteoglycans, able to absorb water. Cartilage is an avascular, non-innervated tissue and also does not contain lymphatic vessels. It can be classified in three subtypes: hyaline cartilage, elastic cartilage and fibrocartilage<sup>1</sup>. These three types of cartilage differ significantly in their structure at a macroscopic, microscopic and molecular level. These differences are related to distinct mechanical properties, which allow for proper function of each subtype of cartilage<sup>2</sup>. For example, hyaline cartilage is rich in collagen type II, which is highly resilient, and therefore it can resist high mechanical stresses. Elastic cartilage, which is found in the outer ear and other structures that provide flexible support, contains a dense network of elastic fibers composed of elastin. Fibrocartilage, found in intervertebral discs, tendon insertions and some joints, is highly resilient to compressive deformation, as a result of a low aggrecan content and fibrous matrix production by embedded fibroblasts. Articular cartilage is hyaline cartilage, and material development facilitating regeneration of this tissue is a major focus of this thesis. Therefore, its anatomy and physiology are described in more detail in the following sections.

### 1.1.2 Anatomy of articular cartilage

Articular cartilage covers the extremities of long bones, and enables proper joint articulation, owing to its smooth and lubricated surface<sup>3</sup>. Moreover, it is capable of transmitting and evenly distributing the load imposed on joints to the underlying bone. In humans, the cartilage thickness is approximately 1-2.5 mm and it can vary for joint type, *e.g.* hip, knee or ankle, and individual characteristics, *e.g.* body mass

and height<sup>4,5</sup>. The extracellular matrix (ECM) is primarily composed of water (60-80% of wet weight), collagen (50-60% of dry weight), proteoglycans (30% of dry weight), as well as glycoproteins and lipids in smaller content<sup>1,3</sup>. Multiple types of collagen are present in cartilage, although collagen type II is the most abundant. Collagen fibers are oriented in an arcade-like fashion, with the apex toward the articular surface. This provides the cartilage with mechanical resilience against tangential compression. Water is attracted and retained in the cartilage matrix due to the hydrophilic character of proteoglycans. Among proteoglycans, aggrecan is most mass-abundant and consists of a core protein covalently linked to highly sulfated glycosaminoglycans (GAGs), *i.e.* chondroitin sulfate and keratan sulfate. Numerous aggrecan molecules are associated with a long hyaluronan backbone via non-covalent binding, forming proteoglycan aggregates<sup>6</sup>. Chondrocytes occupy approximately 2% of the total volume of articular cartilage<sup>3</sup>. These cells are responsible for ECM production and homeostasis, and they respond to several stimuli, such as growth factors, mechanical loads or hydrostatic pressure. As cartilage is avascular, the viability and function of chondrocytes depend on the diffusion of oxygen and nutrients, as well as waste products through the synovial fluid. Chondrocytes are located in small regions in the ECM, called *lacunae*. A lacuna usually contains one chondrocyte, but multiple chondrocytes may be present<sup>1</sup>.

Articular cartilage has a complex and highly organized structure, consisting of four horizontal layers, or “zones”<sup>1,3</sup> (Figure 1). The zones differ in terms of cell morphology and density, content and arrangement of the ECM components, and consequently in their functions. The *superficial (tangential) zone* is a smooth and thin layer, containing flattened chondrocytes and collagen fibers oriented tangentially to the articular surface. This organization allows high resistance to shear stress. The *intermediate (transitional) zone* is rich in proteoglycans and thick collagen fibers are arranged in an oblique fashion with regard to the articular surface. Chondrocytes in the intermediate zone are spherical and present in lower density compared to the superficial layer. The main function of this layer is to resist compressive forces. The *deep zone* contains the highest amount of proteoglycans, yet the lowest amount of water. The collagen fibers have the largest diameter and are positioned perpendicularly to the articular surface. The cell density is the lowest compared to that of all other layers, and chondrocytes are large and stacked into columns. This layer more efficiently resists compressive forces. Finally, the *calcified zone* anchors the articular cartilage to the subchondral bone, and it contains chondrocytes in non-calcified areas. Within each zone, three distinct ECM regions can be distinguished, which are the pericellular, territorial and interterritorial regions<sup>1,3</sup>. The *pericellular region* is located closely around the chondrocytes, it is rich in proteoglycans, and it is involved in the signal transduction in response to load stimuli. The *territorial region* is more fibrillary and surrounds the pericellular region, and it may play a role in the mechanical protection of chondrocytes. The *interterritorial region* is the largest region (approximately 90% of the whole matrix) and it constitutes the rest of the matrix around the territorial regions.

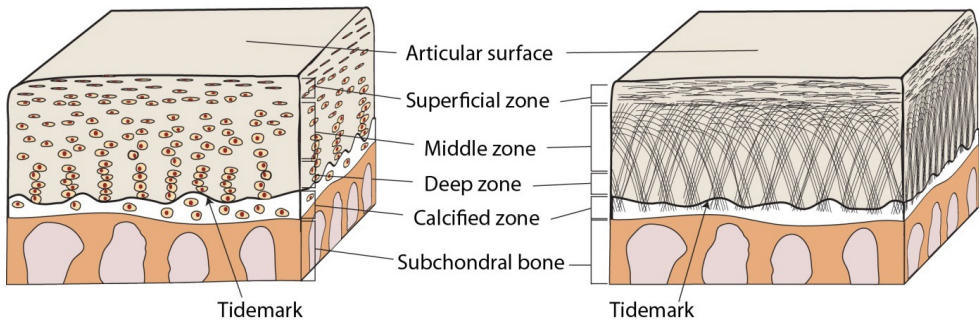


**Figure 1.** Schematic illustration of the depth-dependent structure of articular cartilage, highlighting the different cell organization (left) and collagen fibers arrangement (right) throughout the four horizontal layers<sup>7</sup>.

### 1.1.3 Physiology of articular cartilage

Chondrocytes play an essential role in maintaining the homeostasis of cartilage by producing matrix components, as well as metabolic enzymes<sup>8</sup>. The synthetic activity of chondrocytes is regulated in response to environmental stimuli. For example, the detection of matrix degradation products or the exposure to load due to matrix compression can induce synthetic activity of chondrocytes. This activity mechanism explains the fact that regular movement contributes to the maintenance of healthy articular cartilage<sup>8</sup>. Moreover, the presence of several cytokines and growth factors, such as interleukin-1 (IL-1), tumor necrosis factor- $\alpha$  (TNF- $\alpha$ ), and transforming growth factor- $\beta$  (TGF- $\beta$ ), can affect the proliferation of chondrocytes and regulate the chondrocyte-mediated metabolism of ECM components<sup>3,9</sup>. The turnover of ECM components is regulated by the activity of several specific enzymes, such as metalloproteinases, *e.g.* collagenase, and cathepsins<sup>3</sup>.

Due to its viscoelastic properties, healthy cartilage is capable to respond to compression and tension during the repetitive loading of the joint, generated during movements. An essential aspect in the resistance of cartilage to compression is the regulation of the extrusion and retention of water in the matrix during loading-cycles, which is governed by the combined action of aggrecan and collagen<sup>6</sup>. Aggrecan is negatively charged and thus repulses other aggrecan molecules, attracts fluid and thereby highly contributes to the expansion of the ECM. On the other hand, collagen is specifically capable of resisting tensile forces. Hence, it counteracts the aggrecan-driven expansion of ECM. Upon loading, when the cartilage matrix is compressed, water is extruded and the distance between aggrecan molecules decreases. After the load is removed, the compacted aggrecan molecules re-attract fluid to its thermodynamic equilibrium, thus re-expanding the matrix, but only to a limited extent that is determined by the tensile resistance of the collagen fibers.

Degeneration of cartilage can be due to an acute trauma, experienced during *e.g.* accidents, or it can be caused by age-related tissue deterioration. The spontaneous



repair of damaged cartilage is usually nil or highly insufficient<sup>10,11</sup>. This is partially due to the low number of cells, as well as to their low metabolic activity, imputable to the absence of vascularization. Therefore, partial thickness defects that involve exclusively the cartilage tissue do not heal spontaneously. On the other hand, full-thickness defects that involve the partial deterioration of the subchondral bone, have some regenerative potential<sup>11</sup>. In fact, the damage of the subchondral bone causes rapid influx of subchondral blood into the defect area and migration of mesenchymal stem cells. Although this process results in the production of some ECM and provides a certain degree of repair, the new tissue, *i.e.* fibrocartilage is biomechanically inferior to hyaline cartilage<sup>11</sup>, and an often inevitable consequence of this process is osteoarthritis (OA)<sup>12</sup>.

#### **1.1.4 Clinical approaches for the repair of articular cartilage**

Cartilage defects are currently treated in clinics by using procedures that rely on bone marrow stimulation, osteochondral transplantation or cell delivery. Microfracture, subchondral drilling and abrasion arthroplasty are performed by partial perforation of the subchondral bone to trigger blood influx, and therefore cell migration into the defect area<sup>13</sup>. As explained above, this mechanism leads to the formation of inadequate fibrocartilage, and to a high risk of developing OA. Nevertheless, these techniques are widely applied since they provide a sufficient, yet temporary relief to patients. Alternatively, osteochondral transplantation offers the only efficient method to quickly re-establish hyaline cartilage<sup>11</sup>. However, donor site morbidity, often associated with autograft transplantation and immunogenicity, often caused by allografts are the main limitations here. Autologous chondrocyte implantation (ACI) has also been adopted as a relevant treatment in the clinical routine of some countries<sup>14,15</sup>. This method consists of the isolation of autologous chondrocytes, their *in vitro* expansion and re-injection into the defect area of a patient. More recent modalities of ACI involve the additional use of a porous matrix, on which cells are seeded (matrix-induced autologous chondrocyte implantation, MACI). In matrix-based approaches, the presence of a three dimensional (3D) scaffold can warrant the complete filling of the defect area, and provides a temporary mechanical support.

### **1.2 Tissue engineering for articular cartilage repair**

#### **1.2.1 Scaffold types**

Tissue engineering (TE) involves the use of cells, biomaterials, biochemical factors, *e.g.* growth factors, and/or physical stimulation, *e.g.* pressure, to create constructs able to regenerate damaged tissues<sup>16–18</sup>. Ideally, the purpose of TE constructs is to initially provide a mechanical support and a bio-friendly environment for cells, and later to promote new tissue formation by embedded or recruited cells, while the biomaterial is degrading. The matrices that provide the structural support in a TE-approach are commonly called scaffolds. There are four main types of TE scaffolds: hydrogels, pre-made porous scaffolds, decellularized natural ECM and cell sheets<sup>19</sup>. For engineering load-bearing tissues, such as articular cartilage the first

three types are most relevant. Hydrogels are (visco)elastic materials, consisting of hydrophilic polymeric networks that retain high amounts of water. Cells are usually homogeneously dispersed in neutral aqueous solutions of hydrogel precursors, which are subsequently converted into physically or chemically crosslinked networks. Due to their innate soft and aqueous nature they offer a cell-friendly environment, however for the same reason they are unable to reach the stiffness of native cartilage<sup>20</sup>. Hydrogel scaffolds can be fabricated by mold casting or more sophisticated additive manufacturing procedures, before implantation into tissue defects<sup>21</sup>. Alternatively, injectable hydrogels can be infused directly into the defect area, and subsequently undergo *in situ* gelation<sup>22</sup>. Pre-made porous scaffolds are solid polymeric meshes, which can support cell attachment and inclusion of biologically relevant molecules, e.g. growth factors. They can usually provide mechanical stiffness close to that of native cartilage<sup>14</sup>. Finally, scaffolds for cartilage repair may be formed by naturally derived ECM, upon decellularization<sup>23</sup>. In more recent approaches, combinations of the described scaffold types have been explored. For instance, the placement of a cell-laden (polymeric or tissue-derived) hydrogel within a stiff thermoplastic porous scaffold can offer a hybrid system, where advantages of the two materials can be warranted<sup>14,25</sup>.

### 1.2.2 Requirements for TE scaffolds

Besides the capacity to support tissue regeneration *in vivo*, scaffolds must fulfill several requirements when considering their translation to the clinic, of which the most important ones are biocompatibility, biodegradability, biomechanical and architectural adequacy, as well as possibility to manufacture them at reasonably low cost<sup>26</sup>. Biocompatibility is an essential factor determining the successful application of a scaffold. The immune response induced by the human body against the implanted scaffold largely determines its biocompatibility, therefore this response must be understood, and methods to control it must be devised. Rejection by the human body can be targeted to the biomaterial, to the seeded cells, or to any other included component. Moreover, a reaction against immunogenic materials may consequently damage embedded cells that would otherwise be non-immunogenic. Therefore, when discussing the immunological biocompatibility of a TE construct, all the individual components (biomaterials, cells and included molecules), as well as their immunological interactions, must be regarded. For the maintenance of the biocompatibility of a scaffold, toxic components, possibly used during its manufacturing, must be completely removed, and good manufacturing practices (GMP) must be adopted.

Biodegradability is one of the key-concepts to design scaffolds that are resorbed *in vivo*, while new tissue is synthesized by embedded or recruited cells. Degradation of a scaffold can be achieved via hydrolytic or enzymatic mechanisms<sup>27</sup>. Synthetic hydrogels usually rely on the hydrolysis of esters, or similarly liable groups, located within the polymer network, and that are cleavable under physiological conditions. Alternatively, enzymatic degradation can be exploited for hydrogels containing building blocks with amino acid sequences or other chemical structures,

such as polysaccharidic chains, recognized by endogenous enzymes, *e.g.* matrix metalloproteinases or hyaluronidase, respectively. Importantly, degradation products must be non-toxic and easily metabolized and/or eliminated by the body. Additionally, degradation rates should occur on a time-scale compatible with the new tissue formation. In general, the scaffold should not degrade completely until the new tissue is mechanically adequate. A big challenge here is that regeneration time differs between patients as a result of age or comorbidities.

A TE construct for cartilage repair must be biomechanically adequate to withstand the mechanical stress generated in the joint. Articular cartilage has a Young's modulus between 0.4 and 0.8 MPa<sup>28-30</sup>. Technically speaking, current knowledge does not allow to state that ideal cartilage constructs must have stiffness within the same range as native cartilage. In fact, a TE construct should not necessarily be an exact copy of the tissue that needs to be regenerated. Instead, it must be an instructive environment for cells to regenerate that tissue, and the physical/chemical stimuli for creating such environment are not yet completely understood. Nevertheless, it is intuitive that the mechanical properties of cartilage constructs should be sufficient to guarantee a valid support during the entire regeneration process, and constructs should be easily handled and fixated into the defect area by surgeons at the moment of implantation. The internal architecture of cartilage scaffolds also deserves major attention. Scaffolds must have an interconnected pore structure allowing the diffusion of fluids and nutrients, and enabling cell-to-cell interactions. Additionally, efforts have been devoted in the creation of zonally organized scaffolds able to reproduce, at least to some extent, the hierarchical organization of native cartilage. This has been attempted by employing different material compositions or cell subpopulations for each zone of the scaffold<sup>31-33</sup>.

## 1.3 Hydrogels

### 1.3.1 Classification and crosslinking mechanisms

Hydrogels are one of the most widely investigated materials for the generation of cartilage constructs. They are composed of crosslinked hydrophilic polymeric chains able to retain a high amount of water, while remaining undissolved. Hydrogels offer a three-dimensional aqueous environment, where cells and/or bioactive molecules can be hosted. Hydrogels are often classified according to the origin of the used polymers, which may be natural, synthetic or hybrid. In addition, hydrogels can be classified in bulk matrices, films, micro- or nanogels according to their physical shape. Finally, the method of crosslinking is a very important distinction principle for hydrogels, as it may significantly impact their properties, *e.g.* mechanics, biodegradability and biocompatibility. Crosslinking methods may be classified as either physical or chemical. Table 1 summarizes a number of frequently used chemical crosslinking methods, as well as their advantages and disadvantages<sup>34</sup>.

**Table 1.** Chemical crosslinking methods for the preparation of hydrogels suitable for TE applications.

crosslinking method	mechanism	advantages	disadvantages	ref
Radical polymerization	vinyl group-functionalized polymers react via redox-, thermal- or photo-initiation	fast crosslinking  thermal or redox initiation can be induced transdermally	possible toxicity due to light irradiation, initiators or unreacted vinyl groups  generation of crosslinking chains with uncontrolled molecular weight	35,36
Schiff-base formation	aldehydes react with amine or hydrazide functionalities. Use of crosslinkers (e.g. glutaraldehyde or adipic dihydrazide)	convenient for amine-containing polymers	possible toxicity of crosslinker  aspecific reactivity of residual groups toward endogenous proteins	37-39
Michael-type addition	reaction between a nucleophile (e.g. thiol) and a $\alpha,\beta$ unsaturated carbonyl	1:1 donor/acceptor reaction with no formation of long crosslinking chains  high selectivity of vinyl groups for thiols (low cross-selectivity of vinyl groups with proteins)  mild reaction conditions	possible toxicity due to residual unreacted thiol or vinyl groups	40-42
Native chemical ligation (NCL)	thioester reacts with a thiol of a <i>N</i> -terminal cysteine, followed by a <i>N</i> -to- <i>S</i> rearrangement and formation of an amide bond	high chemo-selectivity  mild reaction conditions  possibility to covalently immobilize peptides	possible toxicity due to formation of thiol-containing byproducts (can be overcome by oxo-ester mediated NCL <sup>43</sup> )	43-45
Click reactions	an azide reacts with an alkyne	quick and efficient  1:1 reaction	possible toxicity due to copper, if used as a catalyst. Copper-free technologies are presently available	46-48

Enzyme-mediated crosslinking	enzymes catalyze polymer crosslinking (e.g. via transglutaminase or horseradish peroxidase, HRP, in presence of H <sub>2</sub> O <sub>2</sub> )	selectivity  crosslinking kinetics tunable by enzyme concentration	toxicity of H <sub>2</sub> O <sub>2</sub> in case of HRP	49-51
------------------------------	---	--	--	-------

Alternatively, physical hydrogels can be obtained by stereocomplexation, *i.e.* co-crystallization of two enantiomers; by formation of inclusion complexes using *host/guest* chemistry; by self-assembly of protein-polymers or temperature/pH sensitive triblock copolymers<sup>22</sup>. Generally speaking, chemical crosslinking methods provide mechanical and degradation properties superior to physical methods, but they may be less biocompatible due to substances used in their manufacturing process<sup>34</sup>. The combination of chemical and physical crosslinking is currently a widely investigated approach to exploit the beneficial properties of both technologies.

### 1.3.2 Building blocks

Hydrogel building blocks can be of natural or synthetic origin. Frequently used natural macromolecules include collagen and its derivative gelatin, fibrin, a vast class of polysaccharides, and DNA<sup>22</sup>. Collagens have cell-adhesive sites and can form physical hydrogels. However, they degrade rapidly and have poor biomechanical properties<sup>52</sup>. Alternatively, chemical crosslinking methods, based on glutaraldehyde- or UV-mediated chemistry have been applied to collagen and gelatin, to obtain significantly stiffer and slower degrading hydrogels<sup>37,53,54</sup>. Fibrin is a protein that has been widely investigated for the preparation of hydrogels for TE applications<sup>55</sup>. Nevertheless, compaction, low mechanical properties and fast degradation kinetics of fibrin hydrogels are three main disadvantages. Attempts to overcome these issues have been undertaken by *e.g.* adding protease inhibitors to the culture medium, as well as by reducing cell density or by applying PEGylation strategies<sup>56</sup>. Among polysaccharidic building blocks, hyaluronic acid (HA) is one of the most commonly used. HA consists of repeating disaccharide units of D-glucuronic acid and *N*-acetyl-D-glucosamine. It is a natural component present in many tissues including cartilage, where it is involved in the lubrication of the articular surface, in the assembly of the matrix and cell functioning. HA is commercially available in different molecular weights, and because it is rich in hydroxyl and carboxylic groups, it can be chemically modified with crosslinkable groups to form hydrogels.

Classic examples of synthetic polymers used for the fabrication of hydrogels are: poly(ethylene glycol) (PEG), polyacrylamide (PAAm) and poly(vinyl alcohol) (PVA). PEG can be chemically modified by introducing crosslinkable or bioactive moieties on the terminal hydroxyl groups<sup>57</sup>. Especially because PEG is bio-inert, its biofunctionalization is often undertaken to enhance its cell adhesion properties. Moreover, PEGs are by themselves not biodegradable. Therefore, biodegradable moieties are often integrated in the final network. This also means that PEG used to design hydrogel building blocks typically have molecular weights below 50 kDa to

make excretion by the kidneys possible.

Generally speaking, natural polymers have the advantage to be biologically active and cost-effective. On the other hand, their natural source may raise immunogenicity issues. Moreover, they are characterized by a high batch-to-batch variability, which may negatively affect the reproducibility of the characteristics of natural hydrogels. Alternatively, the possibility to accurately design synthetic polymers and the opportunity to produce them in a highly reproducible manner make them ideal candidates for the design of hydrogels with tunable properties. Nevertheless, synthetic polymers are bio-inert and, thus synthetic hydrogels are hardly able to give cell-material interactions and trigger the activation of desired biological pathways. Therefore, the combination of synthetic and natural polymers is often undertaken to create hybrid hydrogels displaying advantageous features provided by both components.

Advances in polymer chemistry and engineering have led to the design of several new, synthetic polymers with stimuli-sensitive behavior, which appear to be very promising for the design of *in-situ* gelating, injectable and 3D printable TE materials.

### 1.3.3 Thermosensitive hydrogels

Stimuli-sensitive hydrogels are hydrogels that can reversibly change their physical properties (*e.g.* swelling/shrinking, liquid/solid state) in presence of specific changes in *e.g.* temperature, pH, pressure or light<sup>22,58</sup>. Thermosensitive hydrogels exhibit a temperature-dependent gelation process and can be formed by polymers with Lower Critical Solution Temperature (LCST) or Upper Critical Solution Temperature (UCST) behavior. LCST and UCST are defined as the temperatures above which or below which the polymeric chains are dehydrated and consequently precipitate in aqueous media<sup>22</sup>. Particularly polymers exhibiting LCST behavior slightly below 37 °C have been extensively investigated for the generation of injectable hydrogels<sup>22</sup>. The main advantage of these systems is that they are viscous liquids at low temperatures, which allows easy handling, incorporation of cells or biomolecules, and finally injection in a minimally invasive manner. Importantly, shape stability at the injection site is warranted by their gelation at body temperature. Only a limited number of natural-based polymers, *i.e.* gelatin and some cellulose and chitosan derivatives, exhibit thermosensitive behavior within a physiologically interesting temperature range<sup>59</sup>. Instead, a rich family of synthetic thermosensitive polymers has been reported for hydrogel fabrication. Poly(*N*-isopropylacrylamide) (pNIPAAm) and its copolymers must be mentioned here as the most used and studied thermosensitive polymers for biomedical applications<sup>59</sup>. Other examples are: poly(ethylene oxide)-*b*-poly(propylene oxide)-*b*-poly(ethylene oxide) (PEO-PPO-PEO), poly(d,l-lactide-co-glycolide)-poly(ethylene glycol)-poly(d,l-lactide-co-glycolide) (PLGA-PEG-PLGA), PEG-poly(l-lactide)-PEG (PEG-PLLA-PEG), star PLLA copolymerized with monocarboxy-monomethoxy PEG, or poly(*N*-hydroxypropyl)methacrylamide mono-dilactate-PEG-poly(*N*-hydroxypropyl)methacrylamide mono-dilactate (pHPMAlac-PEG-pHPMAlac) triblock copolymers<sup>22</sup>.

## 1.4 Cells

### 1.4.1 Cell source

A crucial aspect in many TE strategies is the inclusion of viable cells within the polymeric scaffold and the selection of the most relevant cell type. Incorporated cells contribute to the formation of new tissue by producing extracellular matrix and may also modulate the microenvironment in and around the construct, thereby contributing to the success of the therapy. The most frequently used cell types for TE cartilage constructs are mesenchymal stem cells (MSCs) and chondrocytes<sup>60</sup>. Moreover, co-culture of multiple cell types is currently gaining attention<sup>60</sup>. It needs to be noted that in a preclinical research setting, not only human-derived cells are used, but also cells from *e.g.* rodents, dogs and horses. Although using human cells would be the most appropriate approach towards the translation in clinical setting, availability of human cells is often limited. Additionally, human cells can be used only *in vitro* and in immune-deficient small animal models. Therefore, in the preclinical routine, to guarantee a non-xenogenic implantation in large animal models, the species from which cells are isolated is often dictated by the designed large animal model itself, *e.g.* ovine, caprine, porcine or equine<sup>61</sup>.

### 1.4.2 Chondrocytes

In a clinical scenario, autologous chondrocytes are the first choice for a TE application. Autologous chondrocytes are usually harvested from low-weight bearing regions of the joint, and are further isolated and expanded *in vitro*<sup>60</sup>. This expansion is necessary as a result of the scarcity of chondrocytes in articular cartilage and limitations related to the biopsy size. The main advantage of autologous chondrocytes is their non-immunogenicity. On the other hand, long *in vitro* expansion times associated with autologous chondrocytes usually lead to a dedifferentiation process towards fibroblastic lineage<sup>60</sup>. This can be, at least partially, overcome via pre-culture in chondrogenic medium of the cell-laden scaffolds before implantation. Additionally, cell isolation and subsequent cell-laden scaffolds implantation require two different surgical operations. Alternatively, allogenic articular chondrocytes can be used. In this case, larger biopsies can be taken and therefore expansion times and dedifferentiation can be minimized. Nevertheless, a natural higher tendency for immunogenicity is a relevant issue here<sup>60</sup>.

### 1.4.3 Mesenchymal stem cells

MSCs are usually isolated from bone marrow, synovium, periosteum or adipose tissue<sup>60</sup>. MSCs are characterized by high, long-term self-renewal capacity and differentiation potency<sup>62</sup>. The great potential of MSCs to help regenerate cartilage is due to their intrinsic capacity to differentiate towards a chondrogenic phenotype and their “homing” property. In general, MSCs are known to be able to migrate and “home” into damaged areas, where they can differentiate into the desired cell type, release bioactive factors and modulate processes, such as apoptosis and immune



responses<sup>62</sup>. For instance, it has been reported that they are able to reduce the activity of CD4<sup>+</sup>, CD8<sup>+</sup> and T lymphocytes, as well as to inhibit the maturation of dendritic cells<sup>62</sup>. Notably, co-culture of MSCs with chondrocytes may reduce the required amount of chondrocytes and/or expansion time, and could potentially lead to a one step-procedure in a clinical setting. Nevertheless, important disadvantages of using MSCs in 3D culture include the fact that they frequently differentiate to hypertrophic chondrocytes<sup>63</sup>. Such hypertrophic chondrocytes express proteins such as collagen type X, MMP-13 and alkaline phosphatase, which lead to undesired mineralization of the ECM.

## 1.5 Biofabrication of cartilage constructs

### 1.5.1 Biofabrication

Traditional approaches for the generation of TE constructs rely on the use of biomaterials, enriched with homogeneously distributed cells, often in the presence of signaling molecules. This rather simple combination is hardly reflecting the complexity of native tissues, and may explain the failure of numerous TE constructs that have not successfully been translated to clinics. In this regard, *Biofabrication* can be seen as a progressing field that aims to overcome these limitations by the generation of highly organized, tissue-mimicking constructs. An updated working definition of *Biofabrication* for TE and RM has been recently given by Groll *et al.*<sup>64</sup> as ‘*the automated generation of biologically functional products with structural organization from living cells, bioactive molecules, biomaterials, cell aggregates such as micro-tissues, or hybrid cell-material constructs, through Bioprinting or Bioassembly and subsequent tissue maturation processes*’. This definition embraces both the technological aspect of fabricating advanced constructs, and the natural character of some post-fabrication processes that are necessary to obtain a biologically functional final product. In this context, biofabrication employs two different technologies, *i.e.* bioprinting and bioassembly for the accurate positioning of specific *fabrication units*. For bioprinting, these units can be of relative small scale and can be generally addressed as (cell-containing) biomaterials, such as hydrogels. Instead, for bioassembly the fabrication units are pre-formed cellular organizations, including cell aggregates and cell sheets or more complex and organized organoids and hybrid cell-material constructs<sup>64,65</sup>. As biofabrication can lead to the development of constructs able to recapitulate the complex architecture of native tissues, this can be exploited in a cartilage regenerative approach by the generation of *composite constructs*, where each component fulfills a specific role<sup>66</sup>. In this manner, a structural component (*e.g.* a stiff thermoplastic framework) may provide sufficient mechanical support and a cell-containing unit may provide a bio-friendly environment for embedded cells. Furthermore, several cell-containing units may be present and organized in horizontal zones, differing in the type of encapsulated cells or material composition, to reflect the depth-dependent organization of articular cartilage. Finally, lubrication on the articular surface and integration with surrounding tissues may be provided by other specific components.



### 1.5.2 3D bioprinting

3D (bio-)printing is the computer-aided design and generation of 3D constructs, based on a layer-by-layer deposition of one or more materials<sup>20,64</sup>. Materials of different nature (*e.g.* hydrogels, thermoplasts) with or without cells can be processed by 3D printing. Cellularized 3D printable materials are often referred to as bioinks<sup>67,68</sup>. Bioprinting allows the accurate and controllable positioning of different components within a three-dimensional organization, with the opportunity to tune size, shape and internal architecture (*e.g.* porosity and zonal organization) of the final implant. The four most well-established bioprinting techniques are: stereolithography (SLA), laser-induced forward transfer (LIFT), inkjet printing and robotic dispensing<sup>20,69,70</sup>. SLA is the layer-by-layer photo-induced solidification of a liquid resin in a spatially controlled fashion, where the solidification pattern is accurately defined by the movement of a light beam. SLA enables the generation of relatively big objects with a typically high resolution of 20  $\mu\text{m}$ . New generations of SLA based on two-photon polymerization can have even higher resolution (200 nm). Although an increasing amount of resin types is becoming available, SLA can be applied exclusively to photo-sensitive materials. In the LIFT, a pulsed laser hits a donor slide (ribbon), which causes the material to be propelled from the ribbon to the collection plate. Similarly to SLA, LIFT is a nozzle-free procedure and provides a very high resolution (10-100  $\mu\text{m}$ ). Nevertheless, the use of LIFT is limited by the long fabrication times and commercial unavailability of the equipment. In inkjet printing, small droplets of a bioink are generated by thermal or piezoelectric stimulation, expelled through a small nozzle and deposited on a collection plate. In case of inkjet printing the resolution is still high ( $\sim 75 \mu\text{m}$ ), however the typically small orifice diameter limits the range of material viscosities that can be used, and renders this approach very much prone to clogging issues. Robotic dispensing is based on the generation of continuous filaments, which are extruded through the nozzle via a pneumatic, piston- or screw-based dispensing. Although this approach gives the lowest resolution among all the mentioned techniques, it is frequently used due to the much shorter fabrication times and the possibility to print relatively big objects. Additionally, screw-driven robotic dispensing is the most convenient technique for printing high viscosity materials, such as thermoplasts. Printable thermoplastic polymers, *e.g.* polycaprolactone (PCL), are currently widely used for the production of (cell-seeded) pre-made scaffolds and for the mechanical reinforcement of hydrogels<sup>25,71</sup>. Nozzle-based 3D printing, and especially robotic dispensing, is a major objective of this thesis, therefore the material requirements for applying this technology are discussed separately in the following section.

### 1.5.3 Material requirements for nozzle-based 3D printing

An ideal bioink aimed for nozzle-based 3D printing applications must have specific rheological characteristics to ensure a proper material extrusion and the formation of a shape-stable final construct<sup>20,64</sup>. Firstly, the material must be able to flow through the nozzle upon applying a shear force (shear-thinning behavior). Shear-thinning behavior is a common property of polymer solutions and is a result of the polymeric

chains alignment under shear (Figure 2). Therefore, shear-thinning hydrogels in this sense are among the best candidates. Secondly, after extrusion the bioink should be able to rapidly recover its structure and maintain its shape on the collection plate. In this regard, the yield stress of a material plays a crucial role. Yield stress is defined as the stress below which the material is fully shape-stable and above which it starts flowing<sup>72</sup>. Therefore, hydrogels with relatively high yield stress are first-choice materials in this sense<sup>73</sup>. Based on the general considerations elucidated so far, high viscosity materials have good potential in bioprinting. Additionally, high viscosity after cell incorporation may avoid cell sedimentation in the cartridge during printing. Nevertheless, cell mixing into highly viscous materials can be a challenge. In this regard, thermosensitive hydrogels may offer an attractive alternative, where cells can be included at a temperature at which the polymeric mixture is liquid, while physical gelation in the cartridge at a different temperature would avoid cell sedimentation.

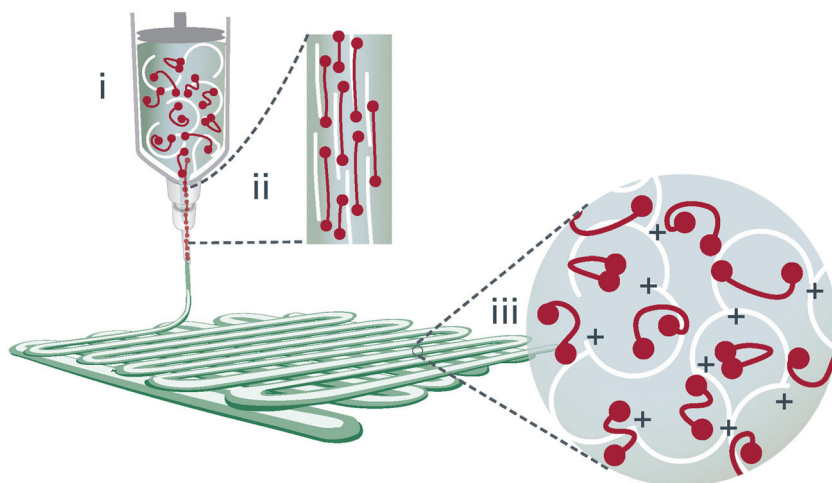


**Figure 2.** Schematic representation of a shear-thinning hydrogel composed of gellan gum and gelatine-methacrylamide<sup>74</sup>. The mixture in the syringe is a physical gel. While applying pressure during the extrusion, the generated shear forces cause the alignment of the polymeric chains and flow of the mixture through the nozzle. Upon stress removal, gelation promptly occurs on the deposition plate and ensures filament shape stability.

## 1.6 Aim and outline of the thesis

The work described in this thesis is part of a research program, which was designed and conducted within the European consortium of HydroZONES (<http://www.hydrozones.eu>). The aim of HydroZONES is to develop hierarchically organized cartilage constructs able to support *in vivo* cartilage regeneration. In order to achieve this, a systematic material development and extensive *in vitro* and *in vivo* assessments are necessary. In this thesis, a major focus is given to the preparation and characterization of thermosensitive and UV-crosslinkable hydrogels based on synthetic triblock copolymers composed of partially methacrylated poly(*N*-(2-hydroxypropyl)methacrylamide mono/dilactate) and PEG (pHPMAlac-PEG) blended with chemically modified natural polysaccharides, *i.e.* methacrylated chondroitin sulfate (CSMA) and hyaluronic acid (HAMA, Figure 3).

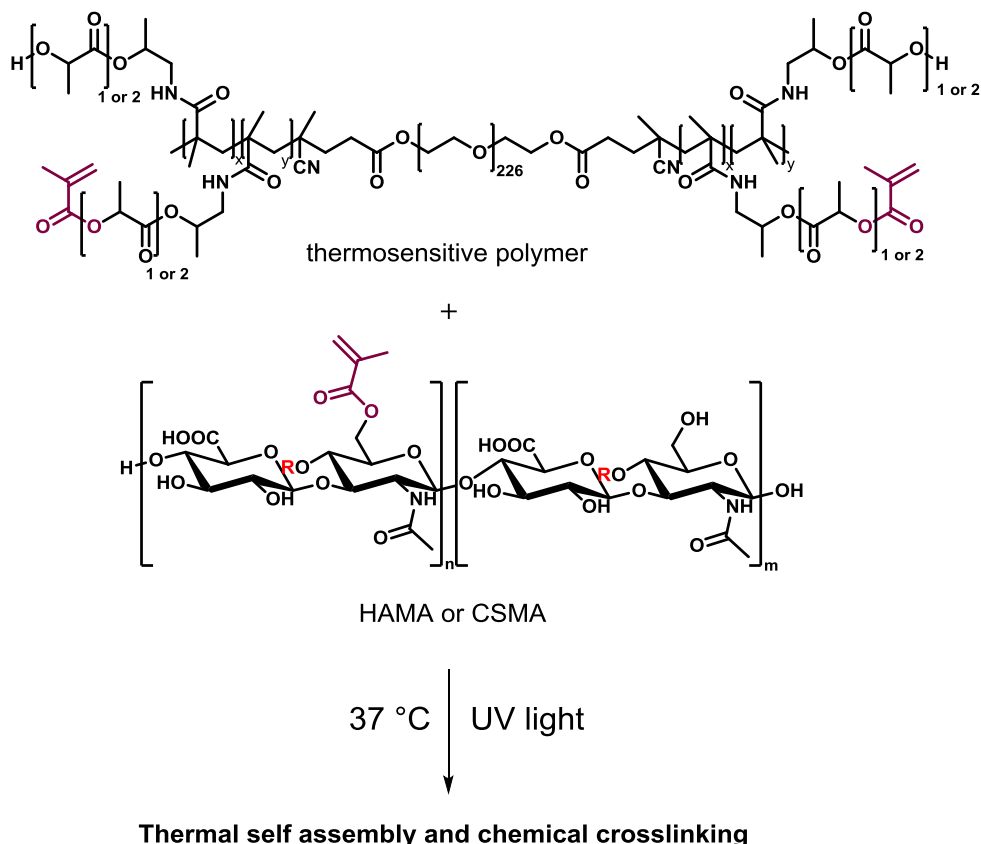


**Figure 3.** Chemical structure of a thermosensitive triblock copolymer based on a PEG mid-block flanked by two partially methacrylated poly(*N*-(2-hydroxypropyl)methacrylamide mono/dilactate) outer blocks (top), and partially methacrylated hyaluronic acid (HAMA, bottom, R = H in equatorial position) or chondroitin sulfate (CSMA, bottom, R = SO<sub>3</sub>H in axial position). Upon exposure to heat and UV light, physical and chemical crosslinking is obtained<sup>75</sup>.

Reproducibility of the building blocks' characteristics is a crucial aspect to obtain reproducible and predictable characteristics of the final hydrogel constructs; therefore, major attention in this thesis is given to synthetic procedures that lead to controlled and reproducible chemical characteristics of polymers. Moreover, mechanical characteristics of the hydrogels are extensively investigated and related to their application as 3D printable, cell-embedding materials. Hence, in **Chapter 2**, an efficient and reproducible method for the methacrylation of CS is reported, together with an extensive pHPMAlac-PEG/CSMA bioink mechanical characterization and cytocompatibility study. In **Chapter 3**, the *in vitro* chondrogenic potential of pHPMAlac-PEG-based hydrogels is investigated. Moreover, the effect of the addition of CSMA and HAMA on degradation, mechanical profile and 3D printability of these hydrogels is assessed.

The internal micro-structure of hydrogels can influence their mechanical properties and their interaction with cells. Hence, an extensive investigation of pHPMAlac-PEG/HAMA hydrogels micro-structure is described in **Chapter 4**. In this chapter, we analyze the relative distribution of the two polymers within the hydrogel network and we investigate the role of micro-phase separation on the rheological characteristics of these hydrogels. Moreover, we report a predictive mathematical model for the design of pHPMAlac-PEG/HAMA hydrogels with desired physical properties.

Inclusion of signaling biomolecules in hydrogel constructs can improve cell-material interactions and trigger desired biological pathways. Therefore, in **Chapter 5**, we explore the possibility to incorporate protein-loaded HAMA microgels in pHPMAlac-PEG hydrogels, for a strong immobilization and *in situ* sustained release of a model protein (lysozyme). For the fabrication of monodisperse HAMA microgels, a microfluidics-based equipment was designed and entirely developed in our laboratory.

The generation of TE constructs able to support chondrogenic cell differentiation as well as capable to withstand the mechanical forces acting in the joint is the “core” of this thesis. **Chapter 6** describes the 3D bioprinting of pHPMAlac-PEG/HAMA hydrogels in combination with thermoplastic reinforcement for the development of cartilage constructs with relevant stiffness and chondrogenic potential.

Finally, in **Chapter 7** extensive *in vivo* investigations in small (murine) and large animal (porcine) models are described as work-up for the final more challenging equine animal model. In **Chapter 8**, a summary of the thesis and perspectives are reported.

## Acknowledgments

A. Talib and D. Saris are thanked for their contribution to this chapter.

## References

- (1) Jung, C. K. Articular Cartilage: Histology and Physiology. In *Techniques in cartilage repair surgery*; Shetty, A. A., Kim, S.-J., Nakamura, N., Brittberg, M., Eds.; Springer Berlin Heidelberg: Berlin, Heidelberg, 2014; pp 17–21.
- (2) Mescher, A. L. Cartilage. In *Junqueira's Basic Histology*; Mescher, A. L., Ed.; New York, NY: McGraw-Hill, 2016.
- (3) Sophia Fox, A. J.; Bedi, A.; Rodeo, S. A. The Basic Science of Articular Cartilage: Structure, Composition, and Function. *Sport. Heal. A Multidiscip. Approach* **2009**, *1* (6), 461–468.
- (4) Malda, J.; Benders, K. E. M.; Klein, T. J.; de Grauw, J. C.; Kik, M. J. L.; Hutmacher, D. W.; Saris, D. B. F.; van Weeren, P. R.; Dhert, W. J. A. Comparative Study of Depth-Dependent Characteristics of Equine and Human Osteochondral Tissue from the Medial and Lateral Femoral Condyles. *Osteoarthr. Cartil.* **2012**, *20* (10), 1147–1151.
- (5) Shepherd, D. E. T.; Seedhom, B. B. Thickness of Human Articular Cartilage in Joints of the Lower Limb. *Ann. Rheum. Dis.* **1999**, *58* (1), 27–34.
- (6) Roughley, P. J.; Mort, J. S. The Role of Aggrecan in Normal and Osteoarthritic Cartilage. *J. Exp. Orthop.* **2014**, *1*, 8.
- (7) Zhang, X.; Blalock, D.; Wang, J. Classifications and Definitions of Normal Joints. In *Osteoarthritis - Progress in Basic Research and Treatment*; Chen, Q., Ed.; InTech, 2015.
- (8) Buckwalter, J. A.; Mankin, H. J. Articular Cartilage: Tissue Design and Chondrocyte-Matrix Interactions. *Instr. Course Lect.* **1998**, *47*, 477–486.
- (9) Goldring, M. B.; Otero, M.; Plumb, D. A.; Dragomir, C.; Favero, M.; El Hachem, K.; Hashimoto, K.; Roach, H. I.; Olivotto, E.; Borzi, R. M.; Marcu, K. B. Roles of Inflammatory and Anabolic Cytokines in Cartilage Metabolism: Signals and Multiple Effectors Converge upon MMP-13 Regulation in Osteoarthritis. *Eur. Cells Mater.* **2011**, *21*, 202–220.
- (10) Heinemeier, K. M.; Schjerling, P.; Heinemeier, J.; Moller, M. B.; Krogsgaard, M. R.; Grum-Schwensen, T.; Petersen, M. M.; Kjaer, M. Radiocarbon Dating Reveals Minimal Collagen Turnover in Both Healthy and Osteoarthritic Human Cartilage. *Sci. Transl. Med.* **2016**, *8* (346), 1–9.
- (11) Hunziker, E. B.; Lippuner, K.; Keel, M. J. B.; Shintani, N. An Educational Review of Cartilage Repair: Precepts & Practice – Myths & Misconceptions – Progress & Prospects. *Osteoarthr. Cartil.* **2015**, *23* (3), 334–350.
- (12) Mandelbaum, B. R.; Browne, J. E.; Fu, F.; Micheli, L.; Mosely, J. B.; Erggelet, C.; Minas, T.; Peterson, L. Articular Cartilage Lesions of the Knee. *Am. J. Sports Med.* **1998**, *26* (6), 853–861.
- (13) Falah, M.; Nierenberg, G.; Soudry, M.; Hayden, M.; Volpin, G. Treatment of Articular Cartilage Lesions of the Knee. *Int. Orthop.* **2010**, *34* (5), 621–630.
- (14) Huang, B. J.; Hu, J. C.; Athanasiou, K. A. Cell-Based Tissue Engineering Strategies Used in the Clinical Repair of Articular Cartilage. *Biomaterials* **2016**, *98*, 1–22.
- (15) Makris, E. A.; Gomoll, A. H.; Malizos, K. N.; Hu, J. C.; Athanasiou, K. A. Repair and Tissue Engineering Techniques for Articular Cartilage. *Nat. Rev. Rheumatol.* **2014**, *11* (1), 21–34.
- (16) Berthiaume, F.; Maguire, T. J.; Yarmush, M. L. Tissue Engineering and Regenerative

- Medicine: History, Progress, and Challenges. *Annu Rev Chem Biomol Eng* **2011**, *2*, 403–430.
- (17) Khademhosseini, A.; Langer, R.; Borenstein, J.; Vacanti, J. P. Microscale Technologies for Tissue Engineering and Biology. *Proc. Natl. Acad. Sci.* **2006**, *103* (8), 2480–2487.
- (18) Khademhosseini, A.; Langer, R. A Decade of Progress in Tissue Engineering. *Nat. Protoc.* **2016**, *11* (10), 1775–1781.
- (19) Chan, B. P.; Leong, K. W. Scaffolding in Tissue Engineering: General Approaches and Tissue-Specific Considerations. *Eur. Spine J.* **2008**, *17* (S4), 467–479.
- (20) Malda, J.; Visser, J.; Melchels, F. P.; Jüngst, T.; Hennink, W. E.; Dhert, W. J. A.; Groll, J.; Hutmacher, D. W. 25th Anniversary Article: Engineering Hydrogels for Biofabrication. *Adv. Mater.* **2013**, *25* (36), 5011–5028.
- (21) Hutmacher, D. W. Scaffold Design and Fabrication Technologies for Engineering Tissues — State of the Art and Future Perspectives. *J. Biomater. Sci. Polym. Ed.* **2001**, *12* (1), 107–124.
- (22) Vermonden, T.; Censi, R.; Hennink, W. E. Hydrogels for Protein Delivery. *Chem. Rev.* **2012**, *112* (5), 2853–2888.
- (23) Visser, J.; Levett, P. A.; te Moller, N. C. R.; Besems, J.; Boere, K. W. M.; van Rijen, M. H. P.; de Grauw, J. C.; Dhert, W. J. A.; van Weeren, P. R.; Malda, J. Crosslinkable Hydrogels Derived from Cartilage, Meniscus, and Tendon Tissue. *Tissue Eng. Part A* **2015**, *21* (7–8), 1195–1206.
- (24) Boere, K. W. M.; Blokzijl, M. M.; Visser, J.; Linssen, J. E. A.; Malda, J.; Hennink, W. E.; Vermonden, T. Biofabrication of Reinforced 3D-Scaffolds Using Two-Component Hydrogels. *J. Mater. Chem. B* **2015**, *3* (46), 9067–9078.
- (25) Visser, J.; Melchels, F. P. W.; Jeon, J. E.; van Bussel, E. M.; Kimpton, L. S.; Byrne, H. M.; Dhert, W. J. A.; Dalton, P. D.; Hutmacher, D. W.; Malda, J. Reinforcement of Hydrogels Using Three-Dimensionally Printed Microfibres. *Nat. Commun.* **2015**, *6*, 6933.
- (26) O'Brien, F. J. Biomaterials and Scaffolds for Tissue Engineering. *Mater. Today* **2011**, *14* (3), 88–95.
- (27) Bajaj, P.; Schweller, R. M.; Khademhosseini, A.; West, J. L.; Bashir, R. 3D Biofabrication Strategies for Tissue Engineering and Regenerative Medicine. *Annu. Rev. Biomed. Eng.* **2014**, *16* (1), 247–276.
- (28) Chen, A. C.; Bae, W. C.; Schinagl, R. M.; Sah, R. L. Depth- and Strain-Dependent Mechanical and Electromechanical Properties of Full-Thickness Bovine Articular Cartilage in Confined Compression. *J. Biomech.* **2001**, *34* (1), 1–12.
- (29) Athanasiou, K. A.; Agarwal, A.; Dzida, F. J. Comparative Study of the Intrinsic Mechanical Properties of the Human Acetabular and Femoral Head Cartilage. *J. Orthop. Res.* **1994**, *12* (3), 340–349.
- (30) Jurvelin, J. S.; Buschmann, M. D.; Hunziker, E. B. Optical and Mechanical Determination of Poisson's Ratio of Adult Bovine Humeral Articular Cartilage. *J. Biomech.* **1997**.
- (31) Schuurman, W.; Gawlitta, D.; Klein, T. J.; Hoop, W. T.; van Rijen, M. H. P.; Dhert, W. J. A.; van Weeren, P. R.; Malda, J. Zonal Chondrocyte Subpopulations Reacquire Zone-Specific Characteristics During In Vitro Redifferentiation. *Am. J. Sports Med.* **2009**, *37* (1\_suppl), 97S–104S.
- (32) Schuurman, W.; Klein, T. J.; Dhert, W. J. A.; van Weeren, P. R.; Hutmacher, D. W.; Malda, J. Cartilage Regeneration Using Zonal Chondrocyte Subpopulations: A



- Promising Approach or an Overcomplicated Strategy? *J. Tissue Eng. Regen. Med.* **2015**, *9* (6), 669–678.
- (33) Sharma, B.; Williams, C. G.; Kim, T. K.; Sun, D.; Malik, A.; Khan, M.; Leong, K.; Elisseeff, J. H. Designing Zonal Organization into Tissue-Engineered Cartilage. *Tissue Eng.* **2007**, *13* (2), 405–414.
- (34) Jin, R.; Dijkstra, P. J. Hydrogels for Tissue Engineering Applications. In *Biomedical Applications of Hydrogels Handbook*; Springer New York: New York, NY, 2010; Vol. c, pp 203–225.
- (35) Skardal, A.; Zhang, J.; McCoard, L.; Xu, X.; Oottamasathien, S.; Prestwich, G. D. Photocrosslinkable Hyaluronan-Gelatin Hydrogels for Two-Step Bioprinting. *Tissue Eng. Part A* **2010**, *16* (8), 2675–2685.
- (36) Hutson, C. B.; Nichol, J. W.; Aubin, H.; Bae, H.; Yamanlar, S.; Al-Haque, S.; Koshy, S. T.; Khademhosseini, A. Synthesis and Characterization of Tunable Poly(Ethylene Glycol): Gelatin Methacrylate Composite Hydrogels. *Tissue Eng. Part A* **2011**, *17* (13–14), 1713–1723.
- (37) Wu, X.; Black, L.; Santacana-Laffitte, G.; Patrick, C. W. Preparation and Assessment of Glutaraldehyde-Crosslinked Collagen–chitosan Hydrogels for Adipose Tissue Engineering. *J. Biomed. Mater. Res. Part A* **2007**, *81A* (1), 59–65.
- (38) Bouhadir, K. H.; Hausman, D. S.; Mooney, D. J. Synthesis of Cross-Linked Poly(aldehyde Guluronate) Hydrogels. *Polymer* **1999**, *40* (12), 3575–3584.
- (39) Su, W.-Y.; Chen, Y.-C.; Lin, F.-H. Injectable Oxidized Hyaluronic Acid/adipic Acid Dihydrazide Hydrogel for Nucleus Pulposus Regeneration. *Acta Biomater.* **2010**, *6* (8), 3044–3055.
- (40) Censi, R.; Fieten, P. J.; di Martino, P.; Hennink, W. E.; Vermonden, T. In Situ Forming Hydrogels by Tandem Thermal Gelling and Michael Addition Reaction between Thermosensitive Triblock Copolymers and Thiolated Hyaluronan. *Macromolecules* **2010**, *43* (13), 5771–5778.
- (41) Lutolf, M. P.; Hubbell, J. A. Synthesis and Physicochemical Characterization of End-Linked Poly(ethylene Glycol)-Co-Peptide Hydrogels Formed by Michael-Type Addition. *Biomacromolecules* **2003**, *4* (3), 713–722.
- (42) Jin, R.; Moreira Teixeira, L. S.; Krouwels, A.; Dijkstra, P. J.; van Blitterswijk, C. A.; Karperien, M.; Feijen, J. Synthesis and Characterization of Hyaluronic Acid–poly(ethylene Glycol) Hydrogels via Michael Addition: An Injectable Biomaterial for Cartilage Repair. *Acta Biomater.* **2010**, *6* (6), 1968–1977.
- (43) Boere, K. W. M.; van den Dikkenberg, J.; Gao, Y.; Visser, J.; Hennink, W. E.; Vermonden, T. Thermogelling and Chemoselectively Cross-Linked Hydrogels with Controlled Mechanical Properties and Degradation Behavior. *Biomacromolecules* **2015**, *16* (9), 2840–2851.
- (44) Boere, K. W. M.; Soliman, B. G.; Rijkers, D. T. S.; Hennink, W. E.; Vermonden, T. Thermoresponsive Injectable Hydrogels Cross-Linked by Native Chemical Ligation. *Macromolecules* **2014**, *47* (7), 2430–2438.
- (45) Hu, B.-H.; Su, J.; Messersmith, P. B. Hydrogels Cross-Linked by Native Chemical Ligation. *Biomacromolecules* **2009**, *10* (8), 2194–2200.
- (46) Crescenzi, V.; Cornelio, L.; Di Meo, C.; Nardecchia, S.; Lamanna, R. Novel Hydrogels via Click Chemistry: Synthesis and Potential Biomedical Applications. *Biomacromolecules* **2007**, *8* (6), 1844–1850.
- (47) Ossipov, D. A.; Hilborn, J. Poly(vinyl Alcohol)-Based Hydrogels Formed by “Click

- Chemistry.” *Macromolecules* **2006**, *39* (5), 1709–1718.
- (48) Takahashi, A.; Suzuki, Y.; Suhara, T.; Omichi, K.; Shimizu, A.; Hasegawa, K.; Kokudo, N.; Ohta, S.; Ito, T. In Situ Cross-Linkable Hydrogel of Hyaluronan Produced via Copper-Free Click Chemistry. *Biomacromolecules* **2013**, *14* (10), 3581–3588.
- (49) Davis, N. E.; Ding, S.; Forster, R. E.; Pinkas, D. M.; Barron, A. E. Modular Enzymatically Crosslinked Protein Polymer Hydrogels for in Situ Gelation. *Biomaterials* **2010**, *31* (28), 7288–7297.
- (50) Lee, F.; Chung, J. E.; Kurisawa, M. An Injectable Enzymatically Crosslinked Hyaluronic Acid–tyramine Hydrogel System with Independent Tuning of Mechanical Strength and Gelation Rate. *Soft Matter* **2008**, *4* (4), 880.
- (51) Jin, R.; Hiemstra, C.; Zhong, Z.; Feijen, J. Enzyme-Mediated Fast in Situ Formation of Hydrogels from Dextran–tyramine Conjugates. *Biomaterials* **2007**, *28* (18), 2791–2800.
- (52) Ma, L.; Gao, C.; Mao, Z.; Zhou, J.; Shen, J.; Hu, X.; Han, C. Collagen/chitosan Porous Scaffolds with Improved Biostability for Skin Tissue Engineering. *Biomaterials* **2003**, *24* (26), 4833–4841.
- (53) Schuurman, W.; Levett, P. A.; Pot, M. W.; van Weeren, P. R.; Dhert, W. J. A.; Hutmacher, D. W.; Melchels, F. P. W.; Klein, T. J.; Malda, J. Gelatin-Methacrylamide Hydrogels as Potential Biomaterials for Fabrication of Tissue-Engineered Cartilage Constructs. *Macromol. Biosci.* **2013**, *13* (5), 551–561.
- (54) Bigi, A.; Cojazzi, G.; Panzavolta, S.; Rubini, K.; Roveri, N. Mechanical and Thermal Properties of Gelatin Films at Different Degrees of Glutaraldehyde Crosslinking. *Biomaterials* **2001**, *22* (8), 763–768.
- (55) Ahmed, T. A. E.; Dare, E. V.; Hincke, M. Fibrin: A Versatile Scaffold for Tissue Engineering Applications. *Tissue Eng. Part B Rev.* **2008**, *14* (2), 199–215.
- (56) Dikovsky, D.; Bianco-Peled, H.; Seliktar, D. The Effect of Structural Alterations of PEG-Fibrinogen Hydrogel Scaffolds on 3-D Cellular Morphology and Cellular Migration. *Biomaterials* **2006**, *27* (8), 1496–1506.
- (57) Zhu, J. Bioactive Modification of Poly(ethylene Glycol) Hydrogels for Tissue Engineering. *Biomaterials* **2010**, *31* (17), 4639–4656.
- (58) Buwalda, S. J.; Boere, K. W. M.; Dijkstra, P. J.; Feijen, J.; Vermonden, T.; Hennink, W. E. Hydrogels in a Historical Perspective: From Simple Networks to Smart Materials. *J. Control. Release* **2014**, *190*, 254–273.
- (59) Klouda, L.; Mikos, A. G. Thermoresponsive Hydrogels in Biomedical Applications. *Eur. J. Pharm. Biopharm.* **2008**, *68* (1), 34–45.
- (60) Leijten, J. C. H.; Georgi, N.; Wu, L.; van Blitterswijk, C. A.; Karperien, M. Cell Sources for Articular Cartilage Repair Strategies: Shifting from Monocultures to Cocultures. *Tissue Eng. Part B Rev.* **2013**, *19* (1), 31–40.
- (61) Vilela, C. A.; Correia, C.; Oliveira, J. M.; Sousa, R. A.; Espregueira-Mendes, J.; Reis, R. L. Cartilage Repair Using Hydrogels: A Critical Review of in Vivo Experimental Designs. *ACS Biomater. Sci. Eng.* **2015**, *1* (9), 726–739.
- (62) Eslaminejad, M. B. Mesenchymal Stem Cells as a Potent Cell Source for Articular Cartilage Regeneration. *World J. Stem Cells* **2014**, *6* (3), 344.
- (63) Sekiya, I.; Vuoristo, J. T.; Larson, B. L.; Prockop, D. J. In Vitro Cartilage Formation by Human Adult Stem Cells from Bone Marrow Stroma Defines the Sequence of Cellular and Molecular Events during Chondrogenesis. *Proc. Natl. Acad. Sci.* **2002**,



- 99 (7), 4397–4402.
- (64) Groll, J.; Boland, T.; Blunk, T.; Burdick, J. A.; Cho, D.-W.; Dalton, P. D.; Derby, B.; Forgacs, G.; Li, Q.; Mironov, V. A.; Moroni, L.; Nakamura, M.; Shu, W.; Takeuchi, S.; Vozzi, G.; Woodfield, T. B. F.; Xu, T.; Yoo, J. J.; Malda, J. Biofabrication: Reappraising the Definition in an Evolving Field. *Biofabrication* **2016**, *13001*, 1–6.
- (65) Nichol, J. W.; Khademhosseini, A. Modular Tissue Engineering: Engineering Biological Tissues from the Bottom up. *Soft Matter* **2009**, *5* (7), 1312.
- (66) Schon, B. S.; Hooper, G. J.; Woodfield, T. B. F. Modular Tissue Assembly Strategies for Biofabrication of Engineered Cartilage. *Ann. Biomed. Eng.* **2016**, 1–15.
- (67) Pati, F.; Jang, J.; Ha, D.-H.; Won Kim, S.; Rhie, J.-W.; Shim, J.-H.; Kim, D.-H.; Cho, D.-W. Printing Three-Dimensional Tissue Analogues with Decellularized Extracellular Matrix Bioink. *Nat. Commun.* **2014**, *5*, 3935.
- (68) Markstedt, K.; Mantas, A.; Tournier, I.; Martínez Ávila, H.; Hägg, D.; Gatenholm, P. 3D Bioprinting Human Chondrocytes with Nanocellulose–Alginate Bioink for Cartilage Tissue Engineering Applications. *Biomacromolecules* **2015**, *16* (5), 1489–1496.
- (69) Jungst, T.; Smolan, W.; Schacht, K.; Scheibel, T.; Groll, J. Strategies and Molecular Design Criteria for 3D Printable Hydrogels. **2016**.
- (70) Melchels, F. P. W.; Feijen, J.; Grijpma, D. W. A Review on Stereolithography and Its Applications in Biomedical Engineering. *Biomaterials* **2010**, *31* (24), 6121–6130.
- (71) Boere, K. W. M.; Visser, J.; Seyednejad, H.; Rahimian, S.; Gawlitta, D.; van Steenbergen, M. J.; Dhert, W. J. A.; Hennink, W. E.; Vermonden, T.; Malda, J. Covalent Attachment of a Three-Dimensionally Printed Thermoplast to a Gelatin Hydrogel for Mechanically Enhanced Cartilage Constructs. *Acta Biomater.* **2014**, *10* (6), 2602–2611.
- (72) Mouser, V. H. M.; Melchels, F. P. W.; Visser, J.; Dhert, W. J. A.; Gawlitta, D.; Malda, J. Yield Stress Determines Bioprintability of Hydrogels Based on Gelatin-Methacryloyl and Gellan Gum for Cartilage Bioprinting. *Biofabrication* **2016**, *8* (3), 35003.
- (73) Mouser, V. H. M.; Melchels, F. P. W.; Visser, J.; Dhert, W. J. A.; Gawlitta, D.; Malda, J. Yield Stress Determines Bioprintability of Hydrogels Based on Gelatin-Methacryloyl and Gellan Gum for Cartilage Bioprinting. *Biofabrication* **2016**, *8* (3), 35003.
- (74) Melchels, F. P. W.; Dhert, W. J. A.; Huttmacher, D. W.; Malda, J. Development and Characterisation of a New Bioink for Additive Tissue Manufacturing. *J. Mater. Chem. B* **2014**, *2* (16), 2282.
- (75) Abbadessa, A.; Mouser, V. H. M.; Blokzijl, M. M.; Gawlitta, D.; Dhert, W. J. A.; Hennink, W. E.; Malda, J.; Vermonden, T. A Synthetic Thermosensitive Hydrogel for Cartilage Bioprinting and Its Biofunctionalization with Polysaccharides. *Biomacromolecules* **2016**, *17* (6), 2137–2147.





## Chapter 2

### **A thermo-responsive and photo-polymerizable chondroitin sulfate-based hydrogel for 3D printing applications**

**A. Abbadessa, M.M. Blokzijl, V.H.M. Mouser, P. Marica, J. Malda,  
W.E. Hennink, T. Vermonden**

*Carbohydrate Polymers*, 2016, 149, 163–174

## Abstract

The aim of this study was to design a hydrogel system based on methacrylated chondroitin sulfate (CSMA) and a thermo-sensitive poly(*N*-(2-hydroxypropyl) methacrylamide-mono/dilactate)-polyethylene glycol triblock copolymer ( $M_{15}P_{10}$ ) as a suitable material for additive manufacturing of scaffolds. CSMA was synthesized by reaction of chondroitin sulfate with glycidyl methacrylate (GMA) in dimethylsulfoxide at 50 °C and its degree of methacrylation was tunable up to 48.5%, by changing reaction time and GMA feed. Unlike polymer solutions composed of CSMA alone (20% w/w), mixtures based on 2% w/w of CSMA and 18% of  $M_{15}P_{10}$  showed strain-softening, thermo-sensitive and shear-thinning properties more pronounced than those found for polymer solutions based on  $M_{15}P_{10}$  alone. Additionally, they displayed a yield stress of  $19.2 \pm 7.0$  Pa. The 3D printing of this hydrogel resulted in the generation of constructs with tailorable porosity and good handling properties. Finally, embedded chondrogenic cells remained viable and proliferating over a culture period of 6 days. The hydrogel described herein represents a promising biomaterial for cartilage 3D printing applications.

## 2.1 Introduction

Tissue-engineered constructs are currently under investigation for the regeneration of several types of tissue, including bony, cartilaginous and vascular tissues. A tissue engineering (TE) approach is of particular relevance for damaged tissues that have a poor capability to regenerate spontaneously, such as articular cartilage defects of critical sizes. Biomimetic hydrogels composed of naturally occurring polysaccharides, *e.g.* chondroitin sulfate (CS) and hyaluronic acid (HA) have already shown significant chondrogenic potential for encapsulated chondrocytes and mesenchymal stem cells<sup>1–8</sup>. Hence, they are promising biopolymers for the development of implantable scaffolds in TE. In native tissue, CS is predominantly present as part of aggrecan and this natural polymer is involved in several biological mechanisms for the physiological maintenance of cartilage and its role in the resistance to compressive loading. More specifically, due to its hydrophilic nature and abundant negative charges, CS is responsible for retaining a large amount of water in the extracellular matrix (ECM), which is partially released upon compression and re-absorbed when the load is removed<sup>9</sup>. This mechanism not only provides mechanical resistance, but also contributes to the nutrients/waste products exchange, and thereby also to functioning/performance of the embedded chondrocytes.

Hydrogel systems based on cross-linked CS offer a suitable *in vitro* platform in which encapsulated cells, particularly chondrocytes and mesenchymal stem cells, can survive, proliferate, as well as produce cartilage-like ECM<sup>10–13</sup>. Moreover, CS is able to confer desirable mechanical properties to implants<sup>14–16</sup>. As a result, CS is currently one of the main components of several recently developed hybrid scaffolds studied *in vitro* and *in vivo*<sup>17–20</sup>.

The clinical applicability of implantable scaffolds requires hydrogels with a tunable shape and size to match the space of the tissue defect. Moreover, the regenerative potential likely depends on the capacity of the scaffold to mimic the inner structural complexity of tissue. For cartilage regeneration, the possibility to create implants having a multi-layer organization, typical of native tissue is believed to be beneficial, but the feasibility of this approach still represents a challenge<sup>21</sup>. These aspects highlight the need for a sophisticated engineering-based approach that guarantees customized scaffolds with tunable degree of complexity. Bioprinting of hydrogels is an attractive technique to generate 3D scaffolds with reproducible and complex structures. It is based on computer aided deposition of hydrogel filaments in a layer-by-layer fashion<sup>22</sup>. By changing certain parameters in the 3D printing settings, it is possible to tune the porosity of printed scaffolds. Porosity is an important parameter that can affect cell survival and activity, because porosity provides higher contact area between the implant and the surrounding fluids and, is thus responsible for better oxygen and nutrient supply to encapsulated cells<sup>22</sup>. The implantation of porous scaffolds may also facilitate cell migration from neighboring tissues that, in turn could offer opportunities to enrich the implant with ECM producing cells<sup>23,24</sup>. Furthermore, 3D bioprinting offers the opportunity to generate customized hydrogel

scaffolds with desired pattern, shape and size.

A 3D printable material needs to have rheological properties allowing its extrusion through a small needle and fast stabilization after deposition to guarantee shape fidelity of the extruded line<sup>22,25</sup>. This implies that hydrogel materials with shear thinning properties complimented with substantial yield stress behavior are attractive candidates.

In this study, we aimed to design a hydrogel based on UV-cross-linkable CS, *i.e.* methacrylated CS (CSMA) as a candidate biomaterial for cartilage 3D printing. As mentioned before, hydrogels composed of CS and/or other similar polysaccharides display high chondrogenic potential. Nevertheless, they usually lack essential mechanical properties needed for 3D printing applications. Therefore, CSMA was blended with a synthetic thermo-sensitive polymer which has an ABA architecture based on polyethylene glycol (PEG) and partially methacrylated poly(*N*-(2-hydroxypropyl) methacrylamide-mono/dilactate) (pHPMAlac), and has already been used for the development of 3D printable hydrogels<sup>26</sup>. Moreover, hydrogels based on methacrylated pHPMAlac-PEG triblock copolymers have been demonstrated to be cytocompatible. In detail, Censi et al. have found an excellent cell survival of embedded equine articular chondrocytes, *i.e.*  $94 \pm 3\%$  and  $85 \pm 7\%$  after 1 and 3 days of culture, respectively<sup>26</sup>. For similar hydrogels, adequate cell viability was also found for goat-derived mesenchymal stem cells cultured over a long culture period of 3 weeks<sup>27</sup>. By combining CSMA with a pHPMAlac-PEG triblock copolymer, we aimed to improve the rheological profile, and thus the 3D printing potential of hydrogels based on CSMA, without compromising cytocompatibility. In this scenario, it is evident that the reproducibility of mechanical and 3D printing properties of the hydrogel depends on the reproducibility of the polymers' characteristics, and thus on the robustness of the synthetic procedure used to obtain the polymers<sup>28</sup>.

Hence, to obtain CS with a controllable and reproducible degree of methacrylation (DM), we firstly focused on the investigation of an efficient method for the synthesis of CSMA. The two most frequently used methods for methacrylating CS consist of reactions in aqueous solutions using methacrylic anhydride (MA) or glycidyl methacrylate (GMA). When MA is chosen, a large excess of this compound is necessary to compensate for its hydrolysis in water-based medium<sup>10,29–32</sup>. Moreover, the adjustment of the pH to basic conditions is crucial for the reaction to proceed. The drawback of adding a basic solution to maintain the pH, is that when not accurately dosed this can cause chain scission of the polysaccharide and hydrolysis of the aimed ester bonds after their formation, as was found by Wang and co-workers<sup>29</sup>. On the other hand, the protocol that employs GMA for the methacrylation of CS in aqueous solution is more efficient<sup>33</sup>. Nevertheless, it leads to the synthesis of a mixture of products originating from trans-esterification and ring-opening mechanisms, and requires a reaction time of 15 days. Our aim was to develop a GMA trans-esterification procedure, similar as used for the methacrylation of dextran in an aprotic and polar solvent, *i.e.* dimethyl sulfoxide (DMSO)<sup>34,35</sup>, to obtain CS modified with methacrylic functionalities in a fast, efficient, and reproducible manner.

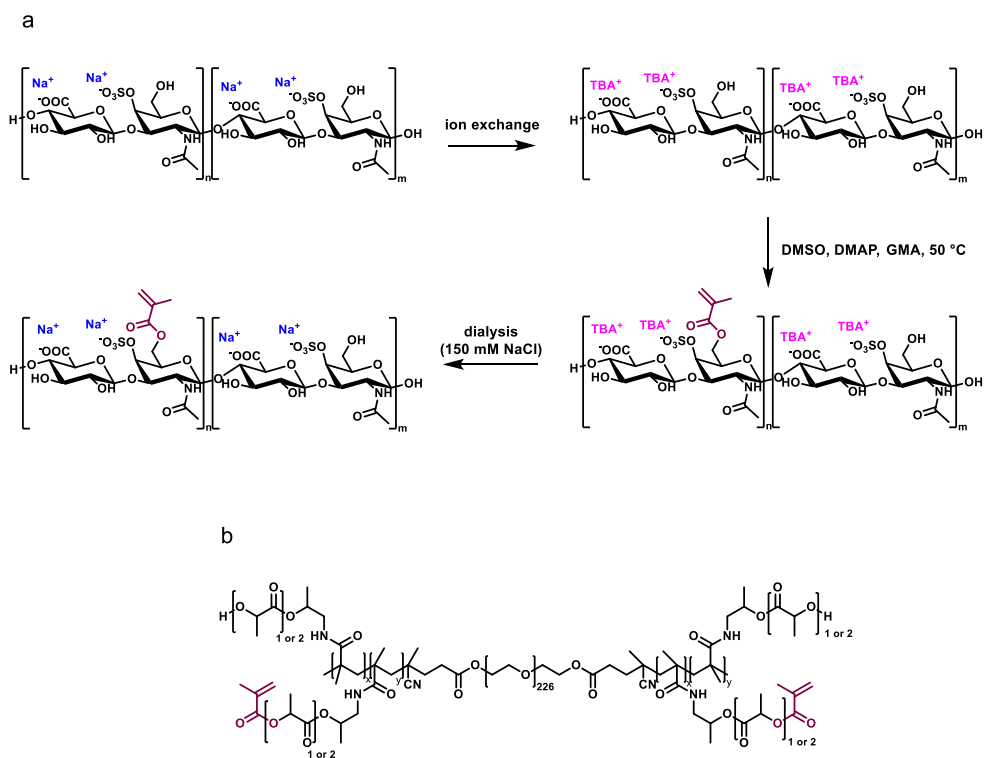
Subsequently, rheological properties of hydrogels composed of CSMA and partially

methacrylated pHPMAlac-PEG triblock copolymer were compared with those of hydrogels only composed of CSMA or partially methacrylated pHPMAlac-PEG triblock. 3D printability of the proposed hydrogel was investigated with the aim to generate 3D printed scaffolds with tunable porosity. Finally, viability and proliferation of chondrogenic cells embedded in the described hydrogel were evaluated.

## 2.2 Materials and Methods

### 2.2.1 Materials

All chemicals and solvents were obtained from Sigma-Aldrich (Zwijndrecht, the Netherlands) and Biosolve (Valkenswaard, the Netherlands), respectively, unless indicated otherwise. Chemicals and solvents were used as received. Chondroitin sulfate A sodium salt from bovine trachea ( $\geq 60\%$  type A (Scheme 1 a), balanced with type C), further referred to as CS, was purchased from Sigma-Aldrich.



**Scheme 1.** Reaction scheme for the synthesis of CSMA (a). In the first step  $\text{Na}^+$  counter ions are replaced by TBA ions. In the second step methacrylation of the hydroxyl groups of CS occurs. CSMA as sodium salt is obtained after dialysis.

Chemical structure of  $\text{M}_{15}\text{-P}_{10}$  (b).  $\text{M}_{15}\text{-P}_{10}$  consists of a  $\text{PEG}_{10000}$  mid-block flanked with two partially methacrylated (DM=15%) pHPMAlac outer blocks, obtained using a feed molar ratio between (hydroxypropyl) methacrylamide mono- and dilactate of 75:25.



CS was analyzed by Gel Permeation Chromatography (GPC), which showed the presence of three molecular weight distributions. Because of the high polydispersity of the sample, the peak molecular weights (Mp) are reported. The Mp values found for CS were 189 kDa, 13 kDa and 3 kDa, when using dextrans as standards (Figure S1 a). A thermo-sensitive triblock copolymer consisting of a PEG (10000 Da, abbreviated as PEG<sub>10000</sub>) mid-block flanked with two partially methacrylated pHPMALac outer blocks (Scheme 1 b) was synthesized and characterized as previously reported<sup>27</sup>. The thermo-sensitive polymer is further referred to as M<sub>15</sub>P<sub>10</sub> (M<sub>15</sub> refers to a degree of methacrylation, DM of 15% and P<sub>10</sub> refers to a PEG chain length of 10 kDa). Characteristics of M<sub>15</sub>P<sub>10</sub> are reported in Table 1. Irgacure 2959 was a kind gift from BASF (Ludwigshafen, Germany) and phosphate buffered saline (PBS) was obtained from Braun (Melsungen, Germany). Dulbecco's Modified Eagle Medium: Nutrient Mixture F-12 supplemented with GlutaMax-1 31331 (further referred to as DMEM/F-12), penicillin/streptomycin (pen/strep; 10.000 units/ml penicillin and 10 mg/ml streptomycin) and Click-iT<sup>®</sup> EdU Imaging Kit C10337 proliferation assay, were supplied by Invitrogen (Carlsbad, California, USA). Fetal bovine serum was purchased from Gibco (Invitrogen corporation), whereas recombinant human Fibroblast Growth Factor-basic (bFGF, 233FB) was supplied by R&D systems (Abingdon, UK).

**Table 1.** Characteristics of M<sub>15</sub>P<sub>10</sub>. Degree of methacrylation (DM), number average molecular weight (Mn), polydispersity index (PDI) and cloud point (CP).

Polymer	DM (%)	Mn (kDa)	PDI	CP (°C)
M <sub>15</sub> P <sub>10</sub>	15 <sup>a</sup>	40.6 <sup>b</sup> 34.3 <sup>c</sup>	2.0 <sup>c</sup>	9 <sup>d</sup>

<sup>a</sup> Defined as the percentage of hydroxyl groups being methacrylated and determined by <sup>1</sup>H-NMR, using DMSO-d<sub>6</sub> as solvent.

<sup>b</sup> Determined by <sup>1</sup>H-NMR, using DMSO-d<sub>6</sub> as solvent and calculated by comparing the signals of the (hydroxypropyl) methacrylamide lactate protons to those of PEG protons.

<sup>c</sup> Determined by GPC, using *N,N*-dimethylformamide enriched with LiCl (10 mM) as eluent and PEG with narrow MW distributions (Polymer Standards Service, Mainz, Germany) as standards.

<sup>d</sup> Determined by UV-VIS spectrophotometry and defined as the onset of increasing light scattering during a temperature ramp measurement (4-50 °C, 1 °C/min, 650 nm).

### 2.2.2 Methacrylation of CS

Methacrylation of CS was carried out using a reaction procedure, as reported by Oudshoorn *et al.*<sup>36</sup> for hyaluronic acid (HA), with some modifications (Scheme 1 a). Briefly, Dowex<sup>®</sup> 50WX8 hydrogen form resin (57.5 g) was initially flushed with 225 ml of a water solution containing tetrabutylammonium (TBA) fluoride (61.6 g) and then extensively washed with MilliQ water until the pH of the eluting solution became neutral. As last step, 1.8 L of an aqueous CS solution (10 mg/ml) was eluted



through the resin and collected. CS in form of TBA salt (CS-TBA) was recovered after freeze-drying. This product was further analyzed by  $^1\text{H}$ -Nuclear Magnetic Resonance ( $^1\text{H}$ -NMR, in  $\text{DMSO-d}_6$ , with chemical shifts referred to the solvent residual peak of 2.50 ppm) and the content of TBA per disaccharide unit of CS (ratio TBA:CS) was determined using the following equation:

$$\text{Ratio TBA:CS} = \frac{\text{average}(I_{1.57}, I_{1.32})}{8} : \frac{I_{1.77}}{3} \quad \text{Equation 1}$$

To study the kinetics of the methacrylation reaction, 1g of CS-TBA (1.141 mmol of disaccharide units) was dissolved in 37 ml of DMSO. Next, 4-(*N,N*-dimethylamino) pyridine (DMAP, 0.1835 g) and GMA (155.2  $\mu\text{l}$ , molar ratio between GMA and CS-TBA disaccharide units = 1:1) were added, and the reaction mixture was stirred under  $\text{N}_2$  atmosphere at 50  $^\circ\text{C}$  for 3 weeks. At several time-points (45 min, 1.5 h, 3 h, 6 h, 21 h, 29 h, 48 h, 54 h, 76 h, 1 week, 2 weeks, 3 weeks) samples of 3 ml were taken, diluted with 9 ml of water and pH-adjusted to 5.5 using a 0.2 M solution of HCl. The polymer solutions were then dialyzed against NaCl 150 mM solution in water for 3 days and against water for an additional 4 days. Purified CSMA samples for each time point were finally collected, as  $\text{Na}^+$  salt, after freeze-drying. This reaction was performed in triplicate.

To study the effect of the GMA feed on the DM of CSMA, several reactions were carried out: 0.545 g of CS-TBA (0.622 mmol of disaccharide units) was dissolved in 20 ml of dry DMSO under  $\text{N}_2$  atmosphere at 50  $^\circ\text{C}$ . After addition of DMAP (0.1 g) and GMA (9.0, 19.7, 39.4, 47.3, 59.1, 84.6, 118.3, 185.6 or 263.5  $\mu\text{l}$ ) the reaction mixtures were stirred at 50  $^\circ\text{C}$  for 48 h. Subsequently, the mixtures were diluted with 60 ml of water, pH-adjusted to 5.5, dialyzed and freeze-dried as described above.

### 2.2.3 Characterization of polysaccharides

CS, CS-TBA and CSMA were characterized by  $^1\text{H}$ -NMR using a Gemini-300 MHz spectrometer (Varian Associates Inc., NMR Instruments, Palo Alto, CA, USA).  $\text{D}_2\text{O}$  was used as solvent for CS and CSMA, and  $\text{DMSO-d}_6$  was used for CS-TBA. Chemical shifts were referred to the solvent residual peak of 4.79 or 2.50 ppm in case of  $\text{D}_2\text{O}$  or  $\text{DMSO-d}_6$ , respectively. The DM of CSMA, defined as the number of methacrylate groups per 100 disaccharide units, was calculated as follows:

$$\text{DM} (\%) = \frac{\text{average}(I_{6.20}, I_{5.77})}{(I_{2.18-1.86} - 3)/3} \times 100 \quad \text{Equation 2}$$

in which the signal at chemical shift 6.20 ppm was normalized for the integration of 1 proton and  $I_{2.18-1.86}$  is referred to the region in which the broad signal at chemical shift 2.04 ppm and the signal at chemical shift 1.96 ppm are fully included. CS and CSMA dissolved in  $\text{D}_2\text{O}$  were also characterized by  $^{13}\text{C}$ -NMR. Spectra were recorded during 21 hours of scanning using an Agilent 400/54 Premium Shielded NMR Magnet System (Agilent Technologies, Santa Clara, CA, USA). In addition,

$^{13}\text{C}$  Attached Proton Test (APT) and Distortionless Enhancement by Polarization Transfer (DEPT) spectra were acquired over a scanning period of 10 hours. CSMA was also characterized by GPC, using the same method described for CS.

### 2.2.4 Rheological measurements

A polymer solution containing 2% w/w of CSMA (DM = 15%) and 18% w/w of  $\text{M}_{15}\text{P}_{10}$  (DM = 15%) was prepared by dissolving the polymers in phosphate buffered saline pH 7.4 (PBS) under mild stirring overnight at 4 °C and it is further referred to as  $\text{CSMP}_{2+18}$ . Polymer solutions containing only CSMA (20% w/w) or  $\text{M}_{15}\text{P}_{10}$  (20% w/w) were prepared in the same manner, used as controls and are further referred to as  $\text{CS}_{20}$  and  $\text{MP}_{20}$ , respectively (Table 2).

**Table 2.** Polymer solution/hydrogel composition for  $\text{CSMP}_{2+18}$ ,  $\text{CS}_{20}$  and  $\text{MP}_{20}$ .

Polymer solution/hydrogel	CSMA (w/w)	$\text{M}_{15}\text{P}_{10}$ (w/w)
$\text{CSMP}_{2+18}$	2%	18%
$\text{CS}_{20}$	20%	-
$\text{MP}_{20}$	-	20%

$\text{CSMP}_{2+18}$ ,  $\text{CS}_{20}$  and  $\text{MP}_{20}$  were analyzed by a Discovery HR-2 rheometer (TA-Instruments, Etten-Leur, The Netherlands) using a cone-plate measuring geometry (cone diameter: 20 mm, cone angle: 1°, truncation: 27  $\mu\text{m}$ ). To identify the linear viscoelastic region (LVR), samples were subjected to strain sweep experiments at 37 °C employing a strain range from 0.01 to 100% and a frequency of 1 Hz. The solutions were further analyzed employing a quick temperature ramp (5 °C/min) from 4 to 40 °C in oscillation mode using a strain of 1% and a frequency of 1 Hz. Furthermore, frequency sweep experiments (0.01-100 rad/s) were performed at 37 °C and 1% strain. To investigate possible shear thinning properties, samples were subjected to an increasing shear rate (from 0.006 to 10000  $\text{s}^{-1}$ ) at 37 °C. Moreover, samples were sheared at 37 °C applying a stress ramp from 0 to 1000 Pa and the shear yield stress ( $\tau_y$ ) was calculated using TA Instruments Trios v3.3.0.4055 software according to the Herschel-Bulkley model<sup>37</sup>. Finally, recovery studies<sup>32,38</sup> were performed at 37 °C in three oscillation steps: first the samples were subjected to a strain of 0.1% for  $\text{CSMP}_{2+18}$  and  $\text{MP}_{20}$ , and 1% for  $\text{CS}_{20}$  (within the LVR), subsequently a strain of 100% (out of the LVR) was applied and finally a step of 0.1% strain for  $\text{CSMP}_{2+18}$  and  $\text{MP}_{20}$ , and 1% strain for  $\text{CS}_{20}$  was implemented. The duration of each step was 1 minute and the frequency was 1 Hz. A strain of 1% instead of 0.1% was chosen for  $\text{CS}_{20}$  because it resulted in a rheogram with higher resolution.

### 2.2.5 Swelling behavior of UV cross-linked hydrogels

CSMP<sub>2+18</sub>, CS<sub>20</sub> and MP<sub>20</sub> polymer solutions prepared as described in section 2.2.4 and supplemented with Irgacure 2959 (0.05% w/w) were injected into a teflon mold containing cylindrical wells (diameter: 6 mm, height: 2 mm). Next, the injected polymer solutions were incubated for 5 min at 37 °C to allow physical gelation of CSMP<sub>2+18</sub> and MP<sub>20</sub>, and further UV-irradiated for 69 sec at 5 cm distance using a Bluepoint 4 UV lamp (point light source, wavelength range: 300-600 nm, intensity at 5 cm: 103 mW/cm<sup>2</sup>, Hönle UV Technology AG, Gräfelfing, Germany). After 3 hours of swelling in PBS (pH 7.4), the swelling ratio (SR) of these chemically cross-linked hydrogel discs was calculated as follows:

$$SR = \frac{V_{3h}}{V_{0h}} \quad \text{Equation 3}$$

where  $V_{3h}$  and  $V_{0h}$  are the measured volumes after 3 hours and before swelling, respectively.

To investigate the effect of the DM of CSMA on the final swelling and mechanical properties of hydrogels, discs only composed of CSMA (20% w/w) having different DM, *i.e.* 7, 20, 27, 35 and 43% were fabricated as described above and the SR was calculated according to equation 3. These hydrogel discs were analyzed for their mechanical properties using a Dynamic Mechanical Analyzer (DMA Q800, TA-Instruments, Etten-Leur, The Netherlands) operating in unconfined compression. Samples were preloaded with a force of 0.001 N, and subsequently compressed using a force ramp rate of 0.1 N/min and an upper force limit of 1 N. The Young's modulus was calculated as the slope of the initial part of the stress/strain curves.

### 2.2.6 3D printing

3D printing of hydrogels was investigated using a 3D Discovery bioprinter platform (RegenHU, Villaz-St-Pierre, Switzerland) equipped with a Bluepoint 4 UV lamp (specifications were given in section 2.2.5). The polymer solution was loaded into a dispensing microvalve CF300H print head (needle diameter: 0.3 mm) pre-heated at 37 °C. The first layer of each construct was generated by dispensing the hydrogel onto glass slides fixed on a baseplate equilibrated at 40 °C. Subsequent layers were obtained by the deposition of alternating horizontal and vertical hydrogel filaments in a bottom-up building fashion. A total of 20 layers for each construct were dispensed and UV-irradiated in a layer-by-layer manner for 3 seconds. After the deposition of the last layer an additional illumination period of 9 seconds was used to guarantee a sufficiently stable construct. To generate constructs with different porosity, three line spacing values were used, *i.e.* 1.25, 1.5 and 2 mm, and the construct dimensions (length and width) were consequently adjusted. Table S1 shows the print-settings used in this study to create 3D porous printed constructs. 3D printed constructs were visualized using an Olympus ZS61 (Tokyo, Japan) microscope fitted with an Olympus (Tokyo, Japan) camera.

### 2.2.7 Cell viability and proliferation

To evaluate cellular behavior in the different hydrogels, ATDC5 cells were mixed into the polymer solutions with a final concentration of  $7.5 \times 10^6$  cells/ml. CSMP<sub>2+18'</sub>, MP<sub>20</sub> and CS<sub>20</sub> cell-laden polymer solutions, containing Irgacure (0.05% w/w) were casted in cylindrical teflon molds as described before (section 2.2.5). Constructs were cultured in ATDC5 expansion medium consisting of DMEM/F-12 supplemented with fetal bovine serum (5%), pen/strep (1%) and bFGF (1 ng/ml) for 6 days with a medium change after 3 days of culture. To three samples of each hydrogel formulation, 5-ethynyl-2'-deoxyuridine (EdU) working solution was added at day 1 according to manufacturer's protocol with a final concentration of 5  $\mu$ M, to be incorporated in the DNA of proliferating cells.

Cell viability was evaluated at day 1, 4 and 6. For all time points, one sample of each formulation was cut in half and stained for 20 min with 4  $\mu$ M calcein MA (live, Life technologies L3224) and 2  $\mu$ M ethidium homodimer-1 (dead, Life technologies L3224) in PBS at 37 °C. Samples were washed 3 times for 5 min with PBS and the staining was visualized using an Olympus BX51 microscope. Images were taken at four different locations of each sample at the cross-sectional area for analysis.

To monitor cellular proliferation a Click-iT® EdU assay was performed on samples that were incubated with EdU working solution, according to manufacturer's protocol. In short, at day 6 samples were collected, fixed overnight in formalin (37%), dehydrated via graded ethanol series and xylene, and embedded in paraffin. Tissue sections with a thickness of 5  $\mu$ m were made and stained for 30 min with the Click-iT reaction cocktail (1x click-iT reaction buffer, CuSO<sub>4</sub>, Alexia Fluor azide, and reaction buffer additive, all provided with the kit) at room temperature to stain the nuclei of proliferated cells green. To stain all cell nuclei blue, samples were incubated for 20 min with 4',6-diamidino-2-phenylindole (DAPI, 0.1  $\mu$ g/ml) solution at room temperature. Next, samples were visualized with an Olympus BX51 microscope.

### 2.2.8 Statistics

Statistical analyses were performed using SPSS software (version 20, IBM Corporation, USA). Differences in viability between groups at each time point were determined with a One-Way ANOVA test with a significance level of 0.05 and a Tukey's Post-hoc analysis. Normality and homogeneity of the data were assumed.

## 2.3 Results and Discussion

### 2.3.1 Synthesis and characterization of CSMA

For the synthesis of CSMA, the Na<sup>+</sup> counter ions were exchanged by the more lipophilic TBA cations to render CS soluble in DMSO. The <sup>1</sup>H-NMR spectrum of CS-TBA (Figure 1, spectrum 2) shows the following signals:  $\delta$  5.01-4.26 and 4.12-3.37 ( $\beta$ -glucuronic acid and *N*-acetyl- $\beta$ -galactosamine-4-sulfate ring protons),  $\delta$  3.16 (8H for each TBA unit, N<sup>+</sup>(CH<sub>2</sub>(CH<sub>2</sub>)<sub>2</sub>CH<sub>3</sub>)<sub>4</sub>),  $\delta$  1.77 (3H for each disaccharide unit, CH<sub>3</sub>CONH),  $\delta$  1.57 (8H for each TBA unit, N<sup>+</sup>(CH<sub>2</sub>CH<sub>2</sub>CH<sub>2</sub>CH<sub>3</sub>)<sub>4</sub>),  $\delta$  1.32 (8H for each TBA unit, N<sup>+</sup>((CH<sub>2</sub>)<sub>2</sub>CH<sub>2</sub>CH<sub>3</sub>)<sub>4</sub>),  $\delta$  0.93 (12H for each TBA unit,

$N^+((CH_2)_3CH_3)_4$ ). The appearance of the signals corresponding to the protons present in the four aliphatic chains of TBA, confirmed that the ion exchange occurred, and showed that almost each disaccharide unit of CS contained two TBA moieties (ratio TBA:CS=1.73). Subsequently, a partial esterification of the hydroxyl groups on CS-TBA was performed in DMSO using GMA as methacrylating agent to obtain CSMA. For CSMA, the following signals were observed:  $\delta$  6.20 and 5.77 (2H for each methacrylate group,  $CH_2=C(CH_3)$ ),  $\delta$  4.71-3.10 ( $\beta$ -glucuronic acid and *N*-acetyl- $\beta$ -galactosamine-4-sulfate ring protons),  $\delta$  2.04 (3H for each disaccharide unit,  $CH_3CONH$ ),  $\delta$  1.96 (3H for each methacrylate group,  $CH_2=C(CH_3)$ ) (Figure 1, spectrum 3). The presence of the signals at chemical shifts 6.20, 5.77 and 1.96 ppm, attributed to the protons present in the methacrylate group, proved that methacrylation occurred. Moreover, the efficient removal of the organic cation after methacrylation and dialysis was confirmed by the disappearance of the above mentioned signals of the TBA protons at 3.16, 1.57, 1.32 and 0.93 ppm (Figure 1, spectrum 3).

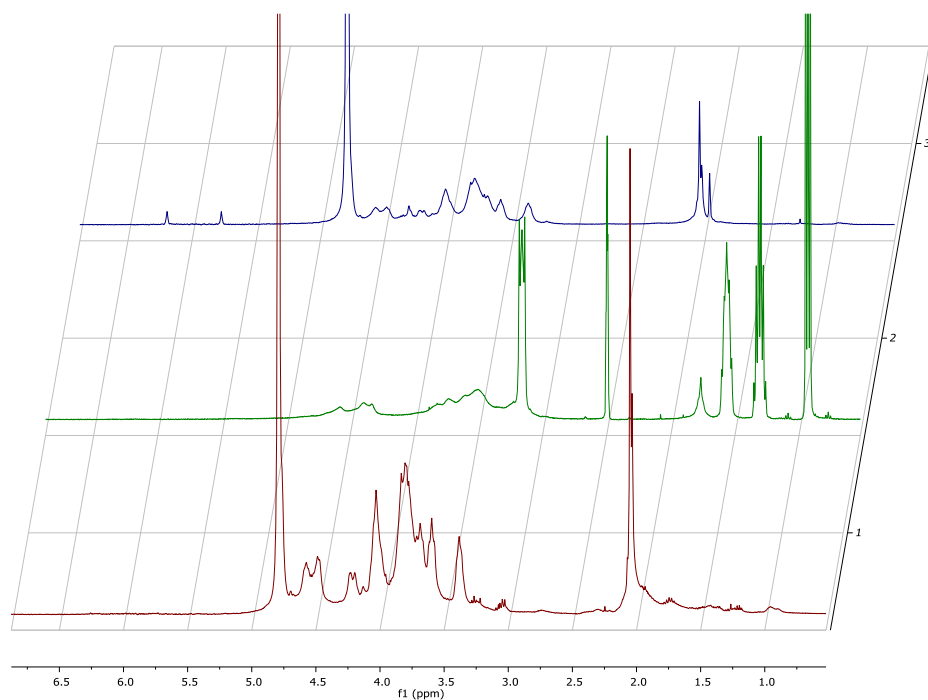


**Figure 1.**  $^1H$ -NMR spectra of CS ( $D_2O$ , bottom spectrum 1, red), CS-TBA ( $DMSO-d_6$ , middle spectrum 2, green) and CSMA ( $D_2O$ , top spectrum 3, blue).

The study on the reaction kinetics was performed using a fixed GMA:CS-TBA disaccharide unit feed ratio of 1:1 and was carried out for 3 weeks. The first time point at which methacrylation of CS was detectable in the  $^1H$ -NMR spectrum was after 1.5 h, where a DM of 4% was found. In Figure 2a,  $^1H$ -NMR spectra of CSMA

recovered after a reaction time of 21h, 48h, 1 week and 3 weeks are reported.

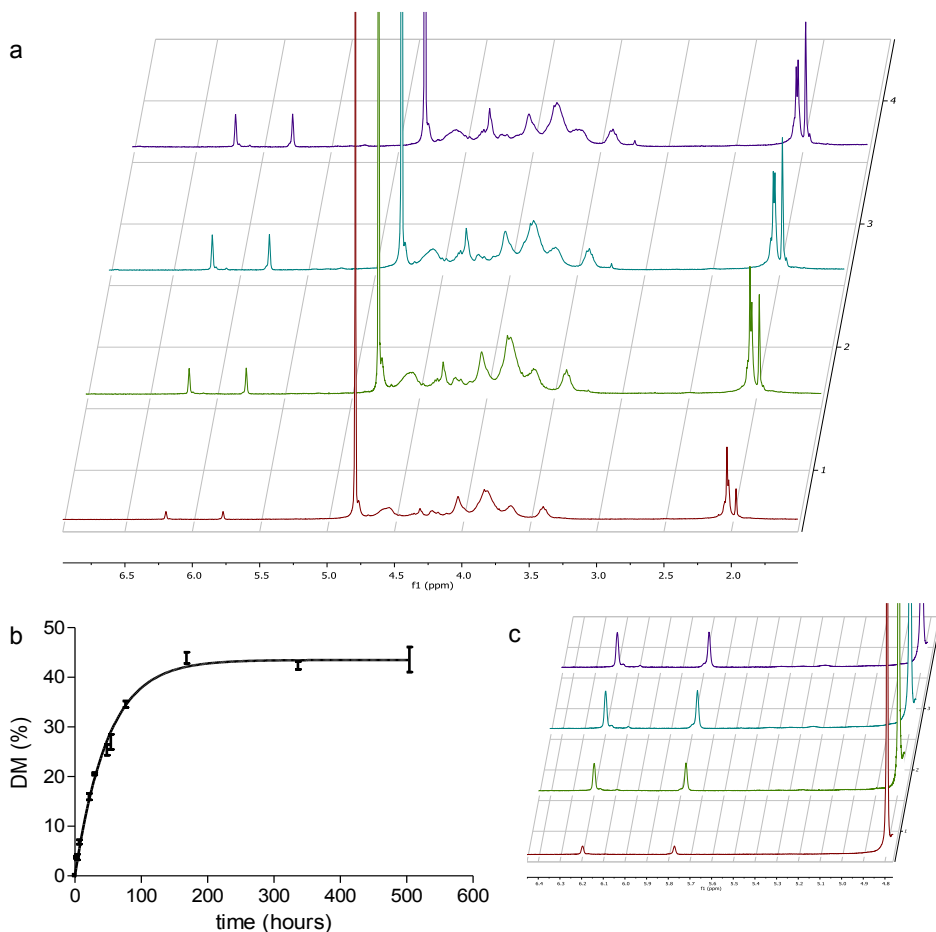


**Figure 2.** Kinetic study for the methacrylation of CS. <sup>1</sup>H-NMR spectra of CSMA (D<sub>2</sub>O) after 21 h (spectrum 1, red), 48 h (spectrum 2, green), 1 week (spectrum 3, blue), and 3 weeks (spectrum 4, purple) (a). DM (%) as a function of time (h) with  $n = 3$  (b). Zoom-in of the region between chemical shift 6.4 and 4.8 ppm of the <sup>1</sup>H-NMR spectra reported in Figure 2a (c).

In the first three spectra, an increase of the signals at 6.20 and 5.77 ppm, representative of the vinyl protons of the methacrylate groups was observed together with a related increase of the signal at 1.96 ppm, representative of the methyl group of the methacrylate functionality. In general, the DM increased by increasing the reaction time for the first 7 days, after which it leveled off at  $43 \pm 1\%$  (Figure 2b). This plateau is likely attributed to an equilibrium-state dictated by the increasing amount of glycidol formed, responsible for competing nucleophilic attack on GMA molecules and/or on CSMA<sup>34,39</sup>. From this study, it was calculated that the minimal unincorporated

GMA was approximately 57%. Based on this observation, the methacrylation of CS under these conditions seems to proceed less efficiently than the methacrylation of dextran, where more than 90% of the added GMA was incorporated under optimized conditions<sup>35</sup>. This might be attributed to the steric hindrance due to the presence of the TBA ions and/or sulfate groups in CS-TBA and/or to the more diluted conditions used for the methacrylation of CS. Nevertheless, to the best of our knowledge, the reaction efficiency found in our study is considerably higher than any other previously reported methods for the methacrylation of CS. More importantly, the methacrylation reaction described herein is highly reproducible, as shown by the low standard deviation found for the DM values reported in Figure 2b.

Another important aspect was to determine whether the described reaction proceeded via ring-opening or trans-esterification or via both mechanisms. When CS was firstly methacrylated in aqueous conditions using GMA by Li and collaborators, the presence of CS derivatives produced by ring-opening was proven by the appearance of signals at 5.5 and 5.2 ppm in the <sup>1</sup>H-NMR spectra, representative of the CH protons on the glyceryl spacer generated by reaction of the sulfate group or the carboxyl group of CS with the epoxide ring of GMA<sup>33</sup>. In contrast, as can be seen in the <sup>1</sup>H-NMR spectra of CSMA synthesized according to our method (Figure 2c), even after 3 weeks of reaction, there is no sign of the above mentioned signals. Hence, ring-opening does not occur under the reaction conditions we used and this observation is in line with the findings reported for the methacrylation of dextran and hyperbranched polyglycerol with GMA in DMSO<sup>34,39</sup>.

To investigate the position of the methacrylate groups in CSMA, <sup>13</sup>C-NMR spectra of CS and CSMA after 48 hours of reaction, in combination with APT and DEPT spectra were used (Figure S2 a-f). These analyses showed that the methacrylation of CS after 48 h of reaction occurs on both primary and secondary OH groups of CS. Nevertheless, considering the integrations of the <sup>13</sup>C-NMR signals, we could observe, as expected that a slightly preferential substitution of primary OH took place.

Several reactions employing different amounts of GMA were used to identify the dependence of the DM on the GMA feed. Figure 3 shows the obtained DM (%) as a function of the feed molar ratio between GMA and the disaccharide units of CS-TBA.

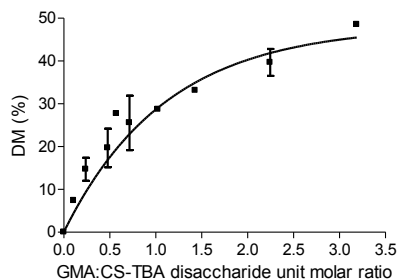


**Figure 3.** DM (%) as a function of GMA:CS-TBA disaccharide unit molar ratio.



As expected, DM increased with increasing GMA feed and a typical variation of  $\sim 6\%$  was found. Finally, GPC analysis on native CS and CSMA (Figure S1 b and c) confirmed that no chain scission occurred during the reaction.

The opportunity to accurately tailor the DM of poly-alcohols via transesterification from GMA is well known in literature and it was extensively applied to dextran<sup>34,35,40,41</sup> as well as to polyglycerol<sup>39</sup>, and to a lesser extent also to HA<sup>36</sup>. To the best of our knowledge, it has not been reported for CS, while this method combines a high efficiency due to water free reaction conditions with a reaction robustness that in turn leads to reproducible tuning of the DM. In summary, the synthesis procedure employed here makes use of an organic solvent, *i.e.* DMSO under water-free conditions, which allows for a highly controlled, reproducible and efficient methacrylation of CS.

### 2.3.2 Rheological properties of polymer solutions

Oscillatory temperature ramp experiments were performed within the linear viscoelastic region (LVR), which was identified by means of strain sweep experiments (Figure S3 a). For CSMP<sub>2+18</sub> it was found that  $G'$  increases by raising the temperature from 4 to 40 °C (Figure 4a). The storage modulus ( $G'$ ) at 40 °C was  $380.8 \pm 2.5$  Pa, whereas the temperature at which  $G'$  crosses the loss modulus ( $G''$ ) was 21.4 °C and this is here referred to as temperature of gelation ( $T_{gel}$ ).

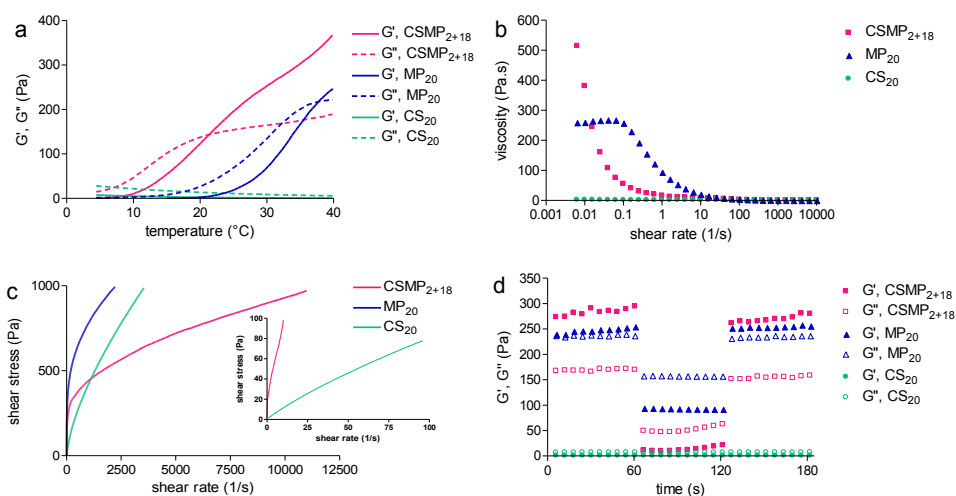


**Figure 4.** Rheological properties of CSMP<sub>2+18</sub>, MP<sub>20</sub> and CS<sub>20</sub>.  $G'$  and  $G''$  as function of temperature for CSMP<sub>2+18</sub>, MP<sub>20</sub> and CS<sub>20</sub>, recorded during a temperature ramp (4-40 °C, 5 °C/min) using a strain value of 1% and a frequency of 1 Hz (a). Viscosity as a function of shear rate for CSMP<sub>2+18</sub>, MP<sub>20</sub> and CS<sub>20</sub>, recorded during a shear rate sweep (0.006-10000 s<sup>-1</sup>) at 37 °C (b). Shear stress as a function of shear rate for CSMP<sub>2+18</sub>, MP<sub>20</sub> and CS<sub>20</sub>, recorded during a stress ramp (0-1000 Pa) at 37 °C. In the insert, zoomed-in view at low shear rate for CSMP<sub>2+18</sub> and CS<sub>20</sub> (c).  $G'$  and  $G''$  as function of three time-steps where strain was applied at 37 °C in a low-high-low (0.1 or 1%-100%-0.1 or 1%) fashion to CSMP<sub>2+18</sub>, MP<sub>20</sub> and CS<sub>20</sub>, using a frequency of 1 Hz (d).



In line with previously reported studies<sup>26,42</sup>, similar behavior was also found for MP<sub>20</sub>. However, a lower  $G'$  at 40 °C ( $248.1 \pm 0.9$  Pa) and a remarkably higher  $T_{\text{gel}}$  (37.8 °C) were found for MP<sub>20</sub> in comparison to CSMP<sub>2+18</sub>. These findings confirm the thermo-responsive character of MP<sub>20</sub> and CSMP<sub>2+18</sub>. In both cases the physical hydrogel formation is imputable to the self-assembly of M<sub>15</sub>P<sub>10</sub> in aqueous medium at elevated temperatures. In fact, pHPMAlac-PEG triblock copolymers and their methacrylated derivatives are known as amphiphilic polymers characterized by a temperature-dependent solubility in water<sup>27,43</sup>. In detail, at sufficiently high temperature, the thermodynamically preferred organization consists of self-assembled polymer chains due to dehydration of the outer blocks of the polymer. Hence, for a certain range of concentrations this phenomenon is responsible for physical gel formation. Importantly, CSMA at the tested concentration does not prevent the temperature-dependent self-assembly of M<sub>15</sub>P<sub>10</sub> and clearly participates in the formation of more stiff physical gels compared with the gels only composed of M<sub>15</sub>P<sub>10</sub>. In line with expectations, CS<sub>20</sub> did not show any thermo-responsivity, since almost constantly low values of  $G'$  and  $G''$  (also with  $G'' > G'$ ) were found indicating liquid-like behavior during the entire temperature ramp.

A general increase of  $G'$  and  $G''$  was visible when CSMP<sub>2+18</sub>, MP<sub>20</sub> and CS<sub>20</sub> samples were sheared at increasing frequency. Nevertheless, only for CSMP<sub>2+18</sub>,  $G'$  was continuously higher than  $G''$  at 37 °C and  $\tan \delta$  ( $G''/G'$ ) was constant ( $0.56 \pm 0.02$ ) over a wide frequency range, indicating critical gel behavior (Figure S3 b)<sup>43</sup>.

A shear rate test was performed on CSMP<sub>2+18</sub> to investigate the material's response under high shear rate and, hence the suitability of this material as a potential bioink. Ideally, a printable hydrogel should decrease its viscosity at the shear forces (approximate shear rate,  $\dot{\gamma} = 100\text{-}500$  s<sup>-1</sup>) acting on it in the syringe of a printer to be able to flow through the needle<sup>22</sup>. Figure 4b shows that the viscosity of CSMP<sub>2+18</sub> hydrogel decreased from 514 Pa.s ( $\dot{\gamma} = 0.006$  s<sup>-1</sup>) to 0.1 Pa.s ( $\dot{\gamma} = 10000$  s<sup>-1</sup>), which demonstrates that this hydrogel displays clear shear-thinning behavior. This feature can be ascribed to the temporarily destruction of the physical interactions and alignment of the polymer chains in the flow direction under high shear rate. On the other hand, MP<sub>20</sub> showed less pronounced shear thinning properties (decrease in viscosity from 259 to 0.2 Pa.s) and CS<sub>20</sub> was characterized by a low viscosity independent of the applied shear rate, suggesting liquid Newtonian behavior not suitable for 3D printing applications.

In Figure 4c shear stress/rate curves are reported. Fitting the curves of both control formulations MP<sub>20</sub> and CS<sub>20</sub> to the Herschel-Bulkley model, no yield stress ( $\tau_y$ ) was found. In contrast, for CSMP<sub>2+18</sub> a  $\tau_y$  of  $19.2 \pm 7.0$  Pa was found (Figure 4c, insert), with a typical  $R^2$  value of 0.99. Having a yield point is a crucial requirement for a printable hydrogel and defines the stress above which the hydrogel starts to flow and below which it maintains its shape<sup>22</sup>.

When recovery tests (Figure 4d) were implemented on CSMP<sub>2+18</sub>, a constant  $G'$  of  $283 \pm 7$  Pa was found at low strain (0.1%) deformation. In the subsequent step, during which a high strain (100%) was applied, an immediate drop of  $G'$  to 10.8 Pa was measured, while in the final step when low strain was applied, the initial  $G'$  value

was rapidly restored. This test indicates that the physical polymer network existing at low strain at 37 °C is efficiently and quickly broken at high strain as proven by  $G''$  values significantly higher than  $G'$  during the second step of the measurement. Moreover, the return of high  $G'$  values, rapidly after lowering the strain is a sign of quick recovery of the physical polymer network. This rapid recovery is a crucial requirement in 3D printing, since it guarantees the good shape fidelity of the hydrogel filament after extrusion.

To summarize, CSMP<sub>2+18</sub> is a thermo-sensitive hydrogel able to form a physically cross-linked polymer network by raising the temperature. It is a critical gel, capable to shear-thin under sufficiently high shear rate and able to quickly recover its initial structure after deformation, thanks to its yield stress behavior.

### 2.3.3 Swelling behavior of UV cross-linked hydrogels

Chemically cross-linked hydrogel discs were obtained using a casting procedure based on injection molding and UV light exposure as described in section 2.2.5. Figure 5a shows the SR of CSMP<sub>2+18</sub>, MP<sub>20</sub> and CS<sub>20</sub> hydrogels. The SR found for CS<sub>20</sub> (SR = 2.06 ± 0.02) was higher than the SR of CSMP<sub>2+18</sub> (SR = 1.34 ± 0.03) and MP<sub>20</sub> (1.37 ± 0.04). The difference in swelling between CSMP<sub>2+18</sub> and CS<sub>20</sub> is also visible from the photographs reported in Figure 5b and c. This phenomenon is likely attributed to the higher CSMA content in CS<sub>20</sub> hydrogels, which is a hydrophilic charged polymer responsible for a large water uptake<sup>44,45</sup>.

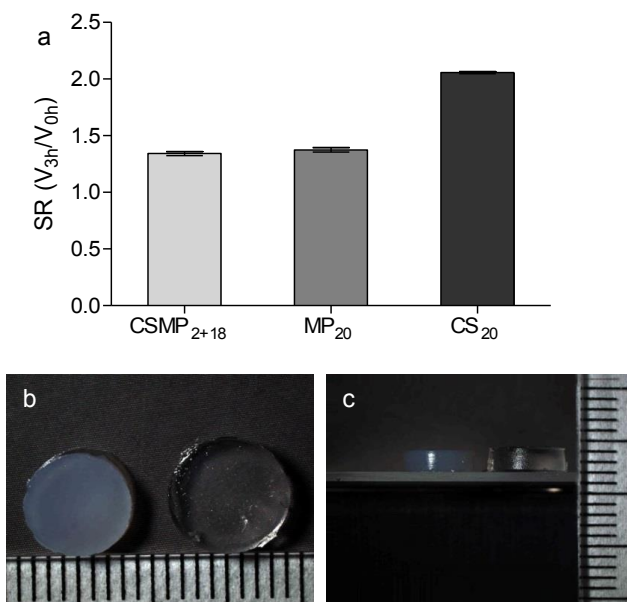


**Figure 5.** Swelling ratios (SR) for CSMP<sub>2+18</sub>, MP<sub>20</sub> and CS<sub>20</sub> hydrogels (a). Photographs of discs composed of CSMP<sub>2+18</sub> (left) and CS<sub>20</sub> (right) from a top view (b) and a side view (c).

Ideally, minimal swelling behavior is often desired for implantable hydrogels to guarantee their stability at the implantation site<sup>46</sup> and to maintain the initial shape of printed constructs. Therefore, the lower swelling of CSMP<sub>2+18</sub> hydrogels compared with CS<sub>20</sub> hydrogels is a relevant feature. Interestingly, the turbidity of CSMP<sub>2+18</sub> hydrogels suggests that these hydrogels are phase-separated systems. Blending the PEG-containing amphiphilic M<sub>15</sub>P<sub>10</sub> with the hydrophilic CSMA at the reported concentrations and temperature seems to lead to the formation of an aqueous polymer/polymer two phase system likely similar to that described for PEG and dextran<sup>47</sup>. Finally, swelling and mechanical studies carried out on hydrogels only composed of CSMA with different DM, showed that the SR of these hydrogels decreased from approximately 4 to 2 by increasing the DM from 7 to 43% (Figure S4). This trend can be explained by the fact that a higher DM of CSMA is responsible for lower polymer hydrophilicity, and more importantly for a higher cross-linking density of the polymer network, which leads to a decreased water uptake. In line with expectations, the Young's modulus increased from  $7.9 \pm 0.8$  kPa to  $59.8 \pm 3.0$  kPa by increasing the DM from 7 to 27%. The absence of a further increase of the Young's modulus for DM higher than 27% can likely be ascribed to a less efficient conversion of the methacrylate groups due to restricted mobility of highly methacrylated CS chains<sup>48</sup>.

### 2.3.4 3D printing of hydrogel

3D printing of CSMP<sub>2+18</sub> under optimized conditions (Table S1) resulted in the deposition of well-defined hydrogel filaments and led to the generation of 3D porous constructs. In Figure 6, photographs of constructs in swollen state, having line spacing of 1.25, 1.5 and 2 mm, respectively are shown.

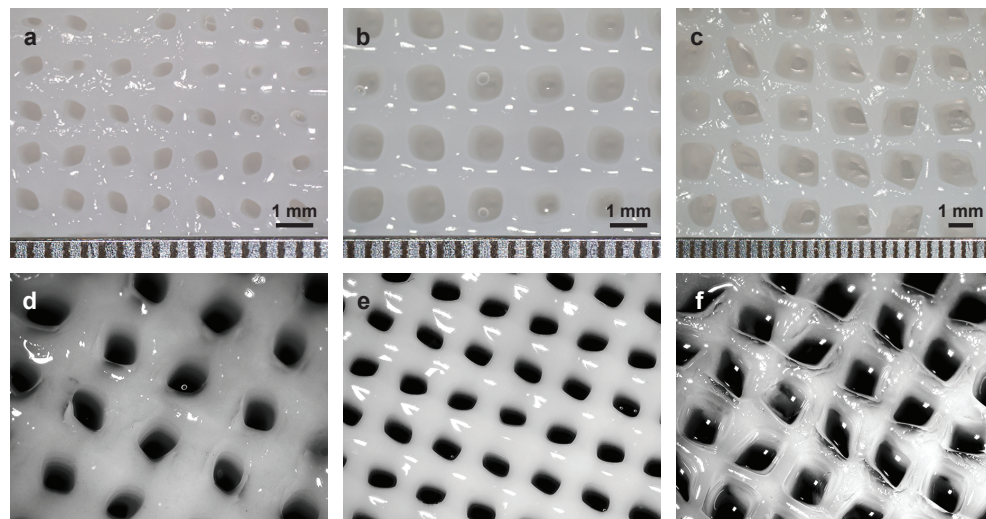


**Figure 6.** Photographs of 3D printed constructs. Top view of constructs printed using a strand spacing of 1.25 mm (a), 1.5 mm (b), and 2 mm (c). Skewed top view of 3D printed constructs having a strand spacing of 1.25 mm (d), 1.5 mm (e), and 2 mm (f).

From these top-viewed pictures, a defined vertical porosity can be appreciated. It needs to be noted that the flexibility of the constructs under handling increased by decreasing the mesh size. For the construct having the widest strand spacing, *i.e.* 2 mm, the flexibility of the cross-linked filaments under handling was higher compared with the other two construct designs. For this reason the pores in the 2 mm strand-spaced construct appear less homogeneously shaped. Nevertheless, all the generated constructs were successfully handled with a spatula without damage. A side view of one of the printed constructs is reported in Figure S5, where it can be observed that the aimed height of 2 mm was accurately achieved.

To summarize, the suitability of CSMP<sub>2+18</sub> as a 3D printable material is in line with the rheological properties described in the section 2.3.2 and a proper 3D printing principle can be described for this hydrogel. In detail, CSMP<sub>2+18</sub> is in a physically cross-linked state when loaded into the cartridge of the printer; subsequently, when a pressure is applied, shear forces cause the temporary disruption of the network and allow the flow of the gel through the needle of the printer. Next, the quick recovery of the physical structure after extrusion, driven by zero-shear rate and high temperature at the deposition site, is responsible for the good shape fidelity of each filament.

### 2.3.5 Cell viability and proliferation

ATDC5 cells were incorporated in the different hydrogel formulations. At day 1 of culture,  $94 \pm 5\%$  of the cells encapsulated in formulation CSMP<sub>2+18</sub> were viable, while significantly less living cells were observed in MP<sub>20</sub> gels ( $80 \pm 3\%$ , Figure 7).

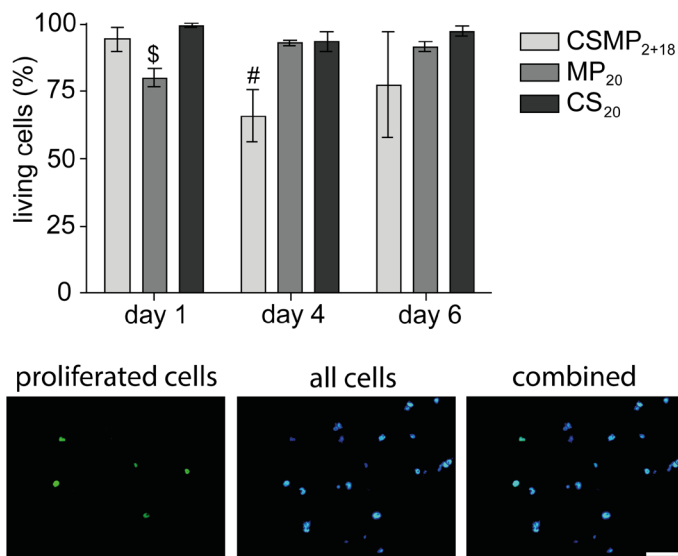


**Figure 7.** Viability of ATDC5 cells embedded in CSMP<sub>2+18</sub>, MP<sub>20</sub> and CS<sub>20</sub> hydrogels. Percentage of living cells after 1, 4 and 6 days of culture, where \$ and # indicate that the group is significantly lower than the other two groups at the same time point (\$  $p = 0.000$ ; #  $p = 0.000$ ) (top). Proliferated cells (left image, green staining), all cells (middle image, blue staining) and combined pictures (right image) after 6 days of culture for CSMP<sub>2+18</sub> hydrogels (bottom). Scale bar represents 50  $\mu\text{m}$ .

In CS<sub>20</sub> gels, 99 ± 1% of the embedded cells were viable at day 1. After 4 days of culture, cell viability decreased in the CSMP<sub>2+18</sub> group to 66 ± 10%, which was significantly lower compared to MP<sub>20</sub> and CS<sub>20</sub> gels (93 ± 1% and 94 ± 4%, respectively) at this time point. After 6 days of culture no significant differences were present between the groups and 78 ± 20%, 92 ± 2%, and 98 ± 2% of the cells were alive in CSMP<sub>2+18</sub>, MP<sub>20</sub> and CS<sub>20</sub>, respectively. Additionally, a typical round morphology of ATDC5 cells was observed for all hydrogels at each time point.

To investigate cellular proliferation, samples were cultured with EdU. Multiple EdU positive cells were detected in CSMP<sub>2+18</sub> hydrogels, indicating that even though some cells died during the first days of culture, the remaining cells were viable and capable of proliferating (Figure 7, EdU staining results of MP<sub>20</sub> and CS<sub>20</sub> hydrogels are shown in Figure S6). Taken together, CSMP<sub>2+18</sub> hydrogels are suitable materials for cell encapsulation showing adequate cell viability and proliferation of ATDC5 cells over a culture period of at least 6 days.

## 2.4 Conclusions

In this work, a novel method for the methacrylation of CS is described and it allows for a tailorable and controllable DM. The reaction proceeds via trans-esterification mechanism and results in the substitution of both primary and secondary hydroxyl groups of CS. Hydrogels based on CSMA and thermo-sensitive M<sub>15</sub>P<sub>10</sub> have been investigated for their rheological properties and revealed their superiority over hydrogels only composed of CSMA or M<sub>15</sub>P<sub>10</sub>. Unlike the control formulations, CSMP<sub>2+18</sub> showed strain-softening, thermo-sensitive and shear thinning behavior combined with yield stress properties. These characteristics render CSMP<sub>2+18</sub> hydrogel suitable for the 3D printing of TE implants. In fact, it was successfully used as a hydrogel-based ink to generate photo-polymerized 3D constructs with tunable porosity. The 3D printability and the opportunity to tailor the porosity of manufactured constructs confer a versatile character to this hydrogel system. Moreover, adequate survival and proliferation were found for chondrogenic cells embedded in this hydrogel. Taken together, the combination of CSMA and a synthetic pHPMAlac-PEG triblock copolymer allowed the design of hydrogels where a cell-friendly environment and desirable mechanical characteristics are warranted.

## Acknowledgements

The research leading to these results has received funding from the European Union's Seventh Framework Programme (FP7/2007-2013) under grant agreement number 309962 (project HydroZONES).

## Supporting Information

### SI 1 Gel Permeation Chromatography (GPC) of chondroitin sulfate and derivatives

CS, CS-TBA and CSMA were characterized by GPC using a Waters 2695 separating module coupled with a 2414 refractive index detector (Waters Corporation, Milford, MA, USA) and equipped with a PL aquagel-OH mixed 8 $\mu$ m column (Agilent Technologies, Santa Clara, CA, USA). Samples of 1 mg/ml in tris(hydroxymethyl) aminomethane (Tris) buffer 0.1 M (pH 7.5) were injected onto the column and the eluent flow was 1 ml/min. Solutions of dextrans with narrow molecular weight distributions (Sigma-Aldrich, Steinheim, Germany) in the same solvent (1 mg/ml) were used as calibration standards. Tris buffer 0.1 M was used as eluent and the temperature of the column and the detector were 30 °C and 40 °C, respectively.

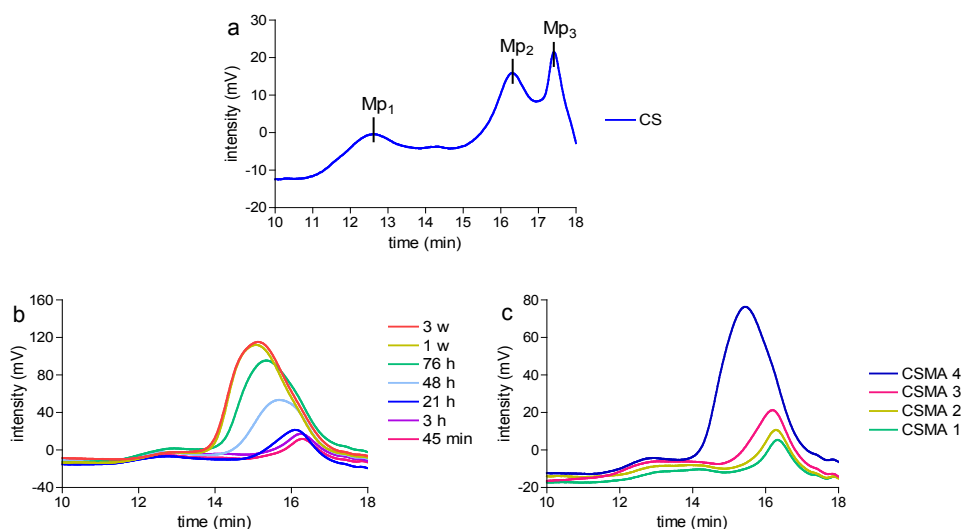


**Figure S1.** GPC characterization of native CS and CSMA. GPC chromatogram of CS (a), where three main molecular weight distributions can be observed. The peak molecular weight (Mp) is provided for each peak. Mp<sub>1</sub> = 189 kDa, Mp<sub>2</sub> = 13 kDa, Mp<sub>3</sub> = 3 kDa. GPC chromatogram for CSMA obtained using increasing reaction times, *i.e.* 45 min, 3 h, 21 h, 48 h, 76 h, 1 week and 3 weeks (b). GPC chromatograms for CSMA obtained employing increasing GMA:CS-TBA molar feed ratios, *i.e.* 0.11, 0.24, 0.71 and 2.24 for CSMA 1, CSMA 2, CSMA 3 and CSMA 4, respectively (c).

After the methacrylation step and purification, the polymer population characterized by the lowest molecular weight (peak corresponding to Mp<sub>3</sub> in Figure S1 a) is lost during the dialysis step (Figure S1 b and c). An unexpected increase of the peak intensity (although the same concentration was used for all the samples) and a decrease of retention time related to the increase of the DM of CSMA was observed. This is a sign of an increase of hydrodynamic volume detectable after methacrylation under



the tested condition. Importantly, premature cross-linking is unlikely considering the symmetrical shape of the peak and the absence of new peaks with shorter elution times. In addition, since no peaks with longer retention times were visible also chain scission can be excluded.

## SI 2 3D printing settings

**Table S1.** Settings used to print CSMP<sub>2+18</sub>.

Parameter	Value
<p><i>Construct</i></p> <ul style="list-style-type: none"> <li>• Dimensions (LxWxH) [mm]</li> <li>• Strand spacing [mm]</li> <li>• Layer height [mm]</li> </ul>	<p>15x15x2<sup>a</sup> or 16x16x2<sup>b</sup></p> <p>1.25, 1.5 and 2</p> <p>0.1</p>
<p><i>Microvalve CF300H</i></p> <ul style="list-style-type: none"> <li>• Inner diameter [mm]</li> <li>• Temperature [°C]</li> <li>• Needle inner diameter [mm]</li> <li>• Valve opening time [μs]</li> <li>• Dosing distance [mm]</li> </ul>	<p>0.3</p> <p>37</p> <p>0.3</p> <p>200</p> <p>0.2</p>
<p><i>Hönle Bluepoint 4</i></p> <ul style="list-style-type: none"> <li>• Distance to sample [mm]</li> <li>• Intensity at 50 mm [mW/cm<sup>2</sup>]</li> <li>• Illumination time (each deposited layer) [s]</li> <li>• Post-curing time [s]</li> <li>• <math>\lambda_{em}</math> [nm]</li> </ul>	<p>50</p> <p>103</p> <p>3</p> <p>9</p> <p>300 – 600</p>
<p><i>RegenHU 3DDiscovery</i></p> <ul style="list-style-type: none"> <li>• Baseplate temperature [°C]</li> <li>• Gel cartridge temperature [°C]</li> <li>• Speed XY [mm/s]</li> <li>• Pressure [bar]</li> </ul>	<p>40</p> <p>37</p> <p>40</p> <p>5.5</p>

<sup>a</sup> when a strand spacing of 1.25 or 1.5 mm is used

<sup>b</sup> when a strand spacing of 2 mm is used

## SI 3 Characterization of CSMA by <sup>13</sup>C-NMR

In the <sup>13</sup>C-NMR spectrum of CS the following signals were identified:  $\delta$  174.9 and 174.4 (C=O), region between 110 and 50 ppm (carbons of the sugar rings),  $\delta$  22.5 (CH<sub>3</sub>CON). After methacrylation, several new signals belonging to the carbons in

the methacrylate units were observed:  $\delta$  169.2 and 168.6 (C=O),  $\delta$  135.5 (C=CH<sub>2</sub>),  $\delta$  127.2 (C=CH<sub>2</sub>),  $\delta$  17.4 (CH<sub>3</sub>C=CH<sub>2</sub>) (Figure S2 a).

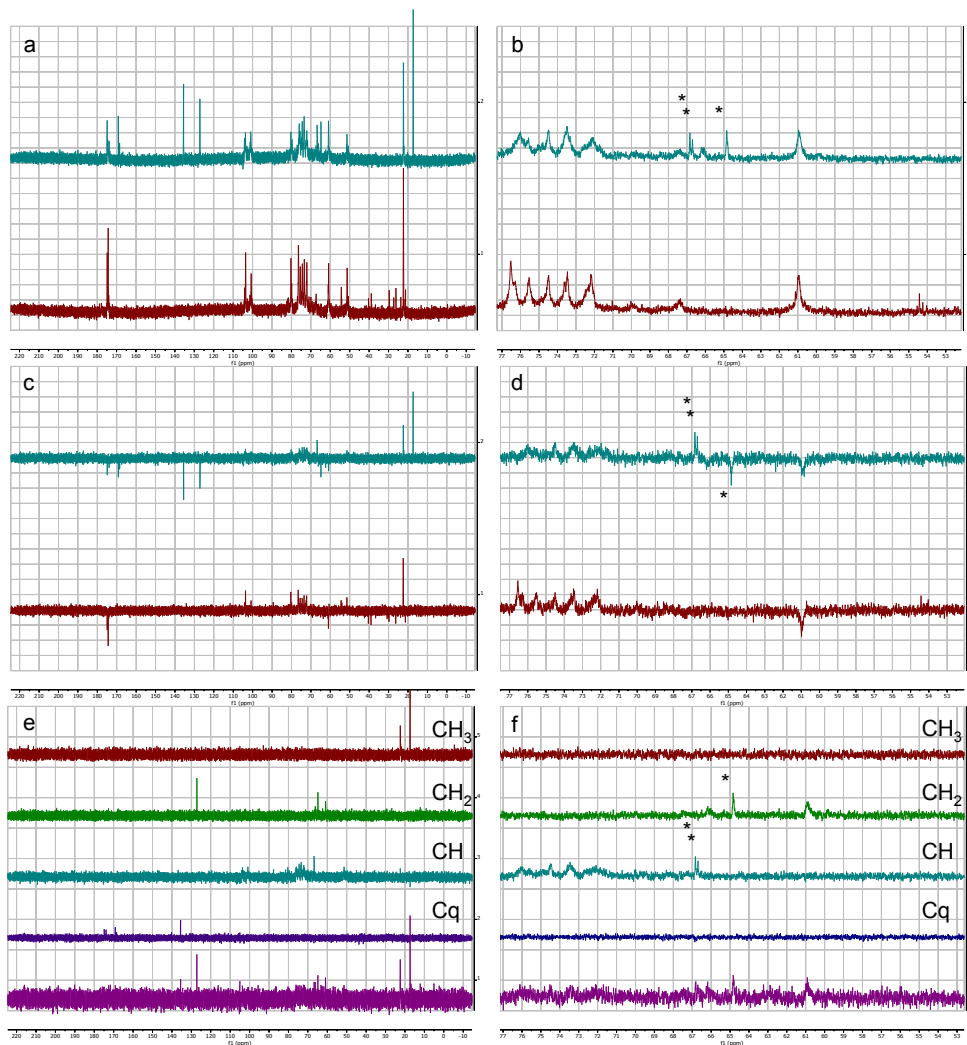


**Figure S2.** <sup>13</sup>C-NMR spectra for CS (red, bottom) and CSMA (blue, top) (a), zoom-in of the region between 77 and 53 ppm (b). <sup>13</sup>C-APT spectra for CS (red, bottom) and CSMA (blue, top) where signals representative of CH and CH<sub>3</sub> carbons point up and signals representative of CH<sub>2</sub> carbons and quaternary carbons (Cq) point down (c), zoom in of the region between 77 and 53 ppm (d). <sup>13</sup>C-DEPT spectra for CSMA (e), zoom in of the region between 77 and 53 ppm (f). The peaks labeled with an asterisk are the peaks at chemical shifts 66.8, 66.7 and 64.9 ppm.

Additionally three extra signals in the region of the sugar ring carbons appeared, *i.e.*  $\delta$  66.8, 66.7 and 64.9 ppm (Figure S2 b). APT and DEPT analysis (Figure S2 c-f) clarified that the signals at 66.8 and 66.7 ppm are representative of carbons attached to one proton (CH), whereas the signal at 64.9 ppm is representative of



carbons attached to two protons ( $\text{CH}_2$ ). Based on this finding, the two CH signals were assigned to the C-2 carbon and the C-3 carbon of the glucuronic acid unit attached to methacrylate groups (methacrylation of secondary OH groups). On the other hand, the  $\text{CH}_2$  signal was attributed to the C-6 carbon of the galactosamine unit attached to a methacrylate group (methacrylation of primary OH groups).

#### SI 4 Rheological behavior of hydrogels in strain sweep and frequency sweep

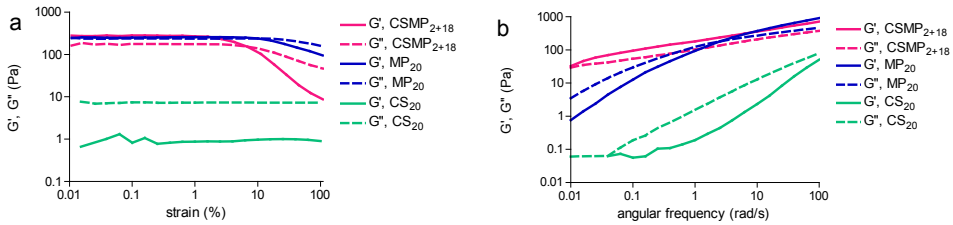


**Figure S3.** Strain sweep and frequency sweep experiments for CSMP<sub>2+18</sub>, MP<sub>20</sub> and CS<sub>20</sub>.  $G'$  and  $G''$  as function of strain, recorded during a strain sweep (0.01-100%) at 37 °C using a frequency of 1 Hz (a). CSMP<sub>2+18</sub> and MP<sub>20</sub> behave as strain-softening materials.  $G'$  and  $G''$  as function of angular frequency, recorded during a frequency sweep (0.01-100 rad/sec) at 37 °C using a strain of 1% (b).

#### SI 5 Swelling/mechanical properties of UV cross-linked CSMA hydrogels

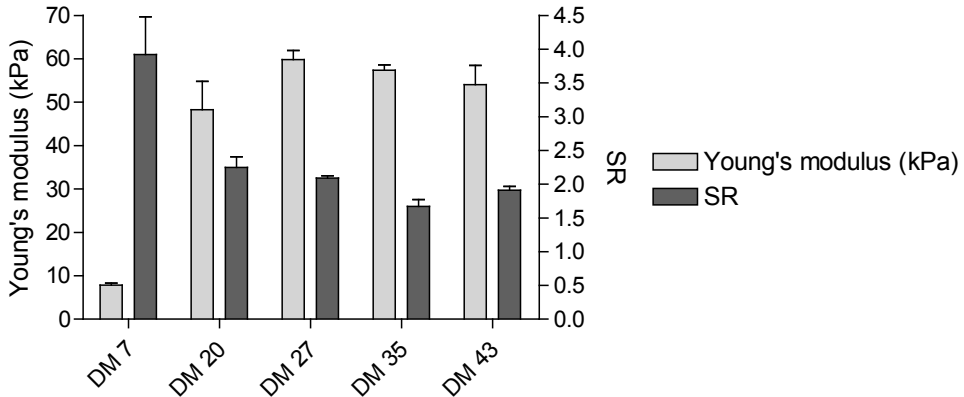


**Figure S4.** Young's modulus and swelling ratio (SR) of hydrogels composed of CSMA with different DM, *i.e.* 7, 20, 27, 35, 43. SR was calculated according to equation 3. Data are shown as mean  $\pm$  standard deviation (n = 3).

## SI 6 3D printed hydrogel constructs

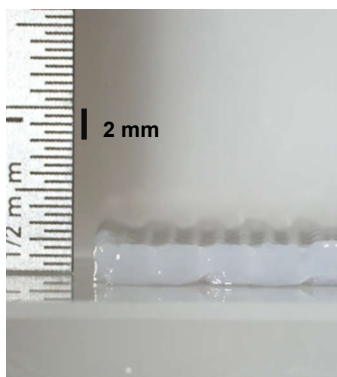


**Figure S5.** Photographs of a 3D printed construct. Side view of a printed construct with a strand spacing of 1.5 mm.

## SI 7 Cell proliferation in hydrogels

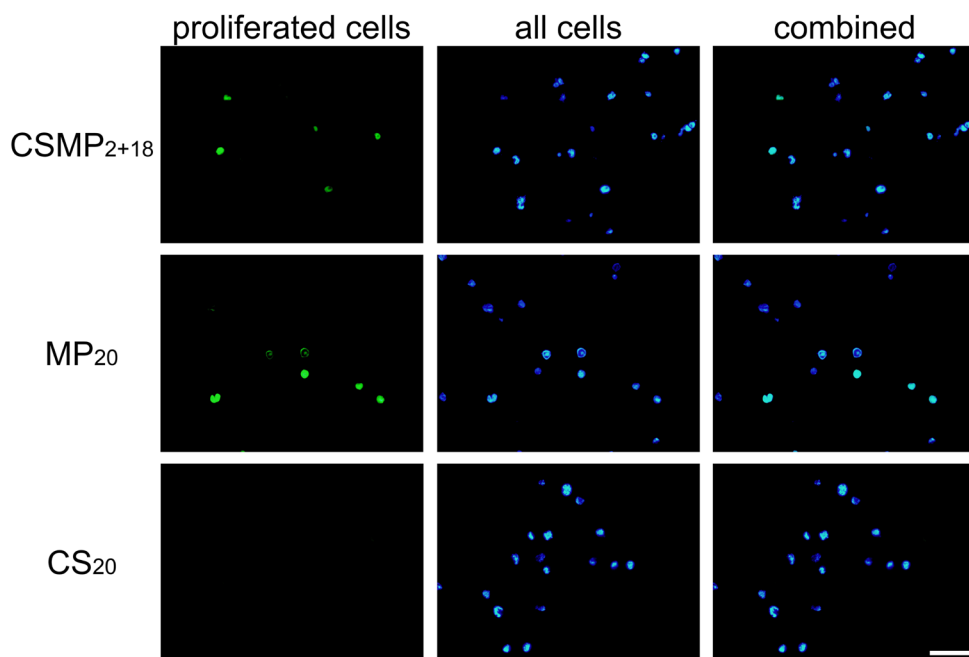


**Figure S6.** EdU/DAPI staining for ATDC5 cells embedded in hydrogels after 6 days of culture. Proliferated cells (first column, green staining), all cells (second column, blue staining) and combined pictures (third column) for CSMP<sub>2+18</sub>, MP<sub>20</sub> and CS<sub>20</sub> hydrogels. Scale bar indicates 50  $\mu\text{m}$ . Cell proliferation is observed in CSMP<sub>2+18</sub> and MP<sub>20</sub> hydrogels. The absence of cell proliferation in CS<sub>20</sub> gels might be due to higher local osmolarities within the hydrogel due to the highly charged CSMA<sup>49</sup>.

## References

- (1) Chung, C.; Beecham, M.; Mauck, R. L.; Burdick, J. A. The Influence of Degradation Characteristics of Hyaluronic Acid Hydrogels on in Vitro Neocartilage Formation by Mesenchymal Stem Cells. *Biomaterials* **2009**, *30* (26), 4287–4296.
- (2) Erickson, I. E.; Huang, A. H.; Sengupta, S.; Kestle, S.; Burdick, J. A.; Mauck, R. L. Macromer Density Influences Mesenchymal Stem Cell Chondrogenesis and Maturation in Photocrosslinked Hyaluronic Acid Hydrogels. *Osteoarthr. Cartil.* **2009**, *17* (12), 1639–1648.
- (3) Ko, C.-S.; Huang, J.-P.; Huang, C.-W.; Chu, I.-M. Type II Collagen-Chondroitin Sulfate-Hyaluronan Scaffold Cross-Linked by Genipin for Cartilage Tissue Engineering. *J. Biosci. Bioeng.* **2009**, *107* (2), 177–182.
- (4) Na, K.; Kim, S.; Woo, D.; Sun, B.; Yang, H.; Chung, H.; Park, K. Synergistic Effect of TGF $\beta$ -3 on Chondrogenic Differentiation of Rabbit Chondrocytes in Thermo-Reversible Hydrogel Constructs Blended with Hyaluronic Acid by in Vivo Test. *J. Biotechnol.* **2007**, *128* (2), 412–422.
- (5) Toh, W. S.; Lim, T. C.; Kurisawa, M.; Spector, M. Modulation of Mesenchymal Stem Cell Chondrogenesis in a Tunable Hyaluronic Acid Hydrogel Microenvironment. *Biomaterials* **2012**, *33* (15), 3835–3845.
- (6) Yoo, H. S.; Lee, E. A.; Yoon, J. J.; Park, T. G. Hyaluronic Acid Modified Biodegradable Scaffolds for Cartilage Tissue Engineering. *Biomaterials* **2005**, *26* (14), 1925–1933.
- (7) Hu, X.; Li, D.; Zhou, F.; Gao, C. Biological Hydrogel Synthesized from Hyaluronic Acid, Gelatin and Chondroitin Sulfate by Click Chemistry. *Acta Biomater.* **2011**, *7* (4), 1618–1626.
- (8) Levett, P. A.; Melchels, F. P. W.; Schrobback, K.; Hutmacher, D. W.; Malda, J.; Klein, T. J. A Biomimetic Extracellular Matrix for Cartilage Tissue Engineering Centered on Photocurable Gelatin, Hyaluronic Acid and Chondroitin Sulfate. *Acta Biomater.* **2014**, *10* (1), 214–223.
- (9) Roughley, P. J.; Mort, J. S. The Role of Aggrecan in Normal and Osteoarthritic Cartilage. *J. Exp. Orthop.* **2014**, *1*, 8.
- (10) Guo, Y.; Yuan, T.; Xiao, Z.; Tang, P.; Xiao, Y.; Fan, Y.; Zhang, X. Hydrogels of Collagen/chondroitin Sulfate/hyaluronan Interpenetrating Polymer Network for Cartilage Tissue Engineering. *J. Mater. Sci. Mater. Med.* **2012**, *23* (9), 2267–2279.
- (11) Ingavle, G. C.; Dormer, N. H.; Gehrke, S. H.; Detamore, M. S. Using Chondroitin Sulfate to Improve the Viability and Biosynthesis of Chondrocytes Encapsulated in Interpenetrating Network (IPN) Hydrogels of Agarose and Poly(ethylene Glycol) Diacrylate. *J. Mater. Sci. Mater. Med.* **2012**, *23* (1), 157–170.
- (12) Huang, Z.; Nooeaid, P.; Kohl, B.; Roether, J. A.; Schubert, D. W.; Meier, C.; Boccaccini, A. R.; Godkin, O.; Ertel, W.; Arens, S.; Schulze-Tanzil, G. Chondrogenesis of Human Bone Marrow Mesenchymal Stromal Cells in Highly Porous Alginate-Foams Supplemented with Chondroitin Sulfate. *Mater. Sci. Eng. C* **2015**, *50*, 160–172.
- (13) Sawatjui, N.; Damrongrungruang, T.; Leeansaksiri, W.; Jearanaikoon, P.; Hongeng, S.; Limpiboon, T. Silk Fibroin/gelatin–chondroitin Sulfate–hyaluronic Acid Effectively Enhances in Vitro Chondrogenesis of Bone Marrow Mesenchymal Stem Cells. *Mater. Sci. Eng. C* **2015**, *52*, 90–96.
- (14) Khanlari, A.; Suekama, T. C.; Detamore, M. S.; Gehrke, S. H. Structurally Diverse and Readily Tunable Photocrosslinked Chondroitin Sulfate Based Copolymers. *J.*

- Polym. Sci. Part B Polym. Phys.* **2015**, 53 (15), 1070–1079.
- (15) Zhang, L.; Li, K.; Xiao, W.; Zheng, L.; Xiao, Y.; Fan, H.; Zhang, X. Preparation of Collagen–chondroitin Sulfate–hyaluronic Acid Hybrid Hydrogel Scaffolds and Cell Compatibility in Vitro. *Carbohydr. Polym.* **2011**, 84 (1), 118–125.
- (16) Sawatjui, N.; Damrongrungruang, T.; Leeansaksiri, W.; Jearanaikoon, P.; Limpai boon, T. Fabrication and Characterization of Silk Fibroin–gelatin/chondroitin Sulfate/hyaluronic Acid Scaffold for Biomedical Applications. *Mater. Lett.* **2014**, 126, 207–210.
- (17) Liao, J.; Qu, Y.; Chu, B.; Zhang, X.; Qian, Z. Biodegradable CSMA/PECA/graphene Porous Hybrid Scaffold for Cartilage Tissue Engineering. *Sci. Rep.* **2015**, 5, 9879.
- (18) Wei, J.; Wang, J.; Su, S.; Wang, S.; Qiu, J. Tough and Fully Recoverable Hydrogels. *J. Mater. Chem. B* **2015**, 3 (26), 5284–5290.
- (19) Kuo, C.-Y.; Chen, C.-H.; Hsiao, C.-Y.; Chen, J.-P. Incorporation of Chitosan in Biomimetic Gelatin/chondroitin-6-Sulfate/hyaluronan Cryogel for Cartilage Tissue Engineering. *Carbohydr. Polym.* **2015**, 117, 722–730.
- (20) Ni, Y.; Tang, Z.; Cao, W.; Lin, H.; Fan, Y.; Guo, L.; Zhang, X. Tough and Elastic Hydrogel of Hyaluronic Acid and Chondroitin Sulfate as Potential Cell Scaffold Materials. *Int. J. Biol. Macromol.* **2015**, 74, 367–375.
- (21) Schuurman, W.; Klein, T. J.; Dhert, W. J. A.; van Weeren, P. R.; Hutmacher, D. W.; Malda, J. Cartilage Regeneration Using Zonal Chondrocyte Subpopulations: A Promising Approach or an Overcomplicated Strategy? *J. Tissue Eng. Regen. Med.* **2015**, 9 (6), 669–678.
- (22) Malda, J.; Visser, J.; Melchels, F. P.; Jüngst, T.; Hennink, W. E.; Dhert, W. J. A.; Groll, J.; Hutmacher, D. W. 25th Anniversary Article: Engineering Hydrogels for Biofabrication. *Adv. Mater.* **2013**, 25 (36), 5011–5028.
- (23) Hunziker, E. B.; Rosenberg, L. C. Repair of Partial-Thickness Defects in Articular Cartilage: Cell Recruitment from the Synovial Membrane. *J. Bone Joint Surg. Am.* **1996**, 78 (5), 721–733.
- (24) Liu, Y.; Shu, X. Z.; Prestwich, G. D. Osteochondral Defect Repair with Autologous Bone Marrow–derived Mesenchymal Stem Cells in an Injectable, in Situ , Cross-Linked Synthetic Extracellular Matrix. *Tissue Eng.* **2006**, 12 (12), 3405–3416.
- (25) Billiet, T.; Vandenhaute, M.; Schelfhout, J.; Van Vlierberghe, S.; Dubruel, P. A Review of Trends and Limitations in Hydrogel-Rapid Prototyping for Tissue Engineering. *Biomaterials* **2012**, 33 (26), 6020–6041.
- (26) Censi, R.; Schuurman, W.; Malda, J.; di Dato, G.; Burgisser, P. E.; Dhert, W. J. A.; van Nostrum, C. F.; di Martino, P.; Vermonden, T.; Hennink, W. E. A Printable Photopolymerizable Thermosensitive p(HPMAm-Lactate)-PEG Hydrogel for Tissue Engineering. *Adv. Funct. Mater.* **2011**, 21 (10), 1833–1842.
- (27) Vermonden, T.; Fedorovich, N. E.; van Geemen, D.; Alblas, J.; van Nostrum, C. F.; Dhert, W. J. A.; Hennink, W. E. Photopolymerized Thermosensitive Hydrogels: Synthesis, Degradation, and Cytocompatibility. *Biomacromolecules* **2008**, 9 (3), 919–926.
- (28) Kirchmayer, D. M.; Gorkin III, R.; in het Panhuis, M. An Overview of the Suitability of Hydrogel-Forming Polymers for Extrusion-Based 3D-Printing. *J. Mater. Chem. B* **2015**, 3 (20), 4105–4117.
- (29) Wang, L.-F.; Shen, S.-S.; Lu, S.-C. Synthesis and Characterization of Chondroitin Sulfate–methacrylate Hydrogels. *Carbohydr. Polym.* **2003**, 52 (4), 389–396.

- (30) Bryant, S. J.; Davis-Arehart, K. A.; Luo, N.; Shoemaker, R. K.; Arthur, J. A.; Anseth, K. S. Synthesis and Characterization of Photopolymerized Multifunctional Hydrogels: Water-Soluble Poly(vinyl Alcohol) and Chondroitin Sulfate Macromers for Chondrocyte Encapsulation. *Macromolecules* **2004**, *37* (18), 6726–6733.
- (31) Steinmetz, N. J.; Bryant, S. J. Chondroitin Sulfate and Dynamic Loading Alter Chondrogenesis of Human MSCs in PEG Hydrogels. *Biotechnol. Bioeng.* **2012**, *109* (10), 2671–2682.
- (32) Kesti, M.; Müller, M.; Becher, J.; Schnabelrauch, M.; D'Este, M.; Eglin, D.; Zenobi-Wong, M. A Versatile Bioink for Three-Dimensional Printing of Cellular Scaffolds Based on Thermally and Photo-Triggered Tandem Gelation. *Acta Biomater.* **2015**, *11*, 162–172.
- (33) Li, Q.; Wang, D.; Elisseeff, J. H. Heterogeneous-Phase Reaction of Glycidyl Methacrylate and Chondroitin Sulfate: Mechanism of Ring-Opening–transesterification Competition. *Macromolecules* **2003**, *36* (7), 2556–2562.
- (34) van Dijk-Wolthuis, W. N. E.; Kettenes-van den Bosch, J. J.; van der Kerk-van Hoof, A.; Hennink, W. E. Reaction of Dextran with Glycidyl Methacrylate: An Unexpected Transesterification. *Macromolecules* **1997**, *30* (11), 3411–3413.
- (35) van Dijk-Wolthuis, W. N. E.; Franssen, O.; Talsma, H.; van Steenbergen, M. J.; Kettenes-van den Bosch, J. J.; Hennink, W. E. Synthesis, Characterization, and Polymerization of Glycidyl Methacrylate Derivatized Dextran. *Macromolecules* **1995**, *28* (18), 6317–6322.
- (36) Oudshoorn, M. H. M.; Rissmann, R.; Bouwstra, J. A.; Hennink, W. E. Synthesis of Methacrylated Hyaluronic Acid with Tailored Degree of Substitution. *Polymer* **2007**, *48* (7), 1915–1920.
- (37) Fu, Q.; Saiz, E.; Tomsia, A. P. Direct Ink Writing of Highly Porous and Strong Glass Scaffolds for Load-Bearing Bone Defects Repair and Regeneration. *Acta Biomater.* **2011**, *7* (10), 3547–3554.
- (38) Liu, Z.; Yao, P. Injectable Thermo-Responsive Hydrogel Composed of Xanthan Gum and Methylcellulose Double Networks with Shear-Thinning Property. *Carbohydr. Polym.* **2015**, *132*, 490–498.
- (39) Oudshoorn, M. H. M.; Rissmann, R.; Bouwstra, J. A.; Hennink, W. E. Synthesis and Characterization of Hyperbranched Polyglycerol Hydrogels. *Biomaterials* **2006**, *27* (32), 5471–5479.
- (40) Chiu, H.-C.; Lin, Y.-F.; Hsu, Y.-H. Effects of Acrylic Acid on Preparation and Swelling Properties of pH-Sensitive Dextran Hydrogels. *Biomaterials* **2002**, *23* (4), 1103–1112.
- (41) Gu, C.; Zheng, R.; Yang, Z.; Wen, A.; Wu, H.; Zhang, H.; Yi, D. Novel Glycidyl Methacrylated Dextran/gelatin Nanoparticles Loaded with Basic Fibroblast Growth Factor: Formulation and Characteristics. *Drug Dev. Ind. Pharm.* **2009**, *35* (12), 1419–1429.
- (42) Vermonden, T.; Jena, S. S.; Barriet, D.; Censi, R.; van der Gucht, J.; Hennink, W. E.; Siegel, R. A. Macromolecular Diffusion in Self-Assembling Biodegradable Thermosensitive Hydrogels. *Macromolecules* **2010**, *43* (2), 782–789.
- (43) Vermonden, T.; Besseling, N. A. M.; van Steenbergen, M. J.; Hennink, W. E. Rheological Studies of Thermosensitive Triblock Copolymer Hydrogels. *Langmuir* **2006**, *22* (24), 10180–10184.
- (44) Lee, C.-T.; Kung, P.-H.; Lee, Y.-D. Preparation of Poly(vinyl Alcohol)-Chondroitin

- Sulfate Hydrogel as Matrices in Tissue Engineering. *Carbohydr. Polym.* **2005**, *61* (3), 348–354.
- (45) Varghese, S.; Hwang, N. S.; Canver, A. C.; Theprungsirikul, P.; Lin, D. W.; Elisseeff, J. Chondroitin Sulfate Based Niches for Chondrogenic Differentiation of Mesenchymal Stem Cells. *Matrix Biol.* **2008**, *27* (1), 12–21.
- (46) Hayami, J. W. S.; Waldman, S. D.; Amsden, B. G. Photo-Cross-Linked Methacrylated Polysaccharide Solution Blends with High Chondrocyte Viability, Minimal Swelling, and Moduli Similar to Load Bearing Soft Tissues. *Eur. Polym. J.* **2015**, *72*, 687–697.
- (47) Albertsson, P.-Å. Particle Fractionation in Liquid Two-Phase Systems. The Composition of Some Phase Systems and the Behaviour of Some Model Particles in Them. Application to the Isolation of Cell Walls from Microorganisms. *Biochim. Biophys. Acta* **1958**, *27*, 378–395.
- (48) Hachet, E.; Van Den Berghe, H.; Bayma, E.; Block, M. R.; Auzély-Velty, R. Design of Biomimetic Cell-Interactive Substrates Using Hyaluronic Acid Hydrogels with Tunable Mechanical Properties. *Biomacromolecules* **2012**, *13* (6), 1818–1827.
- (49) Villanueva, I.; Gladem, S. K.; Kessler, J.; Bryant, S. J. Dynamic Loading Stimulates Chondrocyte Biosynthesis When Encapsulated in Charged Hydrogels Prepared from Poly(ethylene Glycol) and Chondroitin Sulfate. *Matrix Biol.* **2010**, *29* (1), 51–62.





## Chapter 3

### **A synthetic thermo-sensitive hydrogel for cartilage bioprinting and its biofunctionalization with polysaccharides**

**A. Abbadessa\*, V.H.M. Mouser\*, M.M. Blokzijl, D. Gawlitta, W.J.A. Dhert,  
W.E. Hennink, J. Malda, T. Vermonden**

**\*These authors contributed equally**

*Biomacromolecules*, 2016, 17 (6), 2137–2147

This chapter is also included in the PhD thesis of V.H.M. Mouser

## Abstract

Hydrogels based on triblock copolymers of polyethylene glycol and partially methacrylated poly(*N*-(2-hydroxypropyl) methacrylamide mono/dilactate) are an attractive class of biomaterials due to their biodegradability, cytocompatibility, and tunable thermo-responsive and mechanical properties. By fine-tuning these properties, the hydrogels can be 3D biprinted, to generate *e.g.* constructs for cartilage repair. This study investigated whether hydrogels based on the above mentioned polymer with a 10% degree of methacrylation ( $M_{10}P_{10}$ ), support cartilage formation by chondrocytes, and whether the incorporation of methacrylated chondroitin sulfate (CSMA) or methacrylated hyaluronic acid (HAMA) can improve the mechanical properties, long-term stability, and printability. Chondrocyte-laden  $M_{10}P_{10}$  hydrogels were cultured for 42 days to evaluate chondrogenesis.  $M_{10}P_{10}$  hydrogels with or without polysaccharides were evaluated for their mechanical properties (before and after UV photo-cross-linking), degradation kinetics, and printability. Extensive cartilage matrix production occurred in  $M_{10}P_{10}$  hydrogels, highlighting their potential for cartilage repair strategies. The incorporation of polysaccharides increased the storage modulus of polymer mixtures and decreased the degradation kinetics in cross-linked hydrogels. Addition of HAMA to  $M_{10}P_{10}$  hydrogels improved printability and resulted in 3D constructs with excellent cell viability. Hence, this novel combination of  $M_{10}P_{10}$  with HAMA forms an interesting class of hydrogels for cartilage bioprinting.



### 3.1 Introduction

Articular cartilage is the tissue that covers the extremities of the bones inside the joints. The tissue functions as a damper due to its high osmotic pressure and reduces surface friction due to its smooth surface structure. Articular cartilage contains proteoglycans, collagen type II, water, and cells, the chondrocytes. Since the tissue lacks vasculature and innervation, and contains only few chondrocytes, it has a limited regenerative capacity<sup>1,2</sup>. The implantation of cell-laden hydrogel scaffolds is regarded as a promising approach to treat cartilage defects. Hydrogels, networks of hydrophilic polymers, have high water content, which supports cell survival and allow homogeneous encapsulation of cells as well as biological and chemical cues. Therefore, cell-laden hydrogel implants can promote new tissue formation while initially providing structural support. For the generation of successful cell-laden constructs, it is essential to have control over the mechanical properties and degradation kinetics of the construct, as it should progressively be replaced by newly-formed tissue after implantation<sup>3</sup>. The mechanical properties and degradation kinetics of hydrogels can be easily tailored over a broad range and in a highly reproducible manner by a proper design of the building blocks<sup>4-6</sup>. In addition, thermo-responsive functionalities can be introduced in the building blocks, providing the opportunity to generate injectable and three dimensional (3D) printable hydrogels<sup>7</sup>. Copolymers based on a polyethylene glycol (PEG) mid-block flanked by two poly(*N*-(2-hydroxypropyl) methacrylamide mono/dilactate) (polyHPMA-lac) outer blocks have recently been investigated for pharmaceutical and biomedical applications<sup>8-12</sup>. Methacrylated polyHPMA-lac-PEG triblock copolymers display lower critical solution temperature (LCST) behavior in aqueous solutions, meaning that these polymers are soluble at low temperatures and form physical gels, by self-assembly due to dehydration of polymer chains, at temperatures above a critical temperature, called the cloud point (CP)<sup>13</sup>. The thermo-sensitive behavior of methacrylated polyHPMA-lac-PEG triblock copolymers is highly tunable, *e.g.* to physiologically relevant temperatures, by adapting the content of the lactate groups present in the outer blocks as well as the number of methacrylate groups<sup>9,13,14</sup>. In addition, the methacrylate groups allow UV light-mediated photo-cross-linking, which prevents rapid disassembly of the polymer networks<sup>13</sup>. Chemically cross-linked hydrogels with tailored degradation rates and mechanical properties can be obtained by varying the number of methacrylate units per polymer chain, the molecular weight of the PEG mid-block, as well as that of the thermo-sensitive flanking blocks and the polymer concentration in the hydrogel<sup>8,9,11,13</sup>. The thermo-sensitive behavior of methacrylated polyHPMA-lac-PEG triblock copolymers allows easy handling of the polymer solution at low temperatures, when it behaves as a viscous liquid, to incorporate cells. Previous studies have shown high viability of encapsulated articular chondrocytes in methacrylated polyHPMA-lac-PEG triblock copolymer based hydrogels<sup>10</sup>. However, long-term culture and actual cartilage matrix formation in these hydrogels has not been investigated so far.

Cell-laden hydrogels can accurately be shaped with 3D biofabrication techniques to mimic the architecture of native tissues *e.g.* the zonal organization of articular cartilage<sup>15</sup>, and to generate patient specific construct shapes. 3D bioprinting is a form of biofabrication based on computer-aided layer-by-layer material deposition<sup>16–19</sup>. As such, bioprinting also allows the incorporation of pores or perfusable channels in the 3D structure, for easy diffusion of nutrients, oxygen and metabolites during (*in vitro*) construct maturation<sup>7</sup>. Hydrogels composed of methacrylated polyHPMA-lac-PEG triblock copolymers have already been shown to be printable due to their thermo-sensitive behavior<sup>10</sup>. However, this required a relatively high polymer concentration and a high degree of methacrylation (DM)<sup>10</sup>. In general, dense polymer networks due to *e.g.* high polymer concentrations and high DM, have adverse effects on the matrix production of embedded cells<sup>20,21</sup> and are therefore unfavourable for the fabrication of tissue repair constructs. In order to tackle this well-known dilemma in bioprinting<sup>7</sup>, hybrid materials can be designed, for example by incorporating polysaccharides, which increase the viscosity of the polymer solution and can potentially improve the printability without hampering the matrix production of embedded cells<sup>22–26</sup>. In this study, the polysaccharides chondroitin sulfate (CS) and hyaluronic acid (HA) were methacrylated to allow UV photo-cross-linking<sup>27,28</sup> and blended with low DM (10%) polyHPMA-lac-PEG triblock copolymers, as both are natural polysaccharides abundantly present in native cartilage. In addition, they have demonstrated anabolic effects on extracellular matrix synthesis by chondrocytes and stem cells<sup>24,29–34</sup>. Therefore, these polysaccharides are attractive candidates to optimize methacrylated polyHPMA-lac-PEG triblock copolymer based hydrogels for cartilage bioprinting. It is hypothesized that the incorporation of methacrylated HA (HAMA) or methacrylated CS (CSMA) in methacrylated polyHPMA-lac-PEG triblock hydrogels will affect the mechanical properties, decrease the degradation rate and improve the 3D printability in comparison to hydrogels made of methacrylated polyHPMA-lac-PEG triblock only. The aim of this study was to characterize methacrylated polyHPMA-lac-PEG triblock copolymer based hydrogels in terms of chondrogenesis, mechanical behavior, degradation kinetics and printability. It was also investigated whether the incorporation of HAMA or CSMA in this synthetic hydrogel can further improve the mechanical properties, affect the degradation rate, and enhance the printability.

## 3.2 Materials and Methods

### 3.2.1 Materials

All chemicals were obtained from Sigma-Aldrich (Zwijndrecht, the Netherlands) and all solvents from Biosolve (Valkenswaard, the Netherlands) unless indicated otherwise. Chemicals and solvents were used as received. PEG 10 kDa was supplied by Merck (Darmstadt, Germany). HA sodium salt (1560 kDa) was supplied by Lifecore Biomedical (Chaska, MN, USA). CS A sodium salt from bovine trachea (Sigma-Aldrich, Zwijndrecht, the Netherlands) was analyzed with Viscotek Gel Permeation Chromatography (GPC) and showed a bimodal molecular weight

distribution (number average molecular weight,  $M_n$  26.9 kDa, 94% mass content and 353.8 kDa, 6% mass content; details are given in Figure S1). L-lactide was purchased from Corbion Purac (Amsterdam, the Netherlands) and Irgacure 2959 was a kind gift from BASF (Ludwigshafen, Germany). *N*-(2-hydroxypropyl) methacrylamide (HPMA), HPMA mono- and dilactate and PEG<sub>10000</sub>-4,4'-azobis(cyanopentanoate) macroinitiator were synthesized as previously reported<sup>35-37</sup>. Phosphate buffered saline (PBS), penicillin/streptomycin (pen/strep; 10,000 units/ml penicillin and 10 mg/ml streptomycin) and picogreen DNA assay were supplied by Invitrogen (Carlsbad, California, USA). Three different types of Dulbecco's Modified Eagle Medium (DMEM) were used: DMEM 31885 from Gibco (referred to as DMEM), high glucose DMEM D6429 from Sigma-Aldrich (referred to as high glucose DMEM) and DMEM/F-12+GlutaMax-1 31331 from Invitrogen (referred to as DMEM/F-12). Fetal bovine serum (FBS) was obtained from Gibco (Invitrogen corporation) and type II collagenase was purchased from Worthington Biochemical Corp (Lakewood, NJ, USA). ITS+ premix (human recombinant insulin, human transferrin, selenous acid, bovine serum albumin, linoleic acid) was obtained from BD Biosciences (Breda, the Netherlands), recombinant human TGF- $\beta$ 1 from Peprotech (London, UK), pronase (11459643001) from Roche Life Sciences (Indiana, USA), hyaluronidase (H2126) from Sigma-Aldrich and Tissucol Duo S (fibrin and thrombin) from Baxter (Utrecht, the Netherlands). Antibody against collagen type I (1:100; EPR7785, ab138492) was obtained from Abcam (Cambridge, UK). Antibodies against collagen types II and VI (1:100; II-6B3II and 1:5, 5C6, respectively) were obtained from the Developmental Studies Hybridoma Bank (Iowa City, IA, USA). Secondary horse radish-peroxidase conjugated antibodies for collagen type I (EnVision+, K4010), collagen type II (1:100, IgG HRP, P0447), and collagen type VI (EnVision+, K4007) were ordered from DAKO (Heverlee, the Netherlands). Calcein-AM (to stain living cells) and ethidium homodimer-1 (to stain nuclei of dead cells) were obtained from Life Technologies (L3224, Bleiswijk, The Netherlands). Finally, Dye-Trak 'F' microspheres (Fluorescent Orange) were ordered from Triton Technology Inc. (San Diego, CA, USA).

### 3.2.2 Synthesis of methacrylated poly(*N*-(2-hydroxypropyl) methacrylamide mono/dilactate)-PEG triblock

The synthesis of a methacrylated thermo-sensitive triblock copolymer, consisting of a hydrophilic PEG-based mid-block flanked by two partially methacrylated pHPMA-lac outer blocks was carried out as previously described by Vermonden *et al.*<sup>13,14</sup>. Briefly, a free radical polymerization in acetonitrile was carried out at 70 °C for 40 hours under a N<sub>2</sub> atmosphere, using PEG<sub>10000</sub>-4,4'-azobis(cyanopentanoate) as macroinitiator and HPMA mono- and dilactate (molar ratio mono/dilactate = 75:25) as monomers, with a mass ratio monomers/macroinitiator of 4:1. After precipitation in cold diethyl ether, the polymer was collected and further modified via partial esterification of the hydroxyl groups present on the lactate units with methacrylate groups. This reaction was carried out in dry tetrahydrofuran as solvent and methacrylic anhydride (MA, molar feed of 13.3% of the free hydroxyl groups

of the polymer) was used as methacrylating agent in presence of triethylamine and 4-dimethylaminopyridine. The methacrylated polyHPMA-lac-PEG triblock copolymer is further referred to as  $M_{10}P_{10}$  ( $M_{10}$  refers to a DM of 10% and  $P_{10}$  refers to a PEG block with a molecular weight (MW) of 10 kDa) and its precursor as  $M_0P_{10}$ . A low DM of 10% was chosen to achieve a low network density in the cross-linked hydrogel, which is likely beneficial for cell behavior<sup>20</sup>.

### 3.2.3 Methacrylation of polysaccharides

Methacrylation of CS was carried out using a transesterification reaction, as described by Abbadessa *et al.*<sup>38</sup>. Briefly, CS A sodium salt was converted into tetrabutylammonium (TBA) salt (CS-TBA) by using a Dowex® 50WX8 hydrogen form resin, previously saturated with TBA fluoride. Subsequently, 2.7 g (3.08 mmol of disaccharide units) of CS-TBA was dissolved in 100 ml of dry dimethyl sulfoxide (DMSO) under a  $N_2$  atmosphere at 50 °C. Next, 4-dimethylaminopyridine (0.495 g) and glycidyl methacrylate (GMA, 195  $\mu$ l) were added and the reaction mixture was stirred at 50 °C for 48 hours. After the reaction, the mixture was diluted with water and the pH was lowered to 5.5 using a 0.2 M solution of HCl in water. The polymer solution was further dialyzed against a 150 mM NaCl solution in water for 3 days and against water for 4 days. The polymer was finally collected, as  $Na^+$  salt, after freeze-drying and it is further referred to as CSMA.

HA was methacrylated using a slightly modified method from the one reported by Hachet *et al.*<sup>28</sup>. Briefly, 0.5 g (1.25 mmol of disaccharide units) of HA was dissolved in 80 ml of ultrapure water at 4 °C overnight. Subsequently, *N,N*-dimethylformamide (DMF) was added to obtain a mixture with 1:1 water/DMF volume ratio. Next, 926  $\mu$ l (6.25 mmol) of MA was added drop-wise at 4 °C to the HA solution while the pH was kept between 8 and 9 by adding 0.5 M NaOH. The pH was monitored for 4 hours and adjusted to 8-9. After overnight stirring at 4 °C, the polymer was precipitated by addition of NaCl (final concentration in the mixture 0.5 M) and cold ethanol (final ethanol/water ratio of 2.3:1), and further purified by means of dialysis (MWCO 10,000-14,000 Da). Purified HAMA was collected after freeze-drying. The DM of HAMA was investigated using a method based on the detection of methacrylic acid, which is released after basic hydrolysis of the ester bonds present in the methacrylated polysaccharide<sup>39</sup>. The formed methacrylic acid was detected with a High Performance Liquid Chromatography (HPLC) Waters 2695 separating module equipped with a Waters 2487 dual  $\lambda$  absorbance detector ( $\lambda = 210$  nm, Waters Corporation, Milford, MA, USA) and with a C18 column (Sunfire). HAMA (15 mg) was dissolved in 10 ml of 0.02 M NaOH at 37 °C for 2 hours. Subsequently, 2 ml of 2 M acetic acid was added. After filtration using a 0.2  $\mu$ m filter, the samples were injected in the HPLC system and eluted at 1 ml/minute using a mixture of acetonitrile/water (15:85, pH = 2) as mobile phase. Calibration was performed using solutions of methacrylic acid of different concentrations in the same eluent.

### 3.2.4 Experimental design and hydrogel groups

To investigate if  $M_{10}P_{10}$  hydrogels support chondrogenesis of chondrocytes, UV

cross-linked constructs from an equine chondrocyte (passage 1,  $n = 3$  donors) laden  $M_{10}P_{10}$  (18% w/w) polymer mixture were prepared. Constructs were cultured for 42 days and evaluated for evidence of chondrogenesis at days 0 (harvest directly after cell encapsulation), 28 and 42, via quantitative measurements and histology. This gel formulation is further referred to as cell-laden hydrogel M.

To investigate whether the incorporation of HAMA or CSMA in  $M_{10}P_{10}$  can improve the mechanical properties, affect the degradation rate, and enhance the printability, cell-free polymer mixtures based on  $M_{10}P_{10}$  (18% w/w),  $M_{10}P_{10}$  (14% w/w) blended with CSMA (4% w/w), or  $M_{10}P_{10}$  (14% w/w) blended with HAMA (0.9% w/w) were prepared and are further referred to as mixtures M, MCS and MHA, respectively (Table 1). These mixtures were analyzed for their thermo-sensitive properties using rheological measurements. Cell-free UV cross-linked M, MCS and MHA hydrogels were further characterized for their Young's modulus and their degradation/swelling behavior in PBS (pH 7.4) enriched with 0.02% of  $NaN_3$  at 37 °C. Finally, 3D constructs were printed with polymer mixture MHA laden with fluorescent microspheres to assess homogeneous encapsulation, using a 3D bioprinter (regenHU, Villaz-St-Pierre, Switzerland). Additionally, constructs with primary chondrocytes were printed using mixtures M, MCS and MHA to assess viability 1 and 7 days after printing. All measurements were performed in triplicate.

**Table 1.** Compositions of the three hydrogel groups.

hydrogel	polymer concentration (w/w%)		
	$M_{10}P_{10}$	CSMA	HAMA
M	18%	-	-
MCS	14%	4%	-
MHA	14%	-	0.9%

### 3.2.5 Chondrocyte isolation and culture

Primary chondrocytes were isolated from full-thickness cartilage of the stifle joints of fresh equine cadavers ( $n = 3$ ; 3–10 years old horses), with consent of the owners. Macroscopically healthy cartilage was removed from the joint under aseptic conditions and the cartilage was digested overnight at 37 °C in DMEM supplemented with collagenase II (1.5  $\mu$ g/ml), hyaluronidase (1 mg/ml), FBS (10%) and pen/strep (1%). After digestion, the cell suspension was filtered through a 40  $\mu$ m cell strainer. Chondrocytes were washed with PBS and stored in liquid  $N_2$  until further use.

In order to prepare cell-laden constructs, the chondrocytes were expanded in monolayer culture for 14 days (seeding density of  $5 \cdot 10^3$  cells/cm<sup>2</sup>) in chondrocyte expansion medium consisting of DMEM, FBS (10%) and pen/strep (1%). The chondrocytes were harvested and mixed with the polymer mixture at passage 1 when they reached 80-90% confluence. Cell-laden constructs were cultured in chondrogenic differentiation medium consisting of high glucose DMEM supplemented with ITS+ premix (1%), dexamethasone (0.1  $\mu$ M), L-ascorbic acid-2-phosphate (0.2 mM), recombinant human TGF- $\beta$ 1 (10 ng/ml) and pen/strep (1%) to stimulate chondrogenesis and redifferentiation of the chondrocytes<sup>40,41</sup>.

### 3.2.6 Fabrication of cell-laden chemically cross-linked M<sub>10</sub>P<sub>10</sub>-based hydrogels

M<sub>10</sub>P<sub>10</sub> was dissolved in PBS at 4 °C and Irgacure was added (concentration: 0.05% w/w). The resulting mixture (M<sub>10</sub>P<sub>10</sub> concentration: 20.5% w/w) was stirred overnight in the dark at 4 °C. The expanded chondrocytes were mixed on ice with the polymer mixture to obtain a concentration of 15-20  $\cdot 10^6$  chondrocytes/ml (concentration varied per donor). Correcting for the average weight of the added cells, the final concentrations of Irgacure and M<sub>10</sub>P<sub>10</sub> in the cell-laden polymer mixture were 0.044% w/w and 18% w/w, respectively. The cell-laden suspension was injected into a Teflon mold, which was covered with a glass slide to generate cylindrical samples (sample size: 6 mm in diameter, 2 mm in height). The filled molds were placed at 37 °C for 5 minutes to allow physical gelation of the hydrogel. Subsequently, chemical cross-linking was induced with a UV lamp (CL-1000L Model, UVP, Cambridge, UK, Intensity: 7.2 mW/cm<sup>2</sup>, irradiation time: 15 minutes). Next, the samples were cultured at 37 °C and 5% CO<sub>2</sub> for 42 days in chondrogenic differentiation medium. The medium was refreshed twice a week. Fibrin gels were prepared as a positive control for cell behavior. Chondrocytes were mixed with fibrinogen (Tissucol Duo S, diluted 1:15 in PBS) to get a cell density of 30-40  $\cdot 10^6$  cells/ml. Next, 30  $\mu$ l of thrombin (Tissucol Duo S, diluted 1:50 in PBS, 500 IU) was pipetted into the cylindrical molds and 30  $\mu$ l of cell-laden fibrinogen suspension was mixed into the thrombin solution to generate a final cell concentration of 15-20  $\cdot 10^6$  chondrocytes/ml (same as for cell-laden M hydrogels). Samples were incubated for 15 minutes at room temperature and placed in culture with chondrogenic differentiation medium as described above.

### 3.2.7 Histology & Immunohistochemistry

At days 0 (harvest directly after cell encapsulation), 28 and 42, three samples of each hydrogel group (M and fibrin) were harvested. Part of each sample was fixed overnight in formalin (37%) and dehydrated through a graded ethanol series. After clearing in xylene, the samples were embedded in paraffin and sectioned at a thickness of 5  $\mu$ m. Sections were stained with safranin-O to visualize proteoglycans, fast green to visualize collagens, and hematoxylin to stain cell nuclei, as previously described<sup>42</sup>. Collagen types I, II and VI were visualized with immunohistochemistry. First, the sections were deparaffinized and hydrated. Next, antigen retrieval was performed with pronase (1 mg/ml in PBS) and hyaluronidase (10 mg/ml in PBS) for 30 minutes



at 37 °C, followed by a blocking step of 10 minutes with H<sub>2</sub>O<sub>2</sub> (0.3% in PBS) at room temperature. The primary antibody was incubated overnight at 4 °C. Mouse IgG was used at matched concentrations for negative control staining. After incubation, the matching secondary antibody was added and incubated for 30 minutes for collagen type I and 60 minutes for collagen types II and VI, at room temperature. Finally, all stainings were visualized with 3,3'-diaminobenzidine peroxidase substrate solution for 3-10 minutes and counterstained with Mayer's hematoxylin. All stained sections were evaluated and photographed using a light microscope (Olympus BX51 microscope, Olympus DP70 camera, Hamburg, Germany).

### 3.2.8 Biochemical assays

The remaining part of each harvested cell-laden hydrogel was weighed, freeze dried, and weighed again to determine the sample dry weight and water content. Next, the dried hydrogels were digested overnight at 56 °C in 200 μL papain digestion buffer (0.2 M NaH<sub>2</sub>PO<sub>4</sub> + 0.01 M EDTA · 2 H<sub>2</sub>O in milliQ, pH = 6.0) supplemented with 250 μL/ml papain solution (16-40 units/mg protein) and 0.01 M cysteine. To determine the glycosaminoglycan (GAG) content, as a measure for proteoglycan, a dimethylmethylene blue (DMMB)<sup>43</sup> assay was used with known concentrations of chondroitin sulfate C as a reference. The amount of GAG was normalized to the dry weight and DNA content of the samples, as measured by the Quant-iT PicoGreen dsDNA kit and read on a spectrofluorometer (Biorad, Hercules, California, USA), all according to the manufacturer's protocols.

### 3.2.9 Fabrication of chemically cross-linked hydrogels modified with polysaccharides

Defined amounts of M<sub>10</sub>P<sub>10</sub> and CSMA or HAMA (Table 1) were dissolved in PBS at 4 °C and Irgacure was added as the last component (final concentration: 0.044% w/w). The polymer mixture containing CSMA was stirred overnight while the mixture containing HAMA was stirred for 48 hours at 4 °C to allow complete dissolution. Subsequently, the polymer mixtures were injected into Teflon molds (sample size: 6 mm in diameter, 2 mm in height), incubated for 5 minutes at 37 °C and UV irradiated as described for the cell-laden cross-linked M hydrogels (section 3.2.6). Two different hydrogel compositions, MCS and MHA were prepared, in which M<sub>10</sub>P<sub>10</sub> was partially replaced by either CSMA or HAMA, respectively. Finally, hydrogels containing only M<sub>10</sub>P<sub>10</sub> in the maximum total polymer concentration used for hybrid gels were prepared as a control group (18% w/w, hydrogels M). The total polymer concentration in MHA hydrogels was slightly lower compared to the other two hydrogels, since it was not possible to dissolve more than 0.9% w/w of this polysaccharide due to its high MW.

### 3.2.10 Mechanical analysis

Thermo-responsive properties of the polymer mixtures (M, MCS and MHA) before chemical cross-linking were studied using an AR G-2 rheometer (TA-Instruments, Etten-Leur, The Netherlands), equipped with a cone-plate measuring geometry (cone

diameter: 20 mm, angle: 1°). All polymer mixtures were tested under oscillation temperature sweeps from 4 to 50 °C employing a frequency of 1 Hz and a strain of 1%, which was found to be within the linear viscoelastic range of all formulations (Figure S2). Values of storage and loss moduli ( $G'$  and  $G''$ , respectively) were recorded for each sweep and the resulting rheograms were reported showing the lines interconnecting all data points for each run.

To investigate the stiffness of hydrogel constructs after UV cross-linking, all polymer mixtures (M, MCS and MHA) were molded as described in section 3.2.9 and allowed to swell for 3 hours in PBS at room temperature. Next, hydrogels were examined under unconfined compression test using a Dynamic Mechanical Analyzer, DMA (2980 DMA, TA Instruments, Etten-Leur, The Netherlands). The hydrogels were subjected to a preload force of 0.001 N and subsequently compressed with a force ramp rate of 0.25 N/minute and an upper force limit of 1 N<sup>13</sup>. The Young's Modulus was calculated as the slope of the initial linear segment of the stress/strain curve<sup>22</sup>.

### 3.2.11 *In vitro* swelling-degradation study

For all polymer mixtures (M, MCS and MHA) cross-linked samples (6 mm of diameter, 2 mm of height, 56.5  $\mu$ l of volume) prepared as described in section 3.2.9 were placed in glass vials (diameter: 1.75 cm) with 1 ml of PBS (pH 7.4), supplemented with 0.02% of NaN<sub>3</sub>. The vials were incubated at 37 °C and the solutions were refreshed twice per week. At multiple time points, the hydrogels were weighed and the swelling ratio (SR) was calculated as follows:

$$SR = \frac{m_{day\ x}}{m_{day\ 0}} \quad \text{Equation 1}$$

in which  $m_{day\ x}$  represents the hydrogel mass after  $x$  days of incubation and  $m_{day\ 0}$  the hydrogel mass before the hydrogel was placed in PBS.

### 3.2.12 Printing of hydrogels

A 3DDiscovery bioprinter (regenHU, Villaz-St-Pierre, Switzerland) equipped with a Bluepoint 4 UV lamp (point light source, wavelength range: 300-600 nm, UV-A intensity at 5 cm = 103 mW/cm<sup>2</sup>, Hönle UV Technology AG, Gräfelfing, Germany) was used for the 3D printing of hydrogels. Filaments were generated with a micro valve (CF300H) print head, for optimal control over volume deposition rates, using optimized printer settings (Table S1). To generate porous constructs, alternating layers of vertical and horizontal filaments were deposited in the  $x,y$ -plane. Cross-linking was performed in a layer-by-layer fashion, exposing each deposited layer for 3 seconds to UV light from a distance of 5 cm. After printing, the constructs were irradiated for an additional 9 seconds.

### 3.2.13 Printing of hydrogels loaded with fluorescent microspheres and cells

To evaluate the feasibility of homogeneous cell encapsulation, polymer mixture MHA was supplemented with fluorescently labeled microspheres (Fluorescent



Orange Dye-Trak 'F' microspheres, Triton Technology, diameter 15  $\mu\text{m}$  similar as a single cell, concentration in the polymer mixture 0.8 million/ml) and constructs were 3D printed using optimized print settings (Table S1). To visualize the distribution of the microspheres in the constructs, an Olympus BX51 microscope was used.

To evaluate cell viability after printing, primary chondrocytes (harvested and expanded as described in section 3.2.5) were encapsulated in mixtures M, MCS and MHA. The cell-laden mixtures were heated to 37  $^{\circ}\text{C}$  and three constructs were subsequently printed using the aforementioned print method reported in section 3.2.12. As a positive control, cast hydrogels were prepared for each mixture using the same method as for the equine chondrocyte laden hydrogels (section 3.2.6). Each printed construct was cut into four pieces, which were cultured in separate wells with chondrocyte expansion medium. Viability was checked on two pieces at day 1 and for the other pieces after 7 days of culture. To check cell viability, the hydrogels were stained for 20 minutes with calcein-AM (4  $\mu\text{M}$  in PBS) and ethidium homodimer-1 (2  $\mu\text{M}$  in PBS) at 37  $^{\circ}\text{C}$ . After washing three times in PBS, the red and green fluorescent signals were visualized using an Olympus BX51 microscope and three images of each hydrogel quarter were analyzed.

### 3.2.14 Statistics

Statistical analyses were performed using SPSS software (version 20, IBM Corporation, USA). Differences in Young's modulus between the hydrogel groups (M, MHA, MCS) and differences in chondrocyte viability after printing at each time point, were determined with a One-Way ANOVA test. For GAG values normalized to the DNA content, both hydrogels (M and fib) at all time-points (6 groups in total) were compared with each other using a Randomized Block Design ANOVA to correct for donor variability. The GAG, DNA, and water contents normalized to the dry weight at the different time points were compared to each other within each hydrogel formulation by a Randomized Block Design ANOVA. A significance level of 0.05 and a Tukey's Post-hoc analysis were used for all tests.

## 3.3 Results and Discussion

### 3.3.1 Synthesis and characterization of thermo-sensitive polymers and methacrylated polysaccharides

$\text{M}_0\text{P}_{10}$  and  $\text{M}_{10}\text{P}_{10}$  (Figure 1) were obtained in a high yield (80% and 96%, respectively). Their chemical structures, confirmed by  $^1\text{H-NMR}$ , were in accordance to previously reported data<sup>13,14</sup>. The  $\text{M}_n$  and DM of  $\text{M}_{10}\text{P}_{10}$  determined by  $^1\text{H-NMR}$  were 42.4 kDa and 10.7%, respectively, whereas the  $\text{M}_n$  according to GPC was 34.6 kDa with a PDI value of 2.0. The cloud points of  $\text{M}_0\text{P}_{10}$  and  $\text{M}_{10}\text{P}_{10}$  were 35  $^{\circ}\text{C}$  and 20  $^{\circ}\text{C}$ , respectively. Table 2 summarizes the polymer characteristics for  $\text{M}_0\text{P}_{10}$  and  $\text{M}_{10}\text{P}_{10}$ . The methods employed for the methacrylation of CS and HA resulted in high yields of CSMA and HAMA (>84% for both polysaccharides). The methacrylated polysaccharides (chemical structures shown in Figure 1) were analyzed by  $^1\text{H-NMR}$ . The presence of the signals at 6.2 and 5.8 ppm, representative of the two vinyl

protons present in the methacrylate groups, and the signal at 2.0 ppm, typical of the protons belonging to its methyl group, confirmed the partial functionalization of the hydroxyl groups with methacrylate groups.

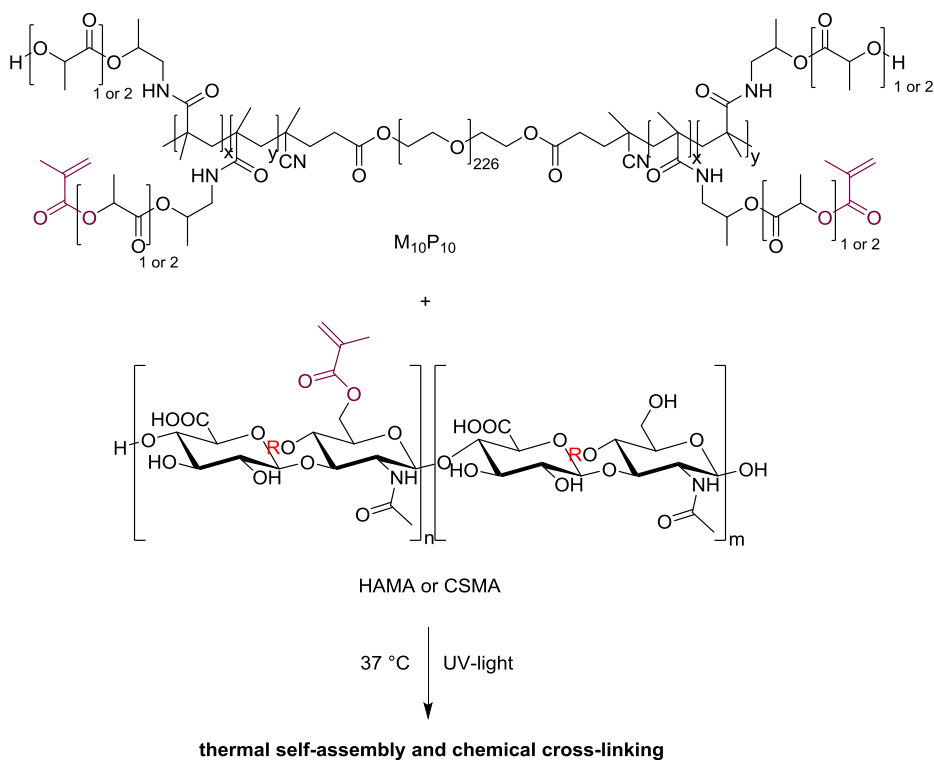


**Figure 1.** Chemical structure of  $M_{10}P_{10}$  (top) and methacrylated HA (bottom, R = H in equatorial position) or CS (bottom, R =  $\text{SO}_3\text{H}$  in axial position).  $M_{10}P_{10}$  confers thermo-sensitive properties to the gel, whereas the presence of methacrylate groups in both polymers allows UV-mediated chemical cross-linking.

The methacrylation of CS was performed in DMSO using GMA as methacrylating agent, and a molar feed of GMA and CS-TBA repeating units of 0.48:1 resulted in a DM of 15.2% (Table 2), calculated according to  $^1\text{H-NMR}$ . Moreover, the absence in the  $^1\text{H-NMR}$  spectrum of the signals at 5.5 and 5.2 ppm representative of a possible glyceryl spacer between the methacrylate group and the disaccharide unit, excluded the presence of products originating from ring opening reaction<sup>44</sup>. Thus, the reaction mechanism follows a transesterification mechanism, which is in line with our previous findings<sup>38</sup>.

For the synthesis of HAMA, we selected the method reported by Hachet *et al.*<sup>28</sup>. This reaction was performed in a mixture of water and DMF using a large excess of MA (molar ratio of 5:1 between MA and repeating units of HA). This high feed ratio is generally used for methacrylation reactions in aqueous environment because it is necessary to compensate for the amount of MA lost as methacrylic acid due

to hydrolysis<sup>45,46</sup>. A lower polymer concentration, 3.1 versus 12.0 mg/ml was used compared to previously reported reactions, which were performed using a lower MW HA<sup>28,47</sup>. The use of relatively low concentration was necessary to facilitate pH monitoring and general handling of the reaction mixture, considering the high viscosity of high MW HA solutions. This low HA concentration likely explains our lower methacrylate incorporation (5%) compared with previous reports ( $\geq 14\%$ )<sup>28,47</sup>. Because of the poor resolution of the <sup>1</sup>H-NMR spectra for high MW HAMA, an HPLC-based method was employed to accurately determine the DM, which was found to be 23.4% (Table 2).

**Table 2.** Characteristics of thermo-sensitive polymers and polysaccharides.

Polymer	DM (%)	M <sub>n</sub> (kDa)	PDI	CP (°C)
<b>M<sub>0</sub>P<sub>10</sub></b>	0 <sup>a</sup>	43.9 <sup>a</sup> 36.2 <sup>b</sup>	1.9 <sup>b</sup>	35 <sup>c</sup>
<b>M<sub>10</sub>P<sub>10</sub></b>	10.7 <sup>a</sup>	42.4 <sup>a</sup> 34.6 <sup>b</sup>	2.0 <sup>b</sup>	20 <sup>c</sup>
<b>CS</b>	0 <sup>a</sup>	26.9 (94%) <sup>d</sup> 353.8 (6%) <sup>d</sup>	1.4 <sup>d</sup> 1.3 <sup>d</sup>	n.a.
<b>CSMA</b>	15.2 <sup>a</sup>	n.d.	n.d.	n.a.
<b>HA</b>	0 <sup>a</sup>	1560 <sup>e</sup>	n.d.	n.a.
<b>HAMA</b>	23.4 <sup>f</sup>	n.d.	n.d.	n.a.

<sup>a</sup> Determined by <sup>1</sup>H-NMR

<sup>b</sup> Determined by GPC

<sup>c</sup> Determined by UV-VIS spectrophotometry

<sup>d</sup> Determined by Viscotek

<sup>e</sup> Average MW determined by Multi-Angle Light Scattering Size Exclusion Chromatography (MALS-SEC) as reported from the supplier

<sup>f</sup> Determined by HPLC

n.d.: not determined

n.a.: not applicable

### 3.3.2 Matrix production of embedded chondrocytes

Hydrogels composed of methacrylated polyHPMA-lac-PEG triblock copolymers have been shown to support the short-term survival of chondrocytes, however, the effect on the matrix production was not yet reported<sup>10</sup>. In this study, equine chondrocytes were encapsulated into an 18%  $M_{10}P_{10}$ -based hydrogel (hydrogel M) and cultured up to 42 days in chondrogenic differentiation medium. The matrix production in this hydrogel was compared to that of chondrocytes embedded in fibrin gel (positive control), which is the golden standard for clinical delivery of cells for cartilage repair procedures and is known to support chondrogenesis due to its bioactive peptide sequences<sup>48,49</sup>. Hydrogel M supported cartilage-like tissue formation of the encapsulated chondrocyte and Safranin-O staining revealed a homogeneous deposition of proteoglycans after 28 and 42 days of culture (Figure 2).

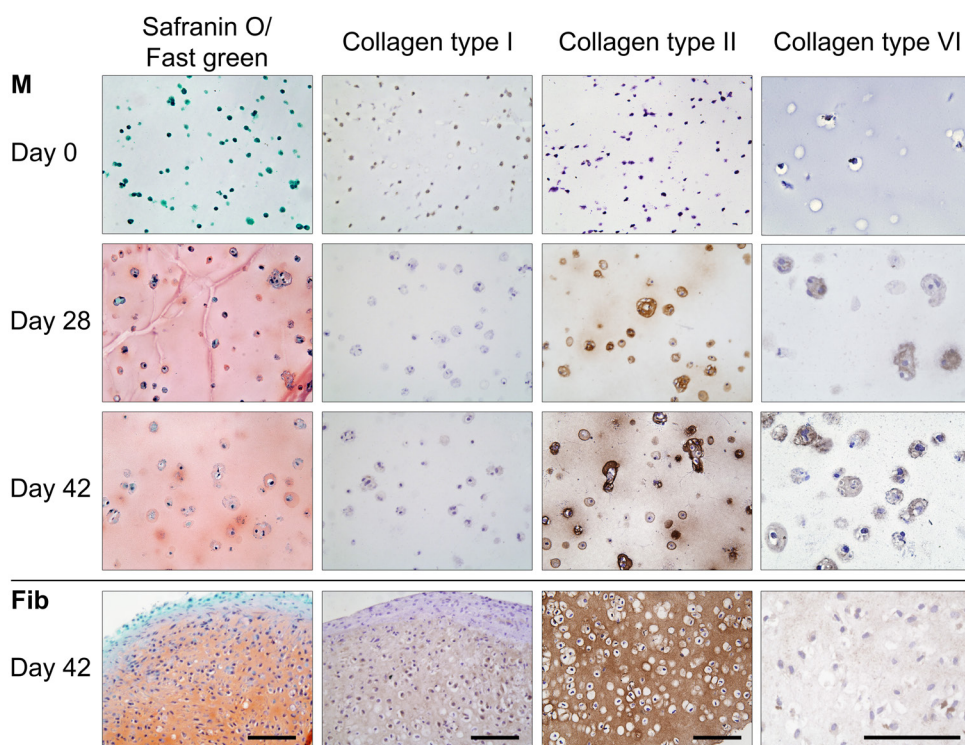


**Figure 2.** Histology and immunohistochemistry of chondrocytes differentiated in  $M_{10}P_{10}$ -based hydrogels (M) with fibrin (fib) as a positive control. From left to right: safranin-O staining, collagen types I, II and VI staining. Scale bar represents 100  $\mu\text{m}$  and it is the same for all images of the same staining (column).

In addition, immunolocalization of collagen type II revealed that its deposition was limited to distinct areas around the cells at day 28. However, after 42 days a more homogeneous distribution was observed. Both stainings were more intense

in the fibrin gels at day 28 and 42 compared to hydrogel M samples at these time points (Figure 2). An explanation for this effect is the compaction of the fibrin gels during the first days of culture<sup>50-52</sup>. Because of this, the relative cell density and amount of matrix per gel volume increased as can be observed in the high DNA/dwt and GAG/dwt values for fibrin samples (Figure 3e, f). The sample dry weight was ten times higher for hydrogels M compared to fibrin gels and this difference remained over time (data not shown). Water volume normalized to the dry weight of M hydrogels increased at day 28 and 42 compared to day 0 (Figure 3d, 250% and 330% respectively). Although hydrogel compaction after implantation in a defect may localize the cells at the bottom of the defect, it will on the other hand result in an incomplete defect-fill. Moreover, contracting materials may be difficult to combine in hybrid scaffolds, e.g. hydrogel constructs reinforced with polymeric fibers, aimed to increase construct stiffness<sup>7,22,53</sup>. In these hybrid constructs, shrinking is a major drawback since it may cause stress at the interface and lead to loss of construct integrity. A collagen type VI staining was performed to visualize chondron formation. Chondrons are chondrocytes with their pericellular matrix, consisting of proteoglycans, collagen types II and VI<sup>54</sup>, and are known to be more active in matrix deposition than chondrocytes<sup>55</sup>. In hydrogels M, collagen type VI positive areas were found around the cells after 28 and 42 days of culture, indicating that chondrocytes formed chondron-like structures during culture. In fibrin samples a slight overall positive collagen type VI staining was found. Further, only limited positive staining for collagen type I was observed in all hydrogel samples, suggesting limited dedifferentiation of the embedded chondrocytes.

Quantitative measurements were performed for GAG, DNA and water content. However, a large variation in cell performance of the three different equine donors (age 3-10 years old) was observed (Figure 3), which is in line with previous reported studies<sup>56</sup>. GAG content normalized to DNA content (GAG/DNA) was similar in M hydrogels at days 28 and 42 ( $27 \pm 9 \mu\text{g}/\mu\text{g}$  and  $26 \pm 10 \mu\text{g}/\mu\text{g}$ , respectively, Figure 3a). At day 28, GAG/DNA was statistically higher compared to the fibrin control gels ( $16 \pm 6 \mu\text{g}/\mu\text{g}$ , Figure 3a) at this time point. After 42 days of culture both hydrogel formulations performed equally. The GAG content normalized to the dry weight of both the M and fibrin hydrogels increased with time (Figure 3b and 3e). However, DNA levels normalized to the dry weight only showed a significant increase for the M hydrogels over time ( $0.52 \pm 0.18 \mu\text{g}/\text{mg}$  at day 0 and  $0.81 \pm 0.30 \mu\text{g}/\text{mg}$  at day 42, Figure 3c), indicating cell proliferation. Finally, higher GAG/dry weight and DNA/dry weight values were found for fibrin gels compared to hydrogels with formulation M, which can be explained by the compaction and relatively fast degradation of the fibrin gels. In addition, M hydrogels seemed to swell during cultures as the  $\text{H}_2\text{O}/\text{dry weight}$  increased during culture. Thus, chondrocytes in hydrogels with formulation M produced similar levels of cartilage-like matrix compared to chondrocytes in fibrin gels. In addition, no compaction occurred for M hydrogels. Encouraged by these results, hydrogels with formulation M were further evaluated and CSMA and HAMA were incorporated to optimize the mechanical properties, degradation kinetics, and printability.

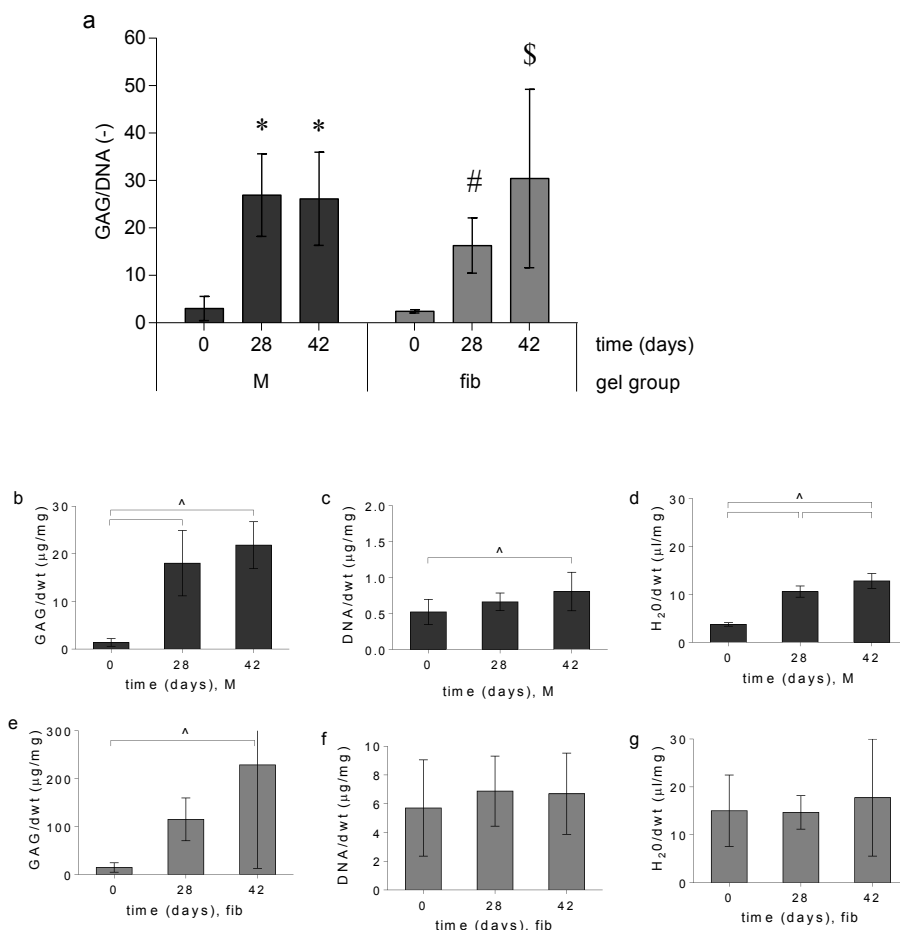


**Figure 3.** Quantitative GAG, DNA, and water measurements for equine chondrocytes encapsulated in  $M_{10}P_{10}$ -based hydrogels (M) and fibrin (fib) gels. a) GAG content normalized to DNA for both hydrogels over time. \* denotes significant differences compared to day 0; # indicates that the group is significantly higher than the day 0 controls but lower compared to fibrin day 42. \$ indicates that the group is significantly higher than the day 0 controls and day 28 fibrin samples but equal to the M hydrogels at days 28 and 42. b, c, d) GAG, DNA and water content normalized to the dry weight (dwt) for M hydrogels over time, respectively. e, f, g) GAG, DNA, and water content, respectively, normalized to the dry weight (dwt) for fibrin gels over time. ^ indicates a significant difference between groups.

### 3.3.3 Thermo-gelation of polymer mixtures before chemical cross-linking

Figure 4 shows storage and loss moduli,  $G'$  and  $G''$ , as a function of temperature for all polymer mixtures. Mixtures based only on  $M_{10}P_{10}$ , exhibited an increase of  $G'$  when increasing the temperature, up to  $29 \pm 2$  Pa at  $50^\circ\text{C}$ , while  $G''$  displayed higher values over the whole temperature range (Figure 4a).

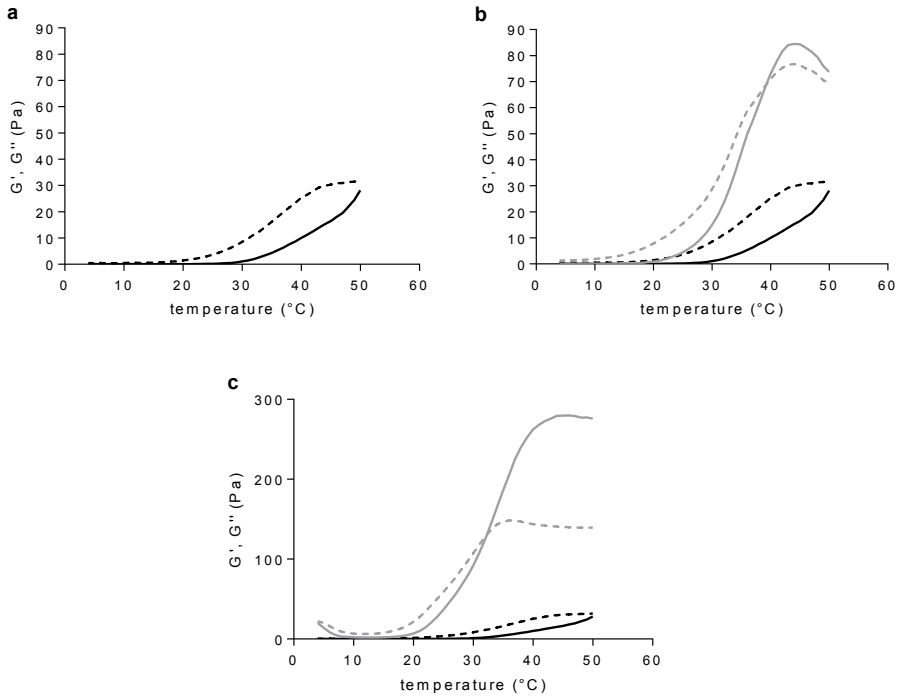


**Figure 4.** Rheograms of polymer mixtures.  $G'$  (solid line) and  $G''$  (dotted line) moduli as a function of temperature, recorded during a temperature sweep experiment from 4 to 50 °C. a) hydrogels based on 18% (w/w)  $M_{10}P_{10}$  (M hydrogels). b) hydrogels based on 14% (w/w)  $M_{10}P_{10}$  and 4% (w/w) CSMA (MCS hydrogels, grey lines) compared with M hydrogels (black lines). c) hydrogels based on 14% (w/w)  $M_{10}P_{10}$  and 0.9% (w/w) HAMA (MHA hydrogels, grey lines) compared with M hydrogels (black lines).

$M_{10}P_{10}$  is a thermo-sensitive polymer capable to self-assemble and to form hydrophobic domains above defined temperatures, leading to a physical gel within a certain range of concentrations<sup>13</sup>. The absence of a gelation temperature ( $T_{gel}$ ), here defined as the temperature at which  $G'$  crosses  $G''$ , as well as the low value of  $G'$  reached upon rising the temperature for polymer mixture M, is due to the relatively low concentration and high CP (20 °C) of the thermo-sensitive polymer used in this study. Figures 4b and 4c show that a continuous increase in  $G'$  as a function of temperature was observed for aqueous systems of MCS and MHA. The values of the storage modulus at 37 and 50 °C were  $56 \pm 6$  and  $84 \pm 24$  Pa, respectively, for MCS hydrogels, and  $216 \pm 14$  and  $263 \pm 12$  Pa, respectively, for MHA hydrogels. For both MCS and MHA mixtures a  $T_{gel}$  was found (39 °C for MCS hydrogels and 32 °C for MHA hydrogels). In line with previous findings, it can be observed that the partial replacement of  $M_{10}P_{10}$  with CSMA or HAMA resulted in the formation of physical



gels with much higher  $G'$  values above 20 °C than polymer mixtures only composed of  $M_{10}P_{10}$ <sup>38</sup>. The beneficial role of the added polysaccharide on the mechanical properties of the hydrogel is more remarkable for MHA hydrogels, where an even lower total polymer concentration (Table 1) led to the formation of the stiffest hydrogel ( $G' = 216 \pm 14$  at 37 °C). The rheological behavior of the polysaccharide-enriched formulations clearly shows that the elastic properties of hydrogels based on  $M_{10}P_{10}$  can be improved by the addition of polysaccharides, without increasing the total polymer concentration.

### 3.3.4 Mechanical properties and *in vitro* swelling-degradation behavior of chemically cross-linked hydrogels

The injection of polymer mixtures in a Teflon mold at 4 °C, followed by a temperature increase to 37 °C and UV irradiation for 15 min, resulted in the formation of cylindrically shaped constructs. Figure 5 shows the Young's moduli for the different hydrogel constructs after 3 hours of swelling in PBS.

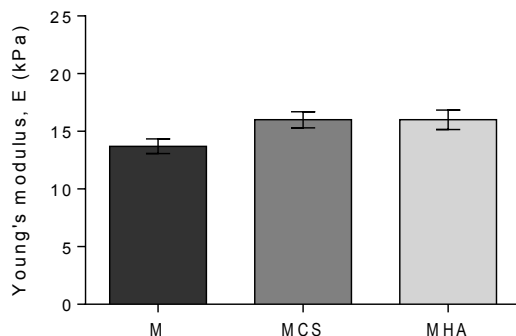


**Figure 5.** Dynamic mechanical analysis on chemically cross-linked hydrogels. Young's moduli for hydrogels based on  $M_{10}P_{10}$  (M), hydrogels based on  $M_{10}P_{10}$  and CSMA (MCS) and hydrogels based on  $M_{10}P_{10}$  and HAMA (MHA), measured under unconfined compression ( $n = 3$ ).

The Young's modulus values were  $13.7 \pm 1.1$ ,  $16.0 \pm 1.4$  and  $16.0 \pm 1.9$  kPa, for M, MCS and MHA hydrogels, respectively. No significant differences between the three hydrogel formulations were found. Hence, no differences in cell response due to different mechanical stimuli can be expected in the three hydrogels. The influence of polysaccharide molecular weight on the final stiffness can be illustrated by comparing MCS and MHA hydrogels. Hydrogels with comparable Young's moduli were obtained, despite the much lower concentration of the higher MW polysaccharide (0.9% vs. 4%) and the lower number of methacrylate groups in MHA hydrogels, calculated considering the slight difference in DM of the two polysaccharides (Figure 5). In line, the positive influence of HA with higher MW has been reported previously for hybrid hydrogel systems based on acrylated HA and thiol-modified 4-arm PEG or thiol-derivatives of HA and PEG-vinylsulfones,

cross-linked via Michael addition-type reaction<sup>57,58</sup>. As can be expected for hydrogel materials, the stiffness of these hydrogel constructs is significantly lower than that of native cartilage (400-800 kPa<sup>59-61</sup>).

Figure 6 shows that M hydrogels initially swelled for 38 days during which the SR reached a maximum of  $2.3 \pm 0.1$ . Complete degradation occurred in 56 days of incubation at 37 °C. This degradation profile is in line with previously reported studies<sup>8,13</sup>.

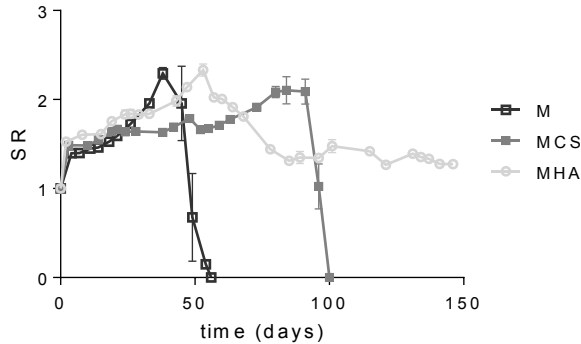


**Figure 6.** Swelling and degradation profiles for hydrogels based on  $M_{10}P_{10}$  (M), hydrogels based on  $M_{10}P_{10}$  and CSMA (MCS), and hydrogels based on  $M_{10}P_{10}$  and HAMA (MHA) in PBS buffer at 37 °C. Error bars represent the standard deviation of experiments performed in triplicate. SR represents the swelling ratio and was calculated according to equation 1.

The degradability of hydrogels based on chemically cross-linked polyHPMA-lac-PEG triblock copolymers at pH 7.4 and 37 °C is due to the hydrolysis of several ester bonds<sup>9</sup>. The first soluble degradation products are lactic acid units obtained by the hydrolysis of OH-terminated lactate side chains. Consequently, the remaining gel matrix exhibits an increased hydrophilic character with a higher water-uptake capacity, leading to the typical swelling phase. Mass loss is seen when the elimination of the water-soluble degradation products from the matrix exceeds the water uptake. This swelling-degradation behavior might also explain the absence of GAG increase in the chondrocyte laden M hydrogels between 28 and 42 days of culture. The swelling process and the presence of a partially degraded and thus less dense hydrogel matrix between day 28 and 42 may have contributed to the leaching of newly formed GAGs out of the gel<sup>62</sup>.

In contrast to M hydrogels, the hydrogels containing polysaccharides degraded much slower (Figure 6). More specifically, MCS hydrogels swelled for 91 days with a maximum SR of  $2.1 \pm 0.2$  and underwent complete disintegration in 100 days, whereas the degradation profile of MHA hydrogels showed a maximum in the SR of  $2.3 \pm 0.1$  at day 53, followed by partial mass loss during the subsequent 32 days and reached a plateau in SR of 1.4 for the subsequent 61 days of monitoring. Thus, the

presence of the two polysaccharides, increased the stability of the hydrogels under the tested conditions. In fact, the loss of polysaccharides from these hydrogels can only occur after the polysaccharide molecules diffuse out of the hydrogel matrix and are dissolved in the surrounding buffer. This phenomenon can take place only after complete hydrolysis of the ester bonds of the polymerized methacrylate groups, which connect a polysaccharide chain to another polysaccharide or  $M_{10}P_{10}$  chain. However, it has been reported that polymerized methacrylate groups directly attached to polysaccharide chains are very stable at pH 7.4 and 37 °C<sup>63,64</sup>. Therefore, it was not surprising that no complete degradation of MHA hydrogels was observed under the applied conditions. Taking this in mind, the full mass loss observed for MCS hydrogels after 100 days can be ascribed to disintegration of the macroscopic hydrogel in smaller fragments, which is confirmed by the observation that the PBS buffer was slightly turbid during the last days of the study.

In general, the highest stability of the hydrogels is observed when  $M_{10}P_{10}$  is partially replaced by HA (MHA hydrogels) at the tested concentrations. Nevertheless, it should be taken into consideration that the degradation profile of the polysaccharide-enriched hydrogels would likely be different if tested *in vivo*, because of the role played by enzymatic degradation via *e.g.* hyaluronidase<sup>65</sup>.

### 3.3.5 Three dimensional printing of hydrogels

Shape stable, 3D printed hydrogel constructs with highly regular internal porosity were obtained, when printing MHA hydrogels, above the  $T_{gel}$  (Figure 7a-c). Polymer mixtures M and MSC could not be printed with high shape fidelity at cell friendly temperature, as polymer mixture M did not form a stable physical gel below 40 °C and the MCS polymer mixture had a too low viscosity at 37 °C, forming only a weak physical gel at cell friendly temperatures. In line with previous observations, polymer mixtures exhibiting physical hydrogel formation and a relatively high  $G'$  (216±14 Pa) at 37 °C allowed adequate stability of the extruded filaments on the deposition plate (pre-heated at 40 °C), and thus 3D printing with high shape fidelity (MHA hydrogels)<sup>38</sup>. On the contrary, the rheological properties of MCS polymer mixture were found insufficient for successful 3D printing.

Fluorescent microbeads with similar sizes as cells (diameter = 15 μm), were homogeneously dispersed in the MHA polymer mixture before printing. This homogeneous distribution was maintained during the printing process (Figure 7d). To investigate the influence of printing on cell viability, primary chondrocytes were dispersed in the three polymer mixtures (M, MCS and MHA) and 3D constructs were printed. The cell viability was found to be between 85% and 95%, at both 1 and 7 days after printing, similar to those of the cast hydrogel controls (Figure 7e) indicating good biocompatibility for all three hydrogel formulations and no adverse effects due to the printing procedure.

In a previous study, a hydrogel based on cross-linkable pHPMA-lac-PEG triblock copolymers was used to print porous 3D structures. However, this required a relatively high polymer concentration (25% w/w) and DM (30%)<sup>10</sup>. The addition of HAMA has led to a hydrogel platform that could be printed at a considerable

lower concentration (14%  $M_{10}P_{10}$  + 0.9% HAMA) and DM of the thermo-sensitive polymer (10%), which is likely beneficial for the cartilage-like matrix deposition of incorporated cells<sup>20,21</sup>.

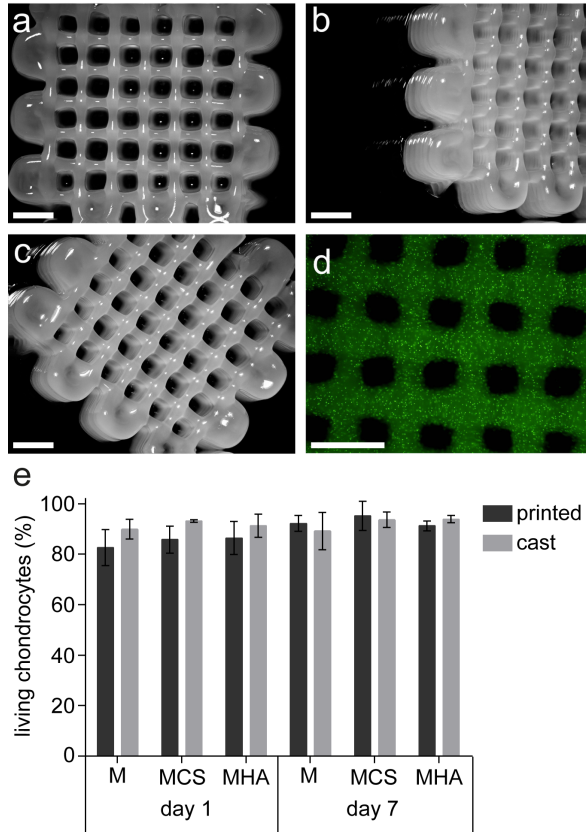


**Figure 7.** 3D printed porous constructs based on MHA. a) top view. b) top-side view. c) top-corner view. d) top view showing a homogeneous distribution of encapsulated green fluorescent beads. e) percentage of living chondrocytes in printed and cast (control) constructs for each hydrogel formulation after 1 and 7 days of culture. No statistical differences were observed between hydrogel formulations. Scale bar represents 2 mm.

In addition, the presence of HAMA itself is likely to improve the cartilage-like tissue production and remodeling by embedded chondrocytes<sup>23,24,29–34,66</sup>. In fact, the differentiation potential of chondrocytes in hydrogels with formulation MHA (and MCS) was confirmed by collagen type II detection after 42 days of culture (Figure S3). Nevertheless, the exact concentration of HAMA still needs further attention for this aspect, as studies have reported a dose-dependent effect in which high HA(MA) concentrations exhibit a less stimulating effect or even a reduction in cartilage-like tissue formation of chondrocytes compared to a lower HA(MA) concentration<sup>24,67–71</sup>. Taken together, the partial replacement of pHPMA-lac-PEG triblock copolymer

with a low amount of HAMA, in combination with a layer-by-layer UV irradiation strategy during the printing process, is a promising approach for cell-friendly additive manufacturing of these hydrogels.

### 3.4 Conclusions

In this study, UV cross-linked hydrogels based on thermo-sensitive methacrylated pHPMA-lac-PEG triblock copolymer, laden with equine chondrocytes showed potential for significant cartilage-like tissue formation *in vitro*. Additionally, mechanical analysis and swelling/degradation studies proved that the partial replacement of methacrylated pHPMA-lac-PEG triblock copolymer with CSMA or HAMA can lead to the design of hydrogels with an improved thermo-sensitive profile, a similar stiffness after UV cross-linking, and a slower degradation rate compared to hydrogels consisting of only pHPMA-lac-PEG triblock copolymers. Moreover, hydrogels containing HAMA (MHA hydrogels) were used to 3D bioprint porous structures without adversely affecting cell viability. Taken together, MHA hydrogels are attractive systems for the design of 3D cell-laden constructs for cartilage regeneration.

#### Acknowledgments

The research leading to these results has received funding from the Dutch Arthritis Foundation (LLP-12), the European Community's Seventh Framework Programme (FP7/2007-2013) under grant agreement n°309962 (HydroZONES) and the European Research Council under grant agreement n°647426 (3D-JOINT). The authors would like to thank Mattie H. P. van Rijen and Caroline C. Tippet for their assistance with the histology and biochemical assays, as well as Paola Marica for her contribution to the synthesis of methacrylated chondroitin sulfate. The primary antibody against collagen type II (II-II6B3) and collagen type VI (5C6), developed by T. F. Linsenmayer and E. S. Engvall respectively, were obtained from the DSHB developed under the auspices of the NICHD and maintained by The University of Iowa, Department of Biology, Iowa City, IA 52242.

## Supporting information

### S1 GPC characterization of chondroitin sulfate (CS)

#### S1.1 Methods

For the detection of the absolute molecular weight of CS, a Viscotek GPC solvent/sample delivery module (GPCmax) coupled with a Triple Detector Array (TDA 302) from Malvern (Malvern, UK), including Refractive Index (RI) and Light Scattering (LS) detectors as well as viscometer, was used. Samples of 5 mg/ml in PBS were injected in PL Aquagel Mixed Column under a flow of 1 ml/min, using PBS as eluent. A solution of Pullulan-P77K from Malvern ( $dn/dc = 0.147$ ;  $M_w = 76,681$  Da;  $M_n = 72,167$  Da) in 0.3 M sodium acetate buffer (pH 6.5) was used as a standard. Data were processed using Omniseq software 4.7.

#### S1.2 Results

Figure S1 shows the RI and Right Angle LS chromatograms obtained for CS. The presence of two partially overlapping peaks indicates the co-existence of two MW distributions.

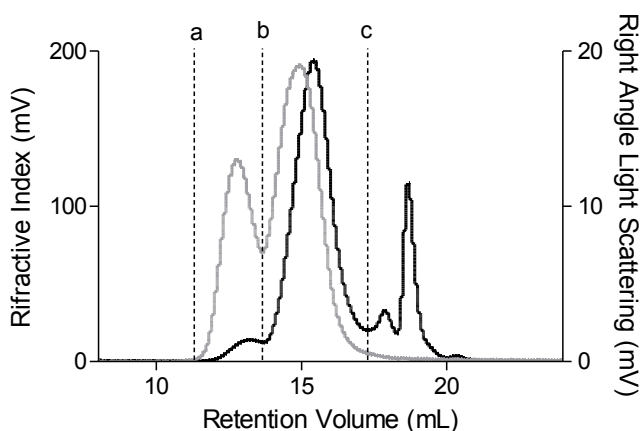


**Figure S1.** GPC-RI (black line, left Y axis, range = 0-200 mV) and -LS (grey line, right Y axis, range = 0-20 mV) chromatogram enlargement (X axis range = 8-24 ml) for CS. The peaks included between lines a and b are attributed to the higher molecular weight chains, whereas those included between lines b and c are representative of the smaller molecular weight chains.

Using the area under the RI peaks, it was found that 6% in weight is composed of polymer chains with a  $M_n$  of 353.8 kDa and a  $M_w$  of 457.5 kDa ( $PDI = 1.3$ ) and the remaining fraction of 94% showed a  $M_n$  of 26.9 kDa and a  $M_w$  of 36.3 kDa ( $PDI = 1.4$ ). It needs to be noticed that the remarkable difference in intensity between the two peaks visible in the RI detection graph is less evident in the LS chromatogram. This is due to the fact that high MW chains give much higher LS signal compared with low MW chains under the same conditions. The  $dn/dc$  found for CS was 0.1136.

## S2 Identification of the linear viscoelastic range (LVR) for physical gels

### S2.1 Methods

For the identification of the Linear Viscoelastic Range (LVR), each gel ( $n = 3$ ) was studied at 37 °C in oscillation amplitude sweep mode (strain sweep from 0.01 to 100%, frequency = 1Hz), using an AR G-2 rheometer (TA-Instruments, Etten-Leur, The Netherlands), equipped with a cone-plate measuring geometry (cone diameter: 20 mm, angle: 1°).

### S2.2 Results

For all thermal gels a LVR from 0.01 to 5-10% was found, after which  $G'$  decreased by increasing the strain (Figure S2). Only MHA gels showed a value of  $G'$  higher than  $G''$  at 37 °C and this is in line with the results found during the temperature sweep runs.

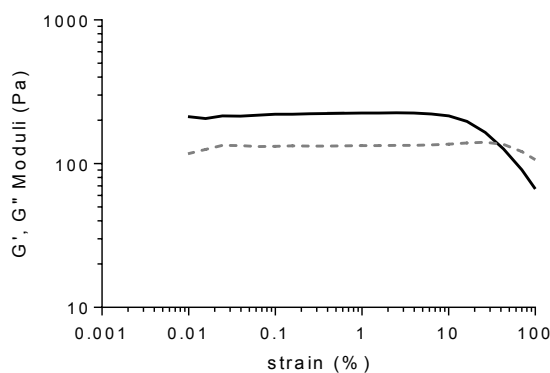


**Figure S2.**  $G'$  (full black line) and  $G''$  (dotted grey line) as function of strain, recorded during a strain sweep experiment for MHA hydrogels (strain ramp from 0.01 to 100%).



### S3 3D printing settings

**Table S1.** Input parameters for creating 3D printed constructs.

Parameter	Value
<p><i>Construct</i></p> <ul style="list-style-type: none"> <li>• Dimensions (LxWxH) [mm]</li> <li>• Line spacing [mm]</li> <li>• Layer height [mm]</li> </ul>	<p>12x12x2 or 10.4x10.4x2 mm 1.5 or 1.3 0.1</p>
<p><i>Microvalve CF300H</i></p> <ul style="list-style-type: none"> <li>• Inner diameter [mm]</li> <li>• Stroke [mm]</li> <li>• Temperature [°C]</li> <li>• Needle inner diameter [mm]</li> <li>• Valve opening time [<math>\mu</math>s]</li> <li>• Dosing distance [mm]</li> </ul>	<p>0.3 0.06 37 0.3 1000 0.05</p>
<p><i>Hönle Bluepoint 4</i></p> <ul style="list-style-type: none"> <li>• Distance to sample [mm]</li> <li>• Intensity at 50 mm [<math>\text{mW}/\text{cm}^2</math>]</li> <li>• Illumination time (each deposited layer) [s]</li> <li>• Post-curing time [s]</li> <li>• <math>\lambda_{\text{em}}</math> [nm]</li> </ul>	<p>50 103 3 9 350 – 450</p>
<p><i>RegenHU 3DDiscovery</i></p> <ul style="list-style-type: none"> <li>• Baseplate temperature [°C]</li> <li>• Gel cartridge temperature [°C]</li> <li>• Speed XY [mm/s]</li> <li>• Pressure [bar]</li> </ul>	<p>40 37 35 1.5</p>

### S4 Differentiation potential of chondrocytes in MCS and MHA hydrogels

#### S4.1 Methods

Equine chondrocytes ( $n = 3$ ,  $15\text{-}20 \cdot 10^6$ , passage 1) were encapsulated in MCS and MHA polymer solutions. Cell laden hydrogels were cast, UV cross-linked, and cultured as described for hydrogels M. To evaluate if chondrocytes had the potential to differentiate and deposit matrix, immunohistochemistry for collagen type II was performed (section 3.2.7).

### S4.2 Results

In MCS and more dominantly in MHA hydrogels, positive areas for collagen type II were observed after 42 days of culture (Figure S3). During this long term culture, cells also maintained their typical round morphology. These aspects indicate that MCS and especially MHA hydrogels have the potential to be used for the fabrication of constructs for cartilage repair.

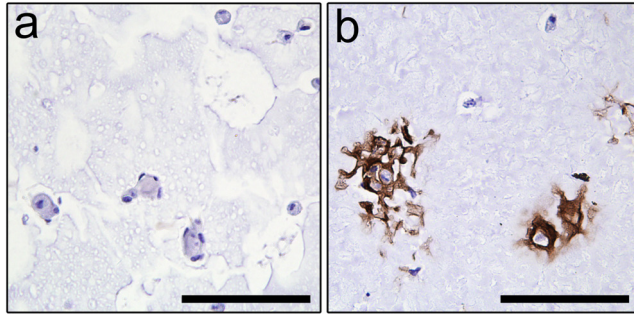


**Figure S3.** Immunohistochemistry for collagen type II (brown) of chondrocytes differentiated in MCS (a) and MHA (b) hydrogels for 42 days. Scale bar represents 100  $\mu\text{m}$ .

## References

- (1) Almarza, A. J.; Athanasiou, K. A. Design Characteristics for the Tissue Engineering of Cartilaginous Tissues. *Ann. Biomed. Eng.* **2004**, *32* (1), 2–17.
- (2) Prakash, D.; Learmonth, D. Natural Progression of Osteo-Chondral Defect in the Femoral Condyle. *Knee* **2002**, *9* (1), 7–10.
- (3) Hutmacher, D. W. Scaffold Design and Fabrication Technologies for Engineering Tissues — State of the Art and Future Perspectives. *J. Biomater. Sci. Polym. Ed.* **2001**, *12* (1), 107–124.
- (4) Vermonden, T.; Censi, R.; Hennink, W. E. Hydrogels for Protein Delivery. *Chem. Rev.* **2012**, *112* (5), 2853–2888.
- (5) Appel, E. A.; del Barrio, J.; Loh, X. J.; Scherman, O. A. Supramolecular Polymeric Hydrogels. *Chem. Soc. Rev.* **2012**, *41* (18), 6195.
- (6) Annabi, N.; Tamayol, A.; Uquillas, J. A.; Akbari, M.; Bertassoni, L. E.; Cha, C.; Camci-Unal, G.; Dokmeci, M. R.; Peppas, N. A.; Khademhosseini, A. 25th Anniversary Article: Rational Design and Applications of Hydrogels in Regenerative Medicine. *Adv. Mater.* **2014**, *26* (1), 85–124.
- (7) Malda, J.; Visser, J.; Melchels, F. P.; Jüngst, T.; Hennink, W. E.; Dhert, W. J. A.; Groll, J.; Hutmacher, D. W. 25th Anniversary Article: Engineering Hydrogels for Biofabrication. *Adv. Mater.* **2013**, *25* (36), 5011–5028.
- (8) Censi, R.; Vermonden, T.; van Steenbergen, M. J.; Deschout, H.; Braeckmans, K.; De Smedt, S. C.; van Nostrum, C. F.; di Martino, P.; Hennink, W. E. Photopolymerized Thermosensitive Hydrogels for Tailorable Diffusion-Controlled Protein Delivery. *J. Control. Release* **2009**, *140* (3), 230–236.
- (9) Censi, R.; Vermonden, T.; Deschout, H.; Braeckmans, K.; di Martino, P.; De Smedt, S. C.; van Nostrum, C. F.; Hennink, W. E. Photopolymerized Thermosensitive poly(HPMA lactate)-PEG-Based Hydrogels: Effect of Network Design on Mechanical Properties, Degradation, and Release Behavior. *Biomacromolecules* **2010**, *11* (8), 2143–2151.
- (10) Censi, R.; Schuurman, W.; Malda, J.; di Dato, G.; Burgisser, P. E.; Dhert, W. J. A.; van Nostrum, C. F.; di Martino, P.; Vermonden, T.; Hennink, W. E. A Printable Photopolymerizable Thermosensitive p(HPMAm-Lactate)-PEG Hydrogel for Tissue Engineering. *Adv. Funct. Mater.* **2011**, *21* (10), 1833–1842.
- (11) Vermonden, T.; Jena, S. S.; Barriet, D.; Censi, R.; van der Gucht, J.; Hennink, W. E.; Siegel, R. A. Macromolecular Diffusion in Self-Assembling Biodegradable Thermosensitive Hydrogels. *Macromolecules* **2010**, *43* (2), 782–789.
- (12) Censi, R.; van Putten, S.; Vermonden, T.; di Martino, P.; van Nostrum, C. F.; Harmsen, M. C.; Bank, R. a; Hennink, W. E. The Tissue Response to Photopolymerized PEG-p(HPMAm-Lactate)-Based Hydrogels. *J. Biomed. Mater. Res. A* **2011**, *97* (3), 219–229.
- (13) Vermonden, T.; Fedorovich, N. E.; van Geemen, D.; Alblas, J.; van Nostrum, C. F.; Dhert, W. J. A.; Hennink, W. E. Photopolymerized Thermosensitive Hydrogels: Synthesis, Degradation, and Cytocompatibility. *Biomacromolecules* **2008**, *9* (3), 919–926.
- (14) Vermonden, T.; Besseling, N. A. M.; van Steenbergen, M. J.; Hennink, W. E. Rheological Studies of Thermosensitive Triblock Copolymer Hydrogels. *Langmuir* **2006**, *22* (24), 10180–10184.

- (15) Klein, T. J.; Rizzi, S. C.; Reichert, J. C.; Georgi, N.; Malda, J.; Schuurman, W.; Crawford, R. W.; Hutmacher, D. W. Strategies for Zonal Cartilage Repair Using Hydrogels. *Macromol. Biosci.* **2009**, *9* (11), 1049–1058.
- (16) Visser, J.; Peters, B.; Burger, T. J.; Boomstra, J.; Dhert, W. J. A.; Melchels, F. P. W.; Malda, J. Biofabrication of Multi-Material Anatomically Shaped Tissue Constructs. *Biofabrication* **2013**, *5* (3), 35007.
- (17) Melchels, F. P. W.; Domingos, M. A. N.; Klein, T. J.; Malda, J.; Bartolo, P. J.; Hutmacher, D. W. Additive Manufacturing of Tissues and Organs. *Prog. Polym. Sci.* **2012**, *37* (8), 1079–1104.
- (18) Levato, R.; Visser, J.; Planell, J. A.; Engel, E.; Malda, J.; Mateos-Timoneda, M. A. Biofabrication of Tissue Constructs by 3D Bioprinting of Cell-Laden Microcarriers. *Biofabrication* **2014**, *6* (3), 35020, 1–12.
- (19) Groll, J.; Boland, T.; Blunk, T.; Burdick, J. A.; Cho, D.-W.; Dalton, P. D.; Derby, B.; Forgacs, G.; Li, Q.; Mironov, V. A.; Moroni, L.; Nakamura, M.; Shu, W.; Takeuchi, S.; Vozzi, G.; Woodfield, T. B. F.; Xu, T.; Yoo, J. J.; Malda, J. Biofabrication: Reappraising the Definition in an Evolving Field. *Biofabrication* **2016**, *8*, 13001, 1–6.
- (20) Seliktar, D. Designing Cell-Compatible Hydrogels for Biomedical Applications. *Science* **2012**, *336* (6085), 1124–1128.
- (21) Bryant, S. J.; Anseth, K. S. Hydrogel Properties Influence ECM Production by Chondrocytes Photoencapsulated in Poly (Ethylene Glycol) Hydrogels. *J. Biomed. Mater. Res.* **2001**, *59* (1), 63–71.
- (22) Schuurman, W.; Levett, P. A.; Pot, M. W.; van Weeren, P. R.; Dhert, W. J. A.; Hutmacher, D. W.; Melchels, F. P. W.; Klein, T. J.; Malda, J. Gelatin-Methacrylamide Hydrogels as Potential Biomaterials for Fabrication of Tissue-Engineered Cartilage Constructs. *Macromol. Biosci.* **2013**, *13* (5), 551–561.
- (23) Levett, P. A.; Hutmacher, D. W.; Malda, J.; Klein, T. J. Hyaluronic Acid Enhances the Mechanical Properties of Tissue-Engineered Cartilage Constructs. *PLoS One* **2014**, *9* (12), e113216.
- (24) Levett, P. A.; Melchels, F. P. W.; Schrobback, K.; Hutmacher, D. W.; Malda, J.; Klein, T. J. A Biomimetic Extracellular Matrix for Cartilage Tissue Engineering Centered on Photocurable Gelatin, Hyaluronic Acid and Chondroitin Sulfate. *Acta Biomater.* **2014**, *10* (1), 214–223.
- (25) Choi, B.; Kim, S.; Lin, B.; Wu, B. M.; Lee, M. Cartilaginous Extracellular Matrix-Modified Chitosan Hydrogels for Cartilage Tissue Engineering. *Appl. Mater. Interfaces* **2014**, *6*, 20110–20121.
- (26) Shim, J.-H.; Jang, K.-M.; Hahn, S. K.; Park, J. Y.; Jung, H.; Oh, K.; Park, K. M.; Yeom, J.; Park, S. H.; Kim, S. W.; Wang, J. H.; Kim, K.; Cho, D.-W. Three-Dimensional Bioprinting of Multilayered Constructs Containing Human Mesenchymal Stromal Cells for Osteochondral Tissue Regeneration in the Rabbit Knee Joint. *Biofabrication* **2016**, *8* (1), 14102.
- (27) Oudshoorn, M. H. M.; Rissmann, R.; Bouwstra, J. A.; Hennink, W. E. Synthesis of Methacrylated Hyaluronic Acid with Tailored Degree of Substitution. *Polymer* **2007**, *48* (7), 1915–1920.
- (28) Hachet, E.; Van Den Berghe, H.; Bayma, E.; Block, M. R.; Auzély-Velty, R. Design of Biomimetic Cell-Interactive Substrates Using Hyaluronic Acid Hydrogels with Tunable Mechanical Properties. *Biomacromolecules* **2012**, *13* (6), 1818–1827.

- (29) Lesley, J.; Hascall, V. C.; Tammi, M.; Hyman, R. Hyaluronan Binding by Cell Surface CD44. *J. Biol. Chem.* **2000**, *275* (35), 26967–26975.
- (30) Chung, C.; Erickson, I. E.; Mauck, R. L.; Burdick, J. a. Differential Behavior of Auricular and Articular Chondrocytes in Hyaluronic Acid Hydrogels. *Tissue Eng. Part A* **2008**, *14* (7), 1121–1131.
- (31) Park, S. H.; Park, S. R.; Chung, S. I.; Pai, K. S.; Min, B. H. Tissue-Engineered Cartilage Using Fibrin / Hyaluronan Composite Gel and Its In Vivo Implantation. *Artif. Organs* **2005**, *29* (10), 838–860.
- (32) Dinescu, S.; Gălățeanu, B.; Albu, M.; Lungu, A.; Radu, E.; Hermenean, A.; Costache, M. Biocompatibility Assessment of Novel Collagen-Sericin Scaffolds Improved with Hyaluronic Acid and Chondroitin Sulfate for Cartilage Regeneration. *Biomed Res. Int.* **2013**, *2013*, 1–11.
- (33) Park, H.; Choi, B.; Hu, J.; Lee, M. Injectable Chitosan Hyaluronic Acid Hydrogels for Cartilage Tissue Engineering. *Acta Biomater.* **2013**, *9* (1), 4779–4786.
- (34) Roberts, J. J.; Nicodemus, G. D.; Ciunta, S.; Bryant, S. J. Incorporation of Biomimetic Matrix Molecules in PEG Hydrogels Enhances Matrix Deposition and Reduces Load-Induced Loss of Chondrocyte-Secreted Matrix. *J. Biomed Mater Res A* **2011**, *97* (3), 281–291.
- (35) Oupický, D.; Konák, C.; Ulbrich, K. DNA Complexes with Block and Graft Copolymers of N-(2-Hydroxypropyl)methacrylamide and 2-(Trimethylammonio)ethyl Methacrylate. *J. Biomater. Sci. Polym. Ed.* **1999**, *10* (5), 573–590.
- (36) Neradovic, D.; van Steenberg, M. J.; Vansteelant, L.; Meijer, Y. J.; van Nostrum, C. F.; Hennink, W. E. Degradation Mechanism and Kinetics of Thermosensitive Polyacrylamides Containing Lactic Acid Side Chains. *Macromolecules* **2003**, *36* (20), 7491–7498.
- (37) Neradovic, D.; van Nostrum, C. F.; Hennink, W. E. Thermoresponsive Polymeric Micelles with Controlled Instability Based on Hydrolytically Sensitive N-Isopropylacrylamide Copolymers. *Macromolecules* **2001**, *34* (22), 7589–7591.
- (38) Abbadessa, A.; Blokzijl, M. M.; Mouser, V. H. M.; Marica, P.; Malda, J.; Hennink, W. E.; Vermonden, T. A Thermo-Responsive and Photo-Polymerizable Chondroitin Sulfate-Based Hydrogel for 3D Printing Applications. *Carbohydr. Polym.* **2016**, *149*, 163–174.
- (39) Stenekes, R. J. H.; Hennink, W. E. Polymerization Kinetics of Dextran-Bound Methacrylate in an Aqueous Two Phase System. *Polymer* **2000**, *41* (15), 5563–5569.
- (40) Benya, P. D.; Shaffer, J. D. Dedifferentiated Chondrocytes Reexpress the Differentiated Collagen Phenotype When Cultured in Agarose Gels. *Cell* **1982**, *30* (1), 215–224.
- (41) Guo, J.; Jourdian, G. W.; Maccallum, D. K. Culture and Growth Characteristics of Chondrocytes Encapsulated in Alginate Beads. *Connect. Tissue Res.* **1989**, *19* (2–4), 277–297.
- (42) Rosenberg, L. Chemical Basis for the Histological Use of Safranin O in the Study of Articular Cartilage. *J. Bone Joint Surg. Am.* **1971**, *53* (1), 69–82.
- (43) Farndale, R. W.; Sayers, C. A.; Barrett, A. J. A Direct Spectrophotometric Microassay for Sulfated Glycosaminoglycans in Cartilage Cultures. *Connect. Tissue Res.* **1982**, *9* (4), 247–248.
- (44) Li, Q.; Wang, D.; Elisseeff, J. H. Heterogeneous-Phase Reaction of Glycidyl Methacrylate and Chondroitin Sulfate: Mechanism of Ring-Opening–

- transesterification Competition. *Macromolecules* **2003**, *36* (7), 2556–2562.
- (45) Burdick, J. A.; Chung, C.; Jia, X.; Randolph, M. A.; Langer, R. Controlled Degradation and Mechanical Behavior of Photopolymerized Hyaluronic Acid Networks. *Biomacromolecules* **2005**, *6* (1), 386–391.
- (46) Smeds, K. A.; Grinstaff, M. W. Photocrosslinkable Polysaccharides for in Situ Hydrogel Formation. *J. Biomed. Mater. Res.* **2001**, *54* (1), 115–121.
- (47) Messenger, L.; Portecop, N.; Hachet, E.; Lapeyre, V.; Pignot-Paintrand, I.; Catargi, B.; Auzély-Velty, R.; Ravaine, V. Photochemical Crosslinking of Hyaluronic Acid Confined in Nanoemulsions: Towards Nanogels with a Controlled Structure. *J. Mater. Chem. B* **2013**, *1* (27), 3369–3379.
- (48) Mastbergen, S. C.; Saris, D. B.; Lafeber, F. P. Functional Articular Cartilage Repair: Here, Near, or Is the Best Approach Not yet Clear? *Nat Rev Rheumatol* **2013**, *9* (5), 277–290.
- (49) Brittberg, M. Cell Carriers as the Next Generation of Cell Therapy for Cartilage Repair: A Review of the Matrix-Induced Autologous Chondrocyte Implantation Procedure. *Am. J. Sports Med.* **2010**, *38* (6), 1259–1271.
- (50) Cummings, C. L.; Gawlitta, D.; Nerem, R. M.; Stegemann, J. P. Properties of Engineered Vascular Constructs Made from Collagen, Fibrin, and Collagen–fibrin Mixtures. *Biomaterials* **2004**, *25* (17), 3699–3706.
- (51) Ahmed, T. A. E.; Dare, E. V.; Hincke, M. Fibrin: A Versatile Scaffold for Tissue Engineering Applications. *Tissue Eng. Part B Rev.* **2008**, *14* (2), 199–215.
- (52) Eyrich, D.; Brandl, F.; Appel, B.; Wiese, H.; Maier, G.; Wenzel, M.; Staudenmaier, R.; Goepferich, A.; Blunk, T. Long-Term Stable Fibrin Gels for Cartilage Engineering. *Biomaterials* **2007**, *28* (1), 55–65.
- (53) Visser, J.; Melchels, F. P. W.; Jeon, J. E.; van Bussel, E. M.; Kimpton, L. S.; Byrne, H. M.; Dhert, W. J. A.; Dalton, P. D.; Hutmacher, D. W.; Malda, J. Reinforcement of Hydrogels Using Three-Dimensionally Printed Microfibres. *Nat. Commun.* **2015**, *6*, 6933.
- (54) Poole, C. A.; Ayad, S.; Schofield, J. R. Chondrons from Articular Cartilage: I. Immunolocalization of Type VI Collagen in the Pericellular Capsule of Isolated Canine Tibial Chondrons. *J. Cell Sci.* **1988**, *90* (Pt 4), 635–643.
- (55) Zhang, Z. Chondrons and the Pericellular Matrix of Chondrocytes. *Tissue Eng. Part B Rev.* **2015**, *21* (3), 267–277.
- (56) Visser, J.; Levett, P. A.; te Moller, N. C. R.; Besems, J.; Boere, K. W. M.; van Rijen, M. H. P.; de Grauw, J. C.; Dhert, W. J. A.; van Weeren, P. R.; Malda, J. Crosslinkable Hydrogels Derived from Cartilage, Meniscus, and Tendon Tissue. *Tissue Eng. Part A* **2015**, *21* (7–8), 1195–1206.
- (57) Kim, J.; Park, Y.; Tae, G.; Lee, K. B.; Hwang, C. M.; Hwang, S. J.; Kim, I. S.; Noh, I.; Sun, K. Characterization of Low-Molecular-Weight Hyaluronic Acid-Based Hydrogel and Differential Stem Cell Responses in the Hydrogel Microenvironments. *J. Biomed. Mater. Res. A* **2009**, *88* (4), 967–975.
- (58) Jeong, C. G.; Francisco, A. T.; Niu, Z.; Mancino, R. L.; Craig, S. L.; Setton, L. A. Screening of Hyaluronic Acid-Poly(ethylene Glycol) Composite Hydrogels to Support Intervertebral Disc Cell Biosynthesis Using Artificial Neural Network Analysis. *Acta Biomater.* **2014**, *10* (8), 3421–3430.
- (59) Chen, A. C.; Bae, W. C.; Schinagl, R. M.; Sah, R. L. Depth- and Strain-Dependent Mechanical and Electromechanical Properties of Full-Thickness Bovine Articular



- Cartilage in Confined Compression. *J. Biomech.* **2001**, *34* (1), 1–12.
- (60) Athanasiou, K. A.; Agarwal, A.; Dzida, F. J. Comparative Study of the Intrinsic Mechanical Properties of the Human Acetabular and Femoral Head Cartilage. *J. Orthop. Res.* **1994**, *12* (3), 340–349.
- (61) Jurvelin, J. S.; Buschmann, M. D.; Hunziker, E. B. Optical and Mechanical Determination of Poisson's Ratio of Adult Bovine Humeral Articular Cartilage. *J. Biomech.* **1997**.
- (62) Bolis, S.; Handley, C. J.; Cornper, W. D. Passive Loss of Proteoglycan from Articular Cartilage Explants. *Biochim. Biophys. Acta - Gen. Subj.* **1989**, *993* (2–3), 157–167.
- (63) van Dijk-Wolthuis, W. N. E.; Hoozeboom, J. A. M.; van Steenberghe, M. J.; Tsang, S. K. Y.; Hennink, W. E. Degradation and Release Behavior of Dextran-Based Hydrogels. *Macromolecules* **1997**, *30* (16), 4639–4645.
- (64) van de Wetering, P.; Zuidam, N. J.; van Steenberghe, M. J.; van der Houwen, O. A. G. J.; Underberg, W. J. M.; Hennink, W. E. A Mechanistic Study of the Hydrolytic Stability of Poly(2-(Dimethylamino)ethyl Methacrylate). *Macromolecules* **1998**, *31* (23), 8063–8068.
- (65) Kurisawa, M.; Chung, J. E.; Yang, Y. Y.; Gao, S. J.; Uyama, H. Injectable Biodegradable Hydrogels Composed of Hyaluronic Acid–tyramine Conjugates for Drug Delivery and Tissue Engineering. *Chem. Commun.* **2005**, No. 34, 4312–4314.
- (66) Hwang, N. S.; Varghese, S.; Lee, H. J.; Theprungsirikul, P.; Canver, A.; Sharma, B.; Elisseff, J. Response of Zonal Chondrocytes to Extracellular Matrix-Hydrogels. *FEBS Lett.* **2007**, *581* (22), 4172–4178.
- (67) Akmal, M.; Singh, A.; Anand, A.; Kesani, A.; Aslam, N.; Goodship, A.; Bentley, G. The Effects of Hyaluronic Acid on Articular Chondrocytes. *J. Bone Jt. Surg. - Br. Vol.* **2005**, *87-B* (8), 1143–1149.
- (68) Allemann, F.; Mizuno, S.; Eid, K.; Yates, K. E.; Zaleske, D.; Glowacki, J. Effects of Hyaluronan on Engineered Articular Cartilage Extracellular Matrix Gene Expression in 3-Dimensional Collagen Scaffolds. *J. Biomed. Mater. Res.* **2001**, *55*, 13–19.
- (69) Callahan, L. A. S.; Ganos, A. M.; McBurney, D. L.; Dilisio, M. F.; Weiner, S. D.; Horton, W. E.; Becker, M. L. ECM Production of Primary Human and Bovine Chondrocytes in Hybrid PEG Hydrogels Containing Type I Collagen and Hyaluronic Acid. *Biomacromolecules* **2012**, *13* (5), 1625–1631.
- (70) Kawasaki, K.; Ochi, M.; Uchio, Y.; Adachi, N.; Matsusaki, M. Hyaluronic Acid Enhances Proliferation and Chondroitin Sulfate Synthesis in Cultured Chondrocytes Embedded in Collagen Gels. *J. Cell. Physiol.* **1999**, *179* (June 1998), 142–148.
- (71) Villanueva, I.; Gladem, S. K.; Kessler, J.; Bryant, S. J. Dynamic Loading Stimulates Chondrocyte Biosynthesis When Encapsulated in Charged Hydrogels Prepared from Poly(ethylene Glycol) and Chondroitin Sulfate. *Matrix Biol.* **2010**, *29* (1), 51–62.







## Chapter 4

### **Two-component thermosensitive hydrogels: phase separation affecting rheological behavior**

**A. Abbadessa, M. Landín, E. Oude Blenke, W.E. Hennink, T. Vermonden**

*Submitted for publication*

## Abstract

Hydrogels based on triblock copolymers of polyethylene glycol (PEG) and methacrylated poly(*N*-(2-hydroxypropyl) methacrylamide-mono/dilactate) (pHPMAlac) with thermoresponsive behavior are currently under investigation for tissue engineering applications. When PEG/pHPMAlac triblock copolymers are mixed with methacrylated polysaccharides, mechanical properties and 3D printability are improved compared with hydrogels only composed of thermosensitive copolymers. The aim of this study was to understand the role of phase separation on the mechanical properties. To this end, hydrogels composed of different concentrations of PEG/pHPMAlac and methacrylated hyaluronic acid (HAMA), were analyzed for phase behavior and rheological properties. Subsequently, phase separation and rheological behavior as function of the two polymer concentrations were mathematically processed to generate a predictive model. Results showed that PEG/pHPMAlac/HAMA hydrogels were characterized by hydrophilic, HAMA-rich internal domains dispersed in a more hydrophobic continuous phase, only composed of PEG/pHPMAlac, and that the volume fraction of the dispersed phase increased by increasing HAMA concentration. Storage modulus, yield stress and viscosity increased with increasing HAMA concentration for low/medium HAMA contents ( $\leq 0.75\%$  w/w), while a further increase of HAMA resulted in a decrease of the mentioned properties. On the other hand, by increasing the concentration of PEG/pHPMAlac these rheological properties were enhanced. The generated models had an appropriate fitting with experimental data, and were used to identify an exemplary 3D printability window for PEG/pHPMAlac/HAMA hydrogels, which was verified by rheological characterization and preparation of 3D printed scaffolds. In conclusion, the dependency of phase separation and rheological behavior in PEG/pHPMAlac/HAMA hydrogels is described by complex functions of the two polymer concentrations. The predictive model generated in this study can be used as a valid tool for the identification of hydrogel compositions with desired, selected characteristics.

## 4.1 Introduction

Hydrogels are networks of hydrophilic natural and/or synthetic polymers, able to absorb and retain large amounts of water. Because of their capacity to entrap cells and biologically active molecules, *e.g.* therapeutic proteins, they are currently under investigation for tissue engineering (TE)<sup>1,2</sup> and drug delivery applications<sup>3-8</sup>. Especially for regenerative medicine purposes, hydrogels are of interest because they can mimic the aqueous nature and mechanical properties of soft tissues and warrant a cell-friendly environment<sup>9</sup>. Moreover, biodegradable hydrogels offer a temporary support, which can be progressively replaced by new tissue components, synthesized by embedded or recruited cells<sup>10-12</sup>. In addition, hydrogels having specific rheological properties can be processed into desired shapes by injection molding or more sophisticated three-dimensional (3D) printing-based manufacturing procedures<sup>13-19</sup>. This aspect is especially important to generate patient-customized implants, which eventually may facilitate clinical translation of TE constructs.

Hydrogels based on triblock copolymers of polyethylene glycol (PEG) and methacrylated poly(*N*-(2-hydroxypropyl) methacrylamide-mono/dilactate) (pHPMAlac) have gained interest during the last decade for their tunable thermosensitive behavior, mechanical and degradation profiles as well as 3D printability and cytocompatibility<sup>20-22</sup>. Our more recent studies have shown that by blending these PEG/methacrylated pHPMAlac triblock copolymers with UV cross-linkable polysaccharides, *i.e.* methacrylated chondroitin sulfate<sup>23</sup> or methacrylated hyaluronic acid<sup>24</sup>, hydrogels with improved mechanical characteristics and degradation profiles can be obtained. Specifically, the more pronounced thermosensitivity, shear thinning and yield stress behavior led to a superior 3D printability of hydrogels based on polysaccharides and PEG/methacrylated pHPMAlac copolymers compared with hydrogels only composed of PEG/methacrylated pHPMAlac copolymers<sup>23,24</sup>. Nevertheless, mechanistic insights behind the beneficial effect on mechanical properties due to the addition of polysaccharides to hydrogels of PEG/methacrylated pHPMAlac are lacking. Visual inspection of these hydrogels pointed to the possibility of aqueous two phase separation (ATPS)<sup>23</sup>, similar to that described for some pairs of water soluble polymers, such as the combination of PEG and dextran<sup>25</sup>. The miscibility of two polymers in water is governed by the following equation:

$$\Delta G_{mix} = \Delta H_{mix} - T\Delta S_{mix} \quad \text{Equation 1}$$

where  $\Delta G_{mix}$  is the free energy of mixing,  $\Delta H_{mix}$  is the enthalpy of mixing,  $T$  is the absolute temperature and  $\Delta S_{mix}$  is the entropy of mixing. Phase separation occurs when  $\Delta G_{mix}$  is positive, and this is possible when  $\Delta H_{mix} > 0$  and  $> T\Delta S_{mix}$ . For polymeric mixtures in water, it has been found that  $\Delta S_{mix}$  is usually very low, and thus even small positive values of  $\Delta H_{mix}$  result in positive  $\Delta G_{mix}$  values<sup>25</sup>. ATPS has found valuable applications in polymeric microparticles fabrication<sup>26,27</sup> as well as in the extraction and separation of biological molecules and cell subtypes<sup>28-30</sup>. Moreover,

ATPS-like phenomena have been observed in hydrogels investigated for biomedical applications, and a positive effect on the morphology of embedded cells as well as on the new tissue formation has been reported<sup>31</sup>.

Interestingly, for telechelic ABA-like amphiphilic triblock copolymers, *e.g.* PEG end-capped with aliphatic blocks<sup>32</sup> and PEG flanked by pHPMAlac outer blocks<sup>21,33</sup>, aqueous phase separation has been described in simple binary systems (one type of polymer in water), at certain conditions of polymer concentration and temperature. In this case, phase separation is attributed to the formation of polymer-rich regions composed of highly “packed” and interconnected polymeric clusters (flower-like micelles), and water-rich regions mainly composed of free micelles and hydrated single polymeric chains<sup>34</sup>. Similarly, phase separation observed for hydrogels composed of highly methacrylated hyperbranched polyglycerol, was explained by the co-existence of polymer-rich regions based on partially dehydrated hydrophobic blocks and water-rich regions containing highly hydrated hydrophilic polymeric portions<sup>35</sup>.

Our hypothesis is that ATPS in hydrogels composed of polysaccharides and PEG/methacrylated pHPMAlac copolymers plays an essential role on the thermosensitivity as well as on fluid-flow properties, *e.g.* shear thinning and yield stress of these hydrogels, and consequently on hydrogel 3D printability. To assess this aspect and to provide a full understanding of the inner micro-organization of these hydrogels, polymeric mixtures of methacrylated hyaluronic acid and PEG/methacrylated pHPMAlac copolymer were prepared and analyzed for their hydrophilic/hydrophobic balance, and possible preferential distribution of the two polymers within the hydrogel. Moreover, rheological properties as function of the two polymers' concentration (and phase separation extent) were studied. Finally, to mathematically study the dependency of phase separation extent and rheological properties from the two polymeric contents, and to create a predictive model, experimental data were integrated using Artificial Neural Networks (ANNs). ANNs have been firstly applied in the pharmaceutical field to overcome the shortcomings of the traditional multiple regression analysis<sup>36</sup>. Due to the complexity of the interpretation of ANNs models, they are often combined with other Artificial Intelligence technologies such as fuzzy logic, giving hybrid systems<sup>37,38</sup>. The neurofuzzy logic technology used in this study combines the adaptive learning capabilities from ANNs and the ability to generalize rules of fuzzy. It allows the definition of the design space with a relative small amount of data and the generation of complex non-linear models of easy and quick numerical solutions. Additionally, fuzzy logic technology enables generation of linguistic rules in order to explain the dependency of the *outputs* from the *input* parameters<sup>39</sup>. In this study, concentrations of PEG/methacrylated pHPMAlac copolymer and methacrylated hyaluronic acid were used as *input* parameters, and phase separation extent and rheological properties were used as *outputs*.

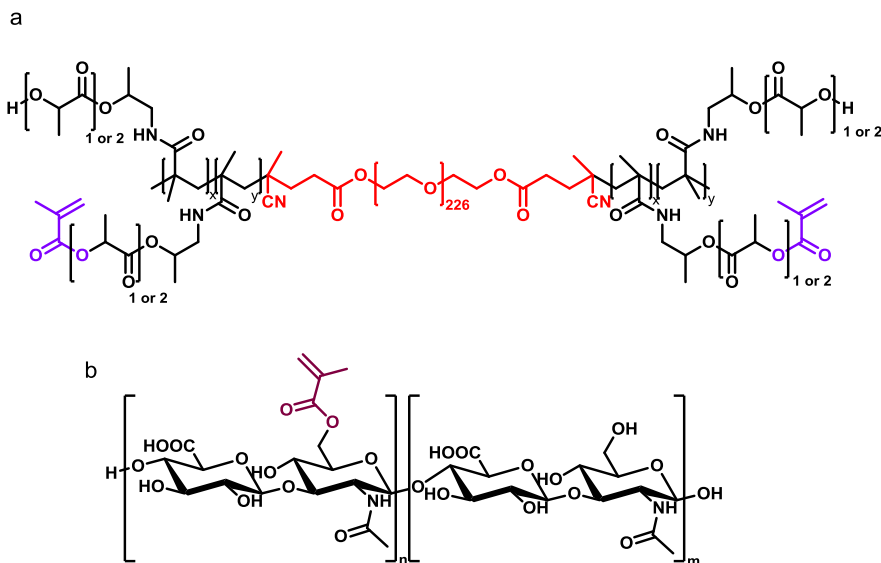
## 4.2 Materials and Methods

### 4.2.1 Materials

All chemicals and solvents were obtained from Sigma-Aldrich (Zwijndrecht, the Netherlands) and Biosolve (Valkenswaard, the Netherlands), respectively, unless indicated otherwise. Chemicals and solvents were used as received. Hyaluronic acid (HA, 120 kDa) was supplied by Lifecore Biomedical (Chaska, MN, USA). L-lactide was obtained from Corbion Purac (Gorinchem, The Netherlands), phosphate buffered saline pH 7.4 (PBS) from Braun (Melsungen, Germany) and Irgacure 2959 was donated by BASF (Ludwigshafen, Germany). Albumin-fluorescein isothiocyanate conjugate (FITC-BSA) and Nile Red (NR) were purchased from Sigma-Aldrich. Weigert's hematoxylin (solution A + B), formaldehyde and xylene were supplied by Klinipath BV (Duiven, The Netherlands). Fast green FCF was ordered from MP Biomedicals (Eindhoven, The Netherlands), safranin-O from VWR (Amsterdam, The Netherlands), and paraffin from Leica Biosystems (Eindhoven, The Netherlands).

### 4.2.2 Synthesis and characterization of polymers

A triblock copolymer composed of a PEG (10 kDa) mid-block flanked by two pHPMAlac (mono/dilactate molar ratio = 75:25) outer blocks (chemical structure reported in Scheme 1a) was synthesized by free radical polymerization, and further partially methacrylated as previously described<sup>20</sup>.



**Scheme 1.** Chemical structure of polymers used in this study. Structure of  $M_{10}P_{10}$ , composed of a PEG-based mid-block (in red) flanked by two pHPMA-lac outer blocks (in black) being partially methacrylated (in purple, a). Chemical structure of HAMA (b).

The triblock copolymer was characterized by Gel Permeation Chromatography (GPC), Proton Nuclear Magnetic Resonance ( $^1\text{H}$  NMR) and UV-VIS spectrophotometry before and after methacrylation as described previously<sup>20,40</sup>. The triblock copolymer is further abbreviated as  $M_0P_{10}$ , whereas its methacrylated derivative as  $M_{10}P_{10}$ , where  $M_0$  and  $M_{10}$  refer to a degree of methacrylation (DM) of 0 and 10% of the lactate side groups, respectively and  $P_{10}$  refers to a PEG mid-block of 10 kDa.

HA was methacrylated as previously reported by Hachet *et al.* with minor adjustments<sup>41</sup>. Briefly, 5 g (12.5 mmol of disaccharide units) of HA was dissolved in 250 ml of ultrapure water and 250 ml of *N,N*-dimethylformamide (DMF). Next, 5 ml of methacrylic anhydride (33.6 mmol) was added drop-wise at 4 °C, while keeping the pH between 8 and 9 by addition of aqueous NaOH solution (0.5 M). Subsequently, the polymer mixture was stirred overnight at 4 °C, and the polymer was purified by precipitation in cold ethanol and subsequently re-dissolved in water. After two days of dialysis (MWCO = 10-14 kDa) against water at 4°C, the polymer solution was freeze-dried and the recovered polymer is further referred to as HAMA (chemical structure reported in Scheme 1b). HA and HAMA were characterized by GPC<sup>23</sup>. HAMA was analyzed by  $^1\text{H}$  NMR ( $\text{D}_2\text{O}$ ) and the DM defined as the number of methacrylate groups per 100 disaccharide units was calculated according to equation 1.

$$DM (\%) = \frac{\text{average } (I_{6.2}, I_{5.8})}{(I_{2.1}-3)/3} \times 100 \quad \text{Equation 2}$$

in which an integration value of 1 is given to the signal at chemical shift of 6.2 ppm. The DM of HAMA was also measured according to a High Performance Liquid Chromatography (HPLC)-based method, as reported previously<sup>24,42</sup>.

### 4.2.3 Preparation of hydrogels and experimental design

Polymer mixtures containing  $M_{10}P_{10}$  and HAMA at different concentrations (Table 1) were prepared by dissolving the two polymers in PBS (pH = 7.4) in the same vial under mild stirring at 4 °C overnight. These polymer mixtures (and the corresponding hydrogels) are further abbreviated as MH (referring to the presence of  $M_{10}P_{10}$  and HAMA) followed by the concentration (w/w %) of the two polymers. For instance, MH 22+1 is composed of 22% (w/w) of  $M_{10}P_{10}$  and 1% (w/w) of HAMA. Contents of  $M_{10}P_{10}$  and HAMA ranging from 22 to 30 and from 0 to 2%, respectively were chosen, based on handling properties and expected thermoresponsivity.

To assess phase separation, hydrogels were analyzed using confocal imaging, safranin-O staining and  $^1\text{H}$  NMR. Additionally, their rheological properties were determined. Results obtained from confocal imaging and rheological measurements were used to create a predictive model based on neurofuzzy logic technology<sup>39</sup>. The generated model was used to identify an exemplary 3D printability window based on applied constraints, and 3D printed porous constructs were fabricated by an extrusion-based 3D printing procedure.



**Table 1.** Polymer mixtures based on different concentrations of  $M_{10}P_{10}$  and HAMA. The combinations of  $M_{10}P_{10}$  and HAMA concentrations marked with a cross (x) were prepared in this study.

$M_{10}P_{10}$	HAMA						
	w/w %	0	0.5	0.75	1	1.5	2
0							X <sup>a</sup>
22	X <sup>a,b</sup>	X <sup>a,b</sup>	X <sup>a,b</sup>	X <sup>a,b</sup>	X <sup>a</sup>		X <sup>a,b</sup>
24		X <sup>a</sup>	X <sup>b</sup>				
26		X <sup>a,b</sup>				X <sup>a,b</sup>	
30		X <sup>b</sup>					

<sup>a</sup>Hydrogel compositions tested by confocal microscopy

<sup>b</sup>Hydrogel compositions tested by rheological analysis

#### 4.2.4 Confocal laser scanning microscopy (CLSM)

Freshly prepared MH polymer mixtures were enriched with FITC-BSA (final concentration = 0.2%) and a few grains of NR, and maintained under stirring overnight at 4 °C. FITC-BSA and NR were chosen to stain hydrophilic and hydrophobic domains, respectively<sup>21,33</sup>. Subsequently 100 µl of each polymer mixture was dispensed in duplo in a 96-well plate and incubated at 37 °C for 1h. Confocal images were obtained using a Yokogawa Cell Voyager 7000S imager (Yokogawa, Tokyo, Japan) at 37 °C. Samples were visualized with a 40x objective employing 488 nm and 561 nm lasers for the excitation of FITC-BSA and NR, respectively. For both fluorophores the used exposure time was 250 ms. Acquisitions were performed using BP525/50 and BP600/37 emission filters for FITC and NR, respectively. Images were recorded for three different locations within each well and for three different Z-stack sections of each location using a Z-stack interval of 3 µm. To quantify the ratio between the domains where NR was dissolved (red areas) and FITC-BSA was predominant (green areas), images were processed using ImageJ 1.45 software. Areas (in pixels) of the red and the green regions were measured for three different acquisition points for each polymer mixture, and a red and a green area were defined as percentage of the total area. From this, a red/green ratio (R/G ratio) was calculated. To investigate the effect of incubation time on phase separation, images were recorded at several time points within the first hour of incubation at 37 °C (*i.e.* 0, 10, 30, 40, 50 and 60 min), and after 2, 3, 8 and 25 hours. For early points (< 1 h) pictures were taken using slightly more intense light for the red channel, to compensate for the slow dissolution of NR.

#### 4.2.5 Safranin-O staining

To assess the localization of HAMA, safranin-O/fast green assay was chosen as a glycosaminoglycan (GAG)-selective staining procedure, which is widely used in tissue engineering for the visualization of GAG-based components in cartilaginous matrices<sup>43-47</sup>. To this end, MH polymer mixtures enriched with 0.05% of Irgacure, were injected into a teflon mold, incubated at 37 °C for 1 hour and UV irradiated for 5 minutes using a Bluepoint 4 UV lamp (point light source, wavelength range: 300-600 nm, intensity at 5 cm: 80 mW/cm<sup>2</sup>, Hönle UV Technology AG, Gräfelfing, Germany) to generate cylindrical UV cross-linked hydrogels. After dehydration using graded series of ethanol/water solutions and a final washing step with xylene, the dehydrated hydrogels were embedded in paraffin and finally sliced into 5 µm thick samples. Safranin-O/fast green assay was performed as previously described in literature<sup>48</sup>, and images were collected using an Olympus microscope equipped with a digital camera (Olympus BX51 microscope, Olympus DP70 camera, Hamburg, Germany).

#### 4.2.6 <sup>1</sup>H NMR analysis of the two phases

A mixture based on MH 22+2 (2.7 ml), prepared as described in section 4.2.3 was incubated for 1 h at 37 °C and centrifuged at maximal speed (5292 x g) for 1.5 hours at 37 °C. Next, the two phases were collected separately, freeze-dried and further analyzed by <sup>1</sup>H NMR (D<sub>2</sub>O) at room temperature.

#### 4.2.7 Rheological measurements

Polymer mixtures prepared as described in section 4.2.3 were analyzed for their rheological properties using a Discovery HR-2 rheometer (TA-Instruments, Etten-Leur, The Netherlands) equipped with a cone-plate measuring geometry (cone diameter: 20 mm, cone angle: 1°, truncation: 27 µm). Samples were analyzed in duplicate using the conditions summarized in Table 2. The temperature of gelation ( $T_{gel}$ ) is defined as the temperature where the storage modulus ( $G'$ ) equals the loss modulus ( $G''$ ) during the temperature ramp experiments<sup>22</sup>, whereas the shear yield stress is defined as the stress at which  $G'$  crosses  $G''$  during the oscillation strain sweep experiments<sup>49,50</sup>. For a few samples, a recovery test was also performed in oscillation and in flow operating mode at 37 °C to investigate if these gels were capable to fully recover after shear stress.

**Table 2.** Settings used for rheological analysis in oscillation and flow mode.

procedure	T (°C)	ramp rate (°C/min)	shear rate (1/s)	frequency (Hz)	strain (%)
<i>oscillation</i> temperature ramp	4-50	5 <sup>a</sup>	-	1	1
<i>oscillation</i> strain sweep	37	-	-	1	0.01-100
<i>flow</i> shear rate sweep	37 <sup>b</sup>	-	0.006-10000	-	-
<i>oscillation</i> recovery	37	-	-	1	step1 <sup>c</sup> : 1 step2 <sup>c</sup> : 100 step3 <sup>c</sup> : 1
<i>flow</i> recovery	37	-	step 1 <sup>c</sup> : 0.05 step 2 <sup>d</sup> : 100 step 3 <sup>c</sup> : 0.05	-	-

<sup>a</sup> For a few hydrogel compositions also at 0.75 °C/min

<sup>b</sup> For a few hydrogel compositions also at T<sub>gel</sub> and 20 °C

<sup>c</sup> Duration step = 60 s

<sup>d</sup> Duration step = 1 s

#### 4.2.8 Computational modeling

To mathematically study the dependency of phase separation extent and rheological properties from M<sub>10</sub>P<sub>10</sub> and HAMA concentrations, and to create a predictive computational model, a database of twelve facts was generated, including MH compositions (Table 1) and corresponding gel properties. Neurofuzzylogic software (FormRules® v4.03, Intelligensys Ltd. UK) was used. The M<sub>10</sub>P<sub>10</sub> and HAMA contents (w/w %) were chosen as *input* parameters, whereas R/G ratio, G' at 37 °C and T<sub>gel</sub> recorded during oscillation temperature ramps, yield stress recorded during oscillation strain sweeps and viscosity at low shear rate (*i.e.* 0.006 1/s) recorded during flow shear rate sweeps were selected as *output* parameters. The default training parameters of the software were used for modeling. The software contains various statistical fitness criteria. Among them, Structural Risk Minimisation (SRM)

was used to model all *outputs* ( $C_1 = 0.8$  and  $C_2 = 4.8$ ), except  $T_{\text{gel}}$  that required the use of Leave One Out Cross Validation (LOOCV) to be properly fitted. The significant effect of a single *input* (HAMA or  $M_{10}P_{10}$  content) or their interaction on each studied property is pointed out by neurofuzzylogic software by generating sub-models for each *output* parameter. Additionally, through “IF...THEN” rules, every *output* parameter (e.g. R/G ratio) is related to the *input* variable (e.g. HAMA content) obtaining statements as follows: “If HAMA content is low, R/G ratio is high and if HAMA content is high, R/G ratio is low”, where *high* and *low* are always flanked by a membership value (ranging from 0 to 1). The membership value describes how close the predicted value of a property (e.g. R/G ratio) is to the highest or lowest experimental value of that property, respectively. To assess the predictability of each generated model, Train Set R-squared values (indicating the percentage of the *output* variability explained by *inputs*) were calculated. Additionally, ANOVA was also carried out to test the statistical significance of each model. Obtaining computed *f* values higher than critical *f* values for the degrees of freedom of the model was used as a necessary condition to assert good performance and accuracy of the model. Subsequently, 3D surface charts were created, where *output* parameter values predicted by the models were reported as function of the two *input* parameters. Finally, to provide a practical example of their predictive capacity, the generated models were used for the identification of MH hydrogel compositions with selected properties. Table 3 contains the inclusion criteria that were used to generate a MH composition range with desirable properties for nozzle-based 3D bioprinting applications. 2D charts originating from the top view of the 3D surface charts for each *output* parameter were overlapped and a region of interest, where all inclusion criteria were satisfied was identified.

#### 4.2.9 3D printing assessment

3D printing of an exemplary MH gel composition with selected properties as predicted by the model was performed using a 3D Discovery bioprinter (RegenHU, Villaz-St-Pierre, Switzerland) equipped with a Bluepoint 4 UV lamp (specifications given in ‘Safranin-O staining’). The polymer mixture was loaded into a cartridge equilibrated at 37 °C, and extruded through a CF300H microvalve by a pneumatically driven robotic dispenser. Hydrogel filaments and hydrogel grids with strand distance ranging from 1.0 to 2.2 mm were obtained by depositing the hydrogel lines on a pre-heated (40 °C) collection plate. Each layer was UV irradiated for 3 seconds from a distance of 2 cm. 3D porous constructs (height = 2 mm) were generated by dispensing horizontal and vertical filaments using a strand distance of 1.5 or 1.3 mm. Samples were UV irradiated in a layer-by-layer fashion (3 s/layer from 2 cm) with additional 15 seconds (from 2 cm) after the printing was completed. 3D printed hydrogels were visualized and photographed using a light microscope connected to a digital camera (specifications given in ‘Safranin-O staining’). Detailed settings used during the 3D printing procedure are reported in Table S1.

**Table 3.** Inclusion criteria for the identification of a MH hydrogel composition range with selected properties.

property	desirable range of values	rationale
yield stress	$\geq 30$ Pa	shape fidelity after 3D printing extrusion
$G'$ at 37 °C	$\geq 150$ Pa	shape fidelity after 3D printing extrusion
$T_{gel}$	$\leq 37$ °C	shape fidelity at physiologically relevant temperatures
viscosity at low shear	$\geq 500$ Pa·s	shape fidelity after 3D printing extrusion
total polymer concentration	$\leq 26$ %	handling, cell incorporation
R/G ratio	$\geq 75/25$	stability of the mixture in the cartridge

## 4.3 Results and Discussion

### 4.3.1 Synthesis and characterization of polymers

The thermosensitive polymer  $M_{10}P_{10}$  was characterized by a number average molecular weight ( $M_n$ ) of 35.6 kDa (according to GPC) and 40.3 (according to  $^1H$  NMR), a DM of 10.7% and a cloud point (CP) of 17 °C. Characteristics of  $M_0P_{10}$  and  $M_{10}P_{10}$  were in line with previously reported findings<sup>20</sup> and are summarized in Table 4. GPC analysis carried out on the polysaccharides showed  $M_n$  values of 96.1 and 90.8 kDa for HA and HAMA, respectively. The similarity in  $M_n$  and PDI of HA and HAMA (chromatograms reported in Figure S1) confirmed that no premature cross-linking or chain scission occurred during the reaction. HAMA was characterized with a DM of 22% as calculated using its  $^1H$  NMR spectrum (equation 1), and the same value of 22% was found by HPLC analysis.

**Table 4.** Characteristics of polymers before and after methacrylation.

polymer	$M_n$ (kDa)	PDI (-)	DM (%)	CP (°C)
$M_0P_{10}$	37.3 <sup>a</sup> 42.6 <sup>b</sup>	2.1 <sup>a</sup>	0 <sup>b</sup>	35 <sup>c</sup>
$M_{10}P_{10}$	35.6 <sup>a</sup> 40.3 <sup>b</sup>	2.2 <sup>a</sup>	10.7 <sup>b</sup>	17 <sup>c</sup>
HA	96.1 <sup>d</sup> 120.0 <sup>e</sup>	1.5 <sup>d</sup>	0 <sup>b</sup>	n.a.
HAMA	90.8 <sup>d</sup>	1.6 <sup>d</sup>	22 <sup>b</sup> 22 <sup>f</sup>	n.a.

<sup>a</sup> Determined by GPC, using DMF containing LiCl (10 mM) as eluent and PEG with narrow molecular weight (MW) distributions as standards.

<sup>b</sup> Determined by <sup>1</sup>H NMR.

<sup>c</sup> Determined by UV-VIS spectrophotometry and defined as the onset of the increasing light scattering during a temperature ramp measurement (4-50 °C, 1 °C/min, 650 nm).

<sup>d</sup> Determined by GPC, using tris(hydroxymethyl)aminomethane buffer 0.1 M (pH 7.5) as eluent and dextrans with narrow MW distributions as standards.

<sup>e</sup> Average MW determined by the supplier using multi-angle light scattering size exclusion chromatography.

<sup>f</sup> Determined by HPLC.

n.a.: not applicable.

### 4.3.2 Phase behavior of aqueous systems of $M_{10}P_{10}$ and HAMA

Phase separation of aqueous polymer mixtures composed of different concentrations of  $M_{10}P_{10}$  and HAMA was studied using CLSM and HAMA-selective staining, *i.e.* safranin-O, combined with <sup>1</sup>H NMR analysis. Figure 1 shows confocal images of polymer mixtures containing  $M_{10}P_{10}$  with a concentration of 22%, and HAMA with a concentration ranging from 0 to 2%, after 1h of incubation at 37 °C. In samples containing only  $M_{10}P_{10}$ , a homogenous distribution of both dyes, *i.e.* FITC-BSA and NR was observed indicating that no phase separation in this system occurred on the scale of the applied magnification. Nevertheless, it needs to be mentioned that (micro-)phase separation in aqueous systems of PEG/pHPMALac triblock copolymers can occur<sup>21,33</sup>.

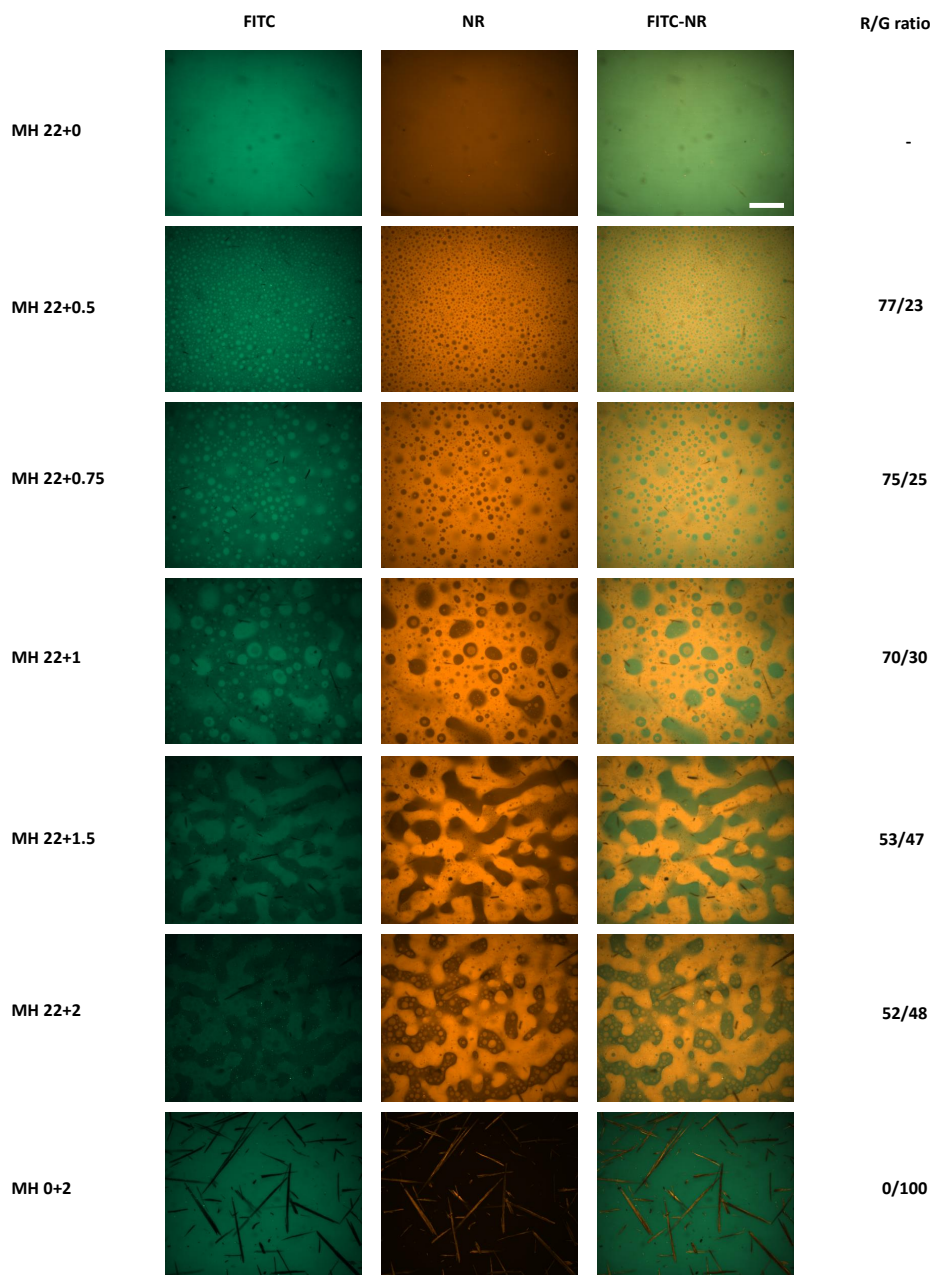


**Figure 1.** Confocal images for different MH compositions after 1 h incubation at 37 °C. FITC-BSA is visualized in green (first and third column) and NR is visualized in red (second and third column). Scale bar represents 50  $\mu\text{m}$ .



In general, ABA-like triblock copolymers with a hydrophilic mid-block and two more hydrophobic outer blocks tend to self-assemble in flower-like micelles. Moreover, by increasing the polymer concentration, bridges between adjacent micelles are formed, generating a transient physical network. In this context, phase separation can be observed between regions with high content of interconnected micelles (more dense, polymer-rich domains) and regions mostly containing isolated micelles and single polymeric chains (less dense, water-rich domains)<sup>34</sup>. Intuitively, this phase behavior is affected by the hydrophilic/hydrophobic balance of the polymer, which is determined by its structural characteristics (*e.g.* block length and composition)<sup>32,51</sup> as well as by the temperature particularly for thermosensitive systems. Therefore, the fact that we did not visualize phase separation for  $M_{10}P_{10}$  mixtures in this study may be explained by the specific molecular architecture of the polymer (PEG and outer blocks length, mono/dilactate ratio in the outer blocks and DM) as well as by the applied magnification.

In samples containing only HAMA, FITC-BSA was fully and homogeneously distributed, whereas NR was visible as undissolved small needles. On the other hand, for all samples containing  $M_{10}P_{10}$  and HAMA a clear preferential distribution of the two dyes in specific regions was observed. FITC-BSA was mainly localized in internal domains whereas NR was dissolved in the surrounding external phase. Although a partial and consistent co-localization of the FITC-BSA in the two phases was visible using the FITC-channel (green)<sup>21</sup>, a clear phase separation was detected using the NR-channel (red) and overlapping both channels (Figure 1). Considering the hydrophilic character of FITC-BSA and the hydrophobic nature of NR, phase separation in  $M_{10}P_{10}$ /HAMA mixtures is characterized by hydrophilic internal regions, dispersed in a more hydrophobic continuous phase. The confocal images and the R/G ratios calculated for each mixture clearly show that the extent of phase separation is dependent on HAMA concentration. In general, with increasing HAMA content, the internal domains became larger and more irregularly shaped, and they seemed even interconnected in MH 22+1.5 and MH 22+2. This suggests that HAMA is predominantly present in the hydrophilic dispersed phase, as also expected considering its high hydrophilicity. Interestingly, the percentage areas measured for the hydrophilic (green) regions in all the mixtures tested are much higher than the expected values based on HAMA and  $M_{10}P_{10}$  solid contents. This discrepancy is likely due to the presence of also  $M_{10}P_{10}$  in those domains, and more importantly, it can be explained by a dehydration process of the hydrophobic regions and consequent increase of the volume fraction of the hydrophilic phase, as it was also reported for mixtures composed of PEG and methacrylated dextran<sup>26</sup>. It should be noted that similar experiments carried out on UV cross-linked hydrogels revealed a similar phase separation profile (data not shown).

Mixtures containing 0.5% of HAMA and increasing concentrations of  $M_{10}P_{10}$ , *i.e.* 24 and 26% showed less extensive phase separation when compared with mixtures containing the same concentration of HAMA and 22% of  $M_{10}P_{10}$  (Figure S2). Similarly, MH 26+1.5 (Figure S2) presented less phase separation in comparison to MH 22+1.5 (Figure 1). Thus, the extent of phase separation decreases with increasing

$M_{10}P_{10}$  content.

To investigate the kinetics of the phase separation of  $M_{10}P_{10}$ /HAMA mixtures, samples were analyzed by confocal microscopy at several time points within the first hour of incubation at 37 °C (Figure S3), and after 2h, 3h, 8h and 25h of incubation at 37 °C (Figure S4). Figure S3 shows that for all samples containing  $M_{10}P_{10}$  or  $M_{10}P_{10}$  and HAMA, the intensity of the red color increased over time, likely due to the more efficient dissolution of NR after longer incubation times. Importantly, in all  $M_{10}P_{10}$ /HAMA blends the shape and the distribution of the internal domains did not change over time, therefore the mixtures were all stable during the first hour of incubation. For incubation times longer than 1 hour, mixtures containing low HAMA concentrations, *i.e.* 0.5 and 0.75% were still stable over a screening period of 25 hours (Figure S4). On the contrary, confocal images of formulations with higher HA content (MH 22+1, MH 22+1.5 and MH 22+2) suggest that the stability over 25 hours is progressively lost with gradually increasing HAMA concentration.

To verify the localization of HAMA in the phase separated gels, safranin-O assay was performed for hydrogels containing  $M_{10}P_{10}$  and increasing amounts of HAMA. UV cross-linked hydrogels were used to fix the 3D polymer network for analysis, because the reversible gelation of uncross-linked samples was not compatible with several steps of this staining procedure. Figure 2 clearly shows red-stained internal domains and an overall phase separation, which increases with increasing HAMA concentration. In MH 22+2 small HAMA-poor (hydrophobic) regions are present throughout HAMA-rich (hydrophilic) domains. Taken altogether, these findings are in line with the confocal images discussed above and confirmed that HAMA was exclusively present in the (more hydrophilic) dispersed phase.

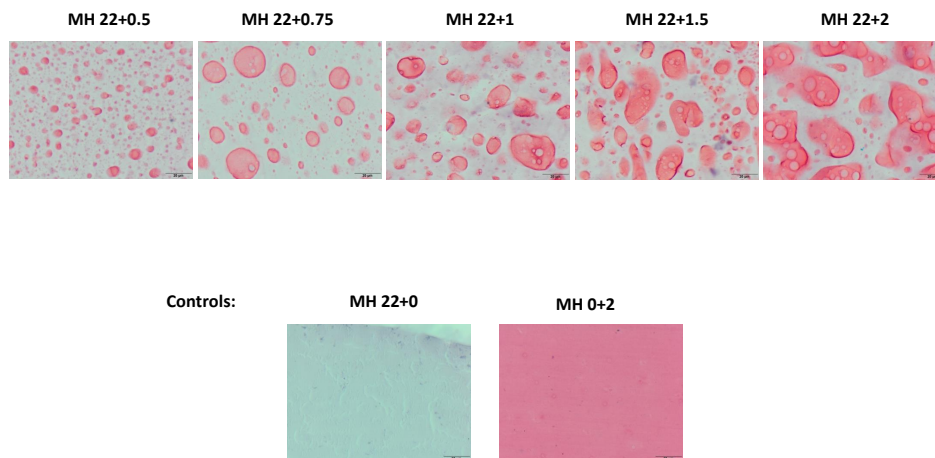


**Figure 2.** Safranin-O staining for different MH compositions. HAMA is stained in red. Scale bar represents 20  $\mu$ m.

To study the composition of each phase quantitatively,  $^1\text{H}$  NMR analysis was used. After 1.5 hours of centrifugation, polymer mixture MH 22+2 showed a clear macro-phase separation.  $^1\text{H}$  NMR spectra of each fraction in comparison to  $\text{M}_{10}\text{P}_{10}$  and HAMA spectra are shown in Figure 3. In the spectrum of the top layer, the presence of the signal at chemical shift 3.7 representative of the  $\text{CH}_2$  PEG protons of  $\text{M}_{10}\text{P}_{10}$  together with the signal at 2.1, representative of the  $\text{CH}_3$  protons of HAMA showed that the top layer contained both  $\text{M}_{10}\text{P}_{10}$  and HAMA, with a prevalence of HAMA (HAMA/ $\text{M}_{10}\text{P}_{10}$  weight ratio  $\sim 12.5/1$ ). In line with the results obtained from the safranin-O staining, in the NMR spectrum of the bottom layer no HAMA was detected, and only the typical signals related to  $\text{M}_{10}\text{P}_{10}$  were observed.

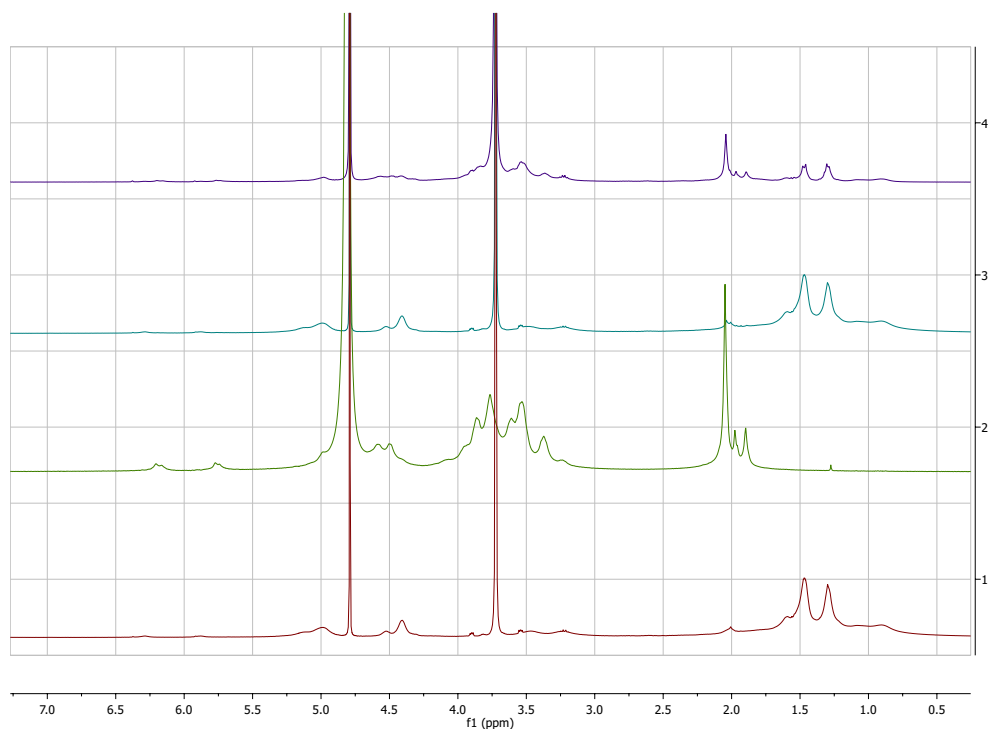


**Figure 3.**  $^1\text{H}$  NMR spectra of  $\text{M}_{10}\text{P}_{10}$  (spectrum 1, red), HAMA (spectrum 2, green), bottom layer (spectrum 3, blue), and top layer (spectrum 4, purple). Chemical shifts were referred to the solvent ( $\text{D}_2\text{O}$ ) residual peak of 4.79 ppm.

In summary, micro-scale ATPS occurs in  $\text{M}_{10}\text{P}_{10}$ /HAMA hydrogel mixtures. Results showed that the dispersed phase is more hydrophilic and is mainly composed of HAMA, whereas the external phase is more hydrophobic and entirely composed of  $\text{M}_{10}\text{P}_{10}$ . Moreover, the extent of phase separation increases with increasing HAMA content. Finally, systems with a low content of HAMA allow the formation of mixtures stable during a period of at least 25 hours, whereas when the content of HAMA exceeds 1% the systems undergo a more dynamic phase separation, which increases over time.

### 4.3.3 Rheological properties

Rheological properties in oscillation and flow mode were studied in  $M_{10}P_{10}$ /HAMA mixtures as function of the two polymers' concentration. Figure 4a shows the storage modulus ( $G'$ ) for polymeric mixtures containing  $M_{10}P_{10}$  (22%) and progressively higher concentrations of HAMA as a function of temperature.

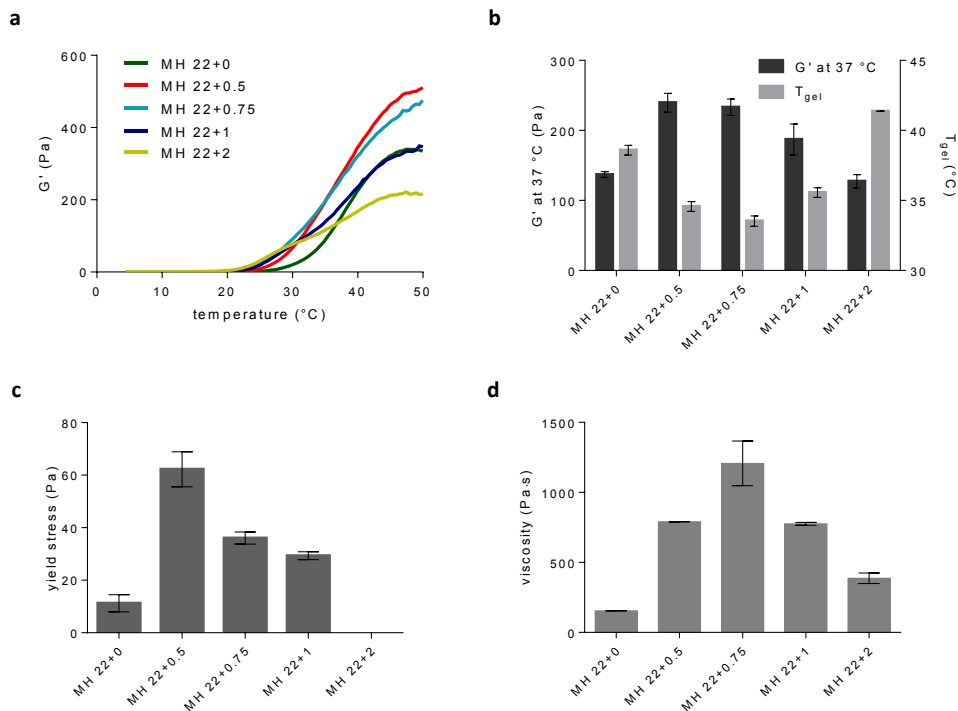


**Figure 4.** Effect of HAMA concentration on hydrogel properties.  $G'$  as function of temperature recorded during a temperature ramp (4-50 °C – 5 °C/min) using a strain of 1% and a frequency of 1 Hz for different MH formulations varying in HAMA content (a).  $G'$  at 37 °C and  $T_{gel}$  (b). Yield stress values obtained at 37 °C during a strain sweep (0.01-100%) using a frequency of 1 Hz (c). Viscosity at 0.006 1/s recorded at 37 °C during a shear rate sweep (0.006-10000 1/s) (d).

For all mixtures, an increase of  $G'$  with increasing temperature was observed and a temperature at which  $G'$  equals  $G''$ , here referred to as  $T_{gel}$  was identified. For samples only composed of  $M_{10}P_{10}$ ,  $G'$  at 37°C was  $137 \pm 4$  Pa and the  $T_{gel}$  was 38.6 °C. The thermosensitive behavior of pHPMAlac/PEG triblock copolymers has been reported in literature<sup>20</sup> and it is due to the self-assembly of polymeric chains driven by dehydration of the pHPMAlac outer blocks upon raising the temperature. In line with previously reported findings<sup>23,24</sup>, the addition of relatively small amounts of polysaccharide, *i.e.* HAMA (0.5-1%) led to higher  $G'$  values at 37 °C and lower  $T_{gel}$  (Figure 4b). Remarkably, a further increase of HAMA up to 2% resulted in a lower  $G'$  and a higher  $T_{gel}$ , despite of a higher total polymer concentration. A possible explanation for this phenomenon lies in the fact that phase separation occurs here to a

higher extent. As described in section 4.3.2, the formation of a hydrophilic dispersed phase is likely related to partial dehydration of the continuous more hydrophobic phase. This leads consequently to a relatively higher  $M_{10}P_{10}$  concentration in the external phase, which in turn can be related to higher  $G'$  values and lower  $T_{gel}$ . Apparently, this phenomenon positively contributes to the thermogelation profile of the hydrogel only when HAMA concentration is relatively low and, therefore when phase separation only leads to relatively small hydrophilic domains. For HAMA contents higher than 1%, when the phase separation becomes more pronounced and the internal domains are interconnected (Figure 1), the continuity of the external phase is lost and this likely leads to the observed lower  $G'$  values of the hydrogel. Moreover, it was found that only for extensively phase-separated hydrogels, *e.g.* MH 22+2, the thermogelation was dependent on the heating rate. For these hydrogels, higher  $G'$  values were obtained when applying a slower temperature ramp (Figure S5 a). This aspect points out the kinetics-dependent effect of phase separation and the consequent impact on rheology. On the other hand, for less phase-separated hydrogels the temperature ramp rate did not affect the thermogelation profile (Figure S5 b).

Figure 4c reports the stress values at which  $G'$  crosses  $G''$ , here referred to as yield stress. In line with the discussion above, a significant increase of yield stress in presence of a low amount of HAMA, *i.e.* 0.5% was observed ( $62.2 \pm 6.7$  Pa for MH 22+0.5) in comparison with hydrogels only composed of  $M_{10}P_{10}$  ( $11.2 \pm 3.2$  Pa). When increasing HAMA content further, a progressive decrease of yield stress was observed, and remarkably, no yield stress was found for blends containing 2% of HAMA. Similar dependency on HAMA concentration was observed for viscosity at low shear and shear thinning properties of the same mixtures (Figure 4d and S6). The rheological study of polymeric mixtures composed of increasing amounts of  $M_{10}P_{10}$  and a fixed low amount of HAMA, *i.e.* 0.5% showed that a higher concentration of  $M_{10}P_{10}$  always contributes positively to the storage modulus, viscosity and yield stress of  $M_{10}P_{10}$ /HAMA mixtures (Figure 5a, b and c).

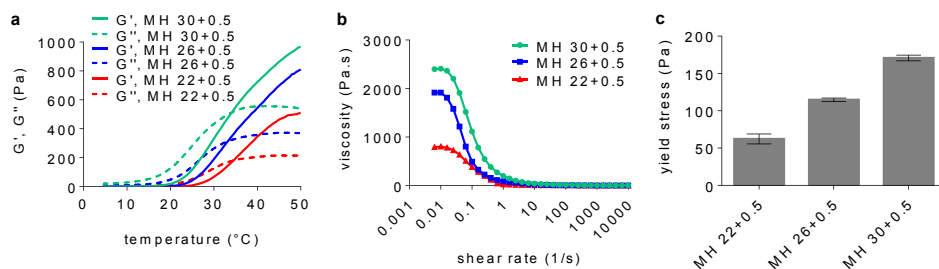


**Figure 5.** Effect of  $M_{10}P_{10}$  concentration on hydrogel properties.  $G'$  as function of temperature recorded during a temperature ramp (4-50 C – 5 °C/min) using a strain of 1% and a frequency of 1 Hz for different MH formulations varying in  $M_{10}P_{10}$  content (a). Viscosity as function of shear rate recorded at 37 °C during a shear rate sweep (0.006-10000 1/s) (b). Yield stress obtained at 37 °C during a strain sweep (0.01-100%) using a frequency of 1 Hz (c).

Similarly to hydrogels composed of pHPMAIac/PEG triblock copolymers and a different polysaccharide, *i.e.* methacrylated chondroitin sulfate<sup>23</sup>, hydrogels based on  $M_{10}P_{10}$  and HAMA showed quick and full recovery after shear at 37 °C, which is a crucial requirement for 3D printable or injectable hydrogels (Figure S7). Moreover, shear rate sweeps demonstrated that the viscosity at low shear rates is highly dependent on temperature. A decrease in temperature from 37 to 20 °C was responsible for significantly lower viscosity in the shear rate range of 0.006-1 1/s (Figure S8 a, b and c). Reasonably, the full hydrogel recovery and high viscosity at elevated temperatures are linked to the thermosensitive character of  $M_{10}P_{10}$ .

#### 4.3.4 Modeling and identification of hydrogels with selected properties

Neurofuzzylogic was employed to model the parameters, R/G ratio,  $G'$  at 37 °C and  $T_{gel}$  recorded during oscillation temperature ramps, yield stress recorded during oscillation strain sweeps and viscosity at low shear rate (*i.e.* 0.006 1/s) recorded during flow shear rate sweeps. Correlation coefficients ( $74.5 < R^2 < 93.5$ ) together with ANOVA parameters (computed f ratio > critical f values for the degrees of freedom) for all modeled properties (Table S2) indicated that there were no statistically significant differences between experimental and predicted results. Therefore, the models can be considered having good performance and predictability. The set of rules generated for each model is reported in Table S3 and a graphical overview of the model outcome is reported in Figure 6, where surface 3D charts are displayed.

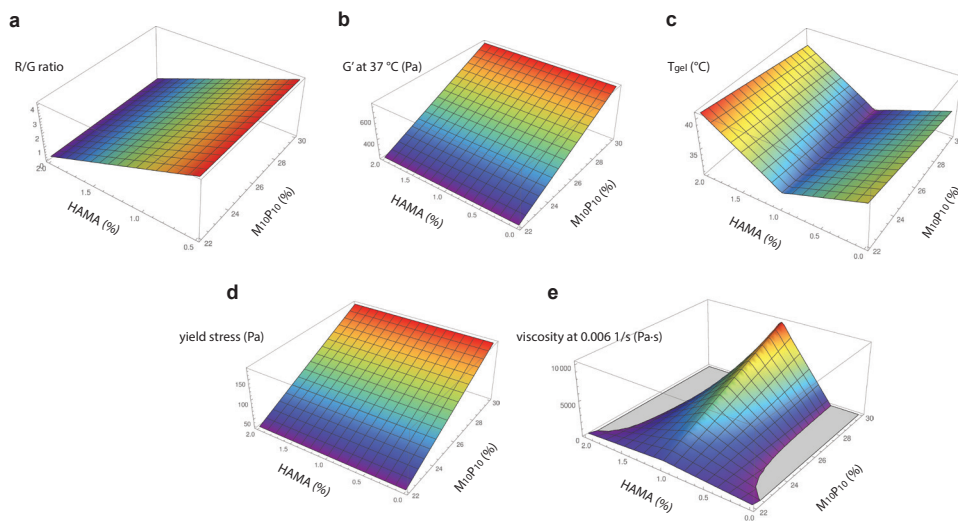


**Figure 6.** Surface 3D charts based on the values predicted by the model. R/G ratio (a),  $G'$  at 37 °C (b),  $T_{gel}$  (c), yield stress (d) and viscosity at 0.006 1/s (e) as function of  $M_{10}P_{10}$  and HAMA concentrations. Only positive Z values were taken into account.



Predicted values for each *output* parameter are reported as function of HAMA and  $M_{10}P_{10}$  contents. Interestingly, single effects of HAMA or/and  $M_{10}P_{10}$  contribute to explain the variability of R/G ratio,  $G'$  at 37 °C,  $T_{gel}$  and yield stress, however an interactive effect between both *inputs* determines the variation of viscosity at low shear. General trends were in line with the experimentally observed trends. Only for viscosity, despite the excellent correlation between the predicted and the experimental results (sufficiently high  $R^2$  and significant model) some spaces were not well sampled. In those areas, the mathematical model may not fit properly.

To provide a practical example of the predictive power of the models, the inclusion criteria reported in Table 3 were used to identify a MH hydrogel composition range with selected characteristics, potentially suitable for the development of a bioink intended for nozzle-based 3D printing applications. An ideal bioink behaves as a shear thinning material able to retain its filament-like shape after extrusion, without any flow on the deposition plate (yield stress behavior). For cell-laden hydrogel printing, stability and relatively high viscosity of the material in the cartridge are desirable features to avoid cell sedimentation. On the other side, high viscosity during cell incorporation may cause handling issues<sup>14</sup>. Consequently, applying these requirements to MH hydrogels, sufficiently high values of yield stress,  $G'$  at 37 °C (with low  $T_{gel}$ ) and viscosity at low shear (Table 3) should ensure shape fidelity after the extrusion process. On the other side, a total polymer concentration lower than 26% (w/w) would guarantee easy handling at low temperatures and a R/G ratio higher than 75/25 would result in sufficient stability of the mixture at 37 °C in the cartridge. It has to be taken into consideration that the numerical ranges for the parameters described in the inclusion criteria were only chosen as examples and different choices can be made with respect to several aspects (*e.g.* cell-type and density, design of the aimed construct, extrusion principle, etc).

The superimposition of the 2D charts generated by the model for each considered *output* parameter (Figure 7) and the implementation of the selected constraints led to the identification of a concentration range of  $M_{10}P_{10}$  and HAMA (dark blue region in Figure 7f) expected to generate hydrogels matching the selected characteristics. MH 24+0.5 % (red dot in Figure 7f) was chosen as an exemplary MH composition (which was not used to generate models for the rheological properties) having  $M_{10}P_{10}$  and HAMA contents in the predicted range. For MH 24+0.5 %,  $G'$  at 37 °C,  $T_{gel}$ , yield stress and viscosity at 0.006 1/s were found to be  $372 \pm 12$  Pa (*vs*  $349 \pm 80$  Pa of predicted value),  $33.3 \pm 0.0$  °C (*vs*  $34.8 \pm 1.1$  °C of predicted value),  $117 \pm 14$  Pa (*vs*  $66 \pm 15$  Pa of predicted value) and  $1445 \pm 36$  Pa·s (*vs*  $1182 \pm 148$  Pa·s of predicted value), respectively. In fact, these values were within the selected ranges and sufficiently close to the predicted values. Moreover, the 3D printing of MH 24+0.5% resulted in the generation of shape-stable filaments and grids with strand distance ranging from 1.0 to 2.2 mm (Figure 8a and b). Furthermore, 2 mm high and porous constructs with variable strand distance (1.3 and 1.5 mm) were successfully printed (Figure 8c-f). All printed constructs were shape-stable, before and after swelling in PBS, as they were handled by the use of a spatula without damage. Taken all together, we developed a valid model for the prediction of the phase behavior



and rheological properties of MH hydrogels and showed its applicability for the identification of hydrogel compositions with pre-designed, desirable profiles.

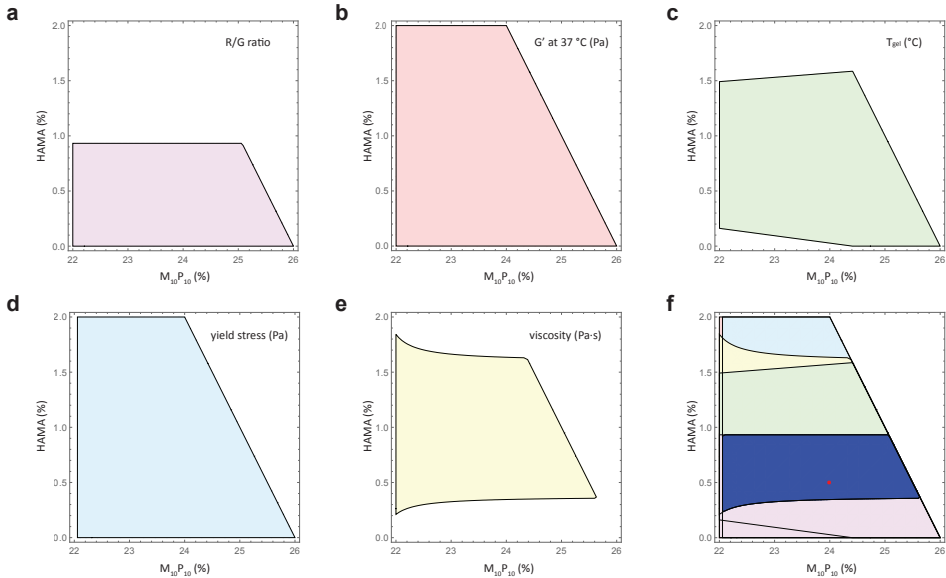


**Figure 7.** 2D graphs for each *output* parameter and selected areas of interest based on the inclusion criteria reported in Table 3. Selected areas for R/G ratio (a, light purple),  $G'$  at 37 °C (b, light pink),  $T_{gel}$  (c, light green), yield stress (d, light blue), viscosity (e, light yellow). Superimposition of selected areas for each *output* parameter; dark blue indicates the region where all the conditions are satisfied and the red dot indicates the exemplary MH composition chosen for validation of the model (f).

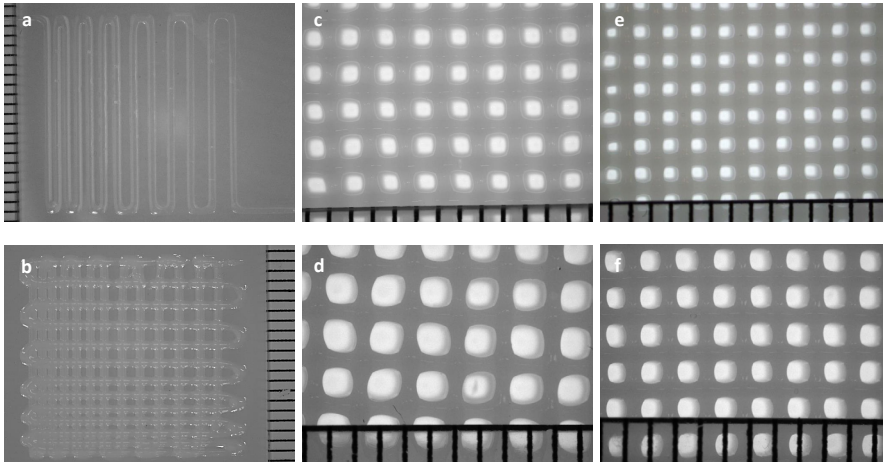


**Figure 8.** 3D printing of an exemplary MH hydrogel composition with selected properties as predicted by the model, *i.e.* MH 24+0.5. Hydrogel filament with strand distance ranging from 1 mm to 2.2 mm (a). Hydrogel grid with strand distance ranging from 1 mm to 2.2 mm (b). 3D construct (20 layers, height = 2 mm) with strand distance 1.5 mm (c and d). 3D construct (20 layers, height = 2 mm) with strand distance 1.3 mm (e and f). Line between two consecutive marks on the ruler indicates 1 mm.

## 4.4 Conclusions

Hydrogels composed of  $M_{10}P_{10}$  and HAMA showed phase separation within the studied concentration range. The co-existence of a more hydrophilic, HAMA-rich dispersed phase together with a more hydrophobic and partially dehydrated  $M_{10}P_{10}$ -based continuous phase was found to be a crucial structural characteristic, that directly affected the rheological behavior of these hydrogels. Limited phase separation, corresponding to low concentrations of HAMA was responsible for higher values of storage modulus, yield stress and viscosity, which is potentially beneficial for nozzle-based 3D printing applications of these materials. Partial dehydration of the continuous phase resulted in a higher concentration of  $M_{10}P_{10}$  in this phase, which is likely responsible for the observed changes in rheological properties. On the other hand, extensive phase separation upon addition of high concentrations of HAMA negatively affected the rheological profile, because of loss of continuity in the external phase. Considering the complex dependency of phase behavior and rheology from the two polymer concentrations, a computational model was generated to predict *a-priori* hydrogel compositions displaying desirable and selected characteristics. In general, the ANNs-based approach can be potentially applied to any kind of hydrogel material and it can be a useful tool especially for developing hydrogels of complex composition.

### Acknowledgments

The authors would like to thank Mattie H. P. van Rijen and Vivian M. Mouser for their assistance with the safranin-O staining assay, and Riccardo Borsato for his handling of 2D and 3D plots in *Mathematica*. The research leading to these results has received funding from the European Community's Seventh Framework Programme (FP7/2007-2013) under grant agreement n°309962 (HydroZONES). ML thanks the Spanish Ministry of Science and Innovation (SAF 2012-39878-C02-01) for financial support.

## Supporting Information

**Table S1.** Settings used during 3D printing of hydrogels.

Parameter	Value
<i>Microvalve CF300H</i> <ul style="list-style-type: none"> <li>• Inner diameter [mm]</li> <li>• Temperature [°C]</li> <li>• Needle inner diameter [mm]</li> <li>• Valve opening time [<math>\mu</math>s]</li> <li>• Dosing distance [mm]</li> </ul>	0.3 37 0.3 400 <sup>a</sup> or 500 <sup>b</sup> 0.1
<i>UV irradiation</i> <ul style="list-style-type: none"> <li>• Distance to sample [mm]</li> <li>• Illumination time (each deposited layer) [s]</li> <li>• Post-printing curing [s]</li> </ul>	20 3 15
<i>RegenHU 3DDiscovery</i> <ul style="list-style-type: none"> <li>• Baseplate temperature [°C]</li> <li>• Gel cartridge temperature [°C]</li> <li>• Speed XY [mm/s]</li> <li>• Pressure [bar]</li> </ul>	40 37 40 1.0

<sup>a</sup> when using a strand spacing of 1.3 mm

<sup>b</sup> when using a strand spacing of 1.5 mm

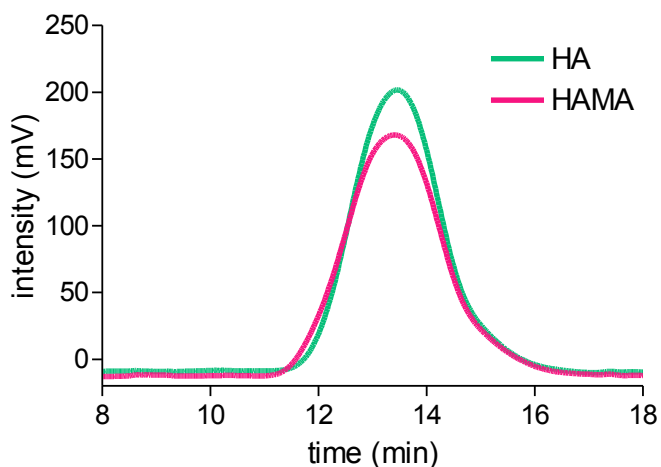


**Figure S1.** GPC chromatograms of HA and HAMA.

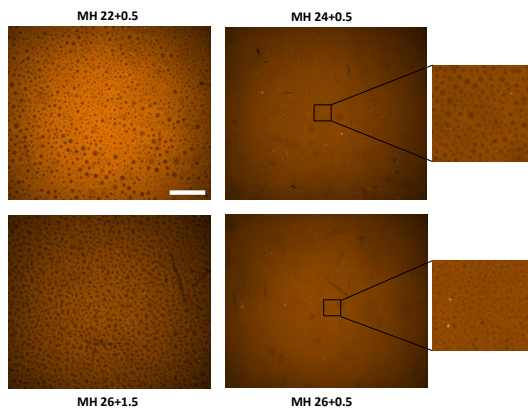


**Figure S2.** Confocal images (NR channel) for MH 22+0.5, MH 24+0.5 (with enlargement), MH 26+0.5 (with enlargement) and MH 26+1.5 after 1 h incubation at 37 °C. Scale bar represents 50  $\mu$ m. Minor phase separation is visible for MH 24+0.5 and MH 26+0.5 in comparison with MH 22+0.5.

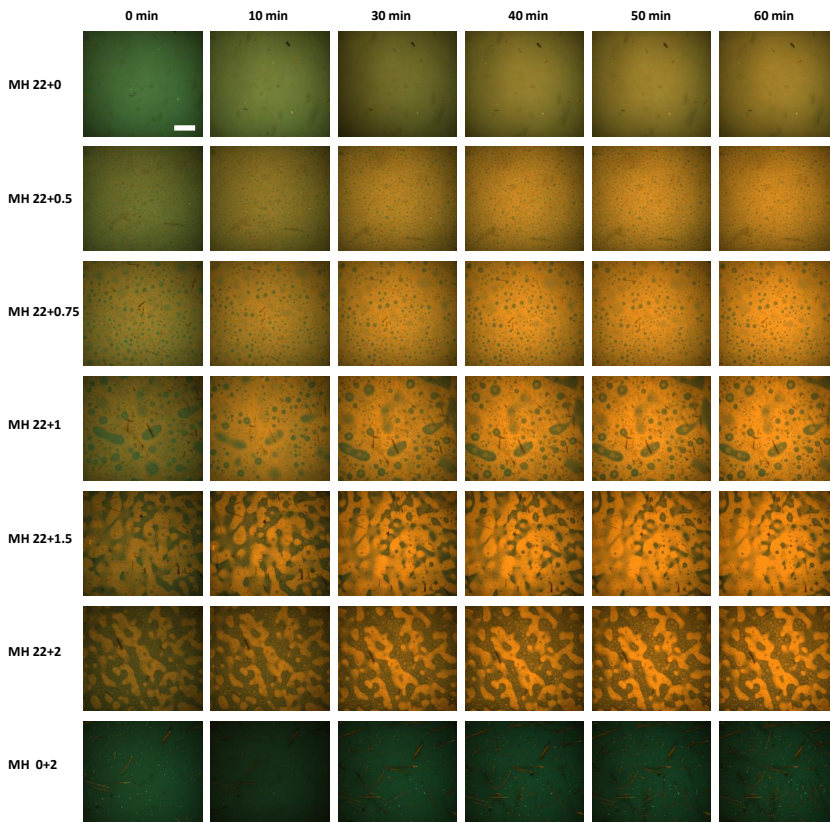


**Figure S3.** Confocal images (FITC/NR overlapped channels) for MH 22+0, MH 22+0.5, MH 22+0.75, MH 22+1, MH 22+1.5, MH 22+2 and MH 0+2 after 0 min, 10 min, 30 min, 40 min, 50 min and 1h of incubation at 37 °C. FITC-BSA is visualized in green and NR is visualized in red. Scale bar represents 50  $\mu$ m.

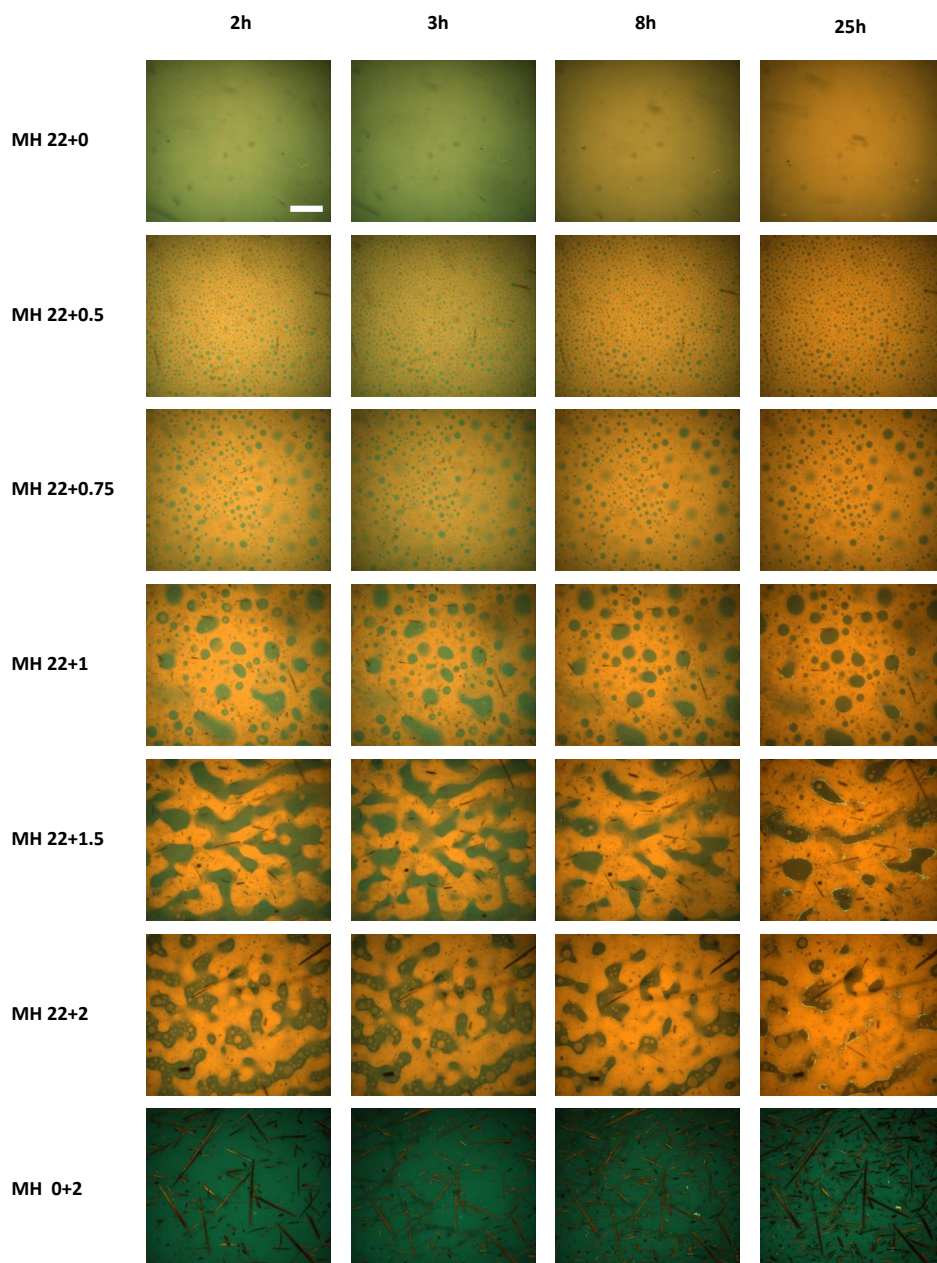


**Figure S4.** Confocal images (FITC/NR overlapped channels) for MH 22+0, MH 22+0.5, MH 22+0.75, MH 22+1, MH 22+1.5, MH 22+2 and MH 0+2 after 2 h, 3h, 8h and 25h of incubation at 37 °C. FITC-BSA is visualized in green and NR is visualized in red. Scale bar represents 50  $\mu\text{m}$ .

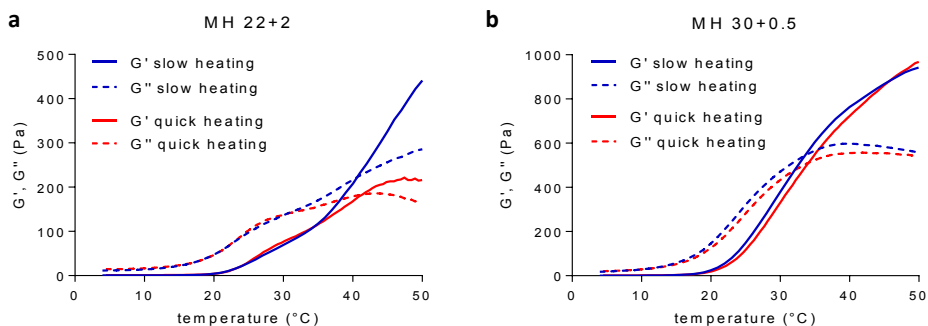


**Figure S5.** Effect of temperature ramp rate on thermogelation.  $G'$  and  $G''$  as function of temperature recorded during a slow temperature sweep ( $0.75\text{ °C/min}$ ) or quick temperature ramp ( $5\text{ °C/min}$ ) for MH 22+2 (a) and MH 30+0.5 (b).

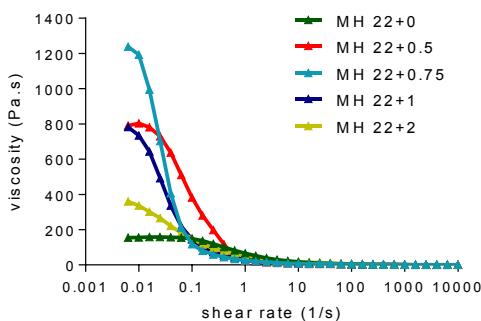


**Figure S6.** Effect of HAMA on shear thinning properties. Viscosity as function of shear rate recorded at  $37\text{ °C}$  during a shear rate sweep ( $0.006\text{-}10000\text{ 1/s}$ ) for several MH compositions varying in HAMA content.

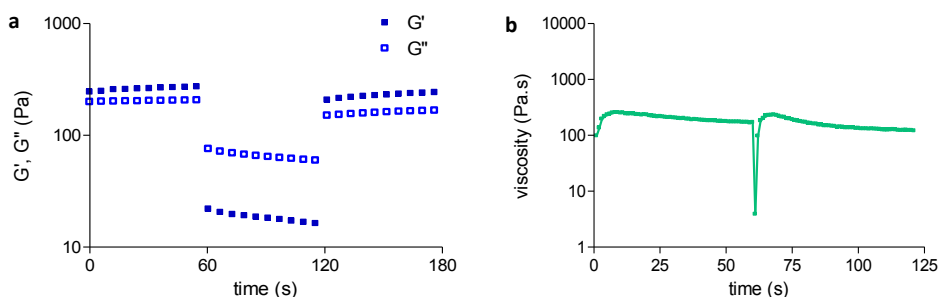


**Figure S7.** Recovery tests for MH 22+0.75.  $G'$  and  $G''$  as function of time recorded during three different time steps where low-high-low strain values (1%-100%-1%) were consecutively applied at  $37\text{ °C}$  (a). Viscosity as function of three different time steps where low-high-low shear rate values ( $0.05\text{ 1/s} - 100\text{ 1/s} - 0.05\text{ 1/s}$ ) were consecutively applied at  $37\text{ °C}$  (b).



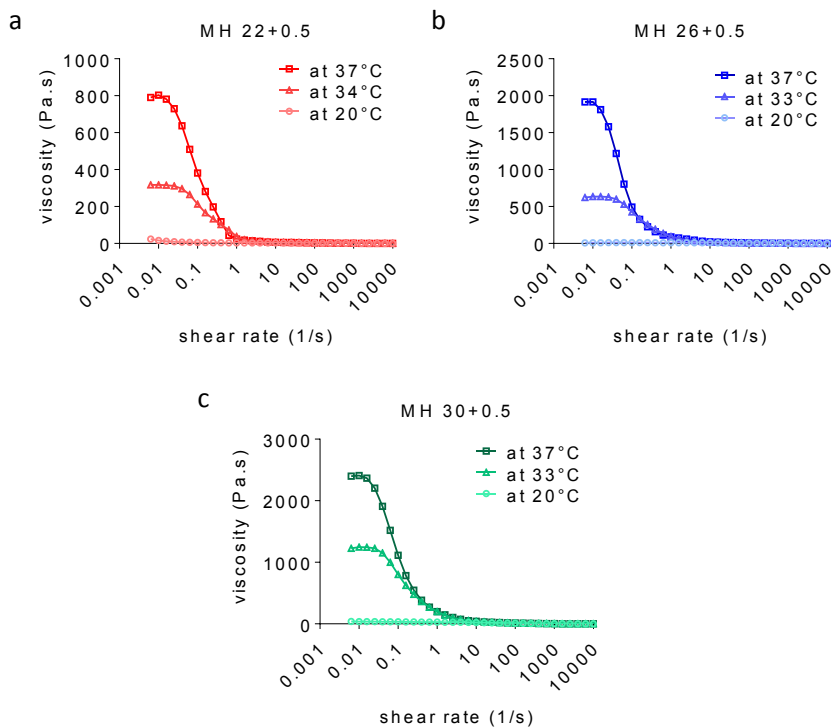


**Figure S8.** Effect of temperature on hydrogel shear thinning. Viscosity as function of shear rate for MH 22+0.5 at 37, 34 ( $T_{gel}$ ) and 20 °C (a), MH 26+0.5 at 37, 33 ( $T_{gel}$ ) and 20 °C (b), and MH 30+0.5 at 37, 33 ( $T_{gel}$ ) and 20 °C (c).

**Table S2.** Significant *inputs* from the neurofuzzy logic submodels for each *output* parameter

<i>output</i> parameter	submodels	<i>inputs</i> from neurofuzzylogic submodels	$R^2$	calculated f value	degrees of freedom	f critical
R/G ratio	submodel 1	HAMA	85.50	17.69	2 and 8	4.45
$G'$ at 37 °C	submodel 1	$M_{10}P_{10}$	74.51	8.77	2 and 8	4.06
$T_{gel}$	submodel 1 submodel 2	HAMA $M_{10}P_{10}$	79.83	3.96	4 and 8	3.83
yield stress	submodel 1	$M_{10}P_{10}$	89.08	16.32	2 and 6	5.14
viscosity at low shear	submodel 1	$M_{10}P_{10}$ x HAMA	93.50	4.80	6 and 8	3.58



**Table S3.** Rules for *output* parameters, R/G ratio, G' at 37 °C and  $T_{gel}$  recorded during oscillation temperature ramps, yield stress recorded during oscillation strain sweeps and viscosity at low shear rate (i.e. 0.006 1/s) recorded during flow shear rate sweeps. Blue color is used to indicate the combination of *inputs* giving the highest value of the *output* and red color is use to indicate the one giving the lowest value of the *output*.

<b>Rules for R/G ratio</b>		
<i>SubModel: 1- HAMA content</i>		
IF HAMA content is LOW	THEN R/G ratio is	HIGH (0.78)
IF HAMA content is HIGH	THEN R/G ratio is	LOW (0.95)
<b>Rules for G' at 37 °C</b>		
<i>SubModel: 1- <math>M_{10}P_{10}</math> content</i>		
IF $M_{10}P_{10}$ content is LOW	THEN G' is	LOW (0.81)
IF $M_{10}P_{10}$ content is HIGH	THEN G' is	HIGH (1.00)
<b>Rules for <math>T_{gel}</math></b>		
<i>SubModel: 1 - HAMA content</i>		
IF HAMA content is LOW	THEN $T_{gel}$ is	LOW (0.57)
IF HAMA content is MID	THEN $T_{gel}$ is	LOW (1.00)
IF HAMA content is HIGH	THEN $T_{gel}$ is	HIGH (1.00)
<i>SubModel: 2 - <math>M_{10}P_{10}</math> content</i>		
IF $M_{10}P_{10}$ content is LOW	THEN $T_{gel}$ is	HIGH (0.77)
IF $M_{10}P_{10}$ content is HIGH	THEN $T_{gel}$ is	LOW (0.77)
<b>Rules for yield stress</b>		
<i>SubModel: 1 - <math>M_{10}P_{10}</math> content</i>		
IF $M_{10}P_{10}$ content is LOW	THEN yield stress is	LOW (0.83)
IF $M_{10}P_{10}$ content is HIGH	THEN yield stress is	HIGH (1.00)
<b>Rules for viscosity at 0.006 1/s</b>		
<i>SubModel: 1- <math>M_{10}P_{10}</math> and HAMA content</i>		
IF $M_{10}P_{10}$ content is LOW AND HAMA content is LOW	THEN viscosity is	LOW (0.92)
IF $M_{10}P_{10}$ content is LOW AND HAMA content is MID	THEN viscosity is	LOW (0.58)
IF $M_{10}P_{10}$ content is LOW AND HAMA content is HIGH	THEN viscosity is	LOW (0.90)
IF $M_{10}P_{10}$ content is HIGH AND HAMA content is LOW	THEN viscosity is	LOW (1.00)
IF $M_{10}P_{10}$ content is HIGH AND HAMA content is MID	THEN viscosity is	HIGH (1.00)
IF $M_{10}P_{10}$ content is HIGH AND HAMA content is HIGH	THEN viscosity is	LOW (1.00)

## References

- (1) Ahadian, S.; Sadeghian, R. B.; Salehi, S.; Ostrovidov, S.; Bae, H.; Ramalingam, M.; Khademhosseini, A. Bioconjugated Hydrogels for Tissue Engineering and Regenerative Medicine. *Bioconjug. Chem.* **2015**, *26* (10), 1984–2001.
- (2) Censi, R.; Di Martino, P.; Vermonden, T.; Hennink, W. E. Hydrogels for Protein Delivery in Tissue Engineering. *J. Control. Release* **2012**, *161* (2), 680–692.
- (3) Vermonden, T.; Censi, R.; Hennink, W. E. Hydrogels for Protein Delivery. *Chem. Rev.* **2012**, *112* (5), 2853–2888.
- (4) Tibbitt, M. W.; Dahlman, J. E.; Langer, R. Emerging Frontiers in Drug Delivery. *J. Am. Chem. Soc.* **2016**, *138* (3), 704–717.
- (5) Caló, E.; Khutoryanskiy, V. V. Biomedical Applications of Hydrogels: A Review of Patents and Commercial Products. *Eur. Polym. J.* **2015**, *65*, 252–267.
- (6) Hammer, N.; Brandl, F. P.; Kirchhof, S.; Messmann, V.; Goepferich, A. M. Protein Compatibility of Selected Cross-Linking Reactions for Hydrogels. *Macromol. Biosci.* **2015**, *15* (3), 405–413.
- (7) Koetting, M. C.; Peters, J. T.; Steichen, S. D.; Peppas, N. A. Stimulus-Responsive Hydrogels: Theory, Modern Advances, and Applications. *Mater. Sci. Eng. R Reports* **2015**, *93*, 1–49.
- (8) Buwalda, S. J.; Boere, K. W. M.; Dijkstra, P. J.; Feijen, J.; Vermonden, T.; Hennink, W. E. Hydrogels in a Historical Perspective: From Simple Networks to Smart Materials. *J. Control. Release* **2014**, *190*, 254–273.
- (9) Annabi, N.; Tamayol, A.; Uquillas, J. A.; Akbari, M.; Bertassoni, L. E.; Cha, C.; Camci-Unal, G.; Dokmeci, M. R.; Peppas, N. A.; Khademhosseini, A. 25th Anniversary Article: Rational Design and Applications of Hydrogels in Regenerative Medicine. *Adv. Mater.* **2014**, *26* (1), 85–124.
- (10) Hutmacher, D. W. Scaffolds in Tissue Engineering Bone and Cartilage. *Biomaterials* **2000**, *21* (24), 2529–2543.
- (11) Madeira, C.; Santhaganam, A.; Salgueiro, J. B.; Cabral, J. M. S. Advanced Cell Therapies for Articular Cartilage Regeneration. *Trends Biotechnol.* **2015**, *33* (1), 35–42.
- (12) Hunt, J. A.; Chen, R.; van Veen, T.; Bryan, N. Hydrogels for Tissue Engineering and Regenerative Medicine. *J. Mater. Chem. B* **2014**, *2* (33), 5319–5338.
- (13) Kirchmayer, D. M.; Gorkin III, R.; in het Panhuis, M. An Overview of the Suitability of Hydrogel-Forming Polymers for Extrusion-Based 3D-Printing. *J. Mater. Chem. B* **2015**, *3* (20), 4105–4117.
- (14) Jungst, T.; Smolan, W.; Schacht, K.; Scheibel, T.; Groll, J. Strategies and Molecular Design Criteria for 3D Printable Hydrogels. *Chem. Rev.* **2016**, *116* (3), 1496–1539.
- (15) Lee, V. K.; Dai, G. Printing of Three-Dimensional Tissue Analogs for Regenerative Medicine. *Ann. Biomed. Eng.* **2016**.
- (16) Jose, R. R.; Rodriguez, M. J.; Dixon, T. A.; Omenetto, F.; Kaplan, D. L. Evolution of Bioinks and Additive Manufacturing Technologies for 3D Bioprinting. *ACS Biomater. Sci. Eng.* **2016**, acsbiomaterials.6b00088.
- (17) Malda, J.; Visser, J.; Melchels, F. P.; Jüngst, T.; Hennink, W. E.; Dhert, W. J. A.; Groll, J.; Hutmacher, D. W. 25th Anniversary Article: Engineering Hydrogels for Biofabrication. *Adv. Mater.* **2013**, *25* (36), 5011–5028.
- (18) Melchels, F. P. W.; Feijen, J.; Grijpma, D. W. A Review on Stereolithography and Its

- Applications in Biomedical Engineering. *Biomaterials* **2010**, *31* (24), 6121–6130.
- (19) Melchels, F. P. W.; Domingos, M. A. N.; Klein, T. J.; Malda, J.; Bartolo, P. J.; Huttmacher, D. W. Additive Manufacturing of Tissues and Organs. *Prog. Polym. Sci.* **2012**, *37* (8), 1079–1104.
- (20) Vermonden, T.; Fedorovich, N. E.; van Geemen, D.; Alblas, J.; van Nostrum, C. F.; Dhert, W. J. A.; Hennink, W. E. Photopolymerized Thermosensitive Hydrogels: Synthesis, Degradation, and Cytocompatibility. *Biomacromolecules* **2008**, *9* (3), 919–926.
- (21) Censi, R.; Vermonden, T.; Deschout, H.; Braeckmans, K.; di Martino, P.; De Smedt, S. C.; van Nostrum, C. F.; Hennink, W. E. Photopolymerized Thermosensitive poly(HPMA lactate)-PEG-Based Hydrogels: Effect of Network Design on Mechanical Properties, Degradation, and Release Behavior. *Biomacromolecules* **2010**, *11* (8), 2143–2151.
- (22) Censi, R.; Schuurman, W.; Malda, J.; di Dato, G.; Burgisser, P. E.; Dhert, W. J. A.; van Nostrum, C. F.; di Martino, P.; Vermonden, T.; Hennink, W. E. A Printable Photopolymerizable Thermosensitive p(HPMAm-Lactate)-PEG Hydrogel for Tissue Engineering. *Adv. Funct. Mater.* **2011**, *21* (10), 1833–1842.
- (23) Abbadessa, A.; Blokzijl, M. M.; Mouser, V. H. M.; Marica, P.; Malda, J.; Hennink, W. E.; Vermonden, T. A Thermo-Responsive and Photo-Polymerizable Chondroitin Sulfate-Based Hydrogel for 3D Printing Applications. *Carbohydr. Polym.* **2016**, *149*, 163–174.
- (24) Abbadessa, A.; Mouser, V. H. M.; Blokzijl, M. M.; Gawlitta, D.; Dhert, W. J. A.; Hennink, W. E.; Malda, J.; Vermonden, T. A Synthetic Thermosensitive Hydrogel for Cartilage Bioprinting and Its Biofunctionalization with Polysaccharides. *Biomacromolecules* **2016**, *17* (6), 2137–2147.
- (25) Albertsson, P.-Å. Particle Fractionation in Liquid Two-Phase Systems. The Composition of Some Phase Systems and the Behaviour of Some Model Particles in Them. Application to the Isolation of Cell Walls from Microorganisms. *Biochim. Biophys. Acta* **1958**, *27*, 378–395.
- (26) Stenekes, R. J. H.; Franssen, O.; van Bommel, E. M. G.; Crommelin, D. J. A.; Hennink, W. E. The Preparation of Dextran Microspheres in an All-Aqueous System: Effect of the Formulation Parameters on Particle Characteristics. *Pharm. Res.* **1998**, *15* (4), 557–561.
- (27) Franssen, O.; Hennink, W. E. A Novel Preparation Method for Polymeric Microparticles without the Use of Organic Solvents. *Int. J. Pharm.* **1998**, *168* (1), 1–7.
- (28) Albertsson, P.-Å. Partition of Cell Particles and Macromolecules in Polymer Two-Phase Systems. In *Archives of Biochemistry and Biophysics*; 1970; Vol. 100, pp 309–341.
- (29) Hatti-Kaul, R. Aqueous Two-Phase Systems: A General Overview. *Mol. Biotechnol.* **2001**, *19* (3), 269–278.
- (30) Johansson, H.-O.; Magaldi, F. M.; Feitosa, E.; Pessoa, A. Protein Partitioning in Poly(ethylene Glycol)/sodium Polyacrylate Aqueous Two-Phase Systems. *J. Chromatogr. A* **2008**, *1178* (1–2), 145–153.
- (31) Levett, P. A.; Melchels, F. P. W.; Schrobback, K.; Huttmacher, D. W.; Malda, J.; Klein, T. J. A Biomimetic Extracellular Matrix for Cartilage Tissue Engineering Centered on Photocurable Gelatin, Hyaluronic Acid and Chondroitin Sulfate. *Acta Biomater.*

- 2014, *10* (1), 214–223.
- (32) François, J.; Beaudoin, E.; Borisov, O. Association of Hydrophobically End-Capped Poly(ethylene Oxide). 2. Phase Diagrams. *Langmuir* **2003**, *19* (24), 10011–10018.
- (33) Vermonden, T.; Jena, S. S.; Barriet, D.; Censi, R.; van der Gucht, J.; Hennink, W. E.; Siegel, R. A. Macromolecular Diffusion in Self-Assembling Biodegradable Thermosensitive Hydrogels. *Macromolecules* **2010**, *43* (2), 782–789.
- (34) Semenov, A. N.; Joanny, J.-F.; Khokhlov, A. R. Associating Polymers: Equilibrium and Linear Viscoelasticity. *Macromolecules* **1995**, *28* (4), 1066–1075.
- (35) Oudshoorn, M. H. M.; Rissmann, R.; Bouwstra, J. A.; Hennink, W. E. Synthesis and Characterization of Hyperbranched Polyglycerol Hydrogels. *Biomaterials* **2006**, *27* (32), 5471–5479.
- (36) Achanta, A. S.; Kowalski, J. G.; Rhodes, C. T. Artificial Neural Networks: Implications for Pharmaceutical Sciences. *Drug Dev. Ind. Pharm.* **1995**, *21* (1), 119–155.
- (37) Kazazi-Hyseni, F.; Landin, M.; Lathuile, A.; Veldhuis, G. J.; Rahimian, S.; Hennink, W. E.; Kok, R. J.; van Nostrum, C. F. Computer Modeling Assisted Design of Monodisperse PLGA Microspheres with Controlled Porosity Affords Zero Order Release of an Encapsulated Macromolecule for 3 Months. *Pharm. Res.* **2014**, 2844–2856.
- (38) Nauck, D.; Kruse, R. A Neuro-Fuzzy Method to Learn Fuzzy Classification Rules from Data. *Fuzzy Sets Syst.* **1997**, *89* (3), 277–288.
- (39) Landin, M.; Rowe, R. C. Artificial Neural Networks Technology to Model, Understand, and Optimize Drug Formulations. In *Formulation Tools for Pharmaceutical Development*; Elsevier, 2013; pp 7–37.
- (40) Rijcken, C. J.; Snel, C. J.; Schifflers, R. M.; van Nostrum, C. F.; Hennink, W. E. Hydrolysable Core-Crosslinked Thermosensitive Polymeric Micelles: Synthesis, Characterisation and in Vivo Studies. *Biomaterials* **2007**, *28* (36), 5581–5593.
- (41) Hachet, E.; Van Den Berghe, H.; Bayma, E.; Block, M. R.; Auzély-Velty, R. Design of Biomimetic Cell-Interactive Substrates Using Hyaluronic Acid Hydrogels with Tunable Mechanical Properties. *Biomacromolecules* **2012**, *13* (6), 1818–1827.
- (42) Stenekes, R. J. H.; Hennink, W. E. Polymerization Kinetics of Dextran-Bound Methacrylate in an Aqueous Two Phase System. *Polymer* **2000**, *41* (15), 5563–5569.
- (43) Gardner, O. F. W.; Musumeci, G.; Neumann, A. J.; Eglin, D.; Archer, C. W.; Alini, M.; Stoddart, M. J. Asymmetrical Seeding of MSCs into Fibrin-Poly(ester-Urethane) Scaffolds and Its Effect on Mechanically Induced Chondrogenesis. *J. Tissue Eng. Regen. Med.* **2016**.
- (44) Shih, C. M.; Chien, J. T. The Microscopic Pictures of Degenerative Intervertebral Disc of Different Diseases with Additional Safranin-O Stain. *J. Clin. Exp. Pathol.* **2015**, *6* (1), 1–5.
- (45) Barandun, M.; Iselin, L. D.; Santini, F.; Pansini, M.; Scotti, C.; Baumhoer, D.; Bieri, O.; Studler, U.; Wirz, D.; Haug, M.; Jakob, M.; Schaefer, D. J.; Martin, I.; Barbero, A. Generation and Characterization of Osteochondral Grafts with Human Nasal Chondrocytes. *J. Orthop. Res.* **2015**, *33* (8), 1111–1119.
- (46) Younesi, M.; Goldberg, V. M.; Akkus, O. A Micro-Architecturally Biomimetic Collagen Template for Mesenchymal Condensation Based Cartilage Regeneration. *Acta Biomater.* **2016**, *30*, 212–221.
- (47) Hsu, H.; Uemura, T.; Yamaguchi, I.; Ikoma, T.; Tanaka, J. Chondrogenic Differentiation of Human Mesenchymal Stem Cells on Fish Scale Collagen. *J. Biosci. Bioeng.* **2016**,

- 122 (2), 219–225.
- (48) Prins, H.-J.; Braat, A. K.; Gawlitta, D.; Dhert, W. J. A.; Egan, D. A.; Tijssen-Slump, E.; Yuan, H.; Coffey, P. J.; Rozemuller, H.; Martens, A. C. In Vitro Induction of Alkaline Phosphatase Levels Predicts in Vivo Bone Forming Capacity of Human Bone Marrow Stromal Cells. *Stem Cell Res.* **2014**, *12* (2), 428–440.
- (49) Kokkinis, D.; Schaffner, M.; Studart, A. R. Multimaterial Magnetically Assisted 3D Printing of Composite Materials. *Nat. Commun.* **2015**, *6*, 8643.
- (50) Zhang, M.; Vora, A.; Han, W.; Wojtecki, R. J.; Maune, H.; Le, A. B. A.; Thompson, L. E.; McClelland, G. M.; Ribet, F.; Engler, A. C.; Nelson, A. Dual-Responsive Hydrogels for Direct-Write 3D Printing. *Macromolecules* **2015**, *48* (18), 6482–6488.
- (51) Sprakel, J.; Besseling, N. A. M.; Cohen Stuart, M. A.; Leermakers, F. A. M. Phase Behavior of Flowerlike Micelles in a SCF Cell Model. *Eur. Phys. J. E* **2008**, *25* (2), 163–173.



## **Chapter 5**

### **Monodisperse hyaluronic acid-based microgels loaded in thermosensitive hydrogels for a sustained release of proteins: an introductory study**

**A. Abbadessa, C.C.L. Schuurmans, M.M. Blokzijl, J.E. Citteren,  
W.E. Hennink, T. Vermonden**



## Abstract

*In situ* controlled release of proteins, e.g. growth factors from tissue-engineered hydrogel constructs is a promising approach to treat tissue defects. The aim of this study was to develop a hydrogel system suitable for tissue engineering applications that releases a positively charged protein, i.e. lysozyme in a sustained manner. To this end, two different UV-crosslinked systems were designed and compared: a lysozyme-loaded hydrogel based on a thermosensitive triblock copolymer of polyethylene glycol (PEG) and methacrylated poly(*N*-(2-hydroxypropyl) methacrylamide-mono/dilactate) (pHPMAlac) blended with methacrylated hyaluronic acid (HAMA) and a PEG-pHPMAlac hydrogel in which HAMA-based monodisperse and lysozyme-loaded microgels were dispersed. Release of lysozyme from hydrogel blends containing different HAMA concentrations of varying molecular weight (MW) was studied. In the second approach, monodisperse crosslinked HAMA microgels were fabricated via microfluidics, post-loaded with lysozyme and further incorporated into the thermosensitive network (further referred to as microcomposite hydrogel). Results for PEG-pHPMAlac/HAMA/lysozyme hydrogel blends showed that complete release of lysozyme occurred within 24 hours, without being affected by HAMA MW or concentration. Monodisperse HAMA microgels had an average diameter ranging from 313 to 557  $\mu\text{m}$ , depending on the processing conditions and HAMA concentration. Lysozyme-loaded HAMA microgels displayed high loading percentage ( $\geq 62\%$ ) and loading efficiency ( $\geq 41\%$ ). Microcomposite HAMA/PEG-pHPMAlac hydrogels showed a sustained release of lysozyme over at least 20 days. The slower kinetics of protein release from microcomposite hydrogels compared to that from PEG-pHPMAlac/HAMA/lysozyme hydrogel blends points to a strong interaction between the protein and the crosslinked HAMA microgels. Importantly, the enzymatic activity of lysozyme after release was fully preserved, demonstrating the protein-friendly character of this technology. In conclusion, monodisperse HAMA microgels loaded in thermosensitive hydrogels are promising delivery systems for the sustained release of proteins.



## 5.1 Introduction

Scaffolds based on biodegradable hydrogels are currently under investigation for their potential in tissue engineering (TE) and drug delivery<sup>1-6</sup>. Because of their soft nature and high water content, hydrogels represent suitable carriers for cells. Moreover hydrogels provide mechanical support to damaged tissue, due to their ability to entirely fill the tissue defect area and to resist stress. However, in an ideal scenario this support is only temporary and it should be progressively replaced by newly formed tissue, synthesized by cells that are embedded into the hydrogel matrix during fabrication or recruited from surrounding tissue<sup>7</sup>. Therefore, hydrogel biodegradability is an important feature, especially when it can be tailored to the time scale of the tissue regeneration process<sup>8</sup>. Tunable biodegradability can be achieved using hydrogels made of synthetic polymers by varying *e.g.* the polymer content of the gels and their crosslink density<sup>9,10</sup>. On the other hand, synthetic hydrogels most often are unable to offer beneficial material-cell interactions, which may trigger the activation of biological pathways crucial for intercellular signaling, cellular differentiation and matrix production. Therefore, inclusion of signaling molecules, *e.g.* growth factors into hydrogels is a commonly investigated strategy to instruct embedded cells or to trigger endogenous cell recruitment<sup>11</sup>. Biologically relevant molecules can be included into hydrogels simply by mixing them into the polymeric mixture prior hydrogel formation, and can be further immobilized into the polymeric network via covalent binding or physical interactions<sup>5</sup>. Generally speaking, covalent binding via a degradable linker to the polymer network can guarantee a long persistence of these molecules in the hydrogels and a prolonged release. Nevertheless, chemical modifications may lead to structural changes and consequent loss of activity, especially when sensitive molecules, *e.g.* growth factors are involved<sup>11,12</sup>. Therefore, in case of growth factors, physical entrapment via, *e.g.* ionic interactions is often preferred<sup>13</sup>. This approach is inspired by the natural mechanism of growth factor sequestration by heparin and other negatively charged biopolymers into the endogenous extracellular matrix, and has been applied for the immobilization of growth factors into hydrogels to increase *e.g.* osteogenic or chondrogenic differentiation of embedded cells<sup>13,14</sup>.

UV-crosslinkable hydrogels based on triblock copolymers of polyethylene glycol (PEG) and methacrylated poly(*N*-(2-hydroxypropyl) methacrylamide-mono/dilactate) (pHPMALac) blended with methacrylated polysaccharides, such as methacrylated hyaluronic acid (HAMA) are currently under investigation for TE applications<sup>15,16</sup>. The presence of HAMA renders these hydrogels negatively charged at physiological conditions and offers the opportunity for the adsorption of positively charged growth factors to the hydrogel network. Examples of relevant growth factors currently under investigation in TE are: angiopoietin 1 and 2 (Ang-1 and -2) and vascular endothelial growth factor (VEGF) for the regeneration of blood vessels; nerve growth factor (NGF) for the regeneration of nerves, spine and brain; and transforming growth factor- $\beta$  (TGF- $\beta$ ) and human platelet-derived growth

factor-BB (hPDGF-BB) for the treatment of cartilage defects<sup>17</sup>. Our hypothesis is that positively charged proteins can be loaded in PEG-pHPMAlac/HAMA hydrogels exploiting protein-HAMA electrostatic interactions. In this context, it is well known that when proteins are included in a hydrogel network, the release kinetics is usually dependent on diffusion kinetics, which can be directly related to protein size and mesh size of the hydrogel network. Therefore, for highly crosslinked hydrogels that have a mesh size in the same range or smaller than the size of the protein, the release can be prolonged and is dependent on the hydrogel degradation kinetics. However, for TE applications in general hydrogels with a relatively low crosslink density are considered beneficial for performance of entrapped cells or to facilitate cell migration. In these hydrogels, entrapped proteins are usually released rapidly according to diffusion-controlled kinetics. Although these kinetics can be often tuned by changing the polymer concentration and number of crosslinkable groups, they generally result in a protein release within few hours or days<sup>18–20</sup>.

The aim of this study was to develop a hydrogel system suitable for TE applications that releases a loaded protein in a sustained manner (at least few weeks). To this end, two different systems were studied: a protein-containing hydrogel blend of PEG-pHPMAlac and HAMA varying in molecular weight (MW) and concentration, and a PEG-pHPMAlac hydrogel in which (protein-loaded) HAMA microgels are dispersed (the latter is further referred to as microcomposite hydrogel). In the present study, we used lysozyme as a model protein, since its size (MW = 14 kDa, hydrodynamic radius = 1.9 nm)<sup>21</sup> and isoelectric point (pI = 11.4) are in the same range as many growth factors<sup>22</sup>. For the fabrication of the microcomposite hydrogel, monodisperse HAMA microgels were fabricated via microfluidics, post-loaded with lysozyme and further encapsulated into PEG-pHPMAlac hydrogels. Recently, the use of two-phase composite hydrogels for biomedical applications has gained attention. Incorporation of micro- and nanoparticles (*e.g.* polymeric, carbon-based or inorganic particles) in polymeric networks is currently exploited to increase mechanical stiffness, to allow encapsulation of hydrophobic drugs, or to obtain a sustained or stimuli-sensitive release of encapsulated molecules<sup>23–27</sup>. Additionally, our choice of using a microfluidics-based system for the preparation of HAMA microgels relies on the fact that microfluidics-based techniques can warrant highly monodisperse droplets/particles formation<sup>28</sup> and have been recently recognized as a smart alternative to classic bulk methods for the fabrication of drug delivery systems<sup>29</sup>. Microfluidics-based technology can be applied to obtain full control over size, shape and micro-architecture (including *e.g.* controllable shell thickness for core-shell systems, multi-shell/multi-chamber design) of particles<sup>29–34</sup>. Importantly, increase of drug loading, more homogeneous drug partition into the matrix, slower drug release and smaller initial burst release have been described for drug delivery systems prepared using microfluidics compared to conventional methods<sup>29</sup>. In this study, we developed a simple and effective microfluidics device with a co-flowing geometry design for the generation of monodisperse aqueous HAMA droplets in oil.

In summary, the aim of this study was to develop a protein delivery system, able to provide sustained release of a loaded protein. To this end, the release kinetics of a

model protein was studied from PEG-pHPMAlac/HAMA hydrogels, where HAMA was included into the PEG-pHPMAlac network either as a building block *per se* or as monodisperse pre-crosslinked microgels.

## 5.2 Materials and Methods

### 5.2.1 Materials

All solvents and chemicals were purchased from Biosolve (Valkenswaard, the Netherlands) and Sigma-Aldrich (Zwijndrecht, the Netherlands), respectively, unless reported otherwise. Solvents and chemicals were used as received. Sodium hyaluronate (HA, 57, 120 and 289 kDa) was purchased from Lifecore Biomedical (Chaska, MN, USA) and lysozyme from chicken egg white was ordered from Sigma-Aldrich. Phosphate buffered saline pH 7.4 (PBS) was supplied by Braun (Melsungen, Germany), L-lactide by Corbion (Gorinchem, The Netherlands), PEG (10 kDa) by Merck (Darmstadt, Germany) and Irgacure 2959 was kindly donated by BASF (Ludwigshafen, Germany). HPMA, HPMA-monolactate, HPMA-dilactate and PEG<sub>10kDa</sub>-4,4'-azobis(cyanopentanoate) macroinitiator were synthesized and characterized as previously reported<sup>35-37</sup>. Mineral oil (light) and Span<sup>®</sup>80 [viscosity = 1000-2000 mPa.s (20 °C)] were purchased from Sigma-Aldrich. Lyophilized *Micrococcus lysodeikticus* bacteria were purchased from Sigma Aldrich.

### 5.2.2 Synthesis and characterization of polymers

A triblock copolymer with an ABA-like architecture composed of a PEG (10 kDa) mid-block and two pHPMAlac (mono/dilactate ratio = 75:25) outer blocks, and its partially methacrylated derivative were synthesized and characterized as previously reported<sup>38,39</sup>. The methacrylated PEG-pHPMAlac triblock copolymer is hereafter abbreviated as M<sub>10</sub>P<sub>10</sub>, where M<sub>10</sub> refers to a degree of methacrylation (DM) of 10% and P<sub>10</sub> refers to the MW of the PEG block. The characteristics of M<sub>10</sub>P<sub>10</sub> were in line with previously reported findings<sup>15,38-40</sup>. HAMA was synthesized according to a previously reported method by Hachet *et al.* with minor adjustments<sup>41</sup>. Briefly, HA (57, 120 or 289 kDa, 0.5 g, 1.25 mmol of disaccharide units) was dissolved in water (25 ml) overnight at 4 °C. *N,N*-dimethylformamide (25 ml) was added. Subsequently, methacrylic anhydride (MA, 2.5 mmol) was added drop-wise at 4 °C, while keeping the pH between 8 and 9 by addition of NaOH solution (0.5 M). HAMA was subsequently precipitated by addition of NaCl (final concentration = 0.5 M) and cold ethanol. The suspension was then centrifuged (14.000 rpm) for 15 minutes at 4 °C. After removal of the supernatant, HAMA pellets were re-dissolved in water and the resulting HAMA solution was dialyzed against water for 2 days. HAMA was characterized by <sup>1</sup>H NMR, and the DM was calculated according to equation 1.

$$DM (\%) = \frac{\text{average}(I_{6.2}, I_{5.8})}{(I_{2.1} - 3)/3} \times 100 \quad \text{Equation 1}$$

in which the signal at chemical shift 6.2 ppm was normalized to an integration value of 1. HAMA with MW of 57, 120 and 289 kDa are further abbreviated as HAMA<sub>57</sub>,

HAMA<sub>120</sub>, HAMA<sub>289</sub>, respectively. The typical DM was  $20 \pm 4\%$ .

### 5.2.3 Protein release study from M<sub>10</sub>P<sub>10</sub>/HAMA hydrogels

M<sub>10</sub>P<sub>10</sub> and HAMA<sub>57</sub>, HAMA<sub>120</sub> or HAMA<sub>289</sub> (polymer concentrations reported in Table 1) and Irgacure 0.05% (w/w) were mixed in PBS at 4 °C. To each polymer mixture, lysozyme was added (final concentration = 10 mg/ml) and the resulting mixtures were stirred overnight at 4 °C.

**Table 1.** Hydrogel compositions and abbreviations for M<sub>10</sub>P<sub>10</sub>/HAMA hydrogels. In the abbreviations, M refers to the presence of  $\underline{M}_{10}P_{10}$ , H to the presence of  $\underline{H}AMA$ , subscript number in parenthesis to the MW of HAMA and following numbers refer to the concentration of M<sub>10</sub>P<sub>10</sub> and HAMA, respectively.

Abbreviation	M <sub>10</sub> P <sub>10</sub> (% w/w)	HAMA <sub>57</sub> (% w/w)	HAMA <sub>120</sub> (% w/w)	HAMA <sub>289</sub> (% w/w)
M 18.5	18.5			
M 19.0	19.0			
M 20.0	20.0			
MH <sub>(57)</sub> 18+0.5	18.0	0.5		
MH <sub>(57)</sub> 18+1.0	18.0	1.0		
MH <sub>(57)</sub> 18+2.0	18.0	2.0		
MH <sub>(120)</sub> 18+0.5	18.0		0.5	
MH <sub>(120)</sub> 18+1.0	18.0		1.0	
MH <sub>(120)</sub> 18+2.0	18.0		2.0	
MH <sub>(289)</sub> 18+0.5	18.0			0.5
MH <sub>(289)</sub> 18+1.0	18.0			1.0
MH <sub>(289)</sub> 18+2.0	18.0			2.0

To obtain cylindrical hydrogels, polymer mixtures were injected into a teflon mold (diameter = 6 mm, height = 2 mm) and incubated at 37 °C for 5 minutes to allow physical thermogelation. Subsequently, hydrogels were UV-irradiated for 5 minutes at a distance of 3 cm from the light source (UV-Handleuchte lamp A. Hartenstein, Germany, wavelength: 365 nm, intensity at 3 cm: 1.2 mW/cm<sup>2</sup>). Lysozyme-loaded

hydrogels were kept in PBS (enriched with 0.02% of  $\text{NaN}_3$ , 900  $\mu\text{l}$  of PBS/gel) at 37  $^\circ\text{C}$ . At several time points 150  $\mu\text{l}$  of medium was removed for analysis and replaced with fresh medium. Quantitative detection of released lysozyme was performed using a Waters Acquity UPLC system equipped with a reversed-phase BEH 300 C18 1.7 $\mu\text{m}$  2.1x50 mm column and connected to a fluorescence detector (excitation wavelength = 280 nm, emission wavelength = 340 nm). A gradient elution (sample injection volume = 7.5  $\mu\text{l}$ , gradient duration = 5 min) was carried out at 0.25 ml/min from 100% of eluent A to 100% of eluent B, where eluent A was a solution of water/acetonitrile (ACN) (95/5), containing 0.1% trifluoroacetic acid (TFA), and eluent B was composed of ACN, containing 0.1% TFA. Calibration curves were obtained using solutions containing known concentration of lysozyme in PBS (5-2000  $\mu\text{g}/\text{ml}$ ). Cumulative release of lysozyme was calculated and reported as the percentage of the actual amount of lysozyme loaded into each hydrogel.

#### 5.2.4 Microfluidics set-up for microgel fabrication

A microfluidics set-up was developed as follows. A dual syringe pump (model 33, Harvard Apparatus) was used to establish two different constant flows. Disposable syringes with luer-lock fittings were used to inject the two different phases and were connected to 1/16<sup>th</sup> inch OD tubing screwing their luer tips into the tubing adapters. Tubes containing the external and the internal phase were let to converge into a customized polyethyletherketone (PEEK) T-junction (Sigma Aldrich). The three T-junction inlets (original ID = 0.020 inch) were drilled out with a micro-drill to an ID roughly equal to 0.040 inch in order to facilitate high fluid flows. The tube containing the external phase was connected to the inlet of the T-junction via a nut and ferrule (orange fluid stream in Figure 1).

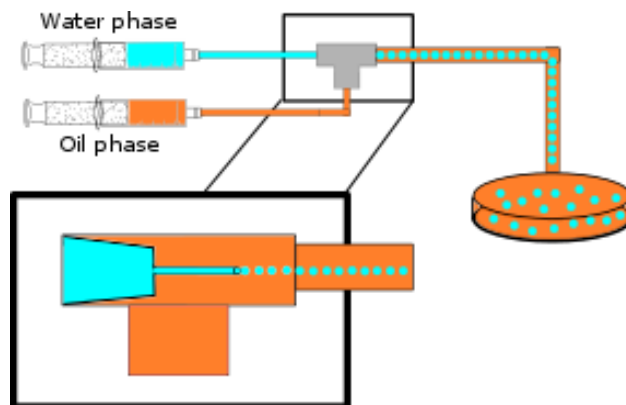


**Figure 1.** Formation of microdroplets using a microfluidics device developed in house. Internal aqueous (dispersed) phase is indicated in blue, external oil (continuous) phase is indicated in orange.

To form micrometer sized droplets of the internal phase, the extremity of the tube containing this phase was equipped with a blunt *Nanofil*<sup>®</sup> needle (World Precision Instruments). To generate a leak-free connection between the tube and the needle, the needle holder was partially inserted into a 1 cm-long tube of chemically resistant, polyolefin-based heat shrink (OD diameter of 3/64<sup>th</sup> inch) and was held above a hot soldering iron to shrink the tubing around the needle. This was then inserted into the 1/16<sup>th</sup> inch tube creating a snug fit. To create a co-flowing geometry, a nut and ferrule were fitted onto the tubing and connected to one of the two straight inlets of the PEEK T-junction. The last opening of the T-junction was connected via a nut to 1/8<sup>th</sup> inch OD tubing acting as the receiving channel for the generated droplets. The droplets were then collected in a petri-dish filled with the external oil phase. The method was validated by studying the formation of water droplets in mineral oil using different needle diameters and external phase flow rates (Figure S1).

### 5.2.5 Fabrication and characterization of HAMA microgels

HAMA microgels were fabricated using the microfluidics device described above. In detail, solutions of HAMA (2.5 or 5% w/w) and Irgacure (0.5%) in milliQ water were filtered through a Schott-Duran P1 glass filter (nominal max. pore size: 100 - 160 μm) and loaded into the internal phase-bearing syringe. A solution of Span 80 in mineral oil (8% w/w) was used as external phase. The flow of HAMA solution was set at 100 μl/min, whereas that of the oil phase at 2 or 6 ml/min. A needle with a diameter of 115 μm was used. After the emulsion was collected, HAMA aqueous droplets were UV irradiated for 10 minutes at a distance of 5 cm using a Bluepoint 4 UV lamp (point light source, wavelength range: 300-600 nm, intensity at 5 cm: 80 mW/cm<sup>2</sup>, Höppler UV Technology AG, Gräfelfing, Germany). The formed crosslinked HAMA microgels were washed three times with excess of tetrahydrofuran (THF, approximately 50 ml of THF for each washing step of 5 mg of microgels). For each washing step, THF was added and the resulting suspensions were vortexed for 30 seconds. Next, the microgels were left to sediment by gravity and the supernatant was removed and replaced with fresh THF. Residual THF after the final washing step was evaporated under mild N<sub>2</sub> flow. Abbreviations for HAMA microgels are reported in Table 2.

HAMA microgels were rehydrated with PBS, placed on a glass slide and visualized and photographed using an Olympus microscope provided with a digital camera (Olympus BX51 microscope, Olympus DP70 camera, Hamburg, Germany). The diameters of a minimum of 100 particles randomly belonging to at least three different batches of microgels with the same composition and prepared using the same processing parameters were measured and used for the calculation of the average diameter and the Coefficient of Variation (CoV) using equation 2<sup>42</sup>. The CoV is a measure for the difference in diameter of each individual microgel compared to the mean, and it is usually conveyed as a percentage<sup>43,44</sup>.

$$CoV = \frac{\text{St.deviation of microgel diameter}}{\text{mean microgel diameter}} * 100 \quad \text{Equation 2}$$



**Table 2.** Compositions and abbreviations for HAMA microgels. In the abbreviations, the numbers following “HAMA” indicate the HAMA concentration in milliQ water and the flow of the continuous phase (in ml/min) used during microgel fabrication, respectively.

Abbreviation	HAMA concentration (% w/w)	Continuous phase flow (ml/min)
HAMA 2.5_2	2.5	2
HAMA 2.5_6	2.5	6
HAMA 5.0_2	5.0	2
HAMA 5.0_6	5.0	6

### 5.2.6 Post-loading of lysozyme into HAMA microgels

The loading of lysozyme post-microgel fabrication was performed according to a previously described method<sup>45</sup>. Briefly, 450  $\mu$ l of microgel suspension (0.5 mg of dry microgels/ml) in 20 mM *N*-(2-hydroxyethyl)piperazine-*N'*-(2-ethanesulfonic acid) (HEPES, pH 7.4) buffer was mixed with 450  $\mu$ l of lysozyme solution (2 mg/ml) in 20 mM HEPES buffer. Samples were gently shaken at room temperature and after 1, 24 and 48 hours of incubation, the supernatant was analyzed to determine the amount of non-loaded lysozyme via UPLC, as described in section 5.2.3. From this, the loaded amount of lysozyme into the microgels was calculated and used to determine the loading percentage (L) and the loading efficiency (LE) according to equation 3 and 4, in which the dry microgel weight is the weight of microgels calculated based on the concentration of initial microgel suspension in HEPES.

$$L (\%) = \frac{\text{weight loaded Lys into microgels}}{\text{weight dry microgels} + \text{loaded Lys}} * 100 \quad \text{Equation 3}$$

$$LE (\%) = \frac{\text{loaded Lys into microgels}}{\text{feed Lys}} * 100 \quad \text{Equation 4}$$

### 5.2.7 Protein release study from microcomposite HAMA/M<sub>10</sub>P<sub>10</sub> hydrogels

Lysozyme-loaded microgels with the four selected compositions (Table 2) were fabricated as reported in the previous section using a higher scale (9 ml *vs* above mentioned 450  $\mu$ l). After 1 hour of incubation of the microgels with the lysozyme solution, samples were centrifuged at 5000 rpm (5311xg), the supernatant was removed and each microgel pellet was mixed with M<sub>10</sub>P<sub>10</sub> polymer solution (18% w/w) at 4 °C. The final concentration of microgels in the M<sub>10</sub>P<sub>10</sub> solution was approximately 8.5 mg/ml. HAMA microgels/M<sub>10</sub>P<sub>10</sub> suspensions were injected into cylindrical glass vials with an approximate internal diameter of 6 mm (100  $\mu$ l of suspension for each vial) and were incubated for 5 minutes at 37 °C to allow thermogelation of M<sub>10</sub>P<sub>10</sub>. Subsequently, the mixtures were UV-irradiated for 3 minutes at a distance of 5 cm using a Bluepoint 4 UV lamp (specifications given in section 5.2.5). Next, PBS (900  $\mu$ l) enriched with 0.02% NaN<sub>3</sub> was added to each hydrogel. Sampling and



detection of the released lysozyme was performed as described in section 5.2.3, and cumulative release of lysozyme was calculated and reported as the percentage of the total lysozyme released after a plateau level was reached (percentage of the total lysozyme mobile fraction).

### 5.2.8 Enzymatic activity of lysozyme

The enzymatic activity of released lysozyme was determined via a turbidity-assay, based on the decrease in optical density of a suspension of *Micrococcus lysodeikticus* bacterium due to the hydrolysis of its outer membrane caused by lysozyme<sup>46,47</sup>. Briefly, samples containing released lysozyme were diluted to match the concentration of a native lysozyme stock solution (30  $\mu\text{g/ml}$  in PBS), which was used as a positive control. Volumes of 5  $\mu\text{l}$  of sample or control were pipetted into individual wells. Next, 195  $\mu\text{l}$  of *Micrococcus lysodeikticus* bacterium suspension (0.2  $\text{mg/ml}$  in 22 mM phosphate buffer,  $\text{pH} = 6.2$ ) was rapidly added to each well. The plate was shaken for 1 minute and the absorbance was measured at 450 nm over 5 minutes. The resulting curves were fitted with linear regression, and their slopes (proportional to lysozyme activity) were calculated and normalized to the slope of the linear curve of the native lysozyme.

## 5.3 Results and Discussion

### 5.3.1 Release of lysozyme from $\text{M}_{10}\text{P}_{10}$ /HAMA hydrogel blends

The aim of this study was to develop a hydrogel system for the sustained release of a loaded protein. To this end, two different systems were evaluated:  $\text{M}_{10}\text{P}_{10}$ /HAMA hydrogel blends and microcomposite  $\text{M}_{10}\text{P}_{10}$  hydrogels, in which HAMA microgels were dispersed. For  $\text{M}_{10}\text{P}_{10}$ /HAMA hydrogel blends, several compositions varying in HAMA MW and concentration were chosen (Table 1) to study the effect of these two parameters on the release kinetics of lysozyme from the obtained hydrogels after photopolymerization. Figure 2 shows the release profile of lysozyme encapsulated in UV-crosslinked  $\text{M}_{10}\text{P}_{10}$ /HAMA hydrogels. For all formulations, lysozyme was completely released in 24 hours with kinetics independent of MH compositions. Furthermore, the hydrogels containing  $\text{M}_{10}\text{P}_{10}$  and HAMA displayed a similar protein release profile as hydrogels only containing  $\text{M}_{10}\text{P}_{10}$ . For all formulations the cumulative release against the square root of time within the first 5 hours (released lysozyme  $\geq 70\%$ ) was properly fitted into a linear regression (Figure S2, Supporting Information). This first order kinetics indicates a diffusion-controlled protein release, typical for protein molecules that are smaller than the mesh size of the hydrogel network<sup>18,20,48</sup>. Surprisingly, neither an increase of HAMA MW nor an increase of its concentration resulted in a slower protein release. Considering the major effect that HAMA MW and concentration have on the stiffness and degradation profile of these hydrogels (these properties were separately studied and results are reported in Figure S3 and S4, Supporting Information), an effect on protein release was intuitively expected. Possibly, although the increase of HAMA MW and concentration seem to contribute for a tighter network, the small dimensions of lysozyme allow an

equally easy diffusion of the protein through all these hydrogels. Notably, for some formulations the maximum released lysozyme was higher than the 100% lysozyme content calculated according to the lysozyme feed of the prepared hydrogels, as observed previously in similar studies using UPLC-based determination of proteins<sup>10,49</sup>. Based on these results, it is evident that the release of lysozyme from  $M_{10}P_{10}$ /HAMA hydrogels is rather rapid and its kinetics cannot be tuned by the hydrogel composition. Therefore, we investigated a different system where HAMA is not included in the hydrogel blend as a building block *per se*, but as pre-crosslinked microgels.

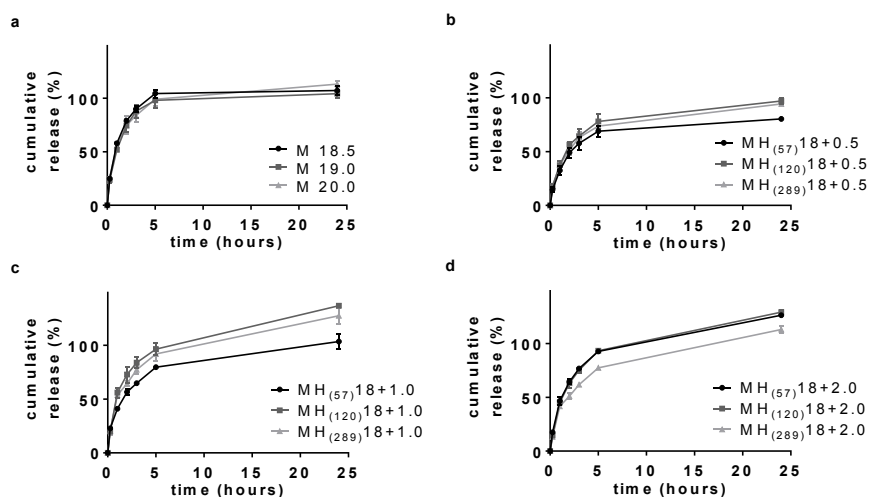


**Figure 2.** Release of lysozyme from hydrogels containing only  $M_{10}P_{10}$  (a), 18% of  $M_{10}P_{10}$  and 0.5% of HAMA (b), 1.0% of HAMA (c) or 2.0% of HAMA (d) varying in HAMA MW.

### 5.3.2 Characteristics of HAMA microgels

Fabrication of HAMA microgels using the microfluidics device described in section 5.2.5 led to the generation of microgels as visualized in Figure 3. Microgels displayed an average diameter ranging from 313 to 557  $\mu\text{m}$  and a CoV ranging from 7 to 14% (Table 3). A  $\text{CoV} \leq 10\%$  is typical for monodisperse particles generated using microfluidic technology<sup>44</sup>. In the present study, all tested conditions (two different HAMA concentrations and continuous phase flow rates) resulted in microgels with a CoV of  $\sim 10\%$ . The microgel size significantly decreased with increasing the continuous phase flow from 2 to 6 ml/min, for both HAMA concentrations. This major effect of the continuous phase flow on particle size can be ascribed to higher shear forces acting on HAMA droplets associated with higher flow rates, in line with literature on comparable systems with a co-flowing geometry<sup>42,50,51</sup>. We also confirmed the effect of the continuous phase flow rate on water droplet size for our microfluidics setup as shown in Figure S4 (Supporting Information).

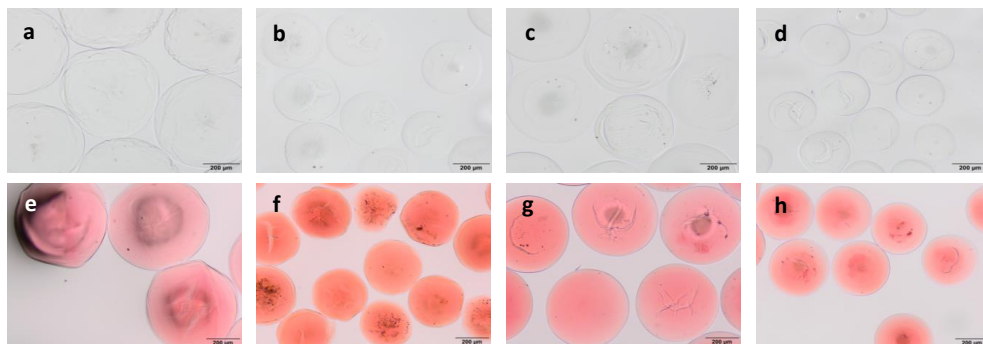


**Figure 3.** Microscopy images of HAMA microgels. HAMA microgels (2.5% w/w) obtained using a dispersed phase flow of 100  $\mu\text{l}/\text{min}$  and a continuous phase flow of 2 ml/min (a) or 6 ml/min (b). HAMA microgels (5.0% w/w) obtained using a dispersed phase flow of 100  $\mu\text{l}/\text{min}$  and a continuous phase flow of 2 ml/min (c) or 6 ml/min (d). Safranin-O was used to stain HAMA microgels (e-h). Scale bar represents 200  $\mu\text{m}$ .

**Table 3.** Size and CoV of HAMA microgels fabricated using different HAMA concentrations and continuous phase flow rates.

Sample	Average diameter ( $\mu\text{m}$ )	CoV (%)
HAMA 2.5_2	557	13
HAMA 2.5_6	342	9
HAMA 5.0_2	496	7
HAMA 5.0_6	313	14

In general, when considering droplet generation using a capillary in a tube with a co-flow of immiscible fluids in a dripping regime, the relation between droplet diameter and flow of the continuous phase can be described by equations 5 and 6, as originally formulated by Umbanhowar *et al.*<sup>28,50</sup>

$$D^3 - \left(1 + \frac{1}{3Ca}\right)D^2 - \frac{\beta}{\alpha}D + \frac{\beta}{\alpha} = 0 \quad \text{Equation 5}$$

$$Ca = \frac{\mu_c Q_c}{\sigma A_0} \quad \text{Equation 6}$$

where  $D$  is the ratio  $D_d / D_c$ , between the diameter of the generated droplet ( $D_d$ ,  $\mu\text{m}$ ) and the inner diameter of the used capillary ( $D_c$ ,  $\mu\text{m}$ ),  $\alpha$  is defined as the ratio

$A_c / A_o$ , between the cross sectional area of the inner capillary ( $A_c$ ,  $\mu\text{m}^2$ ) and the cross sectional area of the outer tube ( $A_o$ ,  $\mu\text{m}^2$ ), and  $\beta$  is the flow rate ratio  $Q_d / Q_c$ , between the dispersed phase flow ( $Q_d$ ,  $\mu\text{l}/\text{min}$ ) and the continuous phase flow ( $Q_c$ ,  $\mu\text{l}/\text{min}$ ). Finally,  $Ca$  is the capillary number defined in equation 6, where  $\mu_c$  is the viscosity of the continuous phase (mPa·s) and  $\sigma$  is the interfacial tension between the dispersed and continuous phase (mN/m). From the definitions of  $Ca$  and  $\beta$ , it is clear that an increase of the continuous phase flow,  $Q_c$  results in an increase of  $Ca$  and a decrease of  $\beta$ , which consequently leads to a decrease of the droplet diameter  $D_d$ , according to equation 5. As an important addition to equation 5, it needs to be noted that  $D_d \geq 2D_c$ , and any average droplet size smaller than twice the capillary inner diameter must be ascribed to satellite droplet formation as reported by Cramer *et al.*<sup>42</sup>. Furthermore, by increasing HAMA concentration, and therefore the viscosity of the dispersed phase, the microgel diameter slightly decreased. An opposite effect would have been expected according to literature<sup>28,42,50,51</sup>. Possibly, the observed smaller size found in our experiments is due to an increase of the resistance that the syringe pump encounters when draining more viscous fluids, *e.g.* HAMA solutions with higher concentration. This would lead to an effective lower dispersed phase flow, responsible for smaller droplet size<sup>50</sup>.

After fabrication, microgels were loaded with lysozyme in a buffer of low ionic strength to favor electrostatic interactions between the negatively charged HAMA matrix and the positively charged protein<sup>19,52</sup>, and loading (%) and LE (%) calculated according to equations 3 and 4 are shown in Figure 4.

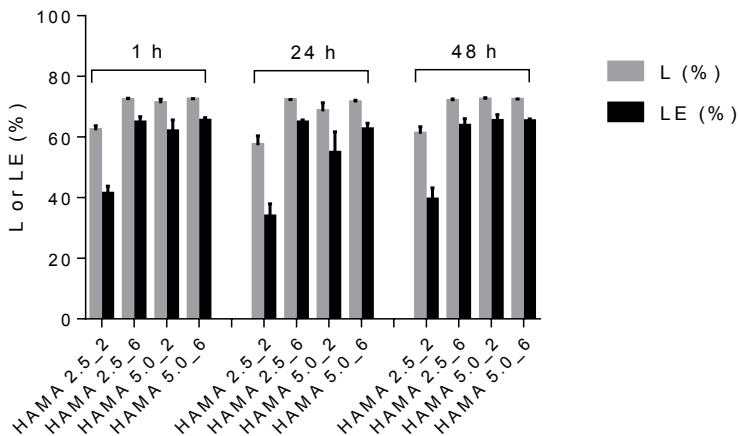


**Figure 4.** L (%) and LE (%) after 1, 24 and 48 hours of incubation of lysozyme with HAMA microgels fabricated using HAMA solutions of different concentrations and continuous phase flow.

HAMA 2.5\_2 showed a loading of  $62.2 \pm 1.5\%$  and a LE of  $41.2 \pm 2.6\%$  after 1h of incubation, whereas all other formulations displayed a loading ranging between  $71.1 \pm 1.3$  and  $72.3 \pm 0.3$ , and a LE ranging between  $61.7 \pm 3.9$  and  $65.3 \pm 1.1$ . Loading and LE did not significantly change at longer incubation times. In line with our results, similar high protein loading was found previously for positively charged microgels loaded with negatively charged ovalbumin<sup>45</sup>. Moreover, for hyaluronic acid mixed with lysozyme, the formation of complex coacervates within the first hour of incubation has been previously reported, which likely explains the possibility to load these high amounts of lysozyme in these microgels<sup>53</sup>.

### 5.3.3 Release of lysozyme from microcomposite HAMA/M<sub>10</sub>P<sub>10</sub> hydrogels

The release of lysozyme from microcomposite HAMA/M<sub>10</sub>P<sub>10</sub> hydrogels in a buffer with physiological ionic strength (PBS) lasted in total 20 days for hydrogels containing HAMA 2.5\_2, HAMA 2.5\_6, HAMA 5.0\_6 and 35 days for hydrogels containing HAMA 5.0\_2 as can be seen in Figure 5a and b. The cumulative release of lysozyme was reported as the percentage of the total lysozyme released after a plateau level was reached. Importantly, the value at the plateau level for each formulation was equal or higher than the calculated total loading. This can be ascribed to a practical issue related to the microgel incorporation in the hydrogels. In fact, lysozyme-loaded microgels are rather heavy and tend to precipitate within the M<sub>10</sub>P<sub>10</sub> mixture during the microcomposite hydrogel fabrication, hampering their perfectly even distribution among the different samples. All formulations showed hardly any burst release, with less than 15% of lysozyme being released in the first 21 hours (Figure 5c and d). Remarkably, the time scale of protein release from these microcomposite systems was significantly longer than that observed for lysozyme-loaded M<sub>10</sub>P<sub>10</sub>/HAMA hydrogel blends (Figure 2). The slower release of lysozyme from microcomposite hydrogels is likely attributed to the strong lysozyme-HAMA interactions, due to the high charge density of the hydrogel network. Nevertheless, it needs to be taken into account that such strong interactions were promoted in a relatively low ionic strength buffer (HEPES buffer 20 mM), used during the post-loading step. In contrast, when preparing lysozyme-loaded M<sub>10</sub>P<sub>10</sub>/HAMA hydrogel blends, lysozyme was mixed with both polymers in PBS at 4 °C, and a selective protein sequestration into HAMA network may not be warranted in this higher ionic strength buffer. Future investigations on the release profile of lysozyme from M<sub>10</sub>P<sub>10</sub>/HAMA hydrogel blends prepared in low ionic strength buffer will clarify the role of the used buffer, and will confirm whether the microcomposite design of this system is the main cause of strong protein-polymer interaction and consequent slow protein release. From the results reported in this study, it is evident that the formation of an efficient and strong lysozyme-HAMA complex driven by electrostatic interactions is crucial for a longer protein immobilization into M<sub>10</sub>P<sub>10</sub>/HAMA hydrogels. The formation of complexes between polycations and polyanions has been previously described in literature<sup>54</sup>, and for a deep characterization of lysozyme-HA complex we refer to a detailed study from Water *et al*<sup>53</sup>. Importantly, the enzymatic activity of the released lysozyme was entirely preserved (Figure S5). Hence, this technology can

be considered protein-friendly and could be potentially applied to the formulation of growth factors for an *in situ* sustained release from hydrogel scaffolds.

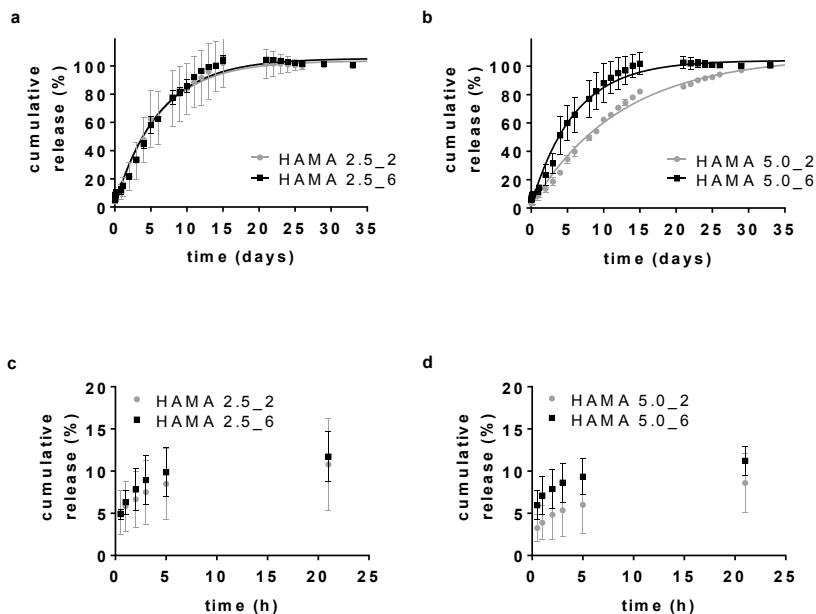


**Figure 5.** Cumulative release of lysozyme over time from microcomposite HAMA/ $M_{10}P_{10}$  hydrogels, containing microgels fabricated using HAMA concentration of 2.5% (a) or 5% (b) and a continuous phase flow of 2 or 6 ml/min. Zoom in of the first 25 h for the same formulations (c and d).

## 5.4 Conclusions

In this study, we developed a facile method for the fabrication of monodisperse HAMA microgels loaded with the model protein lysozyme, which we subsequently encapsulated into  $M_{10}P_{10}$  hydrogel networks. These HAMA/ $M_{10}P_{10}$  microcomposite hydrogels provide a novel alternative to conventional UV-crosslinked  $M_{10}P_{10}$ /HAMA hydrogel blends, where a stronger immobilization of positively charged proteins and a consequently longer sustained release can be obtained. Further investigations are necessary to understand the role of the microcomposite organization on the protein release profile and to gain additional mechanistic insights on the release kinetics. Importantly, this approach can be potentially applied to other GAG molecules, *e.g.* heparin or chondroitin sulfate to obtain microcomposite hydrogels with controllable charge density, which may affect growth factor's loading efficacy and release kinetics.

## Acknowledgments

The authors would like to thank Burak H. Eral, Ivan Rehor and Hans Heessen for their contribution and assistance in developing the microfluidic set-up, as well as Neda Kordalivand for the helpful discussions about the release experiments. The research leading to these results has received funding from the European Community's Seventh Framework Programme (FP7/2007-2013) under grant agreement n°309962 (HydroZONES).

## Supporting Information

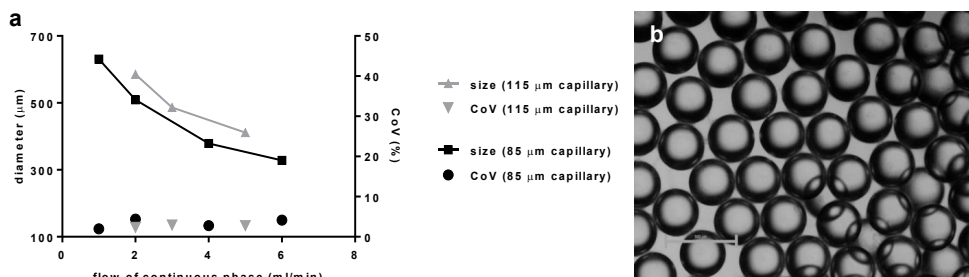


**Figure S1.** Water-in-oil droplet formation. Diameter and CoV of generated droplets as function of continuous phase flow and diameter of the used capillary.

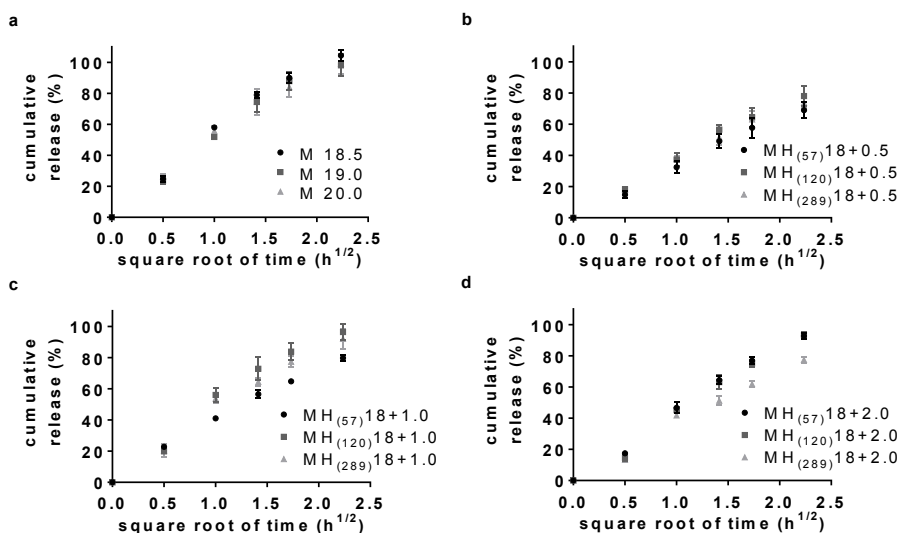


**Figure S2.** Cumulative release of lysozyme as function of square root of time for hydrogels containing only M<sub>10</sub>P<sub>10</sub> (a), 18% of M<sub>10</sub>P<sub>10</sub> and 0.5% of HAMA (b), 1.0% of HAMA (c) or 2.0% of HAMA (d) varying in HAMA MW.



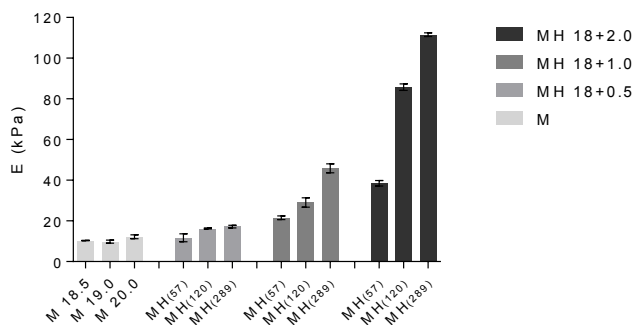


**Figure S3.** Young's modulus ( $E$ , kPa) of UV-crosslinked  $M_{10}P_{10}$ /HAMA hydrogels varying in HAMA MW (57, 120 and 289 kDa) and concentration (0.5, 1.0 and 2.0% w/w). Young's modulus was calculated as the slope of the initial linear segment of the stress/strain curves, recorded during unconfined compression (force ramp rate of 0.1 N/min with a highest force limit of 1 N) of cylindrical samples (diameter = 6 mm, height = 2 mm).

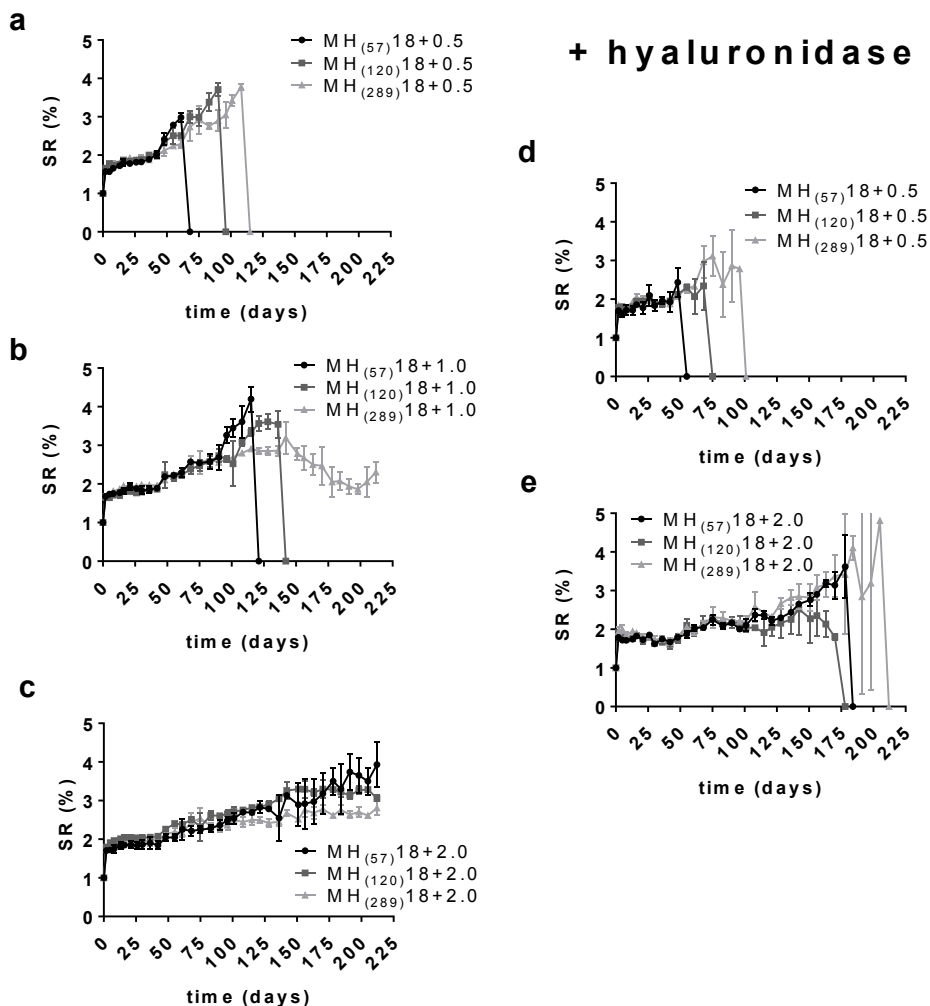


**Figure S4.** Degradation profiles of UV-crosslinked  $M_{10}P_{10}$ /HAMA hydrogels. Effect of HAMA MW on the degradation profile of hydrogels containing 18% of  $M_{10}P_{10}$  and 0.5% of HAMA (a), 1.0% of HAMA (b) or 2.0% of HAMA (c) in PBS. Effect of HAMA MW on hydrogels containing 18% of  $M_{10}P_{10}$  and 0.5% of HAMA (d) or 2.0% of HAMA (e) in PBS enriched with hyaluronidase II (3U/ml). Cylindrical hydrogels were immersed in PBS enriched with  $\text{NaN}_3$  (0.02%) with or without hyaluronidase type II at 37 °C. Medium was refreshed twice per week. Swelling ratio (SR) was calculated as the ratio between the hydrogel weight at each time point and the initial weight of the hydrogel before it was immersed in PBS.

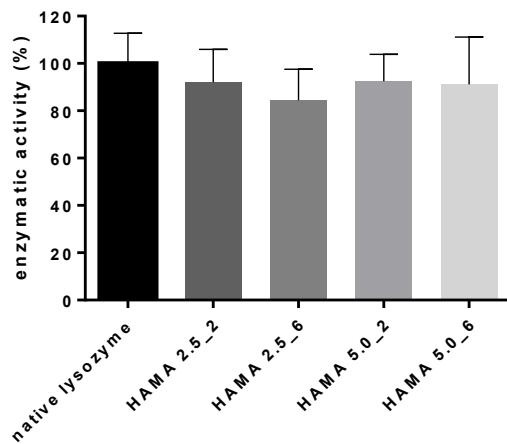


**Figure S5.** Enzymatic activity of lysozyme released after 120 hours from microcomposite HAMA/M<sub>10</sub>P<sub>10</sub> hydrogels.

## References

- (1) Caló, E.; Khutoryanskiy, V. V. Biomedical Applications of Hydrogels: A Review of Patents and Commercial Products. *Eur. Polym. J.* **2015**, *65*, 252–267.
- (2) Tibbitt, M. W.; Dahlman, J. E.; Langer, R. Emerging Frontiers in Drug Delivery. *J. Am. Chem. Soc.* **2016**, *138* (3), 704–717.
- (3) Vashist, A.; Vashist, A.; Gupta, Y. K.; Ahmad, S. Recent Advances in Hydrogel Based Drug Delivery Systems for the Human Body. *J. Mater. Chem. B* **2014**, *2* (2), 147–166.
- (4) Bae, K. H.; Kurisawa, M. Emerging Hydrogel Designs for Controlled Protein Delivery. *Biomater. Sci.* **2016**, *4* (8), 1184–1192.
- (5) Censi, R.; Di Martino, P.; Vermonden, T.; Hennink, W. E. Hydrogels for Protein Delivery in Tissue Engineering. *J. Control. Release* **2012**, *161* (2), 680–692.
- (6) Vermonden, T.; Censi, R.; Hennink, W. E. Hydrogels for Protein Delivery. *Chem. Rev.* **2012**, *112* (5), 2853–2888.
- (7) Malda, J.; Visser, J.; Melchels, F. P.; Jüngst, T.; Hennink, W. E.; Dhert, W. J. A.; Groll, J.; Hutmacher, D. W. 25th Anniversary Article: Engineering Hydrogels for Biofabrication. *Adv. Mater.* **2013**, *25* (36), 5011–5028.
- (8) Seliktar, D. Designing Cell-Compatible Hydrogels for Biomedical Applications. *Science* **2012**, *336* (6085), 1124–1128.
- (9) Bajaj, P.; Schweller, R. M.; Khademhosseini, A.; West, J. L.; Bashir, R. 3D Biofabrication Strategies for Tissue Engineering and Regenerative Medicine. *Annu. Rev. Biomed. Eng.* **2014**, *16* (1), 247–276.
- (10) Boere, K. W. M.; van den Dikkenberg, J.; Gao, Y.; Visser, J.; Hennink, W. E.; Vermonden, T. Thermogelling and Chemoselectively Cross-Linked Hydrogels with Controlled Mechanical Properties and Degradation Behavior. *Biomacromolecules* **2015**, *16* (9), 2840–2851.
- (11) Guvendiren, M.; Burdick, J. A. Engineering Synthetic Hydrogel Microenvironments to Instruct Stem Cells. *Curr. Opin. Biotechnol.* **2013**, *24* (5), 841–846.
- (12) Hammer, N.; Brandl, F. P.; Kirchhof, S.; Messmann, V.; Goepferich, A. M. Protein Compatibility of Selected Cross-Linking Reactions for Hydrogels. *Macromol. Biosci.* **2015**, *15* (3), 405–413.
- (13) Hudalla, G. A.; Murphy, W. L. Biomaterials That Regulate Growth Factor Activity via Bioinspired Interactions. *Adv. Funct. Mater.* **2011**, *21* (10), 1754–1768.
- (14) Freudenberg, U.; Liang, Y.; Kiick, K. L.; Werner, C. Glycosaminoglycan-Based Biohybrid Hydrogels: A Sweet and Smart Choice for Multifunctional Biomaterials. *Adv. Mater.* **2016**, *28* (40), 8861–8891.
- (15) Abbadessa, A.; Mouser, V. H. M.; Blokzijl, M. M.; Gawlitta, D.; Dhert, W. J. A.; Hennink, W. E.; Malda, J.; Vermonden, T. A Synthetic Thermosensitive Hydrogel for Cartilage Bioprinting and Its Biofunctionalization with Polysaccharides. *Biomacromolecules* **2016**, *17* (6), 2137–2147.
- (16) Mouser, V. H. M.; Abbadessa, A.; Levato, R.; Hennink, W. E.; Dhert, W. J. A.; Gawlitta, D.; Vermonden, T.; Malda, J. Bio-Ink Development for Composite Constructs for Cartilage Repair. *Manuscr. Prep.*
- (17) Lee, K.; Silva, E. A.; Mooney, D. J. Growth Factor Delivery-Based Tissue Engineering: General Approaches and a Review of Recent Developments. *J. R. Soc. Interface* **2011**, *8* (55), 153–170.

- (18) Hennink, W. E.; Talsma, H.; Borchert, J. C. H.; De Smedt, S. C.; Demeester, J. Controlled Release of Proteins from Dextran Hydrogels. *J. Control. Release* **1996**, *39* (1), 47–55.
- (19) Schillemans, J. P.; Verheyen, E.; Barendregt, A.; Hennink, W. E.; Van Nostrum, C. F. Anionic and Cationic Dextran Hydrogels for Post-Loading and Release of Proteins. *J. Control. Release* **2011**, *150* (3), 266–271.
- (20) Censi, R.; Vermonden, T.; van Steenberghe, M. J.; Deschout, H.; Braeckmans, K.; De Smedt, S. C.; van Nostrum, C. F.; di Martino, P.; Hennink, W. E. Photopolymerized Thermosensitive Hydrogels for Tailorable Diffusion-Controlled Protein Delivery. *J. Control. Release* **2009**, *140* (3), 230–236.
- (21) Parmar, A. S.; Muschol, M. Hydration and Hydrodynamic Interactions of Lysozyme: Effects of Chaotropic versus Kosmotropic Ions. *Biophys. J.* **2009**, *97* (2), 590–598.
- (22) Cross, M.; Dexter, T. M. Growth Factors in Development, Transformation, and Tumorigenesis. *Cell* **1991**, *64* (2), 271–280.
- (23) Jeon, O.; Wolfson, D. W.; Alsborg, E. In-Situ Formation of Growth-Factor-Loaded Coacervate Microparticle-Embedded Hydrogels for Directing Encapsulated Stem Cell Fate. *Adv. Mater.* **2015**, *27* (13), 2216–2223.
- (24) Hao, J.; Wang, X.; Bi, Y.; Teng, Y.; Wang, J.; Li, F.; Li, Q.; Zhang, J.; Guo, F.; Liu, J. Fabrication of a Composite System Combining Solid Lipid Nanoparticles and Thermosensitive Hydrogel for Challenging Ophthalmic Drug Delivery. *Colloids Surfaces B Biointerfaces* **2014**, *114*, 111–120.
- (25) Merino, S.; Martín, C.; Kostarelos, K.; Prato, M.; Vázquez, E. Nanocomposite Hydrogels: 3D Polymer–Nanoparticle Synergies for On-Demand Drug Delivery. *ACS Nano* **2015**, *9* (5), 4686–4697.
- (26) Lau, H. K.; Kiick, K. L. Opportunities for Multicomponent Hybrid Hydrogels in Biomedical Applications. *Biomacromolecules* **2015**, *16* (1), 28–42.
- (27) Gaharwar, A. K.; Peppas, N. A.; Khademhosseini, A. Nanocomposite Hydrogels for Biomedical Applications. *Biotechnol. Bioeng.* **2014**, *111* (3), 441–453.
- (28) Gordon, C.; Shelley Lynn, A. Microfluidic Methods for Generating Continuous Droplet Streams. *J. Phys. D: Appl. Phys.* **2007**, *40* (19), R319–R336.
- (29) Zhang, Y.; Chan, H. F.; Leong, K. W. Advanced Materials and Processing for Drug Delivery: The Past and the Future. *Adv. Drug Deliv. Rev.* **2013**, *65* (1), 104–120.
- (30) Xu, S.; Nie, Z.; Seo, M.; Lewis, P.; Kumacheva, E.; Stone, H. A.; Garstecki, P.; Weibel, D. B.; Gitlin, I.; Whitesides, G. M. Generation of Monodisperse Particles by Using Microfluidics: Control over Size, Shape, and Composition. *Angew. Chemie Int. Ed.* **2005**, *44* (5), 724–728.
- (31) Nie, Z.; Xu, S.; Seo, M.; Lewis, P. C.; Kumacheva, E. Polymer Particles with Various Shapes and Morphologies Produced in Continuous Microfluidic Reactors. *J. Am. Chem. Soc.* **2005**, *127* (22), 8058–8063.
- (32) Wang, C. X.; Utech, S.; Gopez, J. D.; Mabesoone, M. F. J.; Hawker, C. J.; Klinger, D. Non-Covalent Microgel Particles Containing Functional Payloads: Coacervation of PEG-Based Triblocks via Microfluidics. *ACS Appl. Mater. Interfaces* **2016**, *8* (26), 16914–16921.
- (33) Nisisako, T. Recent Advances in Microfluidic Production of Janus Droplets and Particles. *Curr. Opin. Colloid Interface Sci.* **2016**, *25*, 1–12.
- (34) Nisisako, T.; Hatsuzawa, T. Microfluidic Fabrication of Oil-Filled Polymeric Microcapsules with Independently Controllable Size and Shell Thickness via Janus

- to Core-shell Evolution of Biphasic Droplets. *Sensors Actuators B Chem.* **2016**, *223*, 209–216.
- (35) Oupický, D.; Konák, C.; Ulbrich, K. DNA Complexes with Block and Graft Copolymers of N-(2-Hydroxypropyl)methacrylamide and 2-(Trimethylammonio)ethyl Methacrylate. *J. Biomater. Sci. Polym. Ed.* **1999**, *10* (5), 573–590.
- (36) Neradovic, D.; van Steenberg, M. J.; Vansteelant, L.; Meijer, Y. J.; van Nostrum, C. F.; Hennink, W. E. Degradation Mechanism and Kinetics of Thermosensitive Polyacrylamides Containing Lactic Acid Side Chains. *Macromolecules* **2003**, *36* (20), 7491–7498.
- (37) Neradovic, D.; van Nostrum, C. F.; Hennink, W. E. Thermoresponsive Polymeric Micelles with Controlled Instability Based on Hydrolytically Sensitive N-Isopropylacrylamide Copolymers. *Macromolecules* **2001**, *34* (22), 7589–7591.
- (38) Vermonden, T.; Besseling, N. A. M.; van Steenberg, M. J.; Hennink, W. E. Rheological Studies of Thermosensitive Triblock Copolymer Hydrogels. *Langmuir* **2006**, *22* (24), 10180–10184.
- (39) Vermonden, T.; Fedorovich, N. E.; van Geemen, D.; Alblas, J.; van Nostrum, C. F.; Dhert, W. J. A.; Hennink, W. E. Photopolymerized Thermosensitive Hydrogels: Synthesis, Degradation, and Cytocompatibility. *Biomacromolecules* **2008**, *9* (3), 919–926.
- (40) Abbadessa, A.; Blokzijl, M. M.; Mouser, V. H. M.; Marica, P.; Malda, J.; Hennink, W. E.; Vermonden, T. A Thermo-Responsive and Photo-Polymerizable Chondroitin Sulfate-Based Hydrogel for 3D Printing Applications. *Carbohydr. Polym.* **2016**, *149*, 163–174.
- (41) Hachet, E.; Van Den Berghe, H.; Bayma, E.; Block, M. R.; Auzély-Velty, R. Design of Biomimetic Cell-Interactive Substrates Using Hyaluronic Acid Hydrogels with Tunable Mechanical Properties. *Biomacromolecules* **2012**, *13* (6), 1818–1827.
- (42) Cramer, C.; Fischer, P.; Windhab, E. J. Drop Formation in a Co-Flowing Ambient Fluid. *Chem. Eng. Sci.* **2004**, *59* (15), 3045–3058.
- (43) Abdi, H. Coefficient of Variation. In *Encyclopedia of Research Design*; N.J. Salkind, D.M., D. & B. F., Ed.; SAGE Publications, Inc.: 2455 Teller Road, Thousand Oaks California 91320 United States, 2010; pp 169–171.
- (44) Ziemecka, I.; van Steijn, V.; Koper, G. J. M.; Rosso, M.; Brizard, A. M.; van Esch, J. H.; Kreutzer, M. T. Monodisperse Hydrogel Microspheres by Forced Droplet Formation in Aqueous Two-Phase Systems. *Lab Chip* **2011**, *11* (4), 620–624.
- (45) Li, D.; Kordalivand, N.; Fransen, M. F.; Ossendorp, F.; Raemdonck, K.; Vermonden, T.; Hennink, W. E.; van Nostrum, C. F. Reduction-Sensitive Dextran Nanogels Aimed for Intracellular Delivery of Antigens. *Adv. Funct. Mater.* **2015**, *25* (20), 2993–3003.
- (46) Ghaderi, R.; Carlfors, J. Biological Activity of Lysozyme After Entrapment in Poly (d,l-Lactide-Co-Glycolide)-Microspheres. *Pharm. Res.* **1997**, *14* (11), 1556–1562.
- (47) van de Weert, M.; Hoehstetter, J.; Hennink, W. E.; Crommelin, D. J. . The Effect of a Water/organic Solvent Interface on the Structural Stability of Lysozyme. *J. Control. Release* **2000**, *68* (3), 351–359.
- (48) Peppas, N. A.; Lustig, S. R. Solute Diffusion in Hydrophilic Network Structures. *Hydrogels Med. Pharm.* **1986**, *1*, 57–83.
- (49) Samadi, N.; van Nostrum, C. F.; Vermonden, T.; Amidi, M.; Hennink, W. E. Mechanistic Studies on the Degradation and Protein Release Characteristics of Poly(lactic- Co -Glycolic- Co -Hydroxymethylglycolic Acid) Nanospheres.

- Biomacromolecules* **2013**, *14* (4), 1044–1053.
- (50) Umbanhowar, P. B.; Prasad, V.; Weitz, D. A. Monodisperse Emulsion Generation via Drop Break Off in a Coflowing Stream. *Langmuir* **2000**, *16* (2), 347–351.
- (51) Nunes, J. K.; Tsai, S. S. H.; Wan, J.; Stone, H. A. Dripping and Jetting in Microfluidic Multiphase Flows Applied to Particle and Fibre Synthesis. *J. Phys. D. Appl. Phys.* **2013**, *46* (11), 114002.
- (52) Schillemans, J. P.; Hennink, W. E.; van Nostrum, C. F. The Effect of Network Charge on the Immobilization and Release of Proteins from Chemically Crosslinked Dextran Hydrogels. *Eur. J. Pharm. Biopharm.* **2010**, *76* (3), 329–335.
- (53) Water, J. J.; Schack, M. M.; Velazquez-Campoy, A.; Maltesen, M. J.; van de Weert, M.; Jorgensen, L. Complex Coacervates of Hyaluronic Acid and Lysozyme: Effect on Protein Structure and Physical Stability. *Eur. J. Pharm. Biopharm.* **2014**, *88* (2), 325–331.
- (54) Gucht, J. van der; Spruijt, E.; Lemmers, M.; Cohen Stuart, M. A. Polyelectrolyte Complexes: Bulk Phases and Colloidal Systems. *J. Colloid Interface Sci.* **2011**, *361* (2), 407–422.







# Chapter 6

## **Bio-ink development for the fabrication of composite cartilage repair constructs**

**V.H.M. Mouser\*, A. Abbadessa\*, R. Levato, W.E. Hennink, T. Vermonden,  
D. Gawlitta, J. Malda**

**\*These authors contributed equally**

*Submitted for publication*

This chapter is also included in the PhD thesis of V.H.M. Mouser

## Abstract

Fine-tuning of bio-ink composition and material processing parameters is crucial for the development of biomechanically relevant cartilage constructs. This study aims to design and develop cartilage constructs with tunable internal architectures and relevant mechanical properties. More specifically, the potential of methacrylated hyaluronic acid (HAMA) added to thermosensitive hydrogels composed of methacrylated poly[*N*-(2-hydroxypropyl)methacrylamide mono/dilactate] (pHPMA-lac)/polyethylene glycol (PEG) triblock copolymers, to optimize cartilage-like tissue formation by embedded chondrocytes, and enhance printability was explored. Additionally, co-printing with polycaprolactone (PCL) was performed for mechanical reinforcement. Chondrocyte-laden hydrogels composed of pHPMA-lac-PEG and different concentrations of HAMA (0-1% w/w) were cultured for 28 days *in vitro* and subsequently evaluated for the presence of cartilage-like matrix. Young's moduli were determined for hydrogels with the different HAMA concentrations. Additionally, hydrogel/PCL constructs with different internal architectures were co-printed and analyzed for their mechanical properties. The results of this study demonstrated a dose-dependent effect of HAMA concentration on cartilage matrix synthesis by chondrocytes. Glycosaminoglycans (GAGs) and collagen type II content increased with intermediate HAMA concentrations (0.25-0.5%) compared to HAMA-free controls, while a relatively high HAMA concentration (1%) resulted in increased fibrocartilage formation. Young's moduli of generated hydrogel constructs ranged from 14 to 31 kPa and increased with increasing HAMA concentration. The pHPMA-lac-PEG hydrogels with 0.5% HAMA were found to be optimal for cartilage-like tissue formation. Therefore, this hydrogel system was co-printed with PCL to generate porous or solid constructs with different mesh sizes. Young's moduli of these composite constructs were in the range of native cartilage (3.5-4.6 MPa). Interestingly, the co-printing procedure influenced the mechanical properties of the final constructs. These findings are relevant for future bio-ink development, as they demonstrate the importance of selecting proper HAMA concentrations, as well as appropriate print settings and construct designs for optimal cartilage matrix deposition and final mechanical properties of constructs, respectively.

## 6.1 Introduction

Three dimensional (3D) bioprinting is a promising technique for the fabrication of regenerative constructs. It allows accurate positioning of cells and biomaterials in a layered fashion and can thus be used for the fabrication of organized tissue-like structures<sup>1</sup>, *e.g.* articular cartilage constructs in which a depth-dependent matrix composition and mechanical resistance are addressed<sup>2-4</sup>. Overall, cartilage tissue consists of glycosaminoglycans (GAGs), collagen type II, and water, and contains only a limited number of cells. The low cell number in combination with the lack of vasculature and nerves, leads to the limited regenerative capacity of this tissue<sup>5</sup>. As a consequence, most untreated cartilage defects eventually result in arthritic changes of the whole joint<sup>6</sup>. Therefore, regenerative treatments based on bioprinting to reproduce the cartilaginous organized architecture, are currently under investigation<sup>7,8</sup>.

The most commonly used biomaterials for the 3D bioprinting of cartilage constructs are hydrogels, as they allow homogeneous encapsulation of cells and biological cues, and support survival of relevant cell types, *i.e.* mesenchymal stem cells and chondrocytes. Although hydrogels are potentially suitable for this purpose, optimizing them for bioprinting is challenging. In order to print with high shape-fidelity, the hydrogel needs to possess certain rheological properties, *e.g.* high yield stress and viscosity, while for cell encapsulation and optimal tissue production by embedded cells, low yield stresses and viscosities are favorable<sup>9,10</sup>. Hydrogels based on UV-curable copolymers of a polyethylene glycol (PEG) midblock flanked by two partially methacrylated poly[N-(2-hydroxypropyl)methacrylamide mono/dilactate] (pHPMA-lac) outer blocks are attractive systems for tissue engineering applications because their characteristics, *e.g.* *in vitro* degradation rate and mechanical properties can be accurately tuned via adjustments of the building block's architecture and polymer concentration<sup>11-14</sup>. Recently, we have demonstrated that pHPMA-lac-PEG hydrogels with relatively low concentration and degree of methacrylation supported cartilage matrix deposition by embedded chondrocytes<sup>15</sup>. In addition, the partial replacement of pHPMA-lac-PEG triblock copolymers with methacrylated polysaccharides, *i.e.* hyaluronic acid (HAMA)<sup>15</sup> and chondroitin sulfate<sup>16</sup> further prolonged the *in vitro* degradation profile and enhanced the mechanical properties of the hydrogel blends. Importantly, the addition of HAMA to pHPMA-lac-PEG hydrogels allowed bioprinting with sufficient shape-fidelity of hydrogels even when a relatively low total polymer concentration was used<sup>15</sup>. Hyaluronic acid (HA) is a polysaccharide present in articular cartilage tissue and has been reported to influence multiple biological processes, *e.g.* cell proliferation, migration, attachment, and differentiation<sup>17,18</sup>. Multiple studies have demonstrated an anabolic effect of HA or HAMA on chondrocytes in various culture systems *in vitro* and *in vivo*<sup>19-26</sup>. However, several studies also indicated a critical role of the HA or HAMA concentration on chondrogenesis, as too low or too high HA or HAMA concentrations can be ineffective or even inhibitory<sup>23-26</sup>. Therefore, it is important to identify the currently unknown optimal concentration of HAMA in pHPMA-lac-PEG triblocks/HAMA

hydrogels for cartilage regeneration.

An additional aspect that has to be taken into account for cartilage repair constructs, is the requirement to withstand the high compressive and shear forces present in the articulating joints. However, the maximum stiffness that any hydrogel can reach, without hampering matrix production of embedded cells, is limited<sup>27</sup>. Multiple reinforcement strategies, such as the inclusion of fibers<sup>28,29</sup> or microparticles<sup>30</sup>, consisting of different materials, *e.g.* polycaprolactone (PCL)<sup>31–33</sup>, poloxamer-based hydrogels<sup>34</sup>, and ceramics<sup>35</sup> have been explored. Especially PCL is a promising reinforcement material as it is biocompatible, cost-effective, and it has a relatively slow degradation rate (ranging from months to years)<sup>36</sup>. The co-printing of a (cell-laden) hydrogel with a PCL fiber reinforcement offers a construct design in which the hydrogel provides the necessary milieu for cells to thrive, and the thermoplastic framework provides the required mechanical properties, to overall mimic the biomechanical profile of native cartilage. The mechanical performance of co-printed hydrogel/PCL constructs is dominated by that of the PCL framework<sup>28</sup>. Therefore, by modifying the PCL molecular weight and the geometry of the PCL skeleton, the compressive modulus and tensile strength can be tailored to that of the target tissue<sup>37</sup>. The strand size, strand distance, and to a lesser extent strand orientation, have been identified as the most important geometrical parameters to influence the mechanical features of the printed construct<sup>31,37,38</sup>. Hence, co-printing of pHPMA-lac-PEG triblocks/HAMA hydrogel with PCL might be an attractive approach for the fabrication of cartilage repair constructs. Hence, the aim of this study was to generate bioprinted constructs for cartilage regeneration with optimized bioactivity, and a tunable mechanical performance. As such, the optimal concentration of HAMA in pHPMA-lac-PEG triblocks/HAMA hydrogels for cartilage-like tissue formation of embedded chondrocytes was evaluated, and co-printing with PCL, using multiple construct architectures, was explored to match the mechanical properties of native cartilage.

## 6.2 Materials and Methods

### 6.2.1 Materials

All chemicals were obtained from Sigma-Aldrich (Zwijndrecht, the Netherlands) and all solvents from Biosolve (Valkenswaard, the Netherlands) unless indicated otherwise. Chemicals and solvents were used as received. HA sodium salt (120 kDa) was supplied by Lifecore Biomedical (Chaska, MN, USA) and PEG (10 kDa) by Merck (Darmstadt, Germany). GMP grade homopolymer of  $\epsilon$ -caprolactone (PCL, Parasorb PC 12, 185001) and L-lactide were obtained from Corbion (Gorinchem, The Netherlands), and Irgacure 2959 was a kind gift of BASF (Ludwigshafen, Germany). *N*-(2-hydroxypropyl) methacrylamide mono- and dilactate, and PEG<sub>10 kDa</sub>-4,4'-azobis(cyanopentanoate) macroinitiator were synthesized as previously reported<sup>39,40</sup>. Phosphate buffered saline (PBS), penicillin/streptomycin (pen/strep; 10,000 units/ml penicillin and 10 mg/ml streptomycin) and picogreen DNA assay were supplied by Invitrogen (Carlsbad, California, USA). Fetal bovine serum (FBS) was purchased

from Gibco (Invitrogen corporation) and type II collagenase was obtained from Worthington Biochemical Corp (Lakewood, NJ, USA). Two types of Dulbecco's Modified Eagle Medium (DMEM) were used: DMEM 31885 from Gibco (referred to as DMEM) and high glucose DMEM D6429 from Sigma-Aldrich (referred to as high glucose DMEM). Recombinant human TGF- $\beta$ 1 was obtained from Peprotech (London, UK), hyaluronidase (H2126) from Sigma-Aldrich, pronase (11459643001) from Roche Life Sciences (Indiana, USA), and ITS+ premix (human recombinant insulin, human transferrin, selenous acid, bovine serum albumin, linoleic acid) from BD Biosciences (Breda, the Netherlands). Antibody against collagen type I (1:100; EPR7785, ab138492) was obtained from Abcam (Cambridge, UK). Antibodies against collagen types II and VI (1:100; II-6B3II and 1:5, 5C6, respectively) were obtained from the Developmental Studies Hybridoma Bank (Iowa City, IA, USA). Antibody against proteoglycan IV (1:50; H00010216-M01) was obtained from Novus (Abingdon, United Kingdom). Secondary horse radish-peroxidase conjugated antibodies for collagen type I (EnVision+, K4010), collagen type II (1:100, IgG HRP, P0447), collagen type VI and proteoglycan IV (EnVision+, K4007) were ordered from DAKO (Heverlee, the Netherlands). Calcein-AM (to stain living cells) and ethidium homodimer-1 (to stain nuclei of dead cells) were obtained from Life Technologies (L3224, Bleiswijk, the Netherlands).

### 6.2.2 Synthesis and characterization of polymers

A triblock copolymer composed of two poly[*N*-(2-hydroxypropyl) methacrylamide mono/dilactate] outer blocks (~15 kDa) flanking a PEG (10 kDa) midblock, was synthesized and characterized as previously described, and 10% of the hydroxyl groups from the pendent lactate side-unites were methacrylated<sup>11</sup>. The methacrylated pHPMA-lac-PEG triblock copolymer is hereafter termed  $M_{10}P_{10}$  [ $M_{10}$  refers to a degree of methacrylation (DM) of 10%, and  $P_{10}$  refers to a PEG block with a molecular weight (MW) of 10 kDa]. Hyaluronic acid was methacrylated (DM = 10%, indicating the presence of 10 methacrylate groups per 100 disaccharide units) as previously described<sup>41</sup>. The characteristics of  $M_{10}P_{10}$ , *i.e.* number average molecular weight ( $M_n$ ), polydispersity index (PDI), CP and DM, as well as those of HAMA, *i.e.* MW and DM were in line with our previous findings<sup>11,15,16</sup>.

### 6.2.3 Experimental design

First, a screening of five different hydrogel formulations (Table 1) was performed to find the optimal concentration of HAMA for cartilage tissue engineering with chondrocyte-laden  $M_{10}P_{10}$ /HAMA hydrogels. Equine chondrocytes were encapsulated in the different hydrogel formulations and constructs were cast for *in vitro* culture. At days 1 and 28, the hydrogels were harvested and evaluated for cartilage-like tissue formation. In addition, Young's moduli were evaluated for cell-free cast hydrogel constructs of different compositions (Table 1).

Second, 3D printed constructs were fabricated with the best performing formulation of the first screening, *i.e.*  $MHA_{0.5}$ . Additionally, multiple constructs with different architectures were fabricated by co-printing  $MHA_{0.5}$  and PCL, and the Young's



moduli were determined.

**Table 1.** Overview of the concentrations of  $M_{10}P_{10}$  and HAMA in PBS for the five evaluated hydrogel formulations with their abbreviations.

Abbreviation	Polymer concentration (% w/w)	
	$M_{10}P_{10}$	HAMA
M	20	-
MHA <sub>0.1</sub>	19.9	0.1
MHA <sub>0.25</sub>	19.75	0.25
MHA <sub>0.5</sub>	19.5	0.5
MHA <sub>1</sub>	19	1

#### 6.2.4 Chondrocyte isolation and fabrication of chondrocyte-laden cast hydrogels

Primary chondrocytes were harvested from macroscopically healthy full-thickness cartilage of equine metacarpophalangeal joints ( $n = 3$ ; 3-10 years old), obtained from the local slaughterhouse. Cartilage was removed from the joints and digested overnight at 37°C in DMEM supplemented with collagenase II (1.5 µg/ml), hyaluronidase (1 mg/ml), FBS (10%), and pen/strep (1%). After digestion, the cell suspension was filtered through a 40 µm cell strainer and the chondrocytes were stored in liquid nitrogen until further use.

Before use, chondrocytes (passage 0) were expanded in monolayer culture for ~14 days (seeding density of  $5 \cdot 10^3$  cells/cm<sup>2</sup>) in chondrocyte expansion medium consisting of DMEM, FBS (10%) and pen/strep (1%). The chondrocytes were harvested when they reached 80-90% confluence. Stock solutions of 30%  $M_{10}P_{10}$  and 3% HAMA were prepared by dissolving the right amount of both polymers in PBS with Irgacure (0.05%) at 4°C overnight. Next, the stock solutions were mixed at different ratios and diluted if necessary to obtain the five different formulations (Table 1). Chondrocytes were mixed with the  $M_{10}P_{10}$ /HAMA mixtures on ice, to obtain a final concentration of  $15\text{-}20 \cdot 10^6$  chondrocytes/ml ( $n = 3$ , concentration slightly varied per donor). Constructs were cast by injecting the cell-laden polymer mixtures into cylindrical Teflon molds (sample size: 6 mm in diameter, 2 mm in height). The molds were incubated for 15 minutes at 37°C to allow physical hydrogel formation. Subsequently, chemical cross-linking was induced by irradiation with UV light (UV-Handleuchte lamp A. Hartenstein, Germany, wavelength: 365 nm, intensity at 3 cm: 1.2 mW/cm<sup>2</sup>, irradiation time: 5 minutes). Cross-linked constructs were removed



from the molds and were cultured for 28 days at 37°C and 5% CO<sub>2</sub> in chondrogenic differentiation medium consisting of high glucose DMEM supplemented with ITS+ premix (1%), dexamethasone (0.1 μM), L-ascorbic acid-2-phosphate (0.2 mM), recombinant human TGF-β1 (10 ng/ml), and pen/strep (1%) to stimulate chondrogenesis and redifferentiation of the chondrocytes<sup>42,43</sup>.

### 6.2.5 Histology, immunohistochemistry, and biochemical assays

To evaluate cartilage-like tissue formation, hydrogels were harvested at days 1 and 28. Part of each sample was fixed overnight in formalin (37%) and dehydrated through a graded ethanol series. After a clearing step in xylene, the samples were embedded in paraffin. Sections with a thickness of 5 μm were generated and stained with safranin-O to visualize proteoglycans, fast green to visualize collagens, and hematoxylin to stain cell nuclei, as previously described<sup>44</sup>. Collagen types I, II, and VI were visualized on sections with immunohistochemistry as previously described<sup>15</sup>. For proteoglycan IV immunohistochemistry, the same protocol was used as previously described for collagen type VI, but with only a pronase antigen retrieval. All sections were visualized with a light microscope (Olympus BX51 microscope, Olympus DP70 camera, Hamburg, Germany). The remaining parts of the different harvested cell-laden hydrogels were weighed, freeze dried, and weighed again to determine the water content. Next, the samples were digested overnight at 60°C in digestion buffer (0.2 M NaH<sub>2</sub>PO<sub>4</sub> + 0.01 M EDTA · 2 H<sub>2</sub>O in milliQ, pH = 6.0) supplemented with papain (31 units/mg protein, final concentration of 0.24 mg protein/ml) and cysteine (0.01 M). After digestion, the glycosaminoglycan (GAG) content was determined as a measure for proteoglycan, with a dimethylmethylene blue (DMMB) assay<sup>45</sup>, using chondroitin sulfate C as standard. The amount of DNA was measured with the Quant-iT PicoGreen dsDNA kit and read on a spectrofluorometer (Biorad, Hercules, California, USA), according to the manufacturer's protocols. The GAG content measured at day 28 was corrected for the initial readout at day 0, due to the presence of HAMA (Figure S1). This corrected GAG content was normalized to the DNA content for comparison between groups. In addition, the average change in water content normalized to the samples wet weight (wwt) was determined for each hydrogel formulation. The DNA content was normalized to the dry weight (dwt) of the samples.

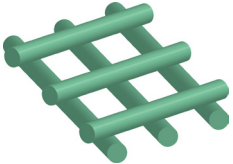
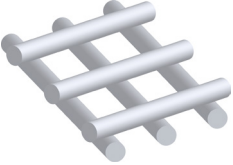
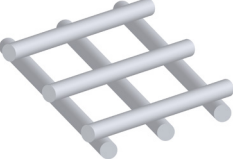
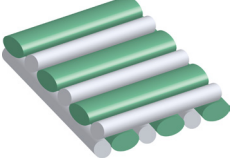
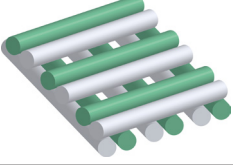
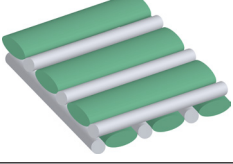
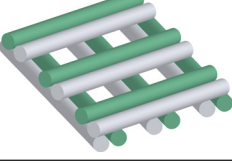
### 6.2.6 Evaluation of mechanical properties of hydrogel constructs

Cell free, cylindrical hydrogels cast as described in section 6.2.4 were analyzed using a Dynamic Mechanical Analyzer, DMA (DMA Q800, TA Instruments, Etten-Leur, The Netherlands) in an uniaxial unconfined compression test, after the equilibrium state of swelling (≥ 5h) was reached in PBS. A preload force of 0.001 N and a ramp force of 0.1 N/min with an upper force limit of 1 N were applied, and the elastic modulus (E, Young's modulus) was calculated as the slope of the initial linear segment of the stress/strain curves (n = 3).

### 6.2.7 Fabrication and characterization of printed constructs with and without reinforcement

Constructs of different designs and with or without PCL reinforcement were printed with formulation M or MHA<sub>0.5</sub> (Table 2) using a 3DDiscovery bioprinter (regenHU, Villaz-St-Pierre, Switzerland) equipped with a Bluepoint 4 UV lamp (point light source, wavelength range: 300-600 nm, UV-A intensity at 5 cm = 103 mW/cm<sup>2</sup>, Hönle UV Technology AG, Gräfelfing, Germany). Pneumatically driven robotic dispensers were used for the extrusion of the hydrogel and PCL filaments. The hydrogel precursor mixture was loaded into a syringe connected to a micro valve (CF300H) nozzle, while PCL pellets were loaded into a stainless steel cartridge furnished with a phosphor bronze thin-wall conical nozzle (inner diameter = 0.56 mm; Integrated Dispensing Solutions, Agoura Hills, CA). Each layer of the PCL/hydrogel hybrid constructs was generated by printing parallel filaments of PCL (strand distance = 1.5 or 2.0 mm), followed by deposition of hydrogel filaments between adjacent PCL strands. Subsequent layers were printed with a filament orientation perpendicular to that of the underlying layer. To achieve a solid or a porous hydrogel filling of the PCL framework, the hydrogel was deposited in the center of adjacent PCL filaments or at a distance of  $\frac{1}{4}$  of the strand distance, respectively. Additionally, the amount of the extruded hydrogel was adjusted by varying the valve opening time (v.o.t.) and pressure (detailed print settings reported in Table S1). Different temperatures of the deposition plate were used to obtain desired flow-behavior of the hydrogel after extrusion. For all designs (Table 2), square sheets (15 x 15 mm) were printed with a height of 2.4 mm, and after each hydrogel layer was printed, chemical cross-linking was induced by 3 seconds of irradiation with the Bluepoint UV lamp from a distance of 5 cm. After printing, constructs were irradiated for an additional time period to reach a total irradiation time of 69 seconds. After crosslinking, cylindrical samples were punched out of the printed sheets with a 6 mm biopsy punch, and visually inspected and photographed using an Olympus ZS61 microscope (Tokyo, Japan) coupled with an Olympus digital camera (Tokyo, Japan). As controls, hydrogel-free PCL constructs and PCL constructs infused with hydrogel by injection molding were generated. More specifically, two PCL sheets with different strand distances, *i.e.* 1.5 or 2.0 mm were printed as described above but without dispensing hydrogel between the PCL filaments. Subsequently, six cylindrical samples were punched out from each sheet, and three constructs per sheet were inserted in a Teflon-based injection mold, infused with the hydrogel, incubated at 37 °C for 5 minutes, and cross-linked for 69 seconds using the Bluepoint UV lamp from a distance of 5 cm. The remaining three constructs per sheet were used as hydrogel-free controls. Finally, the mechanical stiffness of the different printed constructs was evaluated using a DMA with an unconfined compression set up. Samples were preloaded with a force of 0.1 N and further compressed up to 18 N using a force ramp rate of 1.8 N/min. Young's moduli were calculated using stress strain curves.

**Table 2.** Construct designs for printing with hydrogel MHA<sub>0.5</sub> (green) with and without PCL (white) reinforcement.

Abbreviation	Materials	Layer design	Description*
pMH	MHA <sub>0.5</sub>		Porous s.d. = 1.5 mm
pPCL_1	PCL		Porous s.d. = 1.5 mm
pPCL_2	PCL		Porous s.d. = 2.0 mm
pMH/PCL_1	MHA <sub>0.5</sub> + PCL		Solid s.d. = 1.5 mm
pMH/PCL_2	MHA <sub>0.5</sub> + PCL		Porous s.d. = 1.5 mm
pMH/PCL_3	MHA <sub>0.5</sub> + PCL		Solid s.d. = 2.0 mm
pMH/PCL_4	MHA <sub>0.5</sub> + PCL		Porous s.d. = 2.0 mm

\*s.d. = strand distance

### 6.2.8 Statistics

Statistical analysis was performed with SPSS software (version 21, IMB Corp.). For quantitative measurements of matrix production within one cell donor, a one-way analysis of variance (ANOVA) was performed, while a randomized block design ANOVA was performed for the average matrix production, to correct for donor variations. Differences in Young's moduli and viability were determined with a one-way ANOVA. Differences in Young's moduli between constructs fabricated with a different strand distance within each co-print condition were determined with an independent t-test. A significance level of 0.05 was used. When the ANOVA highlighted significant differences, a Bonferroni post hoc test was performed except for the GAG/DNA data in the cast hydrogels which were compared with a Dunnett post hoc test to explore whether the presence of HAMA had an effect compared to HAMA free hydrogels.

## 6.3 Results and Discussion

### 6.3.1 Effect of HAMA concentration on chondrogenesis by embedded chondrocytes

The evaluated hydrogel formulations supported cartilage matrix production of embedded chondrocytes with a hydrogel composition-dependent extent (Figure 1).

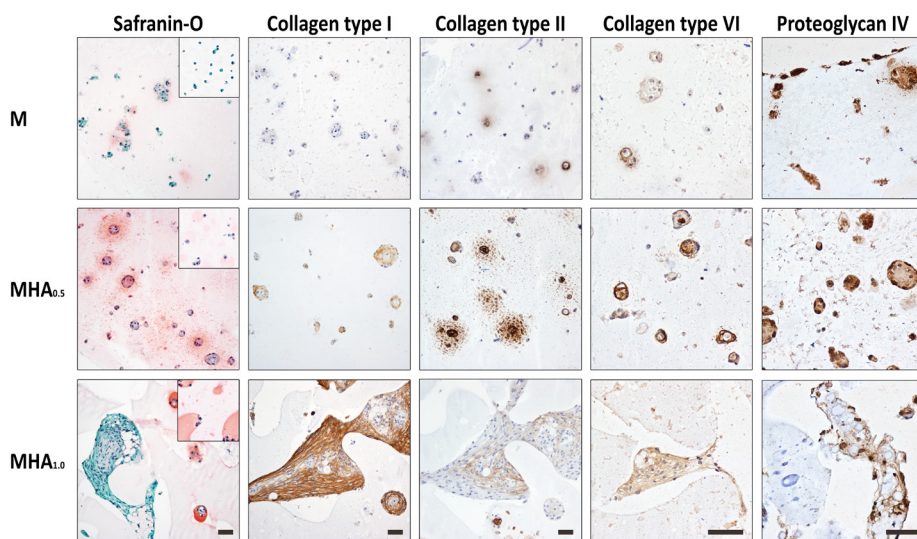


**Figure 1.** Overview of the histology and immunohistochemistry of chondrocytes cultured in  $M_{10}P_{10}$ /HAMA hydrogels with different HAMA concentrations for 28 days. Scale bar represents 50  $\mu\text{m}$  and it is the same for all images of the same staining.

During culture, rounded cell clusters rich in newly formed matrix were observed in samples with average HAMA concentrations ( $MHA_{0.25}$ ,  $MHA_{0.5}$ , Table 1) and to a lesser extent in the hydrogels without HAMA or with the lowest HAMA concentration (M and  $MHA_{0.1}$ ). The largest cell clusters surrounded by newly formed matrix were observed in samples with the highest HAMA concentration ( $MHA_1$ ), however these clusters were observed sporadically and had irregular shapes compared to the rounded clusters in the other formulations. The tissue matrix around the rounded cell clusters reacted strongly with the collagen type II antibody, as well as with safranin-O, indicating the presence of cartilage-like tissue (Figure 1). As safranin-O also stains HAMA, a pink color was observed in all HAMA-containing hydrogels also at day 0. However, the intensity of the staining was higher near the cells for samples at day 28. More collagen type II positive and intense red (safranin-O) areas were observed in hydrogels with intermediate HAMA concentrations ( $MHA_{0.25}$ ,  $MHA_{0.5}$ ) compared to hydrogels without HAMA or with the lowest HAMA concentrations (M and  $MHA_{0.1}$ ). Hydrogels with formulation  $MHA_1$  contained hardly any safranin-O positive areas at day 28, but did reveal intense collagen type II positive areas. However, the collagen type II staining was restricted to the sporadic cell clusters. On the other hand, in hydrogels with intermediate HAMA concentrations ( $MHA_{0.25}$ ,  $MHA_{0.5}$ ) some collagen type II positive areas were also observed in the inter-territorial regions. The presence of collagen type I, a marker for fibrocartilage, increased with increasing HAMA concentration (Figure 1). Additionally, the presence of collagen type VI, a marker of chondron formation, decreased in the areas directly around the chondrocyte membranes in hydrogels with increasing HAMA concentrations, although the matrix clusters in  $MHA_1$  stained overall positive for collagen type VI. Finally, proteoglycan IV, a zonal marker found predominantly in the cartilage surface, was mainly expressed at the hydrogel border of constructs without HAMA or with a low HAMA concentration (0.1%). Overall, all samples showed some proteoglycan IV positive areas.

Quantitative measurements for GAG content normalized to the DNA content of donor 1 and 2 (Figure 2a and b) matched the visualization of GAGs with the safranin-O staining in Figure 1. Contrary, no clear differences between hydrogels with different HAMA concentrations were observed in samples cultured with chondrocytes from donor 3 (Figure 2c). This illustrates that the influence of HAMA on matrix synthesis by the chondrocytes is varying between chondrocyte donor<sup>46,47</sup>. On average, significantly more GAG/DNA was measured in hydrogels with intermediate HAMA concentrations ( $MHA_{0.25}$ ,  $MHA_{0.5}$ ), compared to the hydrogels without HAMA (M) (Figure 2d). Hydrogels with the lowest ( $MHA_{0.1}$ ) and highest ( $MHA_1$ ) HAMA concentrations did not show significant differences in GAG/DNA compared to hydrogels without HAMA (M). Samples with 1% HAMA, cultured with chondrocytes of donor 2, did contain significantly less GAG/DNA compared to the HAMA free hydrogels (Figure 2b).

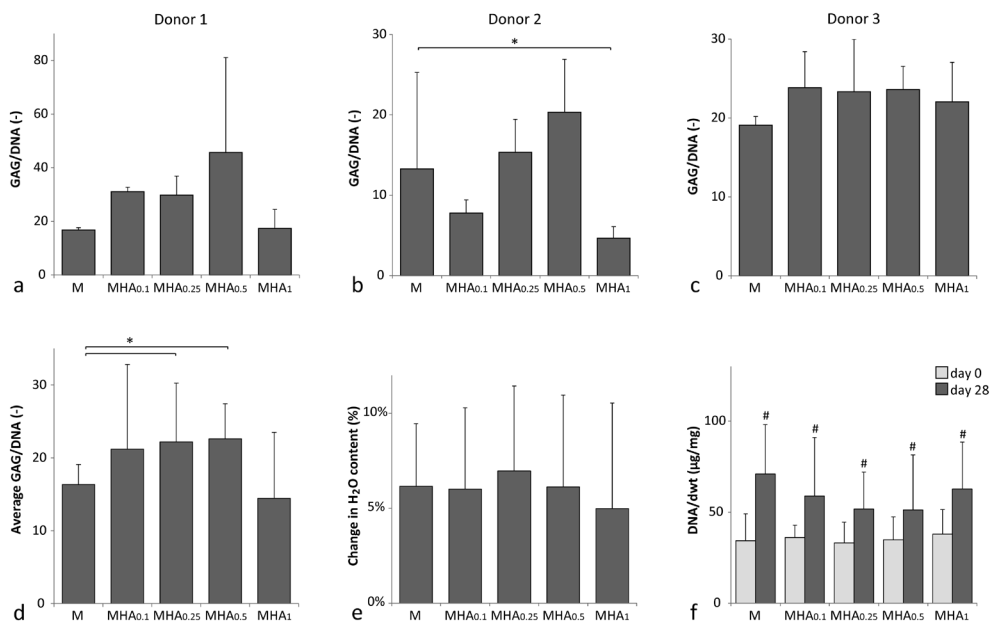


**Figure 2.** Biochemical analysis of multiple chondrocyte-laden hydrogel formulations. a-d) GAG content normalized to the DNA content at day 28 for (a) donor 1, (b) donor 2, (c) donor 3, and (d) the average of all donors. e) Difference in water content between day 28 and day 0. f) DNA content normalized to the dwt. \* indicates a significant difference between the groups. # indicates a significant difference compared to groups without a # but similar to groups with a #.

These observations demonstrate a dose-dependent effect of HAMA on the cartilage matrix production by chondrocytes in pHPMA-lac-PEG/HAMA hydrogels. More specifically, hydrogels with intermediate HAMA concentrations (0.25 and 0.5%) showed increased cartilage-like matrix production by the embedded cells compared to HAMA-free hydrogels, while a higher HAMA concentration (1%) stimulated a shift from hyaline cartilage to fibrocartilage formation. Chondrocytes are known to interact with HA via their membrane receptors *e.g.* CD44, intercellular adhesion molecule-1 (ICAM-1), and receptor for hyaluronan mediated motility (RHAMM)<sup>24,48–51</sup>. This interaction is believed to be responsible for the anabolic effect that HA can have on the matrix production by chondrocytes, as disruption of this HA-chondrocyte binding is associated with matrix degradation in native cartilage<sup>52</sup>. The dose-dependent response of chondrocytes to HA may be attributed to a negative feedback system, in which limited receptor binding with HA, especially via CD44, stimulates matrix production by chondrocytes, while more receptor interactions inhibit chondrocyte redifferentiation<sup>24,41,42,53</sup>. The hypothesis of receptor binding, would also explain why the optimal HA and HAMA concentration for cartilage matrix stimulation appears to increase with increasing cell numbers. In the present study,



we demonstrate an optimum with 0.25-0.5% HAMA in pHPMA-lac-PEG triblock copolymers based hydrogels with  $20 \times 10^6$  chondrocytes/ml. Kawasaki *et al.* (1999)<sup>26</sup> reported an optimum with 0.001-0.01% of HA in collagen-based hydrogels with  $2 \times 10^6$  chondrocytes/ml, Akmal *et al.* (2005)<sup>24</sup> found an optimum with 0.01-0.1% HA in alginate beads with  $5 \times 10^6$  chondrocytes/ml, whereas Levett *et al.* (2014)<sup>25</sup> found an optimum with 0.5% HAMA in collagen type I based hydrogels with  $10 \times 10^6$  chondrocytes/ml. Nevertheless, in contrast to our findings, Levett *et al.* (2014)<sup>25</sup> and Akmal *et al.* (2005)<sup>24</sup> reported a decrease in collagen type I gene expression and protein level, respectively, by chondrocytes in hydrogels with increasing HA or HAMA concentrations. Both studies were conducted with hydrogels based on natural polymers with known cell attachment sites that influence cell behavior, which could explain the different findings<sup>41</sup>. Intuitively, the optimal HA or HAMA concentration for matrix production is likely also dependent on the hydrogel system in which the cells are cultured. The polymer network influences cell migration, which can affect the establishment of a receptor-HA interaction<sup>54</sup>. Additionally, other materials properties, such as construct stiffness and cross-linking densities, have also been demonstrated to influence cell behavior and could, therefore, also influence the response of chondrocytes to the presence of HAMA<sup>55,56</sup>.

The water content normalized to the samples wet weight increased for all hydrogel formulations during culture with approximately 5-7% (Figure 2b). However, no significant differences in swelling were observed between the various formulations, regardless the HAMA content. This finding is in line with previous studies that also reported a negligible change in swelling of samples with 0-1% HAMA<sup>19,25</sup>.

The DNA content normalized to the samples dry weight significantly increased for all hydrogel formulations during the culture period (Figure 2c). All hydrogel formulations reached a similar DNA/dwt content at day 28 (~50-70  $\mu\text{g}/\text{mg}$ ), implying that all hydrogels supported similar proliferation rates. Although HA is capable to influence proliferation of multiple cell types, this was not observed in the current study for chondrocytes, in line with Levett *et al.* (2014)<sup>25</sup>. Contrarily, Kawasaki *et al.* (1999)<sup>26</sup>, Akmal *et al.* (2005)<sup>24</sup>, and Park *et al.* (2013)<sup>21</sup>, reported an increase in DNA content due to the presence of HA. However, the initial cell densities used in those studies were lower compared to the cell density used by Levett *et al.* (2014)<sup>25</sup> and by us in the current study which may explain the observed difference<sup>57</sup>. Additionally, Akmal *et al.* (2005)<sup>24</sup> only observed an increase in proliferation in hydrogels with the lowest HA concentrations, suggesting that this effect can also be dose-dependent and thus not present in the higher HA concentrations used by Levett *et al.* (2014)<sup>25</sup> and in this study.

### 6.3.2 Effect of HAMA concentration on hydrogel mechanical properties

All studied hydrogel formulations were shape-stable after swelling in PBS ( $\geq 5\text{h}$ ). Young's moduli ranged from  $14.0 \pm 0.6$  to  $30.8 \pm 0.9$  kPa (Figure 3). Figure 3 shows that the Young's modulus of  $M_{10}P_{10}$ /HAMA hydrogels increased with increasing HAMA concentration.



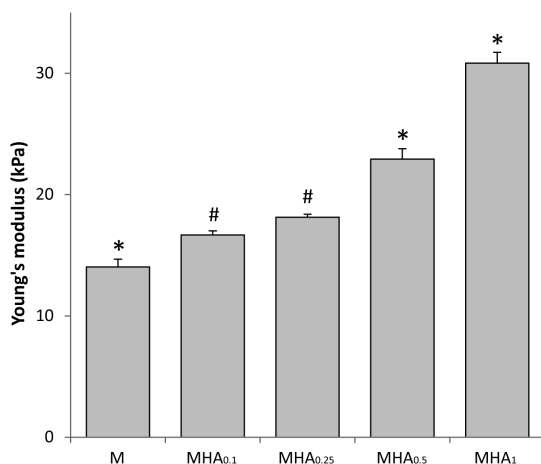


**Figure 3.** Young's moduli obtained from stress/strain curves obtained during unconfined compression, where \* indicates a significant difference ( $p < 0.05$ ) from all other groups and # indicates a significant difference to all groups except to each other.

The Young's moduli of all evaluated hydrogel formulations were statistically different from each other, except for MHA<sub>0.1</sub> and MHA<sub>0.25</sub> that had similar moduli.

Clearly, the presence of HAMA led to stiffer hydrogels compared to hydrogel M, despite an equal total polymer concentration, *i.e.* 20% w/w and a comparable total number of methacrylate groups. These findings are in line with our previous observations<sup>15</sup> and can find an explanation in the microstructure of these hydrogels.  $M_{10}P_{10}$ /HAMA hydrogels are known to exhibit phase separation<sup>58</sup>, as also observed in the safranin-O histology at day 0 (Figure 1) for HAMA-containing hydrogels. We have recently demonstrated that micro-phase separation in these hydrogels leads to the formation of highly hydrated, HAMA-rich domains and partially dehydrated more hydrophobic regions, where the majority of  $M_{10}P_{10}$  is located<sup>58</sup>. The extent of this phase separation is highly dependent on the HAMA concentration. In that study, we have also found that when using low HAMA concentrations ( $< 1\%$  w/w), the relative increase in  $M_{10}P_{10}$  concentration in the hydrophobic domains due to their partial dehydration (driven by the presence of HAMA), resulted in stiffer physical hydrogels. In a similar way, this phenomenon could explain the effect of HAMA concentration on the Young's moduli of chemically cross-linked hydrogels found in the present study. The effect of HAMA on construct stiffness may also be partially attributed to the much higher MW of HAMA (120 kDa) compared to that of  $M_{10}P_{10}$  (40 kDa). In fact, the relatively longer HAMA molecules are likely able to generate more chain entanglements that provide higher stiffness to the entire polymer network. The general increase of hydrogel stiffness with increasing HAMA concentration, likely responsible for a tighter network in hydrogels with higher HAMA content, can also explain the observed cell clusters with irregular shapes and confined matrix deposition in the histological analysis of MHA<sub>1</sub> hydrogels. In fact, it has been

reported that dense polymer networks can hamper the diffusion of newly formed matrix<sup>10,27,59</sup>. In addition, the differences in construct stiffness may also contribute to the difference in matrix production by the embedded chondrocytes<sup>55,56</sup>.

### 6.3.3 Fabrication of hydrogel/PCL co-printed constructs

Among all evaluated hydrogel formulations, hydrogels containing 0.5% HAMA (MHA<sub>0.5</sub>) induced the highest cartilage-like tissue formation, and displayed a medium/high Young's modulus, which is beneficial for the hydrogel filament stability during printing and handling. Hence, the printing experiments were performed with this formulation. Additionally, the incorporation of 0.5% HAMA introduced yield stress behavior to MHA<sub>0.5</sub> (yield stress =  $28.7 \pm 0.2$  Pa), which is reported to improve shape-fidelity of 3D bioprinted constructs<sup>10,15,60,61</sup>, whereas in accordance with our previously reported findings<sup>16</sup>, no yield stress was found for the HAMA-free formulation M (control, Figure S2). In fact, 3D printing of shape-stable MHA<sub>0.5</sub> constructs without supporting structures or reinforcement was successfully achieved (Figure 4a). Printing of PCL under optimized conditions and using a strand distance of 1.5 or 2.0 mm, resulted in the generation of stiff thermoplastic meshes with interconnected pores (Figure 4f). For the co-printing of PCL and MHA<sub>0.5</sub>, constructs with four different designs, having a PCL framework with variable strand distance and a final architecture with or without pores, were printed (Figure b-e and g-j). To obtain porosity in pMH/PCL constructs, a hydrogel dispensing pressure of 0.1 MPa and a valve opening time (v.o.t.) of 300  $\mu$ s were used. To obtain solid co-printed constructs, higher v.o.t. (500 or 1300  $\mu$ s when using a strand distance of 1.5 and 2.0 mm, respectively) and a slightly higher pressure (0.13 MPa, when using a strand distance of 2.0 mm) were used to increase the amount of extruded hydrogel. The temperature of the deposition plate was set at 35°C while printing solid constructs. In contrast, a higher temperature, *i.e.* 40°C was found to be beneficial for the stability of the hydrogel filaments, required to maintain a constant shape and size of the pores in the porous co-printed constructs (pMH/PCL\_2 and pMH/PCL\_4).

Figure 4k shows that PCL meshes without hydrogel and with a strand distance of 1.5 and 2.0 mm possessed Young's moduli of  $7.3 \pm 0.4$  and  $5.1 \pm 0.7$  MPa, respectively. The Young's moduli of pMH/PCL co-printed constructs ranged from 3.5 and 4.6 MPa, with slightly higher values for constructs with lower strand distance (*i.e.* 1.5 mm), and no statistical difference between porous and non-porous constructs. Porosity is considered beneficial for cartilage tissue engineering as it facilitates the nutrients/waste products exchange between the cell-laden hydrogel matrix and the surrounding fluids<sup>62,63</sup>. Moreover, pore size and organization have been shown to affect *in vivo* tissue maturation of tissue engineered constructs<sup>64,65</sup>. Additionally, in an *in vivo* orthotopic scenario, cell-free co-printed porous scaffolds combined with marrow-stimulation techniques *e.g.* microfracture, may facilitate penetration of stem cells from the bone marrow into the implanted hydrogels<sup>66</sup>.

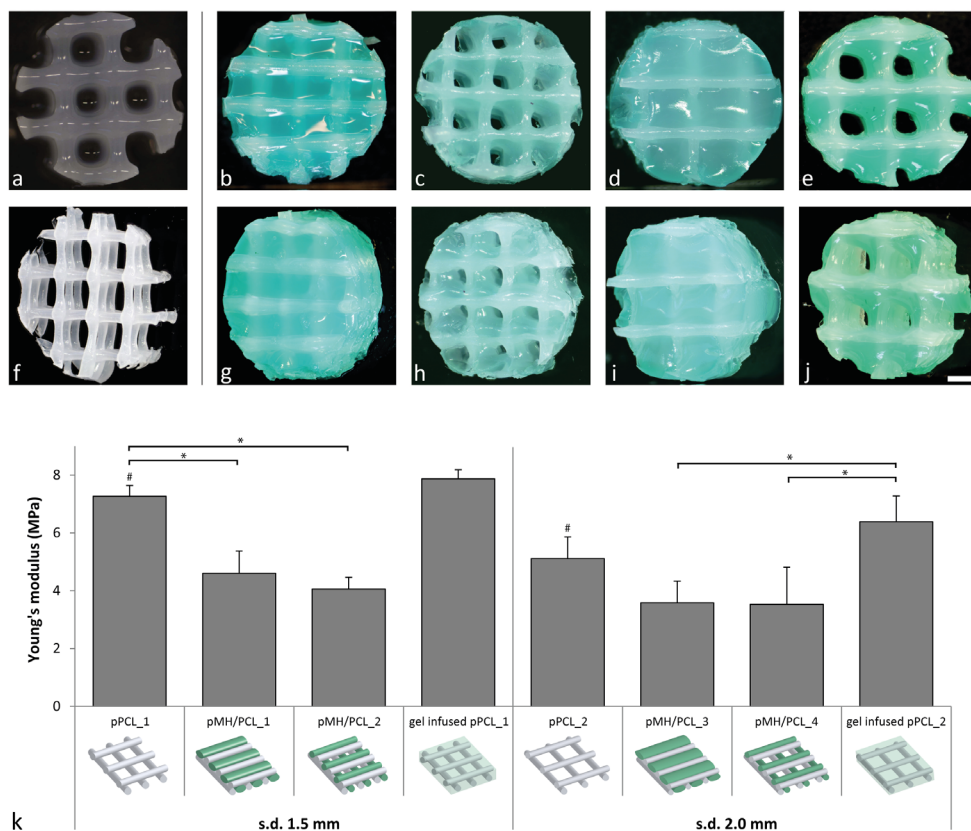


**Figure 4.** Evaluation of co-printed constructs. a) Top view of a 3D shape stable printed hydrogel construct with formulation  $\text{MHA}_{0.5}$ . b and g) Top and top-side view of pMH/PCL<sub>1</sub> ( $\text{MHA}_{0.5}$ /PCL, non-porous, strand distance = 1.5 mm). c and h) Top and top-side view of pMH/PCL<sub>2</sub> ( $\text{MHA}_{0.5}$ /PCL, porous, strand distance = 1.5 mm). d and i) Top and top-side view of pMH/PCL<sub>3</sub> ( $\text{MHA}_{0.5}$ /PCL, non-porous, strand distance = 2.0 mm). e and j) Top and top-side view of pMH/PCL<sub>4</sub> ( $\text{MHA}_{0.5}$ /PCL, porous, strand distance = 2.0 mm). f) Top-side view of a PCL reinforcement structure. k) Young's moduli of the different printed constructs. Significant differences ( $p < 0.05$ ) between conditions with the same strand distance are indicated with \*, while # indicates a significant difference between strand distance within the same print conditions. For visualization purposes,  $\text{MHA}_{0.5}$  hydrogel was stained green in the reinforced constructs. Scale bar represent 1 mm and it is the same for all images, s.d. = strand distance.

Importantly, all the PCL-based constructs had Young's moduli of approximately three orders of magnitude higher than non-reinforced hydrogel constructs (Figure 3), reaching a stiffness comparable to that of native cartilage (0.4-0.8 MPa)<sup>67-69</sup>. This result confirmed the suitability of PCL as reinforcing material for cartilage tissue engineering, in line with previously reported findings<sup>70,71</sup>. Interestingly, co-printed PCL/hydrogel constructs had lower Young's moduli compared to the hydrogel-free PCL meshes. This finding was reproducible and the decrease was significant for constructs with a strand distance of 1.5 mm. In contrast, printed PCL meshes

infused with hydrogel MHA<sub>0.5</sub> had similar Young's moduli as the hydrogel-free PCL meshes ( $7.9 \pm 0.3$  and  $6.4 \pm 0.9$  MPa for constructs with strand distance of 1.5 and 2.0 mm, respectively), indicating that the difference in construct stiffness is a result of the co-printing process. Likely, the layer-by-layer hydrogel deposition partially interfered with the adhesion of newly printed PCL filaments with underlining PCL strands. Nevertheless, co-printed constructs were macroscopically stable and the PCL skeleton appeared intact and coherent to the desired design, after selective removal of the hydrogel for visualization purposes (data not shown). However, this observation highlights the critical role of the chosen print settings and construct design on the mechanical properties of the final construct.

## 6.4 Conclusions

In this study, hydrogel-based cartilage repair constructs with optimized bioactivity and mechanical properties were successfully fabricated, via the addition of HAMA to a thermosensitive pHPMA-lac-PEG hydrogel and via co-printing with PCL. Results of the HAMA concentrations screening demonstrate a dose-dependent effect of HAMA on the cartilage matrix production by embedded chondrocytes. More specifically, intermediate HAMA concentrations (0.25-0.5%) increased cartilage-like matrix production compared to HAMA-free hydrogels, while higher (1%) concentrations resulted in undesirable fibrocartilage formation. These results may impact the choice of HAMA content in bio-ink development. In addition, the presence of HAMA was found to increase the construct stiffness with increasing concentration. These findings allowed the identification of an optimal hydrogel composition of 19.5% pHPMA-lac-PEG with 0.5% HAMA. This formulation supported increased cartilage matrix production compared to HAMA-free hydrogels, contained limited fibrocartilage formation, and displayed a medium/high Young's modulus, and yielding behavior, beneficial for the 3D printing of these hydrogels. Hydrogel/PCL co-printing enabled the generation of complex 3D constructs with mechanical stiffness in the range of native cartilage. However, the co-printing procedure influenced the final construct properties, highlighting the crucial role of the print settings in determining the final construct properties. Further investigations on cell-laden hydrogels co-printed with PCL will clarify the role of the printing procedure on long-term cellular activity and differentiation. In conclusion, we developed advanced composite cartilage repair constructs, with a chondrogenic hydrogel component and a mechanically adequate PCL reinforcement. Whilst this further mimics biomechanical properties of native articular cartilage, this is an interesting approach for further optimization.

**Acknowledgments**

The research leading to these results has received funding from the Dutch Arthritis Foundation (LLP-12), the European Community's Seventh Framework Programme (FP7/2007-2013) under grant agreement n°309962 (HydroZONES) and the European Research Council under grant agreement n°647426 (3D-JOINT). The authors would like to thank Mattie H. P. van Rijen and Naveed A. Rahman for their assistance with histology and biochemical assays, as well as Maarten M. Blokzijl for his contribution to the 3D printing experiments, Anneloes Mensinga for her assistance with the cell cultures, and Carl C. L. Schuurmans for his contribution to the synthesis of  $M_{10}P_{10}$  polymer. The primary antibody against collagen type II (II-II6B3) and collagen type VI (5C6), developed by T. F. Linsenmayer and E. S. Engvall respectively, were obtained from the DSHB developed under the auspices of the NICHD and maintained by The University of Iowa, Department of Biology, Iowa City, IA 52242.

## Supporting Information

**Table S1.** Optimized settings applied for the 3D printing of hydrogel, PCL and hydrogels/PCL constructs.

<b>pMH</b>	<b>Hydrogel print settings</b>	<b>PCL print settings</b>
Pressure Temperature Cartridge Deposition plate XY plane speed Microvalve CF300H Dosing distance Valve opening time	0.1 MPa  37 °C 40 °C 40 mm/s  0.1 mm 300 μs	-
<b>PCL</b>	<b>Hydrogel print settings</b>	<b>PCL print settings</b>
Pressure Temperature Cartridge Deposition plate XY plane speed	-	0.3 MPa  80 °C 35 °C 1 mm/s
<b>pMH/PCL</b>	<b>Hydrogel print settings</b>	<b>PCL print settings</b>
Pressure Temperature Cartridge Deposition plate XY plane speed Microvalve CF300H Dosing distance Valve opening time	0.1 <sup>a</sup> or 0.13 <sup>b</sup> MPa  37 °C 35 <sup>c</sup> or 40 <sup>d</sup> °C 40 mm/s  0.1 mm 300 <sup>e</sup> , 500 <sup>f</sup> or 1300 <sup>g</sup> μs	0.3 MPa  80 °C 35 <sup>c</sup> or 40 <sup>d</sup> °C 1 mm/s

<sup>a</sup> Applied to pMH\_1, pMH\_2 and pMH\_4

<sup>b</sup> Applied to pMH\_3

<sup>c</sup> Applied to pMH\_1 and pMH\_3

<sup>d</sup> Applied to pMH\_2 and pMH\_4

<sup>e</sup> Applied to pMH\_2 and pMH\_4

<sup>f</sup> Applied to pMH\_1

<sup>g</sup> Applied to pMH\_3

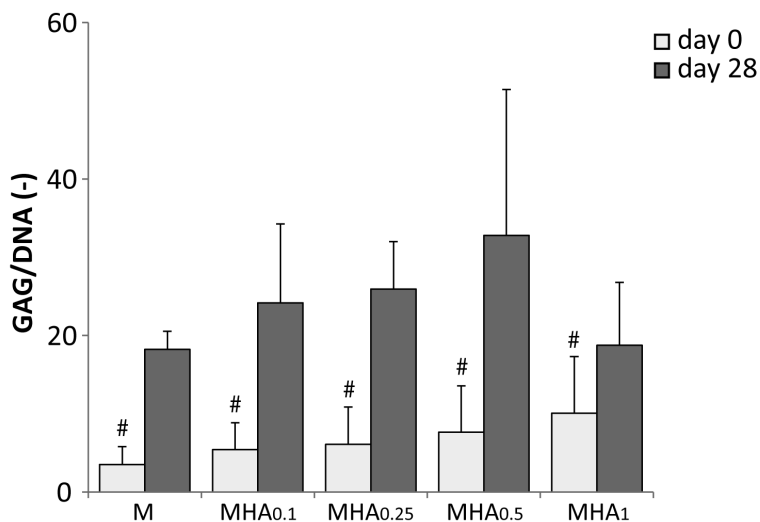


**Figure S1.** GAG/DNA content at day 0 and 28 for the five different hydrogel formulations. # indicates a significant difference compared to groups without a # but similar as groups with a #.

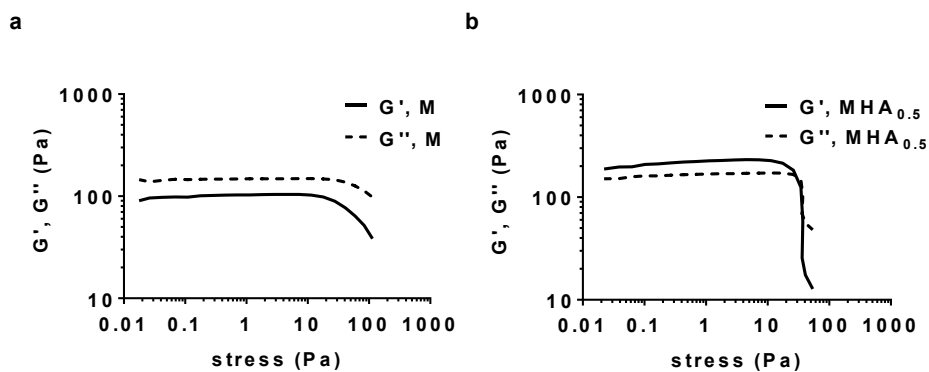


**Figure S2.**  $G'$  and  $G''$  as function of oscillatory stress for formulations M and  $MHA_{0.5}$  before UV-cross-linking, recorded at  $37^\circ\text{C}$  using a frequency of 1 Hz. Yield stress is defined as the stress at which  $G'$  crosses  $G''$ .



## References

- (1) Murphy, S. V.; Atala, A. 3D Bioprinting of Tissues and Organs. *Nat. Biotechnol.* **2014**, *32* (8), 773–785.
- (2) Buckley, M. R.; Gleghorn, J. P.; Bonassar, L. J.; Cohen, I. Mapping the Depth Dependence of Shear Properties in Articular Cartilage. *J. Biomech.* **2008**, *41* (11), 2430–2437.
- (3) Silverberg, J. L.; Barrett, A. R.; Das, M.; Petersen, P. B.; Bonassar, L. J.; Cohen, I. Structure-Function Relations and Rigidity Percolation in the Shear Properties of Articular Cartilage. *Biophys. J.* **2014**, *107* (7), 1721–1730.
- (4) Schuurman, W.; Gawlitta, D.; Klein, T. J.; Hoope, W. T.; van Rijen, M. H. P.; Dhert, W. J. A.; van Weeren, P. R.; Malda, J. Zonal Chondrocyte Subpopulations Reacquire Zone-Specific Characteristics During In Vitro Redifferentiation. *Am. J. Sports Med.* **2009**, *37* (1\_suppl), 97S–104S.
- (5) Almarza, A. J.; Athanasiou, K. A. Design Characteristics for the Tissue Engineering of Cartilaginous Tissues. *Ann. Biomed. Eng.* **2004**, *32* (1), 2–17.
- (6) Prakash, D.; Learmonth, D. Natural Progression of Osteo-Chondral Defect in the Femoral Condyle. *Knee* **2002**, *9* (1), 7–10.
- (7) Mouser, V. H. M.; Levato, R.; Bonassar, L. J.; D’Lima, D. D.; Grande, D. A.; Klein, T. J.; Saris, D. B. F.; Zenobi-Wong, M.; Gawlitta, D.; Malda, J. Three-Dimensional Bioprinting and Its Potential in the Field of Articular Cartilage Regeneration. *Cartilage* **2016**.
- (8) Klein, T. J.; Malda, J.; Sah, R. L.; Hutmacher, D. W. Tissue Engineering of Articular Cartilage with Biomimetic Zones. *Tissue Eng. Part B Rev.* **2009**, *15* (2), 143–157.
- (9) Malda, J.; Visser, J.; Melchels, F. P.; Jüngst, T.; Hennink, W. E.; Dhert, W. J. A.; Groll, J.; Hutmacher, D. W. 25th Anniversary Article: Engineering Hydrogels for Biofabrication. *Adv. Mater.* **2013**, *25* (36), 5011–5028.
- (10) Mouser, V. H. M.; Melchels, F. P. W.; Visser, J.; Dhert, W. J. A.; Gawlitta, D.; Malda, J. Yield Stress Determines Bioprintability of Hydrogels Based on Gelatin-Methacryloyl and Gellan Gum for Cartilage Bioprinting. *Biofabrication* **2016**, *8* (3), 35003.
- (11) Vermonden, T.; Fedorovich, N. E.; van Geemen, D.; Alblas, J.; van Nostrum, C. F.; Dhert, W. J. A.; Hennink, W. E. Photopolymerized Thermosensitive Hydrogels: Synthesis, Degradation, and Cytocompatibility. *Biomacromolecules* **2008**, *9* (3), 919–926.
- (12) Censi, R.; Vermonden, T.; van Steenbergen, M. J.; Deschout, H.; Braeckmans, K.; De Smedt, S. C.; van Nostrum, C. F.; di Martino, P.; Hennink, W. E. Photopolymerized Thermosensitive Hydrogels for Tailorable Diffusion-Controlled Protein Delivery. *J. Control. Release* **2009**, *140* (3), 230–236.
- (13) Censi, R.; Vermonden, T.; Deschout, H.; Braeckmans, K.; di Martino, P.; De Smedt, S. C.; van Nostrum, C. F.; Hennink, W. E. Photopolymerized Thermosensitive poly(HPMA lactate)-PEG-Based Hydrogels: Effect of Network Design on Mechanical Properties, Degradation, and Release Behavior. *Biomacromolecules* **2010**, *11* (8), 2143–2151.
- (14) Censi, R.; Schuurman, W.; Malda, J.; di Dato, G.; Burgisser, P. E.; Dhert, W. J. A.; van Nostrum, C. F.; di Martino, P.; Vermonden, T.; Hennink, W. E. A Printable Photopolymerizable Thermosensitive p(HPMAm-Lactate)-PEG Hydrogel for Tissue

- Engineering. *Adv. Funct. Mater.* **2011**, *21* (10), 1833–1842.
- (15) Abbadessa, A.; Mouser, V. H. M.; Blokzijl, M. M.; Gawlitta, D.; Dhert, W. J. A.; Hennink, W. E.; Malda, J.; Vermonden, T. A Synthetic Thermosensitive Hydrogel for Cartilage Bioprinting and Its Biofunctionalization with Polysaccharides. *Biomacromolecules* **2016**, *17* (6), 2137–2147.
- (16) Abbadessa, A.; Blokzijl, M. M.; Mouser, V. H. M.; Marica, P.; Malda, J.; Hennink, W. E.; Vermonden, T. A Thermo-Responsive and Photo-Polymerizable Chondroitin Sulfate-Based Hydrogel for 3D Printing Applications. *Carbohydr. Polym.* **2016**, *149*, 163–174.
- (17) Ponta, H.; Sherman, L.; Herrlich, P. A. CD44: From Adhesion Molecules to Signalling Regulators. *Nat. Rev. Mol. Cell Biol.* **2003**, *4* (1), 33–45.
- (18) Lesley, J.; Hascall, V. C.; Tammi, M.; Hyman, R. Hyaluronan Binding by Cell Surface CD44. *J. Biol. Chem.* **2000**, *275* (35), 26967–26975.
- (19) Levett, P. A.; Melchels, F. P. W.; Schrobback, K.; Hutmacher, D. W.; Malda, J.; Klein, T. J. A Biomimetic Extracellular Matrix for Cartilage Tissue Engineering Centered on Photocurable Gelatin, Hyaluronic Acid and Chondroitin Sulfate. *Acta Biomater.* **2014**, *10* (1), 214–223.
- (20) Chung, C.; Erickson, I. E.; Mauck, R. L.; Burdick, J. A. Differential Behavior of Auricular and Articular Chondrocytes in Hyaluronic Acid Hydrogels. *Tissue Eng. Part A* **2008**, *14* (7), 1121–1131.
- (21) Park, H.; Choi, B.; Hu, J.; Lee, M. Injectable Chitosan Hyaluronic Acid Hydrogels for Cartilage Tissue Engineering. *Acta Biomater.* **2013**, *9* (1), 4779–4786.
- (22) Liao, E.; Yaszemski, M.; Krebsbach, P.; Hollister, S. Tissue-Engineered Cartilage Constructs Using Composite Hyaluronic Acid/Collagen I Hydrogels and Designed Poly(Propylene Fumarate) Scaffolds. *Tissue Eng.* **2007**, *13* (3), 537–550.
- (23) Allemann, F.; Mizuno, S.; Eid, K.; Yates, K. E.; Zaleske, D.; Glowacki, J. Effects of Hyaluronan on Engineered Articular Cartilage Extracellular Matrix Gene Expression in 3-Dimensional Collagen Scaffolds. *J. Biomed. Mater. Res.* **2001**, *55*, 13–19.
- (24) Akmal, M.; Singh, A.; Anand, A.; Kesani, A.; Aslam, N.; Goodship, A.; Bentley, G. The Effects of Hyaluronic Acid on Articular Chondrocytes. *J. Bone Jt. Surg. - Br. Vol.* **2005**, *87-B* (8), 1143–1149.
- (25) Levett, P. A.; Hutmacher, D. W.; Malda, J.; Klein, T. J. Hyaluronic Acid Enhances the Mechanical Properties of Tissue-Engineered Cartilage Constructs. *PLoS One* **2014**, *9* (12), e113216.
- (26) Kawasaki, K.; Ochi, M.; Uchio, Y.; Adachi, N.; Matsusaki, M. Hyaluronic Acid Enhances Proliferation and Chondroitin Sulfate Synthesis in Cultured Chondrocytes Embedded in Collagen Gels. *J. Cell. Physiol.* **1999**, *179* (2), 142–148.
- (27) Bryant, S. J.; Anseth, K. S. Hydrogel Properties Influence ECM Production by Chondrocytes Photoencapsulated in Poly (Ethylene Glycol) Hydrogels. *J. Biomed. Mater. Res.* **2001**, *59* (1), 63–71.
- (28) Schuurman, W.; Khristov, V.; Pot, M. W.; van Weeren, P. R.; Dhert, W. J. A.; Malda, J. Bioprinting of Hybrid Tissue Constructs with Tailorable Mechanical Properties. *Biofabrication* **2011**, *3* (2), 21001.
- (29) Jang, J.; Lee, J.; Seol, Y.-J.; Jeong, Y. H.; Cho, D.-W. Improving Mechanical Properties of Alginate Hydrogel by Reinforcement with Ethanol Treated Polycaprolactone Nanofibers. *Compos. Part B Eng.* **2013**, *45* (1), 1216–1221.
- (30) Iviglia, G.; Cassinelli, C.; Torre, E.; Baino, F.; Morra, M.; Vitale-Brovarone, C. Novel

- Bioceramic-Reinforced Hydrogel for Alveolar Bone Regeneration. *Acta Biomater.* **2016**, *44*, 97–109.
- (31) Lee, J.-S.; Hong, J. M.; Jung, J. W.; Shim, J.-H.; Oh, J.-H.; Cho, D.-W. 3D Printing of Composite Tissue with Complex Shape Applied to Ear Regeneration. *Biofabrication* **2014**, *6* (2), 24103.
- (32) Kundu, J.; Shim, J.-H. H.; Jang, J.; Kim, S.-W. W.; Cho, D.-W. W. An Additive Manufacturing-Based PCL-Alginate-Chondrocyte Bioprinted Scaffold for Cartilage Tissue Engineering. *J. Tissue Eng. Regen. Med.* **2015**, *9* (11), 1286–1297.
- (33) Visser, J.; Peters, B.; Burger, T. J.; Boomstra, J.; Dhert, W. J. A.; Melchels, F. P. W.; Malda, J. Biofabrication of Multi-Material Anatomically Shaped Tissue Constructs. *Biofabrication* **2013**, *5* (3), 35007.
- (34) Melchels, F. P. W.; Blokzijl, M. M.; Levato, R.; Peiffer, Q. C.; Ruijter, M. De; Hennink, W. E.; Vermonden, T.; Malda, J. Hydrogel-Based Reinforcement of 3D Bioprinted Constructs. *Biofabrication* **2016**, *8* (3), 35004.
- (35) Martin, J. J.; Fiore, B. E.; Erb, R. M. Designing Bioinspired Composite Reinforcement Architectures via 3D Magnetic Printing. *Nat. Commun.* **2015**, *6*, 8641.
- (36) Woodruff, M. A.; Hutmacher, D. W. The Return of a Forgotten polymer—Polycaprolactone in the 21st Century. *Prog. Polym. Sci.* **2010**, *35* (10), 1217–1256.
- (37) Olubamiji, A. D.; Izadifar, Z.; Si, J. L.; Cooper, D. M. L.; Eames, B. F.; Chen, D. X. Modulating Mechanical Behaviour of 3D-Printed Cartilage-Mimetic PCL Scaffolds: Influence of Molecular Weight and Pore Geometry. *Biofabrication* **2016**, *8* (2), 25020.
- (38) Woodfield, T. B. F.; Malda, J.; de Wijn, J.; Péters, F.; Riesle, J.; van Blitterswijk, C. A. Design of Porous Scaffolds for Cartilage Tissue Engineering Using a Three-Dimensional Fiber-Deposition Technique. *Biomaterials* **2004**, *25* (18), 4149–4161.
- (39) Neradovic, D.; van Steenberg, M. J.; Vansteelant, L.; Meijer, Y. J.; van Nostrum, C. F.; Hennink, W. E. Degradation Mechanism and Kinetics of Thermosensitive Polyacrylamides Containing Lactic Acid Side Chains. *Macromolecules* **2003**, *36* (20), 7491–7498.
- (40) Neradovic, D.; van Nostrum, C. F.; Hennink, W. E. Thermoresponsive Polymeric Micelles with Controlled Instability Based on Hydrolytically Sensitive N-Isopropylacrylamide Copolymers. *Macromolecules* **2001**, *34* (22), 7589–7591.
- (41) Hachet, E.; Van Den Berghe, H.; Bayma, E.; Block, M. R.; Auzély-Velty, R. Design of Biomimetic Cell-Interactive Substrates Using Hyaluronic Acid Hydrogels with Tunable Mechanical Properties. *Biomacromolecules* **2012**, *13* (6), 1818–1827.
- (42) Benya, P. D.; Shaffer, J. D. Dedifferentiated Chondrocytes Reexpress the Differentiated Collagen Phenotype When Cultured in Agarose Gels. *Cell* **1982**, *30* (1), 215–224.
- (43) Guo, J.; Jourdian, G. W.; Maccallum, D. K. Culture and Growth Characteristics of Chondrocytes Encapsulated in Alginate Beads. *Connect. Tissue Res.* **1989**, *19* (2–4), 277–297.
- (44) Rosenberg, L. Chemical Basis for the Histological Use of Safranin O in the Study of Articular Cartilage. *J. Bone Joint Surg. Am.* **1971**, *53* (1), 69–82.
- (45) Farndale, R. W.; Sayers, C. A.; Barrett, A. J. A Direct Spectrophotometric Microassay for Sulfated Glycosaminoglycans in Cartilage Cultures. *Connect. Tissue Res.* **1982**, *9* (4), 247–248.
- (46) Gawlitta, D.; van Rijen, M. H. P.; Schrijver, E. J. M.; Alblas, J.; Dhert, W. J. A.

- Hypoxia Impedes Hypertrophic Chondrogenesis of Human Multipotent Stromal Cells. *Tissue Eng. Part A* **2012**, *18* (19–20), 1957–1966.
- (47) Zwickl, H.; Niculescu-Morzsza, E.; Nehrer, S. Investigation of Collagen Transplants Seeded with Human Autologous Chondrocytes at the Time of Transplantation. *Cartilage* **2010**, *1* (3), 194–199.
- (48) Yasuda, T. Nuclear Factor- $\kappa$ B Activation by Type II Collagen Peptide in Articular Chondrocytes: Its Inhibition by Hyaluronan via the Receptors. *Mod. Rheumatol.* **2012**, *23* (6), 1116–1123.
- (49) Viola, M.; Vigetti, D.; Karousou, E.; D'Angelo, M. L.; Caon, I.; Moretto, P.; De Luca, G.; Passi, A. Biology and Biotechnology of Hyaluronan. *Glycoconj. J.* **2015**, *32* (3–4), 93–103.
- (50) Dowthwaite, G. P.; Edwards, J. C. W.; Pitsillides, A. A. An Essential Role for the Interaction Between Hyaluronan and Hyaluronan Binding Proteins During Joint Development. *J. Histochem. Cytochem.* **1998**, *46* (5), 641–651.
- (51) Onodera, Y.; Teramura, T.; Takehara, T.; Fukuda, K. Hyaluronic Acid Regulates a Key Redox Control Factor Nrf2 via Phosphorylation of Akt in Bovine Articular Chondrocytes. *FEBS Open Bio* **2015**, *5* (1), 476–484.
- (52) Ariyoshi, W.; Takahashi, N.; Hida, D.; Knudson, C. B.; Knudson, W. Mechanisms Involved in Enhancement of the Expression and Function of Aggrecanases by Hyaluronan Oligosaccharides. *Arthritis Rheum.* **2012**, *64* (1), 187–197.
- (53) Schuh, E.; Hofmann, S.; Stok, K.; Notbohm, H.; Müller, R.; Rotter, N. Chondrocyte Redifferentiation in 3D: The Effect of Adhesion Site Density and Substrate Elasticity. *J. Biomed. Mater. Res. A* **2012**, *100* (1), 38–47.
- (54) Vu, L. T.; Jain, G.; Veres, B. D.; Rajagopalan, P. Cell Migration on Planar and Three-Dimensional Matrices: A Hydrogel-Based Perspective. *Tissue Eng. Part B Rev.* **2015**, *21* (1), 67–74.
- (55) Discher, D. E.; Janmey, P.; Wang, Y.-L. Tissue Cells Feel and Respond to the Stiffness of Their Substrate. *Science* **2005**, *310* (5751), 1139–1143.
- (56) Huang, G.; Wang, L.; Wang, S.; Han, Y.; Wu, J.; Zhang, Q.; Xu, F.; Lu, T. J. Engineering Three-Dimensional Cell Mechanical Microenvironment with Hydrogels. *Biofabrication* **2012**, *4* (4), 42001.
- (57) Heng, B. C.; Bezerra, P. P.; Preiser, P. R.; Alex Law, S. K.; Xia, Y.; Boey, F.; Venkatraman, S. S. Effect of Cell-Seeding Density on the Proliferation and Gene Expression Profile of Human Umbilical Vein Endothelial Cells within Ex Vivo Culture. *Cytotherapy* **2011**, *13* (5), 606–617.
- (58) Abbadessa, A.; Landin, M.; Blenke, E. O.; Hennink, W. E.; Vermonden, T. Two-Component Thermosensitive Hydrogels: Phase Separation Affecting Rheological Behavior. *Submitt. Publ.*
- (59) Kock, L. M.; Geraedts, J.; Ito, K.; van Donkelaar, C. C. Low Agarose Concentration and TGF- $\beta$ 3 Distribute Extracellular Matrix in Tissue-Engineered Cartilage. *Tissue Eng. Part A* **2013**, *19* (13–14), 1621–1631.
- (60) Jungst, T.; Smolan, W.; Schacht, K.; Scheibel, T.; Groll, J. Strategies and Molecular Design Criteria for 3D Printable Hydrogels. *Chem. Rev.* **2016**, *116* (3), 1496–1539.
- (61) Melchels, F. P. W.; Dhert, W. J. A.; Huttmacher, D. W.; Malda, J. Development and Characterisation of a New Bioink for Additive Tissue Manufacturing. *J. Mater. Chem. B* **2014**, *2* (16), 2282–2289.
- (62) Hollister, S. J. Porous Scaffold Design for Tissue Engineering. *Nat. Mater.* **2005**, *4*

- (7), 518–524.
- (63) Hutmacher, D. W. Scaffolds in Tissue Engineering Bone and Cartilage. *Biomaterials* **2000**, *21* (24), 2529–2543.
- (64) Malda, J.; Woodfield, T. B. F.; van der Vloodt, F.; Kooy, F. K.; Martens, D. E.; Tramper, J.; van Blitterswijk, C. A.; Riesle, J. The Effect of PEGT/PBT Scaffold Architecture on Oxygen Gradients in Tissue Engineered Cartilaginous Constructs. *Biomaterials* **2004**, *25* (26), 5773–5780.
- (65) Malda, J.; Woodfield, T. B. F.; van der Vloodt, F.; Wilson, C.; Martens, D. E.; Tramper, J.; van Blitterswijk, C. A.; Riesle, J. The Effect of PEGT/PBT Scaffold Architecture on the Composition of Tissue Engineered Cartilage. *Biomaterials* **2005**, *26* (1), 63–72.
- (66) Steadman, J. R.; Rodkey, W. G.; Rodrigo, J. J. Microfracture: Surgical Technique and Rehabilitation to Treat Chondral Defects. *Clin Orthop Relat Res* **2001**, No. 391 Suppl, S362-9.
- (67) Chen, A. C.; Bae, W. C.; Schinagl, R. M.; Sah, R. L. Depth- and Strain-Dependent Mechanical and Electromechanical Properties of Full-Thickness Bovine Articular Cartilage in Confined Compression. *J. Biomech.* **2001**, *34* (1), 1–12.
- (68) Athanasiou, K. A.; Agarwal, A.; Dzida, F. J. Comparative Study of the Intrinsic Mechanical Properties of the Human Acetabular and Femoral Head Cartilage. *J. Orthop. Res.* **1994**, *12* (3), 340–349.
- (69) Jurvelin, J. S.; Buschmann, M. D.; Hunziker, E. B. Optical and Mechanical Determination of Poisson's Ratio of Adult Bovine Humeral Articular Cartilage. *J. Biomech.* **1997**.
- (70) Visser, J.; Melchels, F. P. W.; Jeon, J. E.; van Bussel, E. M.; Kimpton, L. S.; Byrne, H. M.; Dhert, W. J. A.; Dalton, P. D.; Hutmacher, D. W.; Malda, J. Reinforcement of Hydrogels Using Three-Dimensionally Printed Microfibres. *Nat. Commun.* **2015**, *6*, 6933.
- (71) Boere, K. W. M.; Blokzijl, M. M.; Visser, J.; Linssen, J. E. A.; Malda, J.; Hennink, W. E.; Vermonden, T. Biofabrication of Reinforced 3D-Scaffolds Using Two-Component Hydrogels. *J. Mater. Chem. B* **2015**, *3* (46), 9067–9078.







## Chapter 7

**PolyHPMA-lac-PEG triblock copolymer/  
HAMA hydrogels for cartilage regeneration:  
*in vivo* studies in mice, mini-pigs and horses**



## Abstract

Hydrogels based on triblock copolymers of polyethylene glycol and methacrylated poly(*N*-(2-hydroxypropyl) methacrylamide-mono/dilactate) (PEG-pHPMAlac) blended with methacrylated hyaluronic acid (HAMA) support cartilage-like tissue formation by embedded chondrocytes *in vitro*. Herein, we report the comprehensive evaluation of biocompatibility and a preliminary investigation on the capacity to support chondrogenesis *in vivo* of these hydrogels in four animal models, *i.e.* two different ectopic murine models, an ectopic equine model and an orthotopic porcine model, as work-up for the final *in vivo* testing in a highly challenging equine orthotopic model. Three different construct designs were used for the fabrication of hydrogels based on PEG-pHPMAlac and HAMA: cast hydrogels, hydrogels reinforced with a PolyActive™ (PA)-based framework and porous 3D printed hydrogels. Cell-free cast, PA-reinforced and printed hydrogels were implanted subcutaneously in immunocompetent mice and horses to evaluate biocompatibility, cell invasion and stability *in vivo*. Hydrogels laden with human mesenchymal stem cells (MSCs) or chondrocytes were implanted ectopically in immune-deficient mice for 42 days to assess cartilage-like matrix formation. Orthotopic implantation for 28 days in mini-pigs was performed to investigate biocompatibility and hydrogel stability in the orthotopic location of a large animal. Results showed no signs of systemic or local adverse reactions after implantation of the different hydrogels in immunocompetent and immune-deficient mice. The stability of cast hydrogels and porous printed hydrogels after four weeks of ectopic implantation in mice was found sufficient. In contrast, PA-reinforced hydrogels were highly invaded by cells and degraded due to a low crosslink density of the hydrogel matrix. Cell-laden cast hydrogels kept their structural integrity and supported partial cartilage-like tissue formation by MSCs and chondrocytes during a culture period of 42 days. Unlike in the ectopic murine implantation, low hydrogel stability combined with high cell infiltration was found for printed hydrogels implanted in horses subcutaneously. On the other hand, cast hydrogels were macroscopically undamaged and poorly invaded by cells. PA-reinforced hydrogels were widely invaded by cells. Printed constructs showed poor stability also in orthotopic location in mini-pigs. In general, the implanted hydrogels did not induce a significant immunoreaction in any of the tested animal models and therefore, they can be considered safe in all tested species. However, improvement of mechanical stability of PA-reinforced and printed constructs, which is currently under investigation, will have to be achieved before long term *in vivo* studies can be initiated. Taken altogether, this study shows that extensive testing in a variety of species is necessary before long-term *in vivo* studies in a challenging large animal model can be undertaken.

## 7.1 Introduction

Degeneration of articular cartilage is currently a major cause for chronic pain and loss of mobility worldwide, especially when it involves a knee or hip joint. Because articular cartilage is not vascularized, not innervated and hosts only a limited number of cells, its spontaneous capacity for repair is virtually nil<sup>1</sup>. Current applied strategies in clinics consist of subchondral drilling or micro-fracturing and abrasion<sup>2</sup>, resulting in bone marrow stimulation and influx of bone marrow-derived cells into the defect. These procedures are relatively cost-effective and provide temporary relief to patients. Nevertheless, they are associated with the formation of a biomechanically inadequate repaired tissue, *i.e.* fibrocartilage, and they can cause changes of the subchondral bone plate with *e.g.* formation of cysts, edema or bony overgrowth<sup>3,4</sup>. At the longer term, development of osteoarthritis (OA) is often the inevitable outcome<sup>5</sup>. Alternatively, osteochondral transplantations have found application in the clinics and seem more promising since hyaline cartilage can be reestablished in the defect area<sup>6</sup>. Nevertheless, morbidity of the donor site in case of autografting, and immunogenicity in case of allografting are notable issues<sup>6</sup>. Also autologous chondrocyte implantation (ACI) is routinely applied in some countries<sup>7,8</sup>. As ACI has the advantage of employing chondrocytes, it has greater potential for hyaline cartilage formation, compared with techniques that rely on bone marrow stimulation<sup>7</sup>. The drawbacks associated with ACI are usually the long recovery time, hypertrophy of chondral flap and lack of a complete filling of the defect area<sup>8</sup>. Limitations of these applied strategies have led to a major interest into cell/scaffold-based approaches, that make use of cells seeded on polymeric membranes (*e.g.* matrix-induced autologous chondrocyte implantation, MACI<sup>9</sup>), in hydrogel-based matrices or on macroporous scaffolds, possibly combined with signaling molecules<sup>7</sup>. In fact, several cell/scaffold-based products are currently under clinical evaluation<sup>7</sup>. Nevertheless, despite often very promising results in *in vitro* investigations and small animal trials, a high failure percentage of clinical trials and a general incapacity of these products of being translated to clinics have been reported<sup>7</sup>. This observation advocates the continued research into new promising biomaterials, as well as more comprehensive screening of those new techniques and materials before they are subjected to final *in vivo* (pre-)clinical applications, in order to overcome the currently faced challenges.

Hydrogels based on triblock copolymers of polyethylene glycol (PEG) and methacrylated poly(*N*-(2-hydroxypropyl) methacrylamide-mono/dilactate) (pHPMAIac) combined with methacrylated hyaluronic acid (HAMA) are an example of hydrogel systems that have shown potential in supporting cartilage-like tissue formation by embedded chondrocytes *in vitro*<sup>10,11</sup>. Moreover, these hydrogels have been used for the fabrication of thermoplastic-reinforced constructs with pre-designed architecture, having mechanical properties comparable to those of native cartilage<sup>11</sup>. This has been successfully achieved using nozzle-based 3D bioprinting and it is of great interest especially for a patient-personalized production of implants

in a future clinical setting. Before that, PEG-pHPMALac/HAMA hydrogels need extensive *in vivo* evaluation to assess their biocompatibility and capacity to support chondrogenesis *in vivo*.

An ideal *in vivo* model for testing biocompatibility and biofunctionality of engineered cartilage constructs, able to fully represent human clinical cases does not exist. Instead, there are several employed animal models, each having their own advantages and disadvantages. According to a recent review of Vilela *et al.*, the most commonly used *in vivo* model for articular cartilage regeneration is the lapine model, due to the fact that, despite their medium-small size, rabbits have a sufficiently large surface in the knee joint (condyles and trochlear groove) where tissue defects can be created<sup>12</sup>. Moreover, housing and care of rabbits are relatively easy and cost-effective. However, cartilage in rabbits has significant spontaneous regenerative capacity and less mechanical challenge than that of humans<sup>13</sup>. Alternative animal models are murine<sup>14</sup>, caprine<sup>15</sup>, ovine<sup>16,17</sup>, porcine<sup>18,19</sup> and equine<sup>20,21</sup> models. In general, small animal models are useful especially for assessing biocompatibility of implants. Particularly, the availability of immune-deficient mice enables testing of human cells incorporated in novel materials. On the other hand, the poor anatomic and biomechanical similarities to the human joint render small animal models insufficient for orthotopic evaluation of scaffolds and hence unsuitable for direct clinical translation<sup>22</sup>.

In this study, we employed two ectopic murine models and one ectopic equine model, to assess biocompatibility, hydrogel stability *in vivo*, and preliminary biofunctionality. Subsequently, we used an orthotopic porcine model as a work-up to the final orthotopic testing in the most challenging large animal model, which is the horse. No small animal models were used for orthotopic evaluation of hydrogel constructs as they were deemed unsuitable for this purpose for three main reasons. Firstly, small animals have a thinner cartilage layer and less strict requirements for load-bearing capacity than humans<sup>12,22,23</sup>. Secondly, their cartilage has a more pronounced spontaneous healing ability than that of human articular cartilage<sup>12,22</sup>. Thirdly, the limited surface area of small animal joints, renders the creation of defects and the implantation of scaffolds difficult. Instead, skeletally mature mini-pigs were chosen for the first orthotopic screening, because of their knee joint size, cartilage thickness, and a naturally poor capacity of their cartilage to regenerate similar to humans<sup>22,24–27</sup>. This large animal study was performed in preparation to a long-term *in vivo* orthotopic model in the horse, which was the designated final large animal model before translation to humans. In fact, the equine model is known to be the most challenging animal model and the horse is one of the few species in which OA is a well-recognized and highly prevalent clinical problem<sup>28</sup>.

In this study, three different hydrogel construct designs were employed: cast hydrogels, hydrogels reinforced with a PolyActive™ (PA)-based framework<sup>29</sup> and porous 3D printed hydrogels. The PA-based reinforcement was chosen as a clinically approved supporting scaffold, that we infused with hydrogel to obtain a two-component construct, where high mechanical stiffness (in the range of a few MPa) is warranted due to the presence of the PA mesh<sup>7</sup>. Additionally, porous hydrogels

fabricated via 3D bioprinting were also evaluated. Three-dimensional printing allows full control over shape, size and internal architecture of hydrogel constructs by an accurate layer-by-layer deposition of dispensed material<sup>30</sup>, and in this study it was employed to create hydrogel constructs with internal macro-porosity. In summary, this study focused on the assessment of biocompatibility and biofunctionality of PEG-pHPMAlac/HAMA hydrogels, as well as on the evaluation of the feasibility of their surgical implantation in large animals. These studies have been designed as a comprehensive preparation for testing the biofunctionality of the mentioned hydrogels in large animal models, which is a crucial step for the translation of new materials to human medicine.

## 7.2 Materials and Methods

### 7.2.1 Materials

All solvents and chemicals were purchased from Biosolve (Valkenswaard, the Netherlands) and Sigma-Aldrich (Zwijndrecht, the Netherlands), respectively, unless reported otherwise. Solvents and chemicals were used as received. Phosphate buffered saline pH 7.4 (PBS) was ordered from Braun (Melsungen, Germany), L-lactide from Corbion Purac (Gorinchem, The Netherlands), and hyaluronic acid (HA, 120 kDa) from Lifecore Biomedical (Chaska, MN, USA). Irgacure 2959 was kindly offered by BASF (Ludwigshafen, Germany) and HPMA was synthesized and characterized as reported in supporting information (S1). A QCL-1000 120 Test Kit for the quantitative determination of endotoxin was obtained from Lonza (Walkersville, MD, USA) and PEG (10 kDa) from Merck (Darmstadt, Germany). HPMA-monolactate, HPMA-dilactate and PEG<sub>10kDa</sub>-4,4'-azobis(cyanopentanoate) macroinitiator were synthesized and characterized as previously reported<sup>31-33</sup>. PolyActive™ (polyethylene oxide terephthalate/polybutylene terephthalate, PEOT/PBT multi-block copolymers)-based implants were donated by CellCoTec (Bilthoven, The Netherlands) and are further abbreviated as PA. Isoflurane and mepivacaine were supplied by B. Braun (Melsungen, Germany), ketoprofen by Merial (Lyon, France) and enrofloxacin by Thermo Fisher Scientific (Waltham, MA, USA). Domosedan® (Detomidine) was obtained from Vêtoquinol (Den Bosch, The Netherlands), Euthasol® (Pentobarbital) from AST farma B.V. (Oudewater, The Netherlands), fibrin glue (Tisseel®) from Baxter (Unterschleißheim, Germany), Chondro-Gide® (collagen I/III membrane) from Geistlich (Baden-Baden, Germany) and Narcoren® (Pentobarbital) from Merial (Hallbergmoos, Germany). Ketamin® (ketamine) was ordered from KLAT-Chemie GmbH (Ahlhorn, Germany), Sedin® (medetomidine hydrochloride) from Alvetra GmbH (Neumünster, Germany), Alazane® (atipamezole) from Zoetis Deutschland GmbH (Berlin, Germany) and Buprenovet® (buprenorphine) from Bayer Vital GmbH (Leverkusen, Germany).

### 7.2.2 Synthesis and characterization of polymers

A triblock copolymer composed of a PEG (10 kDa) mid-block flanked by two pHPMA-lac side blocks (mono-/dilactate molar ratio = 75:25) was synthesized by free radical polymerization as previously reported<sup>34,35</sup>. Briefly, HPMA-monolactate (14.4 g, 67.0 mmol), HPMA-dilactate (6.4 g, 22.3 mmol) and PEG<sub>10kDa</sub>-4,4'-azobis(cyanopentanoate) macroinitiator (5.1 g) were dissolved in dry acetonitrile (80 ml) and flushed with N<sub>2</sub> flow for 20 minutes. The reaction was carried out for 40 hours at 70 °C. Next, the polymer was purified by precipitation in cold diethylether, and is hereafter referred to as M<sub>0</sub>P<sub>10</sub> (where M<sub>0</sub> indicates no presence of methacrylic functionalities and P<sub>10</sub> refers to the molecular weight of the PEG mid-block). Subsequently, M<sub>0</sub>P<sub>10</sub> (19.9 g, containing 64.8 mmol of -OH groups from the side lactate units) was dissolved in dry tetrahydrofuran (THF, 200 ml) under N<sub>2</sub> atmosphere. Dimethylaminopyridine (DMAP, 37.7 mg) and triethylamine (TEA, 1.091 ml) were added. Finally, a 1:1 molar ratio mixture of TEA (1.091 ml) and methacrylic anhydride (1.165 ml) was added. The reaction mixture was stirred for 24 hours at room temperature. Subsequently, THF was evaporated under reduced pressure and the polymer was dissolved in water and purified by dialysis (MWCO = 10-14 kDa) for 3 days at 4 °C. The obtained methacrylated triblock copolymer is hereafter abbreviated as M<sub>10</sub>P<sub>10</sub>. The synthesized polymers (M<sub>0</sub>P<sub>10</sub> and M<sub>10</sub>P<sub>10</sub>) were characterized as previously reported<sup>34,35</sup>. HA was methacrylated and characterized as previously reported<sup>10,36</sup>. Endotoxin levels in M<sub>0</sub>P<sub>10</sub>, M<sub>10</sub>P<sub>10</sub>, HA and HAMA were determined by Endpoint Chromogenic Limulus amoebocyte lysate (LAL) Assay, according to the manufacturer's protocol. For the endotoxin determination, solutions of polymers in endotoxin-free water (0.5 mg/ml) were prepared for testing, and solutions containing known amounts of endotoxin in water (0.1-1 EU/ml) were used as standards.

### 7.2.3 Preparation of hydrogels

Cast hydrogels composed of M<sub>10</sub>P<sub>10</sub> and HAMA were prepared as previously described<sup>10,37</sup>. Briefly, mixtures containing M<sub>10</sub>P<sub>10</sub>, HAMA and Irgacure (0.05% w/w) in PBS were stirred overnight at 4 °C. Subsequently, hydrogel mixtures were injected into teflon molds (diameter = 6 mm, height = 2 mm), incubated at 37 °C for 5 minutes and UV-irradiated for an additional 5 minutes (UV-Handleuchte lamp A. Hartenstein, Germany, wavelength: 365 nm, intensity at 3 cm: 1.2 mW/cm<sup>2</sup>). For the preparation of M<sub>10</sub>P<sub>10</sub>/HAMA hydrogels reinforced with PA-based scaffolds, PA scaffolds (diameter = 6 mm, height = 2 mm, fiber thickness = 170 ± 15 μm, fiber distance = 370 ± 26 μm, layer height = 140 ± 14 μm) after overnight swelling in PBS at room temperature were placed into teflon molds, infused with the hydrogel mixture and cross-linked as described above. Printed hydrogel constructs were generated using a 3DDiscovery bioprinter (regenHU, Villaz-St-Pierre, Switzerland) equipped with a Bluepoint 4 UV lamp (point light source, wavelength range: 300-600 nm, UV-A intensity at 5 cm = 103 mW/cm<sup>2</sup>, Hönlle UV Technology AG, Gräfelfing, Germany). Grid-like hydrogel sheets (typical dimensions = 15 x 20 x 2 mm, l x w x h) were printed using previously reported settings<sup>10</sup>. Six cylindrical

hydrogels were obtained from each printed hydrogel sheet by using a surgical biopsy punch (diameter = 6 mm). For cellularized cast hydrogels, polymer mixtures in PBS were mixed with bone marrow-derived mesenchymal stem cells (MSCs) or chondrocytes (Chs, Table 1, final concentration =  $15\text{-}20 \times 10^6$  cells/ml) before the molding procedure. MSCs were isolated from human bone marrow, which was harvested from the pelvic bone of OA patients. Human Chs were isolated from femoral condyles of OA patients during their total knee replacement operation, after approval by the Institutional Review Board (CEI 095/2012) and informed consent of patients of the Clínica Universidad de Navarra. Cell isolation, seeding and expansion were conducted as previously described<sup>10,38</sup>. Fibrin-based hydrogels prepared as previously described were used as controls<sup>10</sup>. In general, the concentrations of  $M_{10}P_{10}$  and HAMA used in the initial experiments were 14 and 4% (w/w), respectively. In some other experiments, optimized concentrations of 22 and 1% (w/w) of  $M_{10}P_{10}$  and HAMA, respectively, were used. Hydrogels composed of  $M_{10}P_{10}$  and HAMA are further abbreviated as MH (where M refers to the presence of  $M_{10}P_{10}$  and H to the presence of HAMA). Numbers following MH, if present indicate the concentration of  $M_{10}P_{10}$  and HAMA, respectively. Therefore, for instance MH 14+4 indicates that the hydrogel is composed of 14% of  $M_{10}P_{10}$  and 4% of HAMA.

#### 7.2.4 Experimental design

The biocompatibility and stability of cell-free cast, PA-reinforced or printed hydrogel scaffolds were assessed in a subcutaneous murine model. Subsequently, a preliminary functionality assessment of cell-laden cast hydrogels was performed in a second immune-deficient murine model. Additionally, cell-free cast, PA-reinforced or printed hydrogel scaffolds were studied in a subcutaneous equine model. Finally, cell-free hydrogel constructs were implanted orthotopically in a porcine model. Table 1 summarizes aim and conditions for each animal study.

#### 7.2.5 Ectopic murine models

Immunocompetent B6D2F1/Crl mice (BDF-1, Charles River, Sulzfeld, Germany, 12 animals, murine studies 1 and 2, Table 1) were anesthetized using intraperitoneal injection of ketamine (120 mg/kg) and medetomidine hydrochloride (0.5 mg/kg). Each mouse received four implants (hydrogel composition = MH 14+4 or MH 22+1 or MH 25+1) through 4 different subcutaneous incisions of approximately 8 mm each, localized on the dorso-paravertebral sides of the mouse. After surgery, a subcutaneous injection of atipamezol (2.5 mg/kg) partly antagonized the intraperitoneal anesthesia. Subsequently, pain treatment using buprenorphine (0.01-0.05 mg/kg) was provided subcutaneously for two days. After the evaluation time (Table 1), mice were sacrificed by cervical dislocation and the scaffolds were harvested, photographed for visual inspection and further fixed in 4% paraformaldehyde for analysis.



**Table 1.** Experimental conditions for hydrogel implantation in *in vivo* small and large animal models.

Animal model	Site	Scaffold	Cell	Immunology	Duration (days)	Aim
murine	1. s.c. <sup>a</sup>	1. cast/PA+h <sup>b</sup> (MH14+4)	1. cell free	1. competent	1. 14 days	1. bioC <sup>c</sup> /cell invasion
	2. s.c.	2. cast/ printed <sup>d</sup> (MH22+1)	2. cell free	2. competent	2. 28 days <sup>e</sup>	2. stability
murine	3. s.c.	3.cast (MH14+4)	3. cell free/Chs/ MSCs	3. deficient	3. 42 days	3.bioF <sup>f</sup>
equine	1. s.c.	1. cast/PA+h/ printed (MH22+1)	1. cell free	1. competent	1. 14 days	1. bioC/ stability/cell invasion
porcine	1. o.t. <sup>g</sup>	1. printed (MH22+1)	1. cell free	1. competent	1. 28 days	1. bioC/ stability/cell invasion

<sup>a</sup> s.c. = subcutaneous

<sup>b</sup> PA+h = hydrogel reinforced with PolyActive™-based scaffold

<sup>c</sup> bioC = biocompatibility

<sup>d</sup> besides MH 22+1, hydrogels with slightly higher M<sub>10</sub>P<sub>10</sub> content (*i.e.* MH 25+1) were used for comparison

<sup>e</sup> harvest of hydrogels was performed also at intermediate time points of 7 and 14 days

<sup>f</sup> bioF = biofunctionality

<sup>g</sup> o.t. = orthotopic

In a second ectopic murine model, immunodeficient Rag2 mice (Balb/cA Rag2-/- $\gamma$ C-/-, 22 animals, care center: Centro de Investigación Médica Aplicada, CIMA, Pamplona, Spain, murine study 3, Table 1) were anesthetized using an inhalation device delivering isoflurane (1.5-2% in oxygen) at 1 L/min. This rate was maintained during the entire course of the surgical procedure. Before surgery, animals received 5 mg/kg of ketoprofen to prevent inflammation. Subcutaneous implantation of scaffolds was performed as described before for BDF-1 mice. After surgery, oral antibiotic treatment (10 mg/kg of enrofloxacin) was provided through the drinking water and maintained for 7 days. Possible local adverse reactions were evaluated based on the presence of inflammation signs at the implantation site and monitoring the post-surgical wound healing process; whereas weight loss, apathy and unusual behavior (such as immobilization and starvation) were considered signs of an undesired systemic reaction. After the evaluation time, mice were sacrificed by CO<sub>2</sub> inhalation. Cell viability, histology and immunohistochemistry were performed as previously



described<sup>10,39</sup>. The BDF-1 mice study was conducted according to the German animal welfare under the agreement of the local authorities (RP Karlsruhe, G-249/15). Rag2 mice experiments were performed in accordance with the regulations of the University of Navarra's Ethics Committee for Animal Experimentation.

### 7.2.6 Ectopic equine model

Two adult equines (one female horse and one male Shetland pony) were sedated with detomidine (10 µg/kg). Local anesthesia of the cervical area was achieved by injection of 1-2 ml of mepivacaine solution (20 mg/ml) per aimed incision location on the dorsal regions of the horse neck and on the sternum area. A series of subcutaneous pockets were created on the anesthetized locations through small incisions (length = 10 mm) on the skin. Subsequently, each cast, PA-reinforced or printed hydrogel (hydrogel composition = MH 22+1) was placed into one of the subcutaneous pockets and the wounds were sutured. Animals were monitored daily for signs of systemic or local reaction. After 14 days, the two horses were euthanized by administration of Euthasol® (50 mg/kg of body weight) and the entire soft tissue area containing the constructs was harvested for analysis. These animal studies have been approved by the local Ethics Committee for animal experimentation and were performed in accordance with the Institutional Guidelines on the use of laboratory animals.

### 7.2.7 Orthotopic porcine model

One skeletally mature Goettingen minipig (Ellegaard, Denmark, 24 months, 35 kg) was anesthetized, and a full-thickness cartilage defect (diameter = 6 mm) was created in the trochlear groove of each femur using a surgical biopsy punch, without involving subchondral bone. Cartilage tissue was carefully removed and fibrin glue (12.5 µl) was applied into the defect area. Subsequently, a printed hydrogel construct (hydrogel composition = MH 22+1) was placed in each defect on top of the fibrin glue layer. One construct was additionally secured with a Chondro-Gide® membrane disk that was fixed by suturing it to the adjacent cartilage, to distinguish between failure of fixation and loss by hydrogel degradation. After surgery, the animal was treated with pain-killers and antibiotics and left free to move. After 28 days, the minipig was anesthetized and euthanized by administration of Narcoren®. Posterior limbs were harvested by hip joint disarticulation and the joint capsules were isolated and opened for analysis. The study was conducted according to the German animal welfare under the agreement of the local authorities (RP Karlsruhe, G-203/14).

## 7.3 Results and Discussion

### 7.3.1 Characteristics of polymers

Characteristics of  $M_{10}P_{10}$  and HAMA were in line with previously reported data<sup>10,11,40</sup>. Briefly,  $M_{10}P_{10}$  had a degree of methacrylation (DM) of 10.6 % (defined as the percentage of pendent -OH groups being methacrylated) and a number average molecular weight ( $M_n$ ) of 40.1 kDa and 35.6 kDa, measured by Proton Nuclear Magnetic Resonance (<sup>1</sup>H-NMR) and Gel Permeation Chromatography (GPC),

respectively. The DM of HAMA, defined as the number of methacrylate groups on 100 disaccharide units ranged between 10 and 20%. In general, the endotoxin level was significantly lower in  $M_0P_{10}$  and  $M_{10}P_{10}$ , compared to HA and HAMA (Table 2). Furthermore, the endotoxin content of HA slightly increased after methacrylation, whereas no increase in the endotoxin level was observed after the methacrylation of the thermosensitive polymer. These differences might be explained by the fact that  $M_0P_{10}$  and  $M_{10}P_{10}$  were obtained by an entirely synthetic route that involved several steps in organic solvents, where bacteria are unlikely to grow. On the other hand, water was used during the synthesis of HAMA, and this might increase the chance of bacterial contamination. Taking into account the endotoxin values reported in Table 2 and the used solid content of the hydrogels, we estimated a typical endotoxin level of 1.65 EU/implant. To the best of our knowledge, the available literature on endotoxin limits for scaffolds intended for animal implantation is rather poor. According to the United States Pharmacopeia, the endotoxin limit for human use of medical devices that directly or indirectly are in contact with the cardiovascular and lymphatic system is 20 EU/device<sup>41</sup>. Therefore, the measured endotoxin content was considered acceptable for small and large animal studies.

**Table 2.** Endotoxin level in  $M_0P_{10}$ ,  $M_{10}P_{10}$ , HA and HAMA.

Polymer	Endotoxin level (EU/mg)
$M_0P_{10}$	$0.088 \pm 0.037^a$
$M_{10}P_{10}$	$0.069 \pm 0.037^a$
HA	0.460
HAMA	$0.602 \pm 0.123^a$

<sup>a</sup> determined as the average endotoxin level of at least two different polymer batches

### 7.3.2 Ectopic murine models

In the first ectopic murine model (study 1, Table 1), cell-free cast hydrogels and PA-reinforced hydrogels were implanted for 2 weeks in immunocompetent animals to study their biocompatibility and possible host cell infiltration. Neither systemic nor local adverse reactions were observed in these mice for both scaffold types. Cast hydrogel explants were macroscopically intact and poor host cell infiltration was found in these hydrogels (Figure 1a). On the other hand, PA-reinforced hydrogels underwent major resorption (Figure 1b) and were significantly invaded by host cells (Figure 1c). To obtain additional insight in the more pronounced loss of hydrogel matrix and higher cell invasion observed for PA-reinforced scaffolds, methacrylate conversion (MC, defined as the percentage of methacrylate groups that were effectively converted after UV exposure) was calculated for both cast and PA-reinforced scaffolds (Supporting Information S2). The MC for PA-reinforced hydrogels was significantly lower than that of cast hydrogels (*i.e.*  $18.2 \pm 9.5$  vs  $65.5 \pm 10.4$ , for cell-free implants and  $10.8 \pm 12.2$  vs  $72.3 \pm 4.5$  for Chs-laden implants, Figure S2a). This lower MC results in a less tight network, which can explain the faster degradation/disintegration and more intense cell invasion observed for the

PA-reinforced hydrogels. A possible reason for the poor MC of these scaffolds can be the presence of the PA framework itself that hampers light penetration during UV-crosslinking and/or the presence of vitamin E, which is added as an antioxidant during the PA scaffold fabrication. In fact, vitamin E may act as a radical scavenger<sup>42</sup>, limiting radical propagation during UV-polymerization and therefore it can reduce the MC and the network density of the hydrogel matrix. These findings are in line with a previous *in vivo* investigation in an ectopic murine model, that was performed on PEG-pHPMALac hydrogels<sup>43</sup>. In that study hydrogels made of polymers with different DM, and therefore with different network density, were compared, and a higher cell infiltration was observed for PEG-pHPMALac hydrogels with a less tight network and faster degradation profile (hydrogels composed of PEG-pHPMALac with lower DM).

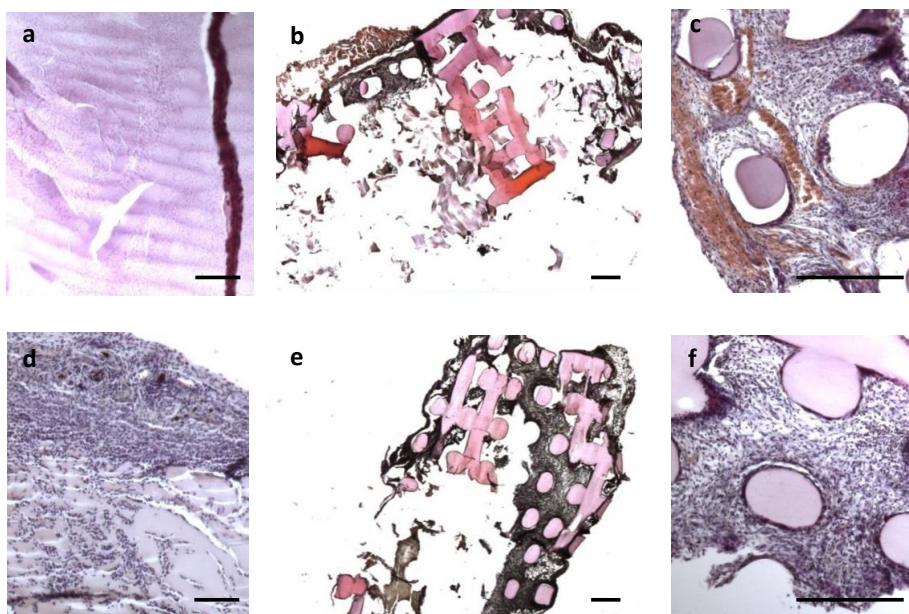


**Figure 1.** Photographs of hematoxylin/eosin (HE) stained sections of explants (cell-free hydrogels, MH 14+4) after 14 days of ectopic implantation in immunocompetent mice. Cast (a) and PA-reinforced hydrogels (b and c) composed of MH. Cast (d) and PA-reinforced hydrogels (e and f) composed of fibrin. Violet dots indicate cells. In PA-reinforced hydrogel, pink color indicates PA-scaffold, violet/grey color indicates hydrogel invaded by cells. Scale bar represents 200  $\mu\text{m}$ .

In the second murine experiment, printed hydrogel constructs prepared from precursor polymeric mixtures of two different concentrations of  $M_{10}P_{10}$ , *i.e.* 22 and 25% (w/w) and a fixed HAMA concentration of 1% were implanted ectopically in immunocompetent mice to evaluate the stability of printed scaffolds compared to cast scaffolds *in vivo* (murine study 2, Table 1). From Figure 2 it can be observed that the integrity of all hydrogel types was maintained *in vivo* after 4 weeks. Importantly,

invasion by host cells was observed within the pores of printed constructs (Figure 2), whereas the hydrogel matrix was free from migrated cells. In line with previous results of hydrogels scaffolds that did not show cell infiltration *in vivo*, the MC for printed hydrogels was high (approx. 80%) and similar to that found for cast controls (Figure S2b).

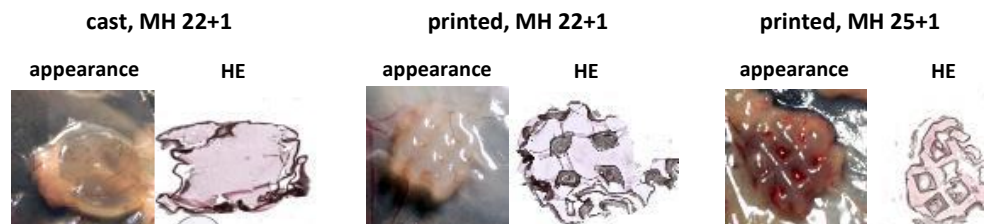


**Figure 2.** Macroscopic appearance and HE-stained hydrogel sections of cell-free, cast and printed (diameter = 6 mm) 4-week explants after ectopic implantation in immunocompetent mice.

In the third ectopic murine study, cast hydrogels laden with Chs or MSCs were implanted in immune-deficient mice to preliminarily evaluate chondrogenesis *in vivo* (murine study 3, Table 1). Hydrogels explanted after 42 days were structurally intact and kept their original size and shape (Figure 3). This indicates that no significant hydrogel degradation occurred at this implantation site in presence of embedded cells in this time frame. These *in vivo* results are in line with previously reported findings for *in vitro* culture of cell-free and equine chondrocyte-laden hydrogels<sup>10,11</sup>. On the other hand, the harvest of the fibrin control hydrogels was challenging due to the significant compaction, which is usually observed for this material after long-term culture (Figure 3)<sup>10,44–46</sup>. No sign of inflammation, calcification or vascularization was visible at the explantation site for MH hydrogels.

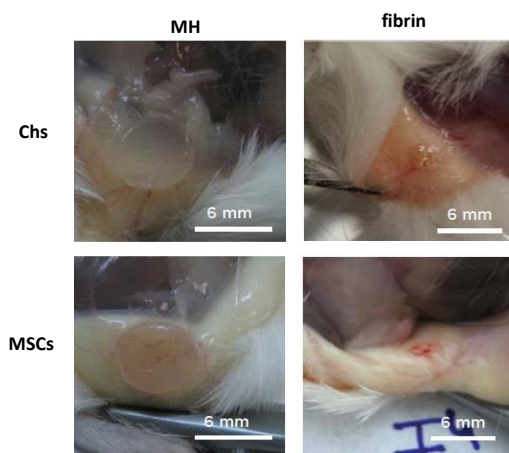


**Figure 3.** Macroscopic appearance of MH 14+4 hydrogels and fibrin explants after 42 days of evaluation in an ectopic murine model (immune-deficient mice).

Appropriate cell viability (65-92%, Figure 4) was obtained for Chs and MSCs directly after hydrogel preparation, which is in line with previously reported findings for these hydrogels<sup>10,37</sup>. Although a decrease in cell survival was observed after 42 days of ectopic culture, a sufficient overall density of viable cells was maintained for each construct. In general, cell viability was slightly higher for Chs compared to MSCs in case of MH hydrogels, while the opposite was found for fibrin gels.

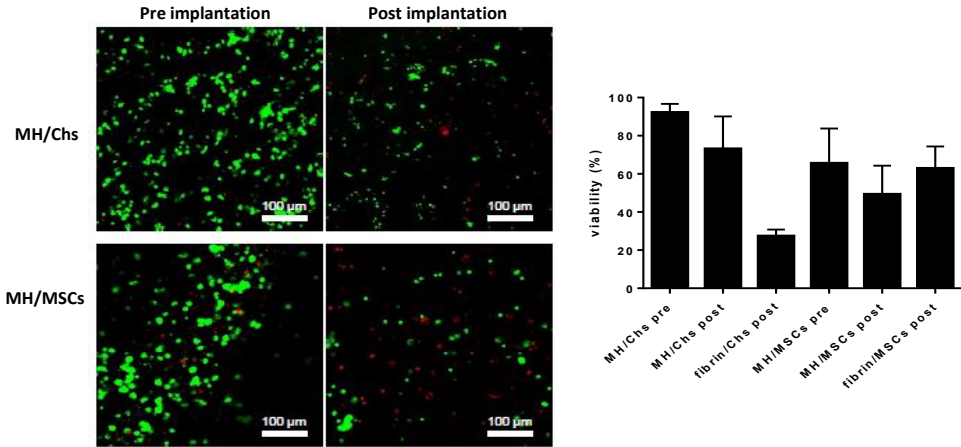


**Figure 4.** Cell viability in MH and fibrin hydrogels. Left side: photographs of Chs and MSCs before implantation and after 42 days of ectopic culture, viable cells are stained with fluorescein diacetate (green) and dead cells are stained with propidium iodide (red). Right side: Viability (%) in MH and fibrin hydrogel pre- and post-implantation.

Using the hematoxylin/eosin (HE) staining, an overall dark blue/violet color was visible for all MH hydrogels pre- and post-implantation (Figure 5).

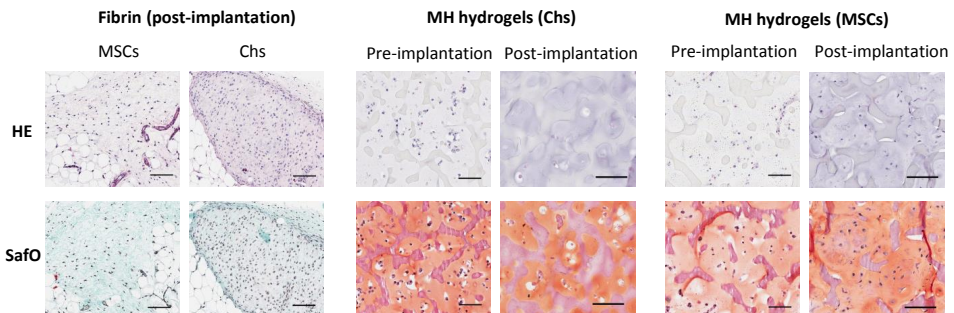


**Figure 5.** Histology of fibrin controls after implantation and for MH hydrogels before and after implantation for 42 days in immune-deficient mice. Hematoxylin/eosin (HE) staining (first row). Safranin-O (SafO) staining (second row). Scale bar represents 100 μm.



Likely due to the unspecific binding of hematoxylin to negatively charged molecules, HAMA that was originally present in the hydrogels cannot easily be distinguished from newly formed glycosaminoglycans (GAGs). Nevertheless, a slightly more intense staining observed for the explants after 42 days, suggests extracellular matrix (ECM) formation (Figure 5). Similarly, safranin-O analysis showed highly intense red staining for all MH hydrogel groups with both cell types and for each time point. Phase separation visible in these hydrogels is in line with our previous findings<sup>40</sup>. Only a few samples among MH hydrogels laden with MSCs showed a visible positive staining for collagens (data not shown). Unexpectedly, the matrix of fibrin gels hardly reacted with Safranin-O, and only positive areas for collagens (green areas) were visible.

Immunohistochemical analysis after explantation revealed the presence of undesirable collagen type I in MH hydrogels as well as in fibrin controls (Figure 6)<sup>10</sup>.

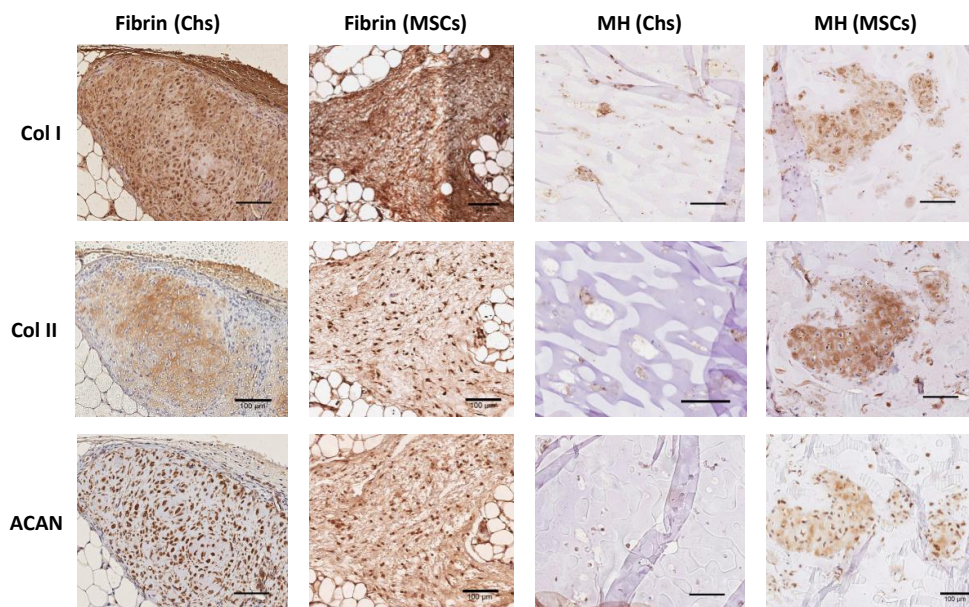


**Figure 6.** Collagen I-, II- and aggrecan-specific immunohistochemical stainings for MH hydrogels and fibrin controls after 42 days of ectopic implantation in immune-deficient mice. Scale bar represents 100  $\mu\text{m}$ .

Importantly, the articular cartilage-specific components collagen type II and aggrecan (ACAN) were visualized with a pericellular localization in case of Chs-laden hydrogels and a more pronounced and inter-territorial localization in MSCs-laden hydrogels. The overall medium-low ECM formation can be partially ascribed to the fact that the constructs were not pre-cultured *in vitro* before ectopic implantation. In fact, cartilage development in tissue engineered constructs is challenging in this ectopic location due to the absence of chondrogenic stimuli (activation of

CD44-mediated pathways, etc.), which may be boosted by *in vitro* pre-culture of cellularized constructs in chondrogenic differentiation medium<sup>47</sup>. Fibrin hydrogels showed extensive compaction during *in vivo* culture, similarly to our previous studies conducted *in vitro*<sup>10</sup>. This likely led to a major concentration of the matrix solid content, and may explain the more intense collagen-specific staining found in the fibrin controls compared with MH hydrogel samples<sup>10</sup>.

Taken altogether, no signs of systemic or local adverse reactions were observed after implantation of MH hydrogels in immunocompetent and immune-deficient mice. Hence, MH hydrogels can be considered biocompatible in these small animal models. In contrast to the poor stability of PA-reinforced hydrogels, the stability of cast hydrogels and porous printed hydrogels after four weeks of ectopic implantation in mice was found sufficient. Cast MH hydrogels laden with Chs or MSCs maintained their structural integrity after a long term *in vivo* culture, and supported partial ECM-like tissue formation by embedded cells.

### 7.3.3 Ectopic equine model

No local or systemic adverse reactions were observed in horses after two weeks of subcutaneous implantation. Cast and PA-reinforced hydrogel explants were macroscopically undamaged and only cast hydrogels were clearly confined in a capsule of fibrous-like tissue (Figure 7a and 7b). In contrast, only fragments of printed constructs were recovered (Figure 7c). Interestingly, this rapid clearance of printed constructs ectopically in horses, which was not observed in the ectopic murine model, suggests that the kinetics of fragmentation/degradation can be species-specific and underlines the importance of studying those aspects independently in multiple relevant models.

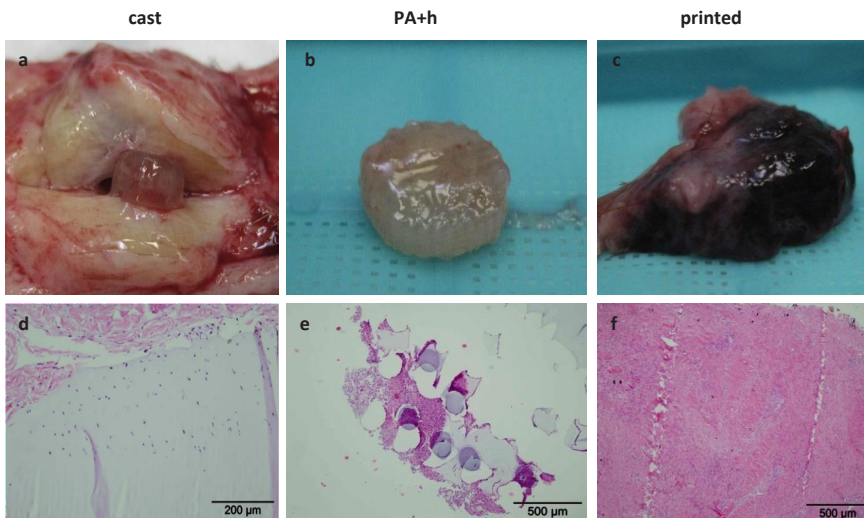


**Figure 7.** Explants (MH 22+1) after 2 weeks of subcutaneous implantation in horses. Macroscopic appearance of cast hydrogel (a), PA-reinforced hydrogel (b), and highly vascularized tissue sample containing fragments of printed hydrogel (c), and corresponding HE-stained sections (d-f).



In line with results found in the ectopic murine model, histology showed that cast hydrogels displayed minimal cell invasion (Figure 7d), with higher cell density on the edges of the constructs, whereas reinforced hydrogels were significantly infiltrated by host cells (Figure 7e). Finally, printed hydrogels underwent massive cell infiltration and extensive degradation (Figure 7f). In general, for all hydrogel types histological images showed that the cell presence was in line with the expected tissue reaction to a wound<sup>48,49</sup>, and no clear indicators of an adverse reaction (such as eosinophils or neutrophils in large amount) were detected. Fibrin controls showed host cell infiltration, with some areas of neutrophils predominance (data not shown). Overall, MH hydrogels did not induce a significant immunoreaction or chemotactic activation of cells that are normally involved in inflammatory processes.

### 7.3.4 Orthotopic porcine model

A preliminary orthotopic implantation of cell-free printed constructs fixed in the defect area with fibrin glue and covered (or not) with a Chondro-Gide<sup>®</sup> membrane disk in mini-pigs (Figure 8) was performed to evaluate biocompatibility and hydrogel stability after 4 weeks.

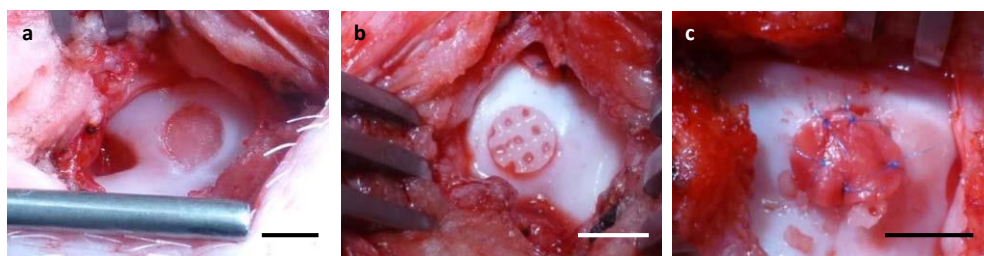


**Figure 8.** Orthotopic implantation of printed hydrogels in minipigs. Full-thickness cartilage defect with a diameter of 6 mm (a), printed construct fixed into the defect site with fibrin glue (b), printed construct fixed with fibrin glue and covered with a Chondro-Gide<sup>®</sup> membrane disk (c). Scale bar represents 6 mm.

At the moment of implantation, partial hydrogel damage was inevitable during suturing, due to the poor mechanical resistance of printed hydrogels (Figure 8c). No adverse reactions were observed locally or systemically in the treated animal after 4 weeks. Visual macroscopic evidence showed the persistence of the Chondro-Gide<sup>®</sup> membrane disk in the defect site where it was originally placed (Figure 9a) and micro-computed tomography ( $\mu$ CT) scans revealed integrity of the subchondral bone underlying in the defect areas (Figure 9a and 9b). Nevertheless, only fragments of hydrogels were retrieved, without any clear sign of host cell invasion. Considering that similar results were obtained with the defect that was covered with Chondro-Gide<sup>®</sup> membrane disk and the defect that was not covered (Figure 9c-h), the insufficient gel persistence may be not purely related to the technical challenge of fixation. More likely the presence of pores (of millimeter range) renders printed

constructs unable to bear load without fragmentation. Fragmentation, in turn may increase degradation rate of the residual hydrogel matrix. In conclusion, MH printed hydrogels showed appropriate biocompatibility in an orthotopic porcine model, but further optimization is required to overcome premature disintegration/degradation of the hydrogels.

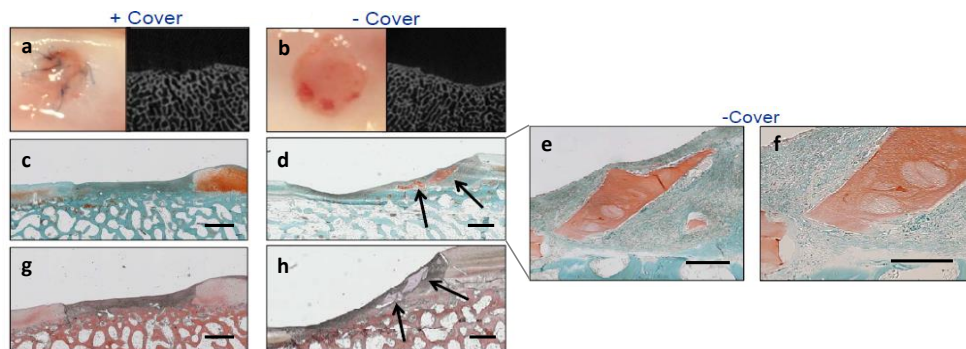


**Figure 9.** Explants after 4 weeks of orthotopic implantation in mini-pigs. Macroscopic appearance of the defect areas (defect diameter = 6 mm) and  $\mu$ CT scans (a and b), Saf-O staining (c-f) and HE-staining (g and h) for printed constructs (MH 22+1) fixed with fibrin glue and covered or not with a Chondro-Gide<sup>®</sup> membrane disk. Scale bar represents 1 mm in images c and g, 500  $\mu$ m in images d and h, 200  $\mu$ m in image e and 100  $\mu$ m in image f.

## 7.4 Conclusions

The extensive testing in a variety of animal models of  $M_{10}P_{10}$ /HAMA hydrogels, before long-term use in a challenging pre-clinical large animal model gave multifaceted and not entirely unambiguous results. Biocompatibility appeared to be sufficient based on the absence of systemic and local adverse reactions in ectopic murine and equine models and in the orthotopic porcine model. Human chondrocytes and MSCs encapsulated in these hydrogels showed some (re)differentiation towards cartilaginous lineage, supported by cartilage-like matrix production in athymic mice. Nevertheless, species-dependent outcome regarding, *e.g.* hydrogel stability stresses the general need for full testing of new materials in the target species, irrespective of earlier *in vitro* results or *in vivo* data from other species. Further, orthotopic implantation in mini-pigs, during which the materials were subjected to both the intra-articular environment and the biomechanical forces associated with locomotion, resulted in degradation profiles that were substantially different to those found in ectopic locations or *in vitro*. Therefore, materials should be tested orthotopically before long-term pre-clinical studies are embarked upon. It can be concluded that comprehensive testing of potentially interesting materials should be always seen as a must. Moreover, it is not unlikely that failure to do so may explain the very limited success of many novel regenerative therapies, which look very promising based on *in vitro* data and limited testing in small animal models, but that fail once they are tested

in highly challenging pre-clinical large animal models or in humans. With respect to the materials tested in this study, further optimization of load-bearing capacity and degradation kinetics of PA-reinforced and printed hydrogels is required to enable long-term orthotopic evaluation in large animal models, which is a crucial step to demonstrate the real regenerative capacity and biofunctionality of these hydrogels.

### **Acknowledgements**

The research leading to these results has received funding from the European Community's Seventh Framework Programme (FP7/2007-2013) under grant agreement n°309962 (HydroZONES). E. Muinos-López and F. Prosper (Clínica Universidad de Navarra), Y. Renz, E. Hesse, F. Bothe and W. Richter (Orthopaedic University Hospital Heidelberg), I. Mancini, H. Brommer, T. van Loon and P.R. van Weeren (Utrecht University), V.H.M. Mouser (University Medical Center Utrecht), M.M. Blokzijl (University Medical Center Utrecht/Utrecht University) and Clayton Wilson (CellCoTec, Bilthoven, The Netherlands) are thanked for their contribution to this chapter.

## Supporting Information

### S1 Synthesis and characterization of HPMA

#### S1.1 Materials and Methods

All chemicals and solvents were supplied by Sigma-Aldrich or Biosolve, except for DL-1-amino-2-propanol (94%), which was purchased from ACROS Organics. DL-1-amino-2-propanol (80 ml), reverse osmosis water (ROW, 400 ml) and NaOH solution (1M, 20 ml) were stirred under vigorous agitation with 400 ml of dichloromethane (DCM). A teaspoon of hydroquinone monomethylether was added to prevent premature polymerization. The reaction mixture was cooled down using a water/ice bath. 110 ml of methacryloyl chloride, previously diluted in DCM, was added drop-wise in a time span of 1.5 h, while the pH was kept between 9.5 and 10 by adding NaOH (5M). The reaction was left overnight at room temperature. Subsequently, the water phase was saturated with NaCl and HPMA was salted out using repeated extractions with DCM (4x). A first fraction of HPMA, referred to as HPMA-1, was obtained as a white powder after evaporation of DCM. Additional HPMA was extracted with water from the DCM phase belonging to the reaction mixture. Afterwards, HPMA was salted out from the aqueous phase to a new DCM phase. The product recovered in this way is referred to as HPMA-2. Both products were analyzed by <sup>1</sup>H-NMR (CDCl<sub>3</sub>) using a Gemini-300 MHz spectrometer. The purity of HPMA-1 and HPMA-2 was tested using a HPLC Waters 2695 separating module coupled with a UV detector (λ=210 nm). A C18 column (Sunfire) under gradient conditions (from 90/10 to 0/100 water:acetonitrile in 20 min, flow 1ml/min) was used. Additionally, the melting point of both products was measured using a Discovery Differential Scanning Calorimetry (DSC) from TA Instruments (Etten-Leur, The Netherlands). The samples underwent a fast heating-slow cooling-fast heating ramp (10 °C/min to 150 °C, followed by 2 °C/min cooling step to 0 °C and 10 °C/min heating ramp to 150 °C) and the melting point was defined as the temperature corresponding to the onset of the melting peak recorded during the second heating ramp.

#### S1.2 Results and Discussion

With the described method, highly pure HPMA could be synthesized in high scale (approximately 120 grams). The yield was 80% (60% of HPMA-1 and 20% of HPMA-2) and the aimed structure of both products was confirmed by <sup>1</sup>H-NMR: 6.8 (broad s, 1H, NH); 5.7 (s, 1H, H<sub>2</sub>C=C(CH<sub>3</sub>)); 5.3 (s, 1H, H<sub>2</sub>C=C(CH<sub>3</sub>)), 3.9 (1H, m, CH<sub>2</sub>CH(CH<sub>3</sub>)OH), 3.7 (s, 1H, OH), 3.4 (m, 1H, CH<sub>2</sub>CH), 3.1 (m, 1H, CH<sub>2</sub>CH), 1.9 (s, 3H, C=C(CH<sub>3</sub>)), 1.1 (d, 3H, CH(CH<sub>3</sub>)). HPLC chromatograms showed the presence of one main peak with a retention time of 4 min attributed to HPMA (Figure 1a). The values of purity were 99.6% and 98.9%, for HPMA-1 and HPMA-2, respectively. The DSC thermograms reported the presence of one sharp melting peak with an onset at 58.7 and 57.9 °C (peak temperature: 64.3 and 63.2 °C) for HPMA-1 and

HPMA-2, respectively (Figure 1b).

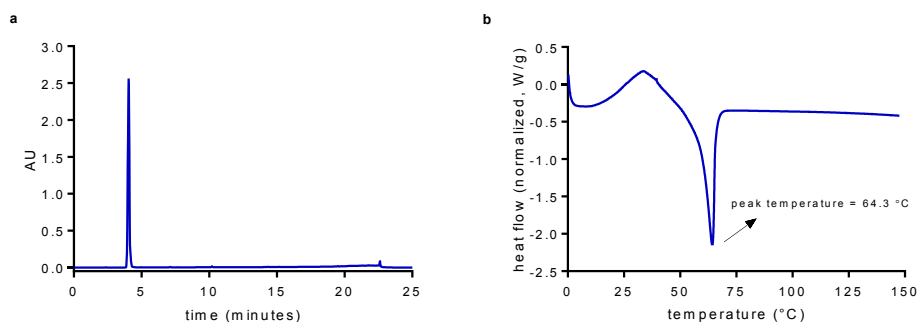


**Figure S1.** HPLC chromatogram (a) and DSC thermogram (b) of HPMA-1.

## S2 Methacrylate conversion (MC) of hydrogel scaffolds

MC was calculated as previously described by Censi *et al*<sup>50</sup>.

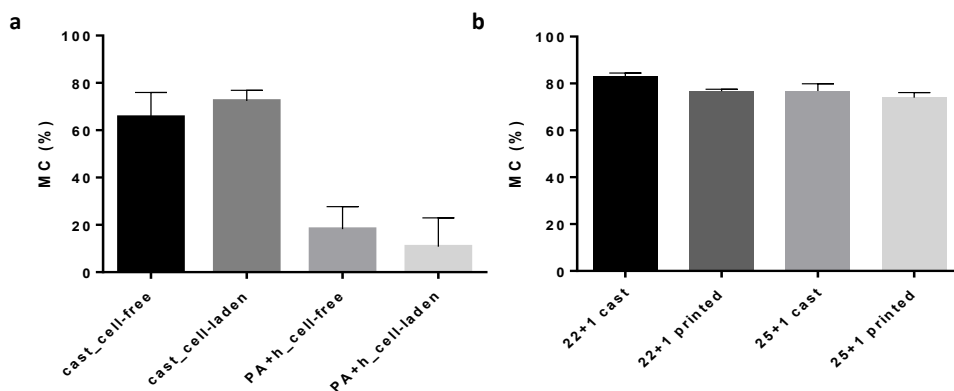


**Figure S2.** MC for cast and PA-reinforced cell-free hydrogels or laden with chondrocytes (a). MC for cell-free printed hydrogels (composed of 22 or 25% of  $M_{10}P_{10}$  and 1% of HAMA) and cast controls (b). The slight difference in MC values reported in figure a for cast hydrogels and those reported in figure b is explained by the use of two slightly different illumination conditions. Cast hydrogels in figure a were crosslinked with 5 minutes of UV irradiation using a relatively weak lamp (UV-Handleuchte lamp A. Hartenstein, Germany, wavelength: 365 nm, intensity at 3 cm: 1.2 mW/cm<sup>2</sup>). Cast hydrogels in figure b were crosslinked for 69 seconds by irradiation using a much stronger lamp (point light source, wavelength range: 300-600 nm, UV-A intensity at 5 cm = 103 mW/cm<sup>2</sup>, Hönle UV Technology AG, Gräfelfing, Germany) to resemble UV-crosslinking conditions during the 3D printing process.

## References

- (1) Heinemeier, K. M.; Schjerling, P.; Heinemeier, J.; Moller, M. B.; Krosgaard, M. R.; Grum-Schwensen, T.; Petersen, M. M.; Kjaer, M. Radiocarbon Dating Reveals Minimal Collagen Turnover in Both Healthy and Osteoarthritic Human Cartilage. *Sci. Transl. Med.* **2016**, *8* (346), 1–9.
- (2) Falah, M.; Nierenberg, G.; Soudry, M.; Hayden, M.; Volpin, G. Treatment of Articular Cartilage Lesions of the Knee. *Int. Orthop.* **2010**, *34* (5), 621–630.
- (3) Mithoefer, K.; Venugopal, V.; Manaqibwala, M. Incidence, Degree, and Clinical Effect of Subchondral Bone Overgrowth After Microfracture in the Knee. *Am. J. Sports Med.* **2016**, *44* (8), 2057–2063.
- (4) Bert, J. M. Abandoning Microfracture of the Knee: Has the Time Come? *Arthrosc. J. Arthrosc. Relat. Surg.* **2015**, *31* (3), 501–505.
- (5) Mandelbaum, B. R.; Browne, J. E.; Fu, F.; Micheli, L.; Mosely, J. B.; Erggelet, C.; Minas, T.; Peterson, L. Articular Cartilage Lesions of the Knee. *Am. J. Sports Med.* **1998**, *26* (6), 853–861.
- (6) Hunziker, E. B.; Lippuner, K.; Keel, M. J. B.; Shintani, N. An Educational Review of Cartilage Repair: Precepts & Practice – Myths & Misconceptions – Progress & Prospects. *Osteoarthr. Cartil.* **2015**, *23* (3), 334–350.
- (7) Huang, B. J.; Hu, J. C.; Athanasiou, K. A. Cell-Based Tissue Engineering Strategies Used in the Clinical Repair of Articular Cartilage. *Biomaterials* **2016**, *98*, 1–22.
- (8) Makris, E. A.; Gomoll, A. H.; Malizos, K. N.; Hu, J. C.; Athanasiou, K. A. Repair and Tissue Engineering Techniques for Articular Cartilage. *Nat. Rev. Rheumatol.* **2014**, *11* (1), 21–34.
- (9) Brittberg, M. Cell Carriers as the Next Generation of Cell Therapy for Cartilage Repair: A Review of the Matrix-Induced Autologous Chondrocyte Implantation Procedure. *Am. J. Sports Med.* **2010**, *38* (6), 1259–1271.
- (10) Abbadessa, A.; Mouser, V. H. M.; Blokzijl, M. M.; Gawlitta, D.; Dhert, W. J. A.; Hennink, W. E.; Malda, J.; Vermonden, T. A Synthetic Thermosensitive Hydrogel for Cartilage Bioprinting and Its Biofunctionalization with Polysaccharides. *Biomacromolecules* **2016**, *17* (6), 2137–2147.
- (11) Mouser, V. H. M.; Abbadessa, A.; Levato, R.; Hennink, W. E.; Dhert, W. J. A.; Gawlitta, D.; Vermonden, T.; Malda, J. Bio-Ink Development for the Fabrication of Composite Cartilage Repair Constructs. *Manuscr. Prep.*
- (12) Vilela, C. A.; Correia, C.; Oliveira, J. M.; Sousa, R. A.; Espregueira-Mendes, J.; Reis, R. L. Cartilage Repair Using Hydrogels: A Critical Review of *in Vivo* Experimental Designs. *ACS Biomater. Sci. Eng.* **2015**, *1* (9), 726–739.
- (13) Shapiro, F.; Koide, S.; Glimcher, M. J. Cell Origin and Differentiation in the Repair of Full-Thickness Defects of Articular Cartilage. *J. Bone Joint Surg. Am.* **1993**, *75* (4), 532–553.
- (14) Dausse, Y.; Grossin, L.; Miralles, G.; Pelletier, S.; Mainard, D.; Hubert, P.; Baptiste, D.; Gillet, P.; Dellacherie, E.; Netter, P.; Payan, E. Cartilage Repair Using New Polysaccharidic Biomaterials: Macroscopic, Histological and Biochemical Approaches in a Rat Model of Cartilage Defect. *Osteoarthr. Cartil.* **2003**, *11* (1), 16–28.
- (15) Brehm, W.; Aklin, B.; Yamashita, T.; Rieser, F.; Trüb, T.; Jakob, R. P.; Mainil-Varlet, P. Repair of Superficial Osteochondral Defects with an Autologous Scaffold-Free



- Cartilage Construct in a Caprine Model: Implantation Method and Short-Term Results. *Osteoarthr. Cartil.* **2006**, *14* (12), 1214–1226.
- (16) Kandel, R. A.; Grynepas, M.; Pilliar, R.; Lee, J.; Wang, J.; Waldman, S.; Zalzal, P.; Hurtig, M. Repair of Osteochondral Defects with Biphasic Cartilage-Calcium Polyphosphate Constructs in a Sheep Model. *Biomaterials* **2006**, *27* (22), 4120–4131.
- (17) Orth, P.; Meyer, H.-L.; Goebel, L.; Eldracher, M.; Ong, M. F.; Cucchiaroni, M.; Madry, H. Improved Repair of Chondral and Osteochondral Defects in the Ovine Trochlea Compared with the Medial Condyle. *J. Orthop. Res.* **2013**, *31* (11), 1772–1779.
- (18) Niemietz, T.; Zass, G.; Hagmann, S.; Diederichs, S.; Gotterbarm, T.; Richter, W. Xenogeneic Transplantation of Articular Chondrocytes into Full-Thickness Articular Cartilage Defects in Minipigs: Fate of Cells and the Role of Macrophages. *Cell Tissue Res.* **2014**, *358* (3), 749–761.
- (19) Liu, Y.; Chen, F.; Liu, W.; Cui, L.; Shang, Q.; Xia, W.; Wang, J.; Cui, Y.; Yang, G.; Liu, D.; Wu, J.; Xu, R.; Buonocore, S. D.; Cao, Y. Repairing Large Porcine Full-Thickness Defects of Articular Cartilage Using Autologous Chondrocyte-Engineered Cartilage. *Tissue Eng.* **2002**, *8* (4), 709–721.
- (20) McIlwraith, C. W.; Fortier, L. A.; Frisbie, D. D.; Nixon, A. J. Equine Models of Articular Cartilage Repair. *Cartilage* **2011**, *2* (4), 317–326.
- (21) Martins, E. A.; Michelacci, Y. M.; Baccarin, R. Y.; Cogliati, B.; Silva, L. C. Evaluation of Chitosan-GP Hydrogel Biocompatibility in Osteochondral Defects: An Experimental Approach. *BMC Vet. Res.* **2014**, *10* (1), 197.
- (22) Chu, C. R.; Szczodry, M.; Bruno, S. Animal Models for Cartilage Regeneration and Repair. *Tissue Eng. Part B Rev.* **2010**, *16* (1), 105–115.
- (23) Malda, J.; de Grauw, J. C.; Benders, K. E. M.; Kik, M. J. L.; van de Lest, C. H. A.; Creemers, L. B.; Dhert, W. J. A.; van Weeren, P. R. Of Mice, Men and Elephants: The Relation between Articular Cartilage Thickness and Body Mass. *PLoS One* **2013**, *8* (2), e57683.
- (24) Hurtig, M. B.; Buschmann, M. D.; Fortier, L. a.; Hoemann, C. D.; Hunziker, E. B.; Jurvelin, J. S.; Mainil-Varlet, P.; McIlwraith, C. W.; Sah, R. L.; Whiteside, R. a. Preclinical Studies for Cartilage Repair: Recommendations from the International Cartilage Repair Society. *Cartilage* **2011**, *2* (2), 137–152.
- (25) Gotterbarm, T.; Breusch, S. J.; Schneider, U.; Jung, M. The Minipig Model for Experimental Chondral and Osteochondral Defect Repair in Tissue Engineering: Retrospective Analysis of 180 Defects. *Lab. Anim.* **2008**, *42* (1), 71–82.
- (26) Malda, J.; Benders, K. E. M.; Klein, T. J.; de Grauw, J. C.; Kik, M. J. L.; Hutmacher, D. W.; Saris, D. B. F.; van Weeren, P. R.; Dhert, W. J. A. Comparative Study of Depth-Dependent Characteristics of Equine and Human Osteochondral Tissue from the Medial and Lateral Femoral Condyles. *Osteoarthr. Cartil.* **2012**, *20* (10), 1147–1151.
- (27) Cokelaere, S.; Malda, J.; van Weeren, R. Cartilage Defect Repair in Horses: Current Strategies and Recent Developments in Regenerative Medicine of the Equine Joint with Emphasis on the Surgical Approach. *Vet. J.* **2016**, *214*, 61–71.
- (28) Moran, C. J.; Ramesh, A.; Brama, P. A. J.; O’Byrne, J. M.; O’Brien, F. J.; Levingstone, T. J. The Benefits and Limitations of Animal Models for Translational Research in Cartilage Repair. *J. Exp. Orthop.* **2016**, *3* (1), 1–12.
- (29) Woodfield, T. B. F.; Malda, J.; de Wijn, J.; Péters, F.; Riesle, J.; van Blitterswijk,



- C. A. Design of Porous Scaffolds for Cartilage Tissue Engineering Using a Three-Dimensional Fiber-Deposition Technique. *Biomaterials* **2004**, 25 (18), 4149–4161.
- (30) Murphy, S. V.; Atala, A. 3D Bioprinting of Tissues and Organs. *Nat. Biotechnol.* **2014**, 32 (8), 773–785.
- (31) Oupický, D.; Konák, C.; Ulbrich, K. DNA Complexes with Block and Graft Copolymers of N-(2-Hydroxypropyl)methacrylamide and 2-(Trimethylammonio)ethyl Methacrylate. *J. Biomater. Sci. Polym. Ed.* **1999**, 10 (5), 573–590.
- (32) Neradovic, D.; van Nostrum, C. F.; Hennink, W. E. Thermoresponsive Polymeric Micelles with Controlled Instability Based on Hydrolytically Sensitive N-Isopropylacrylamide Copolymers. *Macromolecules* **2001**, 34 (22), 7589–7591.
- (33) Neradovic, D.; van Steenberg, M. J.; Vansteelant, L.; Meijer, Y. J.; van Nostrum, C. F.; Hennink, W. E. Degradation Mechanism and Kinetics of Thermosensitive Polyacrylamides Containing Lactic Acid Side Chains. *Macromolecules* **2003**, 36 (20), 7491–7498.
- (34) Vermonden, T.; Besseling, N. A. M.; van Steenberg, M. J.; Hennink, W. E. Rheological Studies of Thermosensitive Triblock Copolymer Hydrogels. *Langmuir* **2006**, 22 (24), 10180–10184.
- (35) Vermonden, T.; Fedorovich, N. E.; van Geemen, D.; Alblas, J.; van Nostrum, C. F.; Dhert, W. J. A.; Hennink, W. E. Photopolymerized Thermosensitive Hydrogels: Synthesis, Degradation, and Cytocompatibility. *Biomacromolecules* **2008**, 9 (3), 919–926.
- (36) Hachet, E.; Van Den Berghe, H.; Bayma, E.; Block, M. R.; Auzély-Velty, R. Design of Biomimetic Cell-Interactive Substrates Using Hyaluronic Acid Hydrogels with Tunable Mechanical Properties. *Biomacromolecules* **2012**, 13 (6), 1818–1827.
- (37) Abbadessa, A.; Blokzijl, M. M.; Mouser, V. H. M.; Marica, P.; Malda, J.; Hennink, W. E.; Vermonden, T. A Thermo-Responsive and Photo-Polymerizable Chondroitin Sulfate-Based Hydrogel for 3D Printing Applications. *Carbohydr. Polym.* **2016**, 149, 163–174.
- (38) Lamo-Espinosa, J. M.; Mora, G.; Blanco, J. F.; Granero-Moltó, F.; Nuñez-Córdoba, J. M.; Sánchez-Echenique, C.; Bondía, J. M.; Aquerreta, J. D.; Andreu, E. J.; Ormilla, E.; Villarón, E. M.; Valentí-Azcárate, A.; Sánchez-Guijo, F.; del Cañizo, M. C.; Valentí-Nin, J. R.; Prósper, F. Intra-Articular Injection of Two Different Doses of Autologous Bone Marrow Mesenchymal Stem Cells versus Hyaluronic Acid in the Treatment of Knee Osteoarthritis: Multicenter Randomized Controlled Clinical Trial (Phase I/II). *J. Transl. Med.* **2016**, 14 (1), 246.
- (39) Muinos-López, E.; Ripalda-Cemboráin, P.; López-Martínez, T.; González-Gil, A. B.; Lamo-Espinosa, J. M.; Valentí, A.; Mortlock, D. P.; Valentí, J. R.; Prósper, F.; Granero-Moltó, F. Hypoxia and Reactive Oxygen Species Homeostasis in Mesenchymal Progenitor Cells Define a Molecular Mechanism for Fracture Nonunion. *Stem Cells* **2016**, 34 (9), 2342–2353.
- (40) Abbadessa, A.; Landín, M.; Blenke, E. O.; Hennink, W. E.; Vermonden, T. Two-Component Thermosensitive Hydrogels: Phase Separation Affecting Rheological Behavior. *Submitt. Publ.*
- (41) Guidance for Industry Pyrogen and Endotoxins Testing: Questions and Answers. <http://www.fda.gov/> **2012**, 1–10.
- (42) Burton, G. W.; Ingold, K. U. Vitamin E: Application of the Principles of Physical Organic Chemistry to the Exploration of Its Structure and Function. *Acc. Chem. Res.*

- 1986, 19 (7), 194–201.
- (43) Censi, R.; van Putten, S.; Vermonden, T.; di Martino, P.; van Nostrum, C. F.; Harmsen, M. C.; Bank, R. A.; Hennink, W. E. The Tissue Response to Photopolymerized PEG-p(HPMAm-Lactate)-Based Hydrogels. *J. Biomed. Mater. Res. Part A* **2011**, 97A (3), 219–229.
- (44) Cummings, C. L.; Gawlitta, D.; Nerem, R. M.; Stegemann, J. P. Properties of Engineered Vascular Constructs Made from Collagen, Fibrin, and Collagen–fibrin Mixtures. *Biomaterials* **2004**, 25 (17), 3699–3706.
- (45) Ahmed, T. A. E.; Dare, E. V.; Hincke, M. Fibrin: A Versatile Scaffold for Tissue Engineering Applications. *Tissue Eng. Part B Rev.* **2008**, 14 (2), 199–215.
- (46) Eyrich, D.; Brandl, F.; Appel, B.; Wiese, H.; Maier, G.; Wenzel, M.; Staudenmaier, R.; Goepferich, A.; Blunk, T. Long-Term Stable Fibrin Gels for Cartilage Engineering. *Biomaterials* **2007**, 28 (1), 55–65.
- (47) Moretti, M.; Wendt, D.; Dickinson, S. C.; Sims, T. J.; Hollander, A. P.; Kelly, D. J.; Prendergast, P. J.; Heberer, M.; Martin, I. Effects of in Vitro Preculture on in Vivo Development of Human Engineered Cartilage in an Ectopic Model. *Tissue Eng.* **2005**, 11 (9–10), 1421–1428.
- (48) Koh, T. J.; DiPietro, L. A. Inflammation and Wound Healing: The Role of the Macrophage. *Expert Rev. Mol. Med.* **2011**, 13 (2008), e23.
- (49) Anderson, J. M.; Cook, G.; Costerton, B.; Hanson, S. R.; Hensten-Pettersen, A.; Jacobsen, N.; Johnson, R. J.; Mitchell, R. N.; Pasmore, M.; Schoen, F. J.; Shirliff, M.; Stoodley, P. Host Reactions to Biomaterials and Their Evaluation. In *Biomaterials science: An introduction to materials in medicine.*; Ratner, B., Hoffman, A., Schoen, F., Lemons, J., Eds.; San Diego, CA: Academic Press: San Diego, CA, 1996; pp 293–304.
- (50) Censi, R.; Vermonden, T.; Deschout, H.; Braeckmans, K.; di Martino, P.; De Smedt, S. C.; van Nostrum, C. F.; Hennink, W. E. Photopolymerized Thermosensitive poly(HPMA lactate)-PEG-Based Hydrogels: Effect of Network Design on Mechanical Properties, Degradation, and Release Behavior. *Biomacromolecules* **2010**, 11 (8), 2143–2151.



# **Chapter 8**

## **Summary and Perspectives**

## 8.1 Summary

Tissue engineering (TE) aims to regenerate damaged tissues by the combined use of biomaterials and cells, often in presence of bioactive molecules, such as growth factors. Particularly for tissues with poor regenerative capacity, such as articular cartilage, TE approaches may lead to promising treatments. Articular cartilage is a connective tissue responsible for absorbing and distributing the load acting on the joint, to the underlying bone. The limited regenerative capacity of articular cartilage is due to the absence of blood vessels in this tissue and consequent low cellular activity. Currently, an optimal treatment for cartilage defects does not exist. Therefore, TE strategies are exploited to obtain cell-laden scaffolds able to provide an initial mechanical support that over time degrades, while new tissue is formed by the embedded cells. The aim of this thesis was to develop biomechanically advanced hydrogel constructs for articular cartilage regeneration. The described work is part of a research program, which was designed and conducted within the European consortium of HydroZONES (<http://www.hydrozones.eu>). The interactive environment of HydroZONES provided the opportunity to address the objective of this thesis using an interdisciplinary approach, with a major focus on the biomaterial manufacturing and characterization, as well as *in vitro* and *in vivo* assessment.

**Chapter 1** provides a general introduction of the anatomy and the physiology of articular cartilage, as well as the current clinically relevant techniques for its repair. Considering the limitations of present treatments, TE strategies for cartilage regeneration are presented as a promising alternative. In this chapter, attention is also given to currently investigated biomaterials for TE applications (with a particular emphasis on hydrogels) and used cell types. Three-dimensional bioprinting is presented as a novel and versatile technology for the accurate design and generation of cartilage constructs. The experimental “core” of this thesis describes a step-by-step development of thermosensitive and photo-crosslinkable hydrogels based on partially methacrylated poly[*N*-(2-hydroxypropyl)methacrylamide mono-dilactate]/polyethylene glycol triblock copolymers (pHPMAlac-PEG) and chemically modified polysaccharides, *i.e.* methacrylated chondroitin sulfate (CSMA) or hyaluronic acid (HAMA), for 3D bioprinting of cartilage constructs.

As reproducibility and tailorability of hydrogel properties highly depends on the reproducibility of synthesized building blocks, in **Chapter 2** a major focus is given to the application of an efficient and reproducible method for the methacrylation of chondroitin sulfate (CS) using glycidyl methacrylate as methacrylating agent and 4-(*N,N*-dimethylamino)pyridine as catalyst in a polar and aprotic organic solvent, *i.e.* dimethylsulfoxide. The degree of methacrylation of CSMA was tuned over a broad range (4–48 %) by varying the methacrylating agent feed and the reaction time. In this chapter, it is also described that the combination of pHPMAlac-PEG with CSMA resulted in hydrogels with improved rheological characteristics with respect to thermogelation profile and yield stress behavior, compared with hydrogels only composed of pHPMAlac-PEG. The superior rheological behavior allowed the

generation of 3D printed constructs with tunable porosity by using a nozzle-based 3D printing technology. Moreover, in these hydrogels chondrogenic cells could be embedded with high viability.

The assessment of chondrogenic differentiation of embedded cells in novel biomaterials is a crucial aspect when developing tissue-engineered cartilage constructs. As discussed in **Chapter 3**, we demonstrated that pHPMAlac-PEG-based hydrogels support *in vitro* chondrogenesis of embedded chondrocytes. After 42 days of culture, equine chondrocytes embedded in pHPMAlac-PEG hydrogels synthesized significant amounts of articular cartilage-specific components, *i.e.* glycosaminoglycans (GAGs), collagens type II and VI. Moreover, the addition of CSMA or HAMA improved the degradation profile and the mechanical properties of the hydrogels. Shape-stable 3D printed porous hydrogels, based on pHPMAlac-PEG and HAMA were generated, and supported excellent viability of chondrocytes.

Hydrogels composed of pHPMAlac-PEG and HAMA are two-component systems in aqueous medium, and as such they may be susceptible for micro-phase separation, which in turn can play a role on the final hydrogel properties. Driven by this research question, in **Chapter 4**, hydrogels with varying pHPMAlac-PEG and HAMA concentrations were studied, to explore phase separation and its impact on the rheological behavior of these hydrogels. Phase separation was indeed observed and resulted in hydrophilic, HAMA-richer internal domains and a more hydrophobic and partially dehydrated external continuous phase, essentially composed of pHPMAlac-PEG. Furthermore, when using low HAMA concentrations (< 1% w/w), the relative increase of pHPMAlac-PEG concentration in the external phase, due to partial dehydration (driven by the presence of HAMA), resulted in stiffer physical hydrogels with more favorable rheological characteristics for 3D printing applications. Conversely, when the HAMA concentration was further increased, this beneficial effect was no longer observed, since the extensive phase separation disrupted the continuity of the external phase. The dependency of phase separation and rheological properties on the polymers' concentration was mathematically studied, and models were generated to design *a priori* pHPMAlac-PEG/HAMA hydrogels with desired properties.

Inclusion of signaling molecules, *e.g.* growth factors, in hydrogels is a promising strategy to modulate biological events, such as the formation of extracellular matrix by embedded cells and/or the chemotactic migration of cells from the surrounding environment. In this context, it is preferable that these proteinaceous molecules are present for prolonged times. **Chapter 5** describes an introductory study on the possibility to enrich pHPMAlac-PEG hydrogels with protein releasing microgels. A user-friendly microfluidics-based equipment was developed in our laboratory for the generation of monodisperse HAMA microgels. Subsequently, HAMA microgels loaded with the model protein lysozyme (Lys) were encapsulated in pHPMAlac-PEG hydrogels. Microgel diameter ranged from 313 to 557  $\mu\text{m}$  by varying HAMA concentration and processing conditions. Importantly, HAMA microgels showed high Lys loading, and the microcomposite hydrogels released Lys over at least 20 days. These release kinetics were significantly slower than those from



pHPMAlac-PEG/HAMA hydrogels. Future investigations will clarify the role of the microcomposite design and fabrication conditions on the slower protein release. The findings reported in this chapter open a large number of possibilities since microgels made of other GAG molecules, *e.g.* heparin or chondroitin sulfate may be used to obtain microcomposite hydrogels with a controllable charge density, which is likely to affect growth factor loading and release kinetics.

One of the major limitations regarding the use of hydrogels for cartilage regeneration is their low stiffness and often incapacity to withstand the high mechanical stresses generated in the joint during movements. Although the stiffness of pHPMAlac-PEG/HAMA hydrogels can be tuned over a broad range (as discussed in chapter 5), this range may be not sufficient in case of orthotopic implantation *in vivo*, where biochemical stimulation from the environment and high loading associated with locomotion are present. One way to reinforce hydrogel constructs is by using thermoplastic fibers. **Chapter 6** describes the 3D bioprinting of pHPMAlac-PEG/HAMA hydrogels in combination with a polycaprolactone (PCL)-based reinforcement for the development of cartilage composite constructs with relevant stiffness and high chondrogenic potential. Firstly, cell studies on cast hydrogels demonstrated a dose-dependent effect of HAMA on the chondrogenic potential of embedded chondrocytes. This allowed the identification of an optimal composition of pHPMAlac-PEG/HAMA hydrogel, which was subsequently co-printed with PCL. The PCL/hydrogel co-printing allowed the generation of several scaffold types with varying internal architecture, and having mechanical resistance in the range of native cartilage. Future studies on cell-laden hydrogel/PCL printed constructs will elucidate the role of the printing process on long-term activity and differentiation of embedded cells.

Besides all the aspects discussed so far, biocompatibility and functionality of cartilage constructs assessed in relevant *in vivo* models are crucial steps, when considering translation of these materials to the clinic. In **Chapter 7**, we report about the ectopic implantation of pHPMAlac-PEG/HAMA hydrogels in small animal (murine) and large animal (equine) models, as well as the orthotopic implantation in a large animal (porcine) model, as a work up for the future orthotopic implantation in a highly challenging equine model. Importantly, pHPMAlac-PEG/HAMA hydrogels showed adequate biocompatibility in the tested species and locations. Nevertheless, variability in hydrogel stability and resistance between different implantation sites and among the different species highlights the need for further optimization before an orthotopic, long-term screening in horses is undertaken.

## 8.2 Perspectives

Based on the studies reported in this thesis, hydrogels composed of pHPMAlac-PEG triblock copolymers and polysaccharides are promising biomaterials for cartilage tissue regeneration. Chondrogenic differentiation of embedded cells, *in vivo* biocompatibility, as well as possibility to process the hydrogel via 3D bioprinting technology to achieve porous and tunable architectures render these materials potential candidates for future clinical translation. Nevertheless, further optimization must be undertaken and technical considerations have to be taken into account to facilitate the progress of this material into the clinic.

### 8.2.1 Hydrogel composition and manufacturing

Additive manufacturing, *e.g.* 3D bioprinting is a promising technology for the generation of customized TE scaffolds having complex and tissue-mimicking architectures<sup>1,2</sup>. The applicability of this technology to pHPMAlac-PEG/HAMA or CSMA hydrogels allowed the fabrication of shape-stable hydrogel constructs with tunable porosity, as well as thermoplastic-reinforced hydrogels with mechanical properties in the range of native cartilage. Additionally, a preliminary attempt towards zonally organized hydrogel constructs, able to mimic the depth-dependent architecture of articular cartilage has been also performed. In a simplified design, the consecutive deposition of two layers, mimicking the middle-deep zone and the superficial zone of articular cartilage was achieved using two different print-heads, dispensing two different hydrogel compositions (Figure 1). Nevertheless, the creation of zonally organized tissue-constructs is not only a technical challenge related to the manufacturing process *per se*. Each layer not only has to be well-integrated with the others, but it has to be also carefully and rationally designed in terms of material and cell compositions<sup>3</sup>. Furthermore, each layer has to be individually studied and assessed for its potential in supporting the expression of specific zonal markers, *e.g.* proteoglycan IV (also named lubricin)<sup>4</sup> and clusterin<sup>5,6</sup> for the superficial zone; cartilage intermediate layer protein (CILP)<sup>7</sup> for the middle zone and cartilage oligomeric matrix protein (COMP)<sup>8</sup> for the middle and deep zone. In chapter 6, we report that pHPMAlac-PEG hydrogels and pHPMAlac-PEG/HAMA hydrogels containing low amount of HAMA (0.1%) supported the deposition of proteoglycan IV, which is a lubricant component of the superficial zone of cartilage<sup>4</sup>. The more limited presence of this marker in pHPMAlac-PEG/HAMA hydrogels with higher HAMA content (1%) suggests a dose-dependent effect of HAMA on the proteoglycan IV deposition, and in general highlights the need for a careful fine-tuning of the hydrogel composition to maximize the zone-mimicking capacity of each layer. Alternatively, different cell types (mesenchymal stem cells, chondrocytes or embryonic stem cells) or different cell subpopulations (chondrocytes isolated from different zones of articular cartilage) may be used<sup>9-11</sup>. Furthermore, layered constructs having a depth-dependent mechanical performance can be engineered<sup>3</sup>. Finally, signaling molecules can be included in the hydrogel to selectively stimulate



the zone-specific cellular differentiation and tissue remodeling<sup>3</sup>. In chapter 5, we developed a microcomposite hydrogel as a promising delivery system to achieve an *in situ* sustained release of a model protein. Further research may demonstrate the feasibility of this approach for the immobilization and sustained release of growth factors and their effect on relevant cell types.

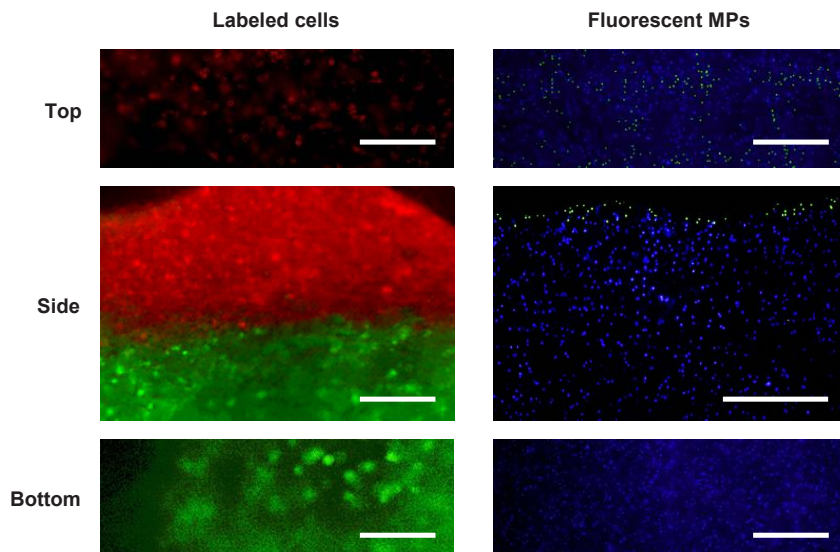


**Figure 1.** Layered constructs of pHPMAlac-PEG/HAMA hydrogels. A bottom layer (thickness = 1.8 mm) mimics the middle-deep zone (green or blue layer in the left and right column, respectively). A thin top layer (0.2 mm) mimics the superficial zone (red or green layer in the left and right column, respectively). The two hydrogels were enriched with dye-labeled cells (left, scale bar indicates 100  $\mu\text{m}$ ) or fluorescent microparticles (MPs, right, scale bar indicates 1 mm) for visualization purposes.

### 8.2.2 Translational aspects

Hydrogels composed of pHPMAlac-PEG and HAMA showed to support *in vitro* chondrogenesis of embedded chondrocytes. Moreover, short-term *in vivo* screening conducted in ectopic small animal (murine) and large animal (equine) models, as well as in an orthotopic large animal (porcine) model showed sufficient biocompatibility of these hydrogels in all tested species and implantation sites. Nevertheless, long-term *in vivo* studies in challenging large animal models, such as the horse, will be crucial to confirm the real applicability and regenerative potential of these hydrogels. In fact, often a discrepancy is observed between very promising results found *in vitro* or *in vivo* during short-term studies and the poor outcome of long-term studies in large animal models<sup>12</sup>.

In our studies, the species-dependent and implantation site-dependent character of some outcomes suggests the need for further material optimization before future long-term studies. For instance, the *in vivo* stability of porous printed constructs was maintained during the ectopic implantation in mice. However, the ectopic implantation of the same constructs in an equine model and the orthotopic implantation in a porcine

model resulted in an insufficient persistence of the hydrogels over time. Porosity of hydrogel constructs is considered a beneficial feature affecting nutrient/waste product exchange between the cell-containing matrix and the surrounding fluid, and avoiding the formation of poorly supplied core, especially for large TE constructs. Moreover, pore size and organization have been reported as important parameters affecting *in vivo* tissue maturation of TE constructs<sup>13,14</sup>. However, in our studies 3D printed porous hydrogels were significantly less stable than cast hydrogel controls, indicating the ambiguous role of pores in the millimeter range. This issue may be overcome by adjusting the pores size or, more efficiently by combining the hydrogel printing with thermoplastic extrusion, as we demonstrated in chapter 6. Overall, the superiority of porous printed constructs over cast hydrogels must be validated in appropriate *in vivo* settings, for instance in case of orthotopic implantation in large animal models associated with bone marrow stimulation procedures. In this scenario, porosity may facilitate cell penetration into the hydrogels from the underlying tissue. Another crucial aspect that needs further investigation is the development of valid strategies for the fixation of the hydrogel constructs in the defect area and their integration with the surrounding healthy cartilage. An often adopted strategy for the fixation of TE constructs is the use of fibrin-based adhesive materials, which are also employed in clinical settings<sup>15-17</sup>. In chapter 7 of this thesis, fibrin glue was used to fixate hydrogel constructs in a cartilaginous patellofemoral defect of a porcine limb. Nevertheless, our preliminary results conducted with pHPMAlac-PEG/HAMA hydrogels in an orthotopic equine model (results not reported in this thesis) suggest that xenogenic (human) fibrin glue may trigger an immunological reaction, and consequently lead to undesired resorption of the underlying bony tissue. This concern may find a solution in the isolation of species-specific fibrin glue or in the use of biodegradable covering membranes. Alternatively, a completely different approach would be the design of TE osteochondral-plugs intended for implantation in osteochondral defects. For this aim, constructs most preferably possess a stiff, bone-mimicking bottom layer and a cartilage-mimicking top layer. In this case, the press-fitting of the construct into the bone may guarantee early fixation of the constructs, while bony tissue ingrowth into the bone-mimicking zone of the construct can lead to long term stability<sup>18</sup>.

Finally, a crucial step for successful translation of TE implants is the development of procedures allowing the scale up and the production of materials according to Good Manufacturing Practice (GMP). Triblock copolymers of pHPMAlac and PEG are currently synthesized in our laboratory using a five-step procedure. Although a relatively high scale (max 25 g) was employed in the experiments described in this thesis, the applicability of a much larger scale has to be obviously considered.

## References

- (1) Malda, J.; Visser, J.; Melchels, F. P.; Jüngst, T.; Hennink, W. E.; Dhert, W. J. A.; Groll, J.; Hutmacher, D. W. 25th Anniversary Article: Engineering Hydrogels for Biofabrication. *Adv. Mater.* **2013**, *25* (36), 5011–5028.
- (2) Annabi, N.; Tamayol, A.; Uquillas, J. A.; Akbari, M.; Bertassoni, L. E.; Cha, C.; Camci-Unal, G.; Dokmeci, M. R.; Peppas, N. A.; Khademhosseini, A. 25th Anniversary Article: Rational Design and Applications of Hydrogels in Regenerative Medicine. *Adv. Mater.* **2014**, *26* (1), 85–124.
- (3) Klein, T. J.; Rizzi, S. C.; Reichert, J. C.; Georgi, N.; Malda, J.; Schuurman, W.; Crawford, R. W.; Hutmacher, D. W. Strategies for Zonal Cartilage Repair Using Hydrogels. *Macromol. Biosci.* **2009**, *9* (11), 1049–1058.
- (4) Li, Z.; Yao, S.; Alini, M.; Grad, S. Different Response of Articular Chondrocyte Subpopulations to Surface Motion. *Osteoarthr. Cartil.* **2007**, *15* (9), 1034–1041.
- (5) Khan, I. M.; Salter, D. M.; Bayliss, M. T.; Thomson, B. M.; Archer, C. W. Expression of Clusterin in the Superficial Zone of Bovine Articular Cartilage. *Arthritis Rheum.* **2001**, *44* (8), 1795–1799.
- (6) Malda, J.; ten Hoope, W.; Schuurman, W.; van Osch, G. J. V. M.; van Weeren, P. R.; Dhert, W. J. A. Localization of the Potential Zonal Marker Clusterin in Native Cartilage and in Tissue-Engineered Constructs. *Tissue Eng. Part A* **2010**, *16* (3), 897–904.
- (7) Lorenzo, P.; Bayliss, M. T.; Heinegard, D. A Novel Cartilage Protein (CILP) Present in the Mid-Zone of Human Articular Cartilage Increases with Age. *J. Biol. Chem.* **1998**, *273* (36), 23463–23468.
- (8) Murray, R. C.; Smith, R. K.; Henson, F. M. D.; Goodship, A. The Distribution of Cartilage Oligomeric Matrix Protein (COMP) in Equine Carpal Articular Cartilage and Its Variation with Exercise and Cartilage Deterioration. *Vet. J.* **2001**, *162* (2), 121–128.
- (9) Klein, T. J.; Malda, J.; Sah, R. L.; Hutmacher, D. W. Tissue Engineering of Articular Cartilage with Biomimetic Zones. *Tissue Eng. Part B Rev.* **2009**, *15* (2), 143–157.
- (10) Schuurman, W.; Klein, T. J.; Dhert, W. J. A.; van Weeren, P. R.; Hutmacher, D. W.; Malda, J. Cartilage Regeneration Using Zonal Chondrocyte Subpopulations: A Promising Approach or an Overcomplicated Strategy? *J. Tissue Eng. Regen. Med.* **2015**, *9* (6), 669–678.
- (11) Schuurman, W.; Gawlitta, D.; Klein, T. J.; Hoope, W. T.; van Rijen, M. H. P.; Dhert, W. J. A.; van Weeren, P. R.; Malda, J. Zonal Chondrocyte Subpopulations Reacquire Zone-Specific Characteristics During In Vitro Redifferentiation. *Am. J. Sports Med.* **2009**, *37* (1\_suppl), 97S–104S.
- (12) Vindas Bolaños, R. A.; Cokelaere, S. M.; McDermott, J. M. E.; Benders, K. E. M.; Gbureck, U.; Plomp, S. G. M.; Harrie, W.; Groll, J.; van Weeren, P. R.; Malda, J. The Use of a Cartilage Decellularized Matrix Scaffold for the Repair of Osteochondral Defects: The Importance of Long-Term Studies in a Large Animal Model. *Osteoarthr. Cartil.* **2016**, 1–8.
- (13) Malda, J.; Woodfield, T. B. F.; van der Vloodt, F.; Kooy, F. K.; Martens, D. E.; Tramper, J.; van Blitterswijk, C. A.; Riesle, J. The Effect of PEGT/PBT Scaffold Architecture on Oxygen Gradients in Tissue Engineered Cartilaginous Constructs. *Biomaterials* **2004**, *25* (26), 5773–5780.

- (14) Malda, J.; Woodfield, T. B. F.; van der Vloodt, F.; Wilson, C.; Martens, D. E.; Tramper, J.; van Blitterswijk, C. A.; Riesle, J. The Effect of PEGT/PBT Scaffold Architecture on the Composition of Tissue Engineered Cartilage. *Biomaterials* **2005**, *26* (1), 63–72.
- (15) Lewis, P. B.; McCarty, L. P.; Yao, J. Q.; Williams, J. M.; Kang, R.; Cole, B. J. Fixation of Tissue-Engineered Human Neocartilage Constructs with Human Fibrin in a Caprine Model. *J. Knee Surg.* **2009**, *22* (3), 196–204.
- (16) Jordan, M. A.; Van Thiel, G. S.; Chahal, J.; Nho, S. J. Operative Treatment of Chondral Defects in the Hip Joint: A Systematic Review. *Curr. Rev. Musculoskelet. Med.* **2012**, *5* (3), 244–253.
- (17) Falah, M.; Nierenberg, G.; Soudry, M.; Hayden, M.; Volpin, G. Treatment of Articular Cartilage Lesions of the Knee. *Int. Orthop.* **2010**, *34* (5), 621–630.
- (18) Kandel, R. A.; Grynepas, M.; Pilliar, R.; Lee, J.; Wang, J.; Waldman, S.; Zalzal, P.; Hurtig, M. Repair of Osteochondral Defects with Biphasic Cartilage-Calcium Polyphosphate Constructs in a Sheep Model. *Biomaterials* **2006**, *27* (22), 4120–4131.





# **Appendix A**

## **Nederlandse Samenvatting**



## Nederlandse samenvatting

Regeneratieve geneeskunde houdt zich bezig met het ontwikkelen van methoden om beschadigde weefsels te herstellen door gebruik te maken van onder andere biomaterialen, cellen en biologische signaalmoleculen. Met name voor weefsels met een beperkt natuurlijk herstellervermogen, zoals bijvoorbeeld kraakbeen, spelen de ontwikkelingen in de regeneratieve geneeskunde een steeds belangrijkere rol. Kraakbeen is een weefsel dat de uiteinden van beenderen in gewrichten bedekt en hiermee zware belasting opvangt en soepele bewegingen mogelijk maakt. Onder andere, omdat het niet doorbloed is, geneest beschadigd kraakbeen moeilijker dan andere weefsels. Aangezien er tot op heden geen optimale behandeling beschikbaar is voor kraakbeendefecten worden er verschillende regeneratieve strategieën onderzocht. Hiervoor worden biomaterialen gemaakt die in de eerste plaats zorgen voor mechanische ondersteuning en daarnaast een celvriendelijk milieu waarborgen. Deze biomaterialen degraderen langzaam gedurende een bepaalde tijd waarin nieuw weefsel wordt gevormd door de aanwezige cellen.

Het doel van het werk beschreven in dit proefschrift was het ontwikkelen van een geavanceerd hydrogelimplantaat voor de regeneratie van kraakbeen. Dit werk is uitgevoerd als onderdeel van het Europese consortium genaamd HydroZones ([www.hydrozones.eu](http://www.hydrozones.eu)) waarbij de ontwikkeling van biomaterialen, en hun *in vitro* en *in vivo* evaluatie centraal staan.

**Hoofdstuk 1** geeft een algemene introductie van de anatomie en fysiologie van kraakbeen en de huidige klinische behandelingsmethoden voor kraakbeendefecten. Daarnaast worden de ontwikkelingen in de regeneratieve geneeskunde t.a.v. kraakbeenherstel besproken. Verschillende biomaterialen, celtypen en fabricatiemethoden komen in dit hoofdstuk aan bod, waarbij speciaal aandacht wordt besteed aan het maken van geavanceerde 3D geprinte constructen.

De ontwikkeling van temperatuurgevoelige hydrogelen die gestabiliseerd worden door fotopolymerisatie staat centraal in dit proefschrift. Als basispolymeer is gekozen voor het triblok polymeer: gemethacyleerd poly[*N*-(2-hydroxypropyl) methacrylamide mono-dilactaat]/polyethylene glycol (pHPMAlac-PEG-pHPMAlac) gemengd met gemodificeerde polysacchariden zoals gemethacyleerde chondroïtine sulfaat (CSMA) of gemethacyleerd hyaluraanzuur (HAMA).

**Hoofdstuk 2** beschrijft een nieuwe methode om chondroïtine sulfaat (CS) te methacryleren op een efficiënte en reproduceerbare manier in een organisch oplosmiddel. De methacryleringsgraad was controleerbaar tot 48,5% door de hoeveelheid reagens en reactietijd te variëren. Door CSMA op te lossen met pHPMAlac-PEG in buffer werd na UV polymerisatie een hydrogel verkregen met verbeterde mechanische eigenschappen in vergelijking met hydrogelen zonder de aanwezigheid van CSMA. Deze goede mechanische eigenschappen maakten het mogelijk om deze hydrogelen in 3D te printen met goede controle over de vorm en



poreusheid. Daarnaast is aangetoond dat chondrocyten die beladen waren in deze hydrogel het fabricatieproces overleefden.

Naast overleving is differentiatie van chondrocyten van groot belang en dit aspect is bestudeerd in **hoofdstuk 3** voor pHPMAlac-PEG hydrogelen. *In vitro* experimenten toonden aan dat na 42 dagen significante hoeveelheden kraakbeenspecifieke componenten zoals glycosaminoglycanen, collageen II en VI werden geproduceerd door chondrocyten afkomstig van paarden. De toevoeging van CSMA of HAMA vertraagde de afbraaksnelheid van de hydrogelen en versterkte de mechanische eigenschappen. Vormvaste poreuze 3D geprinte matrices zijn gefabriceerd die wederom een excellente celoverleving lieten zien.

Hydrogelen gebaseerd op een mengsel van pHPMAlac-PEG en HAMA zijn twee-componenten systemen in waterig milieu waarbij fasescheiding werd waargenomen op microschaal. Fasescheiding kan een rol spelen in de uiteindelijke hydrogeleigenschappen. Daarom is in **hoofdstuk 4** fasescheiding als functie van pHPMAlac-PEG en HAMA concentraties bestudeerd in relatie tot de bijbehorende mechanische eigenschappen. Fasescheiding leidde tot een hydrofiele HAMA-rijke fase en een meer hydrofobe fase bestaande uit uitsluitend pHPMAlac-PEG. Een hogere concentratie HAMA leidde tot een grotere mate van fasescheiding. Mathematische modelering gaf een duidelijk beeld van de afhankelijkheid van de relatieve polymeerconcentraties op de mate van fasescheiding en mechanische eigenschappen van de hydrogelen. Deze modelering kan gebruikt worden als hulpmiddel bij het ontwerpen van een biomateriaal met de gewenste eigenschappen.

Belading van signaal moleculen zoals groeifactoren in hydrogelen is een veelbelovende strategie om gereguleerde afgifte van deze moleculen te bewerkstelligen. **Hoofdstuk 5** beschrijft een methode om monodisperse HAMA microgelen te maken met behulp van microfluidica en deze te beladen met een positief geladen model eiwit (lysozym). De diameter van de microgeldeeltjes varieerde van 313 tot 557  $\mu\text{m}$  door variaties in HAMA concentratie en fabricatiecondities. Een opmerkelijk hoge lysozymconcentratie in de microdeeltjes werd geobserveerd, waarschijnlijk veroorzaakt door de gunstige ladingsinteracties tussen lysozym en HAMA. Deze microgelen werden vervolgens geïmmobiliseerd in een pHPMAlac-PEG hydrogel en de afgifte van lysozym vanuit deze composietgel bleek vele malen trager dan wanneer lysozym zonder microgelen beladen was. Hieruit blijkt dat het gebruik van HAMA microgelen een toegevoegde waarde heeft voor de gereguleerde afgifte van eiwitten.

Aangezien een hydrogel minder sterk en stijf is dan kraakbeen, zijn in **hoofdstuk 6** de eerder beschreven pHPMAlac-PEG/HAMA gels geprint met poly- $\epsilon$ -caprolacton (PCL) vezels resulterend in stevigere constructen. Als eerste is de ideale HAMA concentratie bepaald voor optimale prestatie van beladen chondrocyten. Daarna is deze optimale formulering gebruikt om PCL en hydrogel samen in 3D te printen.

Verschillende constructen zijn gefabriceerd met dit geavanceerde printproces resulterend in materialen met variaties in interne structuur en vorm. De mechanische eigenschappen van deze hybride materialen lag in dezelfde orde van grootte als de mechanische eigenschappen van gezond kraakbeen.

Naast alle aspecten beschreven in de eerste zes hoofdstukken is natuurlijk de evaluatie van de biocompatibiliteit en functionaliteit van de gemaakte kraakbeenconstructen *in vivo* van cruciaal belang om uiteindelijk translatie naar de kliniek mogelijk te maken. In **hoofdstuk 7** wordt de *in vivo* evaluatie van pHPMAlac-PEG/HAMA hydrogels in muizen, paarden (ectopisch) en varkens (orthotopisch) beschreven. Een goede biocompatibiliteit is waargenomen in de diermodellen. Desalniettemin is een grote variabiliteit waargenomen in stabiliteit van de gelen tussen de verschillende diersoorten. Deze experimenten laten duidelijk zien dat verdere optimalisatie nodig is alvorens lange termijn regeneratie van kraakbeendefecten in paarden kan worden onderzocht.



# **Appendix B**

## **Curriculum Vitae and List of Publications**

## Curriculum Vitae

Anna Abbadessa was born on the 26<sup>th</sup> of February 1986 in San Severo, Italy. She obtained a Master degree *cum laude* in Pharmacy, at University "G. d'Annunzio", Chieti, Italy, in 2010. Subsequently, she started a research programme in Pharmaceutical Chemistry and Technology in the same university under the supervision of prof. A. Di Stefano. During this programme she worked on the synthesis of novel pro-co-drugs for anti-Alzheimer's and anti-Parkinson's disease applications. In 2012, she performed a 10-months internship in the department of Pharmaceutics at Utrecht University, Utrecht, The Netherlands, focusing on the development of polymeric particles for protein delivery. In January 2013, she started a PhD programme in polymer chemistry for tissue engineering under the supervision of prof. W.E. Hennink, dr. T. Vermonden and dr. J. Malda, and within the research programme of the European consortium HydroZONES ([www.hydrozones.eu](http://www.hydrozones.eu)). During her PhD, she focused on the development of thermosensitive, photo-curable hydrogels for 3D bioprinting of cartilage constructs.

## Publications included in this thesis

A. Abbadessa, M. M. Blokzijl, V. H. M. Mouser, P. Marica, J. Malda, W. E. Hennink, T. Vermonden

A thermo-responsive and photo-polymerizable chondroitin sulfate-based hydrogel for 3D printing applications, *Carbohydrate Polymers*, 2016, 149, pp 163-174.

A. Abbadessa\*, V. H. M. Mouser\*, M. M. Blokzijl, D. Gawlitta, W. J. A. Dhert, W. E. Hennink, J. Malda, T. Vermonden

A synthetic thermosensitive hydrogel for cartilage bioprinting and its biofunctionalization with polysaccharides, *Biomacromolecules*, 2016, 17 (6), pp 2137-2147.

A. Abbadessa, M. Landín, E. Oude Blenke, W. E. Hennink, T. Vermonden

Two-component thermosensitive hydrogels: phase separation affecting rheological behavior, *submitted for publication*.

V.H.M. Mouser\*, A. Abbadessa\*, R. Levato, W.E. Hennink, T. Vermonden, D. Gawlitta, J. Malda

Bio-ink development for the fabrication of composite cartilage repair constructs, *submitted for publication*.

\* these authors contributed equally

## Other publications

N. Samadi\*, A. Abbadessa\*, A. Di Stefano, C. F. van Nostrum, T. Vermonden, S. Rahimian, E. A. Teunissen, M. J. van Steenberg, M. Amidi, W. E. Hennink

The effect of lauryl capping group on protein release and degradation of poly (D,L-lactic-co-glycolic acid) particles, *Journal of Controlled Release*, 2013, 172 (2), pp 436-443.

P. Sozio, L. S. Cerasa, A. Abbadessa, A. Di Stefano

Designing prodrugs for the treatment of Parkinson's disease, *Expert opinion on drug discovery*, 2012, 7 (5), pp 385-406.

\* these authors contributed equally

## **Selected oral presentations**

A. Abbadessa, V. H. M. Mouser, M. M. Blokzijl, D. Gawlitta, W. J. A. Dhert, W. E. Hennink, J. Malda, T. Vermonden  
Novel thermosensitive photo-crosslinkable hydrogels for zonal 3D bioprinting,  
*Würzburger Initiative in Tissue Engineering 2015*, Würzburg, Germany.

A. Abbadessa, M. Landín, E. Oude Blenke, W. E. Hennink, T. Vermonden  
Rheology: an attractive tool to predict 3D printability of thermosensitive hydrogels,  
*Biofabrication 2015*, Utrecht, The Netherlands.

A. Abbadessa, V. H. M. Mouser, M. M. Blokzijl, D. Gawlitta, W. J. A. Dhert, W. E. Hennink, J. Malda, T. Vermonden  
Novel hybrid photo-crosslinkable and thermosensitive hydrogels for biofabrication,  
*Dutch Polymer Days 2015*, Lunteren, The Netherlands.

## **Selected poster presentations**

A. Abbadessa, M. Landín, E. Oude Blenke, W. E. Hennink, T. Vermonden  
Thermosensitive polysaccharide based-hydrogels with tunable rheological properties: a novel class of bioinks for cartilage 3D bioprinting,  
*World Biomaterials Conference 2016*, Montreal, Canada.

A. Abbadessa, C. C. L. Schuurmans, W. E. Hennink, T. Vermonden  
Glycosaminoglycan-based microgels for controlled release of proteins from hydrogel scaffolds,  
*Netherlands Society for Biomaterials and Tissue Engineering 2015*, Lunteren, The Netherlands.

A. Abbadessa, V. H. M. Mouser, M. M. Blokzijl, D. Gawlitta, W. J. A. Dhert, W. E. Hennink, J. Malda, T. Vermonden  
3D printed thermosensitive hydrogel scaffolds for articular cartilage regeneration,  
*Dutch Polymer Days 2014*, Lunteren, The Netherlands.



# **Appendix C**

## **Acknowledgements**



## Acknowledgements

Dear Tina, it is hard for me to express with simple words all my gratitude towards you. Your approach to science and to life has been incredibly inspiring for me. Thanks for sharing with me the thoughts of your brilliant mind, your knowledge, your time, your enthusiasm, and for granting me scientific freedom and trust. Thanks for your endless dedication to our shared work and for all the times that there was no need for me to talk, because you had already understood everything by looking at me. I could always find in you a professional mentor and an adorable person. Thanks, because with your character you have enriched my personality. And thanks for making me, as you always say, an “independent researcher”.

Dear Wim, although in this last year I finally learned to remove the salutation “prof” next to your name, you will always be prof. Wim for me. Thanks for hosting me in the department of Pharmaceutics for five wonderful years. You are an extremely knowledgeable scientist and friendly person. Although you are now a very busy professor, you still like to carefully check each manuscript (we all know that the first version of a manuscript that we send to you will be back soon completely red!). In our meetings I have always enjoyed our scientific discussions, and I will never forget your attention to the smallest details, such as the use of “must” in a sentence. Besides, you always have a funny story to tell while drinking a beer with us. I hope you know how precious it is to have a prof like you!

Dear Jos, thanks for supporting and trusting me during these years. Thanks for introducing me to the world of “biofabrication” and for many inspiring meetings and discussions. Your passion for this job and your knowledge are a beautiful source of inspiration for a young scientist like me. Thank you because you always did your best to help me despite your busy agenda.

Dear Debby, thanks a lot for all you did for me, for all your nice suggestions to improve my experiments and manuscripts, and for all our constructive meetings.

A special thank goes to my closest collaborators. Dear Vivian, Maarten, Irina, Emma, Riccardo, we shared so many challenges and successes, difficult and wonderful moments that we can really say: we have been a great team! Dear Vivian, our “scientific marriage” was something extremely intense! Thanks for every single time you were there for me. Your dedication and passion to our shared work, as well as our perfect and natural connection made many nice things possible. Not only things that are reported in this thesis, but also beautiful memories for ever printed in my heart. Dear Maarten, thanks a lot for all your help, especially for introducing me to the world of 3D printers and for being always there if I needed any technical and moral support.

Thanks, HydroZONES! Thanks, because you are not a simple European Consortium, but a real life experience. Thanks to the people who made HydroZONES possible in the first place, Prof. Groll, Prof. Prosper and Jos, and the rest of the people who every day work together to accomplish the final goal of this ambitious project. Especially, I would like to thank Jörg, Simone, Uwe, Ralf, Felix, Clayton and Dirk for our constructive WP1 teleconferences; Thomas, Andrea, Franziska, Linda, Froi, Yvonne, Friederike, Eliane; Reka and Stefanie for your professional and passionate contribution to HydroZONES.

I would like to acknowledge also prof. René van Weeren for his precious contribution to chapter 8 of this thesis, and for his professional attitude and always enthusiastic support during our meetings.

Thanks to prof. Daan Saris and Ali Talib for their contribution to chapter 1.

Dear prof. Roos Masereeuw, I really enjoyed our meetings and discussions. Thanks for introducing me to the “bioartificial kidney” topic. Thanks Michele, because of your enthusiasm in our shared work. Unfortunately, we didn’t have the chance to complete our project. I hope it will be eventually possible to fulfil our goal.

To my lovely colleagues from Pharmaceutics: thanks for being always very kind and helpful to me, especially during the last months of my PhD. When I was a kind of anti-social human being, too focused only in writing my thesis and last papers, you always had a smile for me. Thanks!

Thanks to my students Birgit, Paola, Carl, Jennifer, Claudia, Ali. From each of you I have a special memory and from each of you I have learned something important. I wish you all good luck with your future life!

Dear Roberta Censi, thanks for your thesis! Besides mine, yours is the only PhD thesis that I have read from the first to the last word. Your thesis has been on my desk every single day of my PhD. From your beautiful book, I could perfectly feel all your passion for science and your dedication.

Dear prof. Di Stefano, thanks for introducing me to the world of pharmaceutics in the first place. Thanks for all your trust and your help. You have been an important guide for me, from the classes at university to my first steps into research.

Dear Mies, thanks for every time you helped me with passion and positivity! Thanks for all the care you have for us and our lab! Thanks for every loud song you sang in the lab, for every time you scared me shouting for who-knows-what, and thanks for your delicious “erwtensoeep”!

Dear Barbara, Joep, Roel, Mattie and Anneloes thanks for all your help! Every time I came to you, you were always willing to help me!

Dear Netherlands, thanks to you! I will never forget all you gave me! You have been my window to the world!

Dear Marco and Shima, you have been like family for me and Riccardo during these years. Thanks for all you did for me with love and care, thanks for all the unforgettable moments together.

Thanks to all my friends in Utrecht, Carlo, Gosia, Alessia, Jorgos, Michele, Giuliana, Lisa and many others. Thanks also to all my friends from Italy. Marilena, I have missed you so much while living apart during the last five years. You have been the perfect housemate and the most intimate friend I have ever had. Chiara, thanks for all the help you always offered me and for discovering the Netherlands with me in the really beginning of my Dutch experience.

Thanks to my family and my family in law, who always helped and supported me. Thanks for loving me so much!

Cara mamma, thanks for your infinite love and for making me the person I am. Even in the most difficult moments, you always had a smile for me! Thanks, because with your love you took what was impossible in our lives and made it possible.

My dear Riccardo, thanks for all these years together! Thanks for making my life so beautiful and for giving me your love every day in the most graceful way. You are the most precious thing I have in my life.

